Respiratory Systems

Modeling, Analysis, and Control

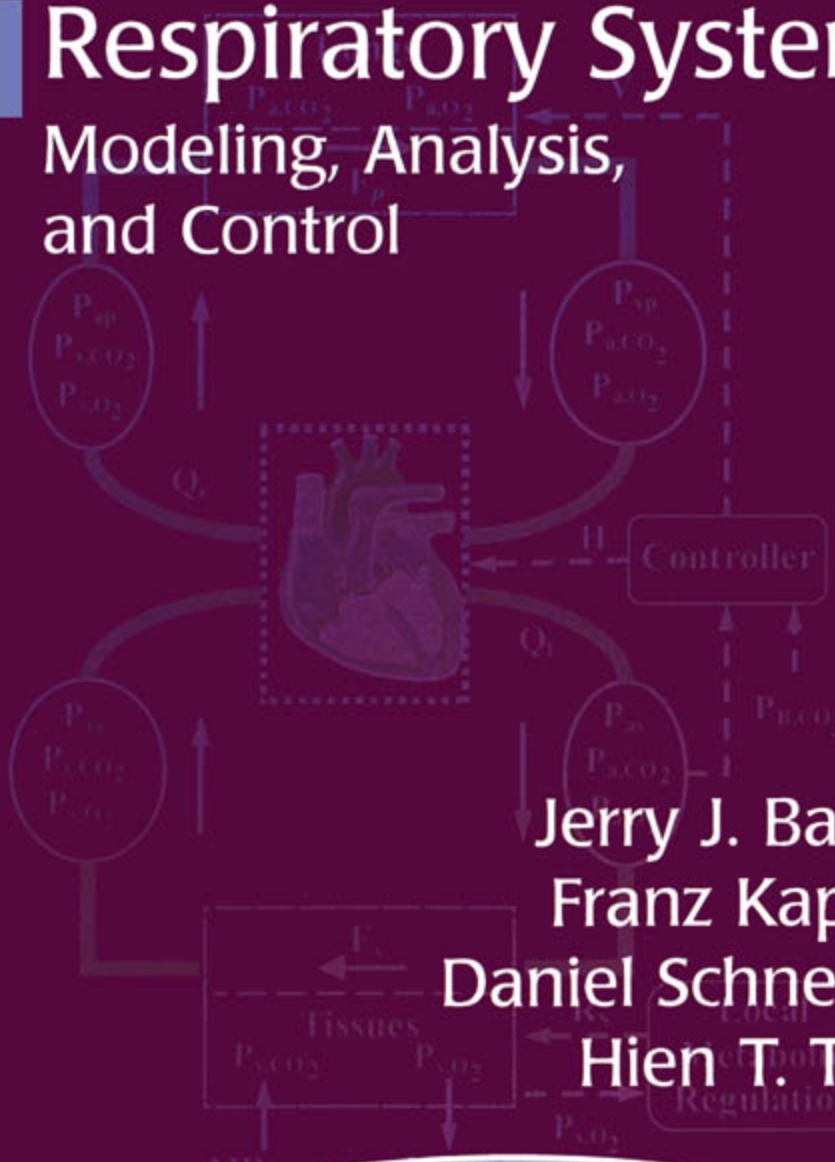

Jerry J. Batzel
Franz Kappel
Daniel Schneditz
Hien T. Tran

siam FRONTIERS IN APPLIED MATHEMATICS

Cardiovascular and Respiratory Systems

This page intentionally left blank

The SIAM series on Frontiers in Applied Mathematics publishes monographs dealing with creative work in a substantive field involving applied mathematics or scientific computation. All works focus on emerging or rapidly developing research areas that report on new techniques to solve mainstream problems in science or engineering.

The goal of the series is to promote, through short, inexpensive, expertly written monographs, cutting edge research poised to have a substantial impact on the solutions of problems that advance science and technology. The volumes encompass a broad spectrum of topics important to the applied mathematical areas of education, government, and industry.

EDITORIAL BOARD

BOOKS PUBLISHED IN FRONTIERS IN APPLIED MATHEMATICS

Batzel, Jerry J.; Kappel, Franz; Schneditz, Daniel; and Tran, Hien T., *Cardiovascular and Respiratory Systems: Modeling, Analysis, and Control*

Li, Zhilin and Ito, Kazufumi, *The Immersed Interface Method: Numerical Solutions of PDEs Involving Interfaces and Irregular Domains*

Smith, Ralph C., *Smart Material Systems: Model Development*

Iannelli, M.; Martcheva, M.; and Milner, F. A., *Gender-Structured Population Modeling: Mathematical Methods, Numerics, and Simulations*

Pironneau, O. and Achdou, Y., *Computational Methods in Option Pricing*

Day, William H. E. and McMorris, F. R., *Axiomatic Consensus Theory in Group Choice and Biomathematics*

Banks, H. T. and Castillo-Chavez, Carlos, editors, *Bioterrorism: Mathematical Modeling Applications in Homeland Security*

Smith, Ralph C. and Demetriou, Michael, editors, *Research Directions in Distributed Parameter Systems*

Höllig, Klaus, *Finite Element Methods with B-Splines*

Stanley, Lisa G. and Stewart, Dawn L., *Design Sensitivity Analysis: Computational Issues of Sensitivity Equation Methods*

Vogel, Curtis R., *Computational Methods for Inverse Problems*

Lewis, F. L.; Campos, J.; and Selmic, R., *Neuro-Fuzzy Control of Industrial Systems with Actuator Nonlinearities*

Bao, Gang; Cowsar, Lawrence; and Masters, Wen, editors, *Mathematical Modeling in Optical Science*

Banks, H. T.; Buksas, M. W.; and Lin, T., *Electromagnetic Material Interrogation Using Conductive Interfaces and Acoustic Wavefronts*

Oostveen, Job, *Strongly Stabilizable Distributed Parameter Systems*

Griewank, Andreas, *Evaluating Derivatives: Principles and Techniques of Algorithmic Differentiation*

Kelley, C. T., *Iterative Methods for Optimization*

Greenbaum, Anne, *Iterative Methods for Solving Linear Systems*

Kelley, C. T., *Iterative Methods for Linear and Nonlinear Equations*

Bank, Randolph E., *PLTMG: A Software Package for Solving Elliptic Partial Differential Equations. Users' Guide 7.0*

Moré, Jorge J. and Wright, Stephen J., *Optimization Software Guide*

Rüde, Ulrich, *Mathematical and Computational Techniques for Multilevel Adaptive Methods*

Cook, L. Pamela, *Transonic Aerodynamics: Problems in Asymptotic Theory*

Banks, H. T. , *Control and Estimation in Distributed Parameter Systems*

Van Loan, Charles, *Computational Frameworks for the Fast Fourier Transform*

Van Huffel, Sabine and Vandewalle, Joos, *The Total Least Squares Problem: Computational Aspects and Analysis*

Castillo, José E., *Mathematical Aspects of Numerical Grid Generation*

Bank, R. E., *PLTMG: A Software Package for Solving Elliptic Partial Differential Equations. Users' Guide 6.0*

McCormick, Stephen F., *Multilevel Adaptive Methods for Partial Differential Equations*

Grossman, Robert, *Symbolic Computation: Applications to Scientific Computing*

Coleman, Thomas F. and Van Loan, Charles, *Handbook for Matrix Computations*

McCormick, Stephen F., *Multigrid Methods*

Buckmaster, John D., *The Mathematics of Combustion*

Ewing, Richard E., *The Mathematics of Reservoir Simulation*

Cardiovascular and Respiratory Systems

Modeling, Analysis, and Control

Jerry J. Batzel
Franz Kappel
University of Graz
Graz, Austria

Daniel Schneditz
Medical University of Graz
Graz, Austria

Hien T. Tran
North Carolina State University
Raleigh, North Carolina

siam
Society for Industrial and Applied Mathematics
Philadelphia

10 9 8 7 6 5 4 3 2 1

Library of Congress Cataloging-in-Publication Data:

Cardiovascular and respiratory systems : modeling, analysis, and control \ Jerry J. Batzel ...[et al.].
p. cm. — (Frontiers in applied mathematics)
Includes bibliographical references and index.
ISBN-13: 978-0-898716-17-7 (pbk.)
ISBN-10: 89871-617-9 (pbk.)
1. Cardiovascular system—Mathematical models. 2. Respiratory organs—Mathematical models. I. Batzel, Jerry J.

QP105.C37 2006
612.1—dc22 2006051174

Contents

This page intentionally left blank

List of Symbols and Abbreviations

Symbols

a_o, b_o, c_o	dissociation parameters for oxygen
η	viscosity
Π_{cap}	colloid osmotic pressure in capillaries
Π_{tis}	colloid osmotic pressure in tissue
c	compliance
c_{ap}	arterial pulmonary compliance
c_{as}	arterial systemic compliance
c_{is}	compliance of interstitial tissue
c_{ps}	peripheral systemic compliance
c_{ra}	right atrial compliance
c_{vp}	venous pulmonary compliance
c_{vs}	venous systemic compliance
C_{a,CO_2}	carbon dioxide concentration in arterial blood
C_{a,O_2}	oxygen concentration in arterial blood
C_{am,O_2}	oxygen concentration in mixed shunted venous and lung capillary blood
C_{B,CO_2}	carbon dioxide concentration in brain tissue
C_{T,CO_2}	carbon dioxide concentration in tissue
C_{T,O_2}	oxygen concentration in tissue
C_{v,CO_2}	carbon dioxide concentration in venous blood
C_{v,O_2}	oxygen concentration of venous blood
C_{v,B,CO_2}	carbon dioxide concentration in venous blood in brain
C_{ind}	volume concentration of indicator
C_{pl}	protein concentration in plasma
C_{ref}	refilling protein concentration
E_F	factor for ventilatory dead space
f_{cell}	fraction of cells
F	blood flow
F_B	cerebral blood flow
f_v	ventilatory frequency

F_p	pulmonary blood flow
F_s	systemic blood flow
G_{aff}	afferent gain
G_{cap}	capillary pressure drop gain
$G_{eff,i}$	peripheral gains
G_C	central ventilatory gain
G_P	peripheral ventilatory gain
G_S	ventilatory sleep gain factor
$G_{S,min}$	minimum ventilatory sleep gain factor
H	heart rate
C_{hct}	hematocrit
$C_{hct,lv}$	hematocrit in large vessels
$C_{hct,wb}$	hematocrit in the whole body
$\dot{H}$	change in heart rate
I_C	threshold of the central ventilatory control cutoff
I_P	threshold of the peripheral ventilatory control cutoff
K_{CO_2}	dissociation constant for carbon dioxide
K_{fil}	filtration coefficient
M	body mass
m_{ind}	mass of indicator
MR	metabolic rate
MR_B	cerebral metabolic rate
P	pressure
$P_{A\text{-}a,O_2}$	alveolar-arterial O_2 gradient
P_{amb}	ambient pressure
P_{as}	arterial systemic blood pressure
P_{ap}	arterial pulmonary blood pressure
P_{cap}	capillary hydrostatic pressure
P_{dcap}	drop of the capillary hydrostatic pressure
P_{is}	interstitial tissue pressure
P_{ps}	peripheral systemic pressure
P_{ra}	right atrial pressure
P_{tis}	tissue hydrostatic pressure
P_{vp}	venous pulmonary blood pressure
P_{vs}	venous systemic blood pressure
P_{CO_2}	partial pressure of carbon dioxide
P_{O_2}	partial pressure of oxygen
P_{a,CO_2}	partial pressure of carbon dioxide in arterial blood
P_{a,O_2}	partial pressure of oxygen in arterial blood
P_{am,O_2}	partial pressure of oxygen in mixed shunted venous and lung capillary blood
P_{i,CO_2}	partial pressure of carbon dioxide in inhaled air
P_{i,O_2}	partial pressure of oxygen in inhaled air
P_{mcf}	mean circulatory filling pressure
P_t	transmural pressure
P_{T,CO_2}	partial pressure of carbon dioxide in tissue

P_{T,O_2}	partial pressure of oxygen in tissue
P_{v,CO_2}	partial pressure of carbon dioxide in venous blood
P_{v,O_2}	partial pressure of oxygen in venous blood
P_{v,B,CO_2}	partial pressure of carbon dioxide in brain
Q	generic fluid flow
Q_{co}	cardiac output
Q_{fil}	filtration flow
Q_{ly}	lymph flow
Q_ℓ	left cardiac output
Q_r	right cardiac output
Q_{uf}	ultrafiltration rate
R	resistance
R_{as}	arterial systemic resistance
R_p	pulmonary resistance
R_{ps}	peripheral systemic resistance
R_{ra}	right atrial resistance
R_s	systemic resistance
R_{vs}	venous systemic resistance
S_ℓ	left cardiac contractility
σ_ℓ	rate of change in S_ℓ
S_r	right cardiac contractility
σ_r	rate of change in S_r
$\gamma_\ell, \alpha_\ell, \beta_\ell$	parameters for S_ℓ equations
$\gamma_r, \alpha_r, \beta_r$	parameters for S_r equations
S_{a,O_2}	oxygen saturation
S_K	ventilatory operating point
S_{K_M}	minimum of the ventilatory operating point
S	surface area
T	temperature
T_{aff}	afferent tone
τ	delay
T_I	duration of inspiration
T_E	duration of expiration
V	volume
$\dot{V}_{ar}$	arousal threshold of the ventilatory drive
V_D	dead space volume
V_{ind}	distribution volume of an indicator
V_{is}	interstitial tissue volume
$\dot{V}_{min}$	minimum ventilation before collapse of airways
V_b	blood volume
V_{pl}	plasma volume
$V_{pl,wb}$	whole body plasma volume
V_{RBC}	red blood cell volume
$V_{RBC,wb}$	whole body red blood cell volume
$V_{b,rel}$	relative blood volume
$V_{pl,rel}$	relative plasma volume

V_s	stressed volume
V_u	unstressed volume
V_{as}	arterial stressed volume
V_{ps}	peripheral stressed volume
V_{rs}	right atrial stressed volume
V_{vs}	venous stressed volume
V_{A,CO_2}	effective CO_2 volume of the lung compartment
V_{A,O_2}	effective O_2 volume of the lung compartment
V_{B,CO_2}	effective CO_2 volume of the brain compartment
V_{T,CO_2}	effective CO_2 volume of the tissue compartment
V_{T,O_2}	effective O_2 volume of the tissue compartment
V_T	tidal volume
$\dot{V}_A$	alveolar ventilation rate
$\ddot{V}_A$	change in alveolar ventilation rate
$\dot{V}_C$	central ventilatory controller
$\dot{V}_D$	dead space ventilation
$\dot{V}_E$	minute ventilation
$\dot{V}_P$	peripheral ventilatory controller

Abbreviations

ADH	antidiuretic hormone
Ang-II	angiotensin II
ANP	atrial natriuretic peptide
BTPS	body temperature and ambient pressure, water saturated
CA	central apnea
CBF	cerebral blood flow
CHF	congestive heart failure
CNS	central nervous system
COPD	chronic obstructive pulmonary disease
CSA	central sleep apnea
CSF	cerebral spinal fluid
CSR	Cheyne–Stokes respiration
CT	computed tomography
CVRS	cardiovascular-respiratory system
CVS	cardiovascular system
2,3-DPG	2,3-diphosphoglycerate
Hb	hemoglobin
Hb-A	adult hemoglobin
Hb-F	fetal hemoglobin
HF	heart failure
HRV	heart rate variability
HUT	head up tilt
ICG	indocyanine green
LBNP	lower body negative pressure
L-R shunt	left-right shunt

MAP	mean arterial pressure
MRI	magnetic resonance imaging
NA	noradrenaline
NREM	nonrapid eye movement
OA	obstructive apnea
ODE	ordinary differential equation
OI	orthostatic intolerance
OID	orthostatic intolerance disorder
OLS	output least-squares
OSA	obstructive sleep apnea
PAT	peripheral arterial tonometry
PB	periodic breathing
RAAS	renin-angiotensin-aldosterone system
RBC	red blood cells
REM	rapid eye movement
R-L shunt	right-left shunt
RQ	respiratory quotient
RS	respiratory system
RSA	respiratory sinus arrhythmia
SIDS	sudden infant death syndrome
SNA	sympathetic nerve activity
STPD	standard temperature and pressure, dry

This page intentionally left blank

Preface

Efforts in modeling cardiovascular and respiratory control have been ongoing for a number of years. These efforts include seminal work by A. C. Guyton and coworkers and F. Grodins and coworkers in the 1950s and 1960s. In particular, over the last decade there has been a rapid increase in modeling activities in this area as technology has advanced both for simulation and for data collection. It is now possible to consider a wide range of features from the cellular level to the macroscopic level as well as the complex interaction of control processes and to ask harder questions concerning interdependencies between systems. Indeed, as a consequence of these capabilities, the Physiome project (see Section 5.3) was recently formed to coordinate knowledge about such issues. Often, asking the right question or focusing on a crucial physiological mechanism is more important than utilizing sheer computational power to simulate and capture data behavior.

Control mechanisms provide the basis for maintaining homeostasis at various levels in living systems. Such processes tend to have their own local operational goals, and yet physiological systems are interdependent and interact. However, such interaction could conceivably diminish overall performance. Nevertheless, these critical control systems seem to be well coordinated and to function complementarily. This raises very interesting evolutionary and organizational questions. The range of control processes involved in the effective regulation of human cardiovascular and respiratory systems includes a number of global and local mechanisms. Modeling efforts are certainly required to elucidate these complex interdependencies. As a consequence of the progress in relevant mathematical disciplines and the availability of increasingly powerful computing tools, models are becoming more realistic which allows for the adaptation to individual persons in the clinical setting and thereby makes possible the development of diagnostic and therapeutic tools. This book does not aim to exhaustively examine all research efforts in this field, but to selectively develop some important themes and modeling strategies.

The modeling of physiological control systems has resulted in numerous research monographs written over the years. The cardiovascular and respiratory control systems represent an important focal point for developing physiological control theory given the complexity of the control mechanisms involved, the important modes of interaction between cardiovascular and respiratory function, as well as their importance in many clinical situations. In this volume we will bring together contemporary mathematical and control methodologies to study these systems. We will highlight a number of analytical techniques and ideas from optimal control theory, systems theory, and parameter estimation to give the reader an appreciation of how these tools can be utilized to better understand the regulation processes in the cardiovascular and respiratory systems. Modeling efforts are arranged

around specific questions or conditions such as exercise or sleep transition and, generally, are based on physiological mechanisms rather than on formal description of input-output behavior. We make an effort to emphasize open questions relevant to medical and clinical applications. The context for discussion is on elucidating underlying themes of physiological control organization such as optimization of some process, minimization of quantities such as energy, and possible critical state values, which seem to drive the control design such as maintaining pH levels in a narrow band. We also strive to highlight important questions to be resolved and areas where knowledge is lacking. Throughout the book, we seek to uncover or explain physiological relationships through a first principle-based modeling approach and, in particular, through the analysis of feedback control regulation.

This monograph is intended for researchers in this field, but is also written in such a way as to be accessible to graduate students in biomedical engineering, life sciences, and applied mathematics, as well as to scientists interested in beginning research in this area. Topics are organized around specific questions of control interactions and physiologically based modeling approaches. The primary goals of this volume are: (i) providing an overview that highlights the complex nature of control processes and interactions between the cardiovascular and respiratory systems; (ii) describing state-of-the-art developments in modeling the control processes of the cardiovascular and respiratory systems; (iii) illustrating and developing some basic underlying principles of physiological control organization; and finally (iv) pointing out the direction of future research arranged around natural analytical questions. In summary, we strive to provide insight into organizational principles of cardiovascular and respiratory control and a clear and workable picture of research efforts in this area and possible areas of medical applications.

The material presented in this monograph is organized into five chapters and three appendices. Each chapter provides physiologically relevant background as well as physiologically based approaches to modeling. In addition, analytical issues associated with the mathematical model are also discussed. Chapter 1 introduces basic elements of cardiovascular modeling including key physiological concepts, some analytical tools, and the application of optimal control to model the baroreceptor loop. To illustrate the modeling philosophy used in this book and the applicability of the model, the transition of the cardiovascular system from rest to ergometric exercise is given as an example. In a similar way, Chapter 2 presents the basic elements of the respiratory control system and the development of a mathematical model with the same level of complexity as the cardiovascular model of the first chapter. Time delays play an important role in respiratory control. Such delays are included in the model and their influence on the dynamics of the respiratory system is discussed. A number of important clinically relevant applications are also provided. In Chapter 3 the models developed in Chapters 1 and 2 are integrated into a model for the cardiovascular-respiratory system. Aspects of control theory, steady state analysis, and state-dependent delays are discussed in the context of this more complex model. Furthermore, interaction of respiratory and cardiovascular control is discussed in great detail. Clinically, relevant applications are given which also illustrate how models can be extended to cover new situations. These applications include congestive heart failure, which was already discussed in Chapter 2, as well as new applications to orthostatic stress and basic reactions of the cardiovascular-respiratory system to hemorrhage. Chapter 4 gives a thorough discussion on how the venous system and blood volume control influence the cardiovascular system. This role of the venous system is often underestimated, partly

because the arterial system parameters and the control mechanisms, such as the arterial baroflex, have been more accessible to measurement. These issues play an important role in hemodialysis, which is given as a modeling application. Chapter 5 provides a detailed evaluation of the state of the art in areas related to the themes developed in this book. In particular, important questions are raised, the answers to which should have an impact on the further development of the field. This includes some well-accepted principles which are currently being re-examined.

The appendices provide detailed computations, which would interrupt the presentation in the chapters, and provides short descriptions of important analytical topics which can be pursued in greater detail using the references provided. In particular, Appendix A gives an introduction to generalized sensitivity analysis. Appendix B provides background on nonlinear feedback control. In Appendix C we present basic facts and ideas on delay equations which, in particular, are used in Chapters 2 and 3.

Acknowledgments

We wish to express our gratitude to a number of researchers who shared their insight into current problems in cardiovascular and respiratory control, thus enhancing our presentation in Chapter 5. We especially mention A. De Gaetano, R. Hughson, T. Kenner, R. Kerbl, P. Kerkhof, M. C. K. Khoo, P. Kotanko, R. Panerrai, V. Somers, E. Weibel, P. Robbins, L. Rowell, and N. Westerhof. Of course, the research results presented in this monograph are based on intensive cooperations with a number of colleagues. In particular, we want to mention the intensive discussions with M. S. Olufsen, J. T. Ottesen, and V. Novak at the regular meetings of the RGHBCS group. Interdisciplinary research of the type presented in this monograph relies also on the involvement and contributions of PhD students. We want to acknowledge the work of L. Ellwein, M. Fink, S. Lafer, R. O. Peer, and S. Timischl-Teschl. We especially thank M. Fink for his further contribution and technical support to the production of this manuscript.

We are grateful for the financial support we received for our work on topics presented in this monograph. H. T. Tran was supported by the National Science Foundation (USA), Grant 0437037 "US-Austria-Denmark Cooperative Research: Modeling and Control of the Cardiovascular-Respiratory System" and by the joint DMS/NIGMS Initiative to Support Research in the Area of Mathematical Biology under Grant 1RO1GM67299-01. Furthermore, J. J. Batzel, F. Kappel, and D. Schneditz acknowledge support by the FWF (Austria) in the framework of the Center for Excellence F300 "Optimization and Control."

Graz and Raleigh, November 2005

Jerry J. Batzel
Franz Kappel
Daniel Schneditz
Hien T. Tran

This page intentionally left blank

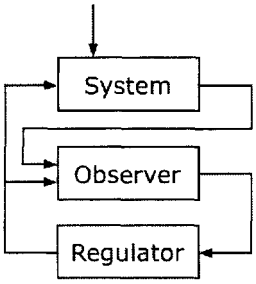

Chapter 1

The Cardiovascular System under an Ergometric Workload

In this chapter we present the basic model for the cardiovascular system under a low to medium ergometric workload. The model is an extension of a model proposed by Grodins for the so-called mechanical part of the cardiovascular system (see Grodins, 1963). The main additions are, a submodel for the local metabolic control process in muscle perfusion and a model for the baroreceptor loop. We also present some of the extensive numerical computations carried out for simulations and parameter identification.

1.1 Some Physiological Facts

In this section we discuss some physiological facts concerning the cardiovascular system which are necessary for the modeling process in this chapter. Most of the facts presented in this section are standard knowledge and can be found in the literature (see for instance Levick, 2003; Westerhof, Stergiopulos, and Noble, 2005). We also refer the reader to Section 3.1 for more details.

The basic task of the cardiovascular system is to satisfy, for each individual cell of the organism, the requirements of metabolism for O_2 and other substrates. At the same time CO_2 and the other end products of metabolism have to be removed. In addition, the cardiovascular system transports hormones and enzymes which regulate cell functions. In order to fulfill these tasks, the blood is pumped by the heart through two vascular circuits: the pulmonary circuit which transports blood through the lungs and the systemic circuit which transports blood through the tissues.

The heart consists of four chambers of two types: atria and ventricles. The atria efficiently load the ventricles which serve as the primary pumps to generate flow through the system. The right atrium and right ventricle function together as a single pump as do the left atrium and left ventricle. For simplicity, we will sometimes refer to the right atrium and right ventricle as the *right heart* and similarly refer to the left atrium and left ventricle as the *left heart*. The left heart receives blood coming from the lungs, which is rich in O_2, and pumps it into the aorta, the first vessel of the arterial tree which distributes the blood to all regions of the body. The vasculature bifurcates into progressively smaller vessels, from larger to smaller systemic arteries and further to systemic arterioles down to the systemic

capillaries. In the capillaries the substrates needed for metabolism by the cells as well as O_2 are delivered and metabolic end products, in particular CO_2, are removed. Leaving the systemic capillaries, the blood, now enriched with CO_2 and depleted of O_2, enters the systemic venous system and reaches the right atrium through veins of progressively larger diameter (venules, small veins, superior and inferior vena cava). The right ventricle pumps the blood into the pulmonary artery and the pulmonary arterial tree, which distributes the blood to the alveolar region of the lungs. In the pulmonary capillaries CO_2 is removed and O_2 enters the blood. Leaving this region, the blood flows through the pulmonary veins to the left atrium. Under resting conditions one circuit through both the systemic and pulmonary circulations takes around one minute. Note that in this configuration the left and right hearts act as two pumps in series. The coordination of flows in this configuration is not a trivial task.

The vessels of the systemic circuit can be grouped according to their total cross section, or, equivalently, the resulting flow velocity and corresponding pressure drop. Along the aorta and the large and small arteries, the total cross-sectional area does not change much and correspondingly the flow velocity decreases only slightly (from about 0.2 [m/sec] to 0.15 [m/sec]). At the same time the average blood pressure decreases from around 100 [mmHg] to approximately 90 [mmHg]. This also means that the resistance against blood flow in this part of the systemic circuit is very small. The main pressure drop in the systemic circuit occurs in the arterioles, which have a diameter smaller than 30–50 [μm]. Consequently, the resistance against blood flow is high. Moreover, this resistance can be varied considerably by vasoconstriction and vasodilation, because the walls of these vessels are equipped with smooth muscle fibers to increase wall tension and thus reduce vessel diameter.[1] This allows for the control of perfusion of different organs or tissues according to their metabolic needs. Along the arterioles there is a tremendous increase in the total cross-sectional area up to approximately 0.3 [m^2], which implies that the flow velocity along the arterioles decreases to around 0.5 [mm/sec] in the capillaries. Therefore, there is sufficient time for the exchange processes with the interstitium (O_2, CO_2, metabolites, fluids, etc.) across the capillary walls, which provide a huge surface for these exchange processes. Blood is collected in the venules which also contribute to the exchange of fluids.

Depending on the pressures in various parts of the cardiovascular system, one can distinguish a high-pressure part and a low-pressure part. The high-pressure part consists of the arteries in the systemic circuit and the left ventricle during the systole (see below), whereas the low-pressure part comprises the veins of the systemic circuit, the vessels of the pulmonary circuit, the right heart, the left atrium as well as the left ventricle during the diastole. The boundary between the two parts is given by the left ventricle (which belongs to the high-pressure part during systole and to the low-pressure part during diastole) and the capillary region of the systemic circuit. At rest, about 85% of the total blood volume is in the low-pressure part and about 15% is in the high-pressure part. The flux distribution at rest in various organs or tissues is also quite interesting (see Table 1.1).

One usually considers two phases of the heart cycle, the *systole* and the *diastole* (see Figure 1.1, upper panel). A systole starts with the contraction of the heart muscle. As a consequence, the ventricular pressure increases and the atrioventricular valves (i.e., the

[1] In fact, all arteries have walls of muscle fibers. However, the density of these muscle fibers increases from central to peripheral arteries.

Organ	Perfusion
Lungs	100%
Myocard	5%
Brain	15%
Kidneys	20%
Skeletal muscles	15%
Skin	10%
Liver	10%
Spleen and intestines	25%

Table 1.1: Perfusion of organs in % of total blood flow.

tricuspid valve for the left ventricle and the mitral valve for the right ventricle) close. As long as the ventricular pressure is lower than the pressure in the aorta (in the pulmonary artery for the right ventricle), the outflow valves (i.e., the aortic valve for the left ventricle and the pulmonary valve for the right ventricle) close. Since the blood volume in the ventricle does not change during this phase of the contraction, this phase is called the isovolumetric contraction. When the ventricular pressure reaches the pressure in the artery (about 80 [mmHg] for the left ventricle and about 10 [mmHg] for the right ventricle), the outflow valve opens and the ejection phase of the systole starts. At rest, each ventricle ejects approximately 65% of the blood volume which was in the ventricle at the beginning of the systole. The quotient "ejected volume" over "ventricular volume at the beginning of the systole" is called the ejection fraction of the ventricle. The pressure in the ventricle continues to increase during the ejection phase (up to approximately 120 [mmHg] for the left ventricle and 25 [mmHg] for the right ventricle). At the end of the systole, the heart muscle starts to relax which causes a rapid decrease in the ventricular pressure. When the ventricular pressure falls below arterial pressure, which now is higher than the pressure at the beginning of the systole, the outflow valve closes and the diastole starts. In fact the outflow valve closes when the ventricular pressure is slightly below the arterial pressure, because of the kinetic energy of the ejected blood.

The first phase of the diastole is an isovolumetric relaxation of the heart muscle. The ventricular pressure drops till it reaches the pressure in the atria (about 5 [mmHg] for the left ventricle and 8 [mmHg] for the right ventricle) and the inflow valve opens. The relaxation of the heart muscle continues, which causes a further drop in the ventricular pressure below the pressure in the atria. As a result of the pressure difference, blood flows into the ventricle. The diastole comes to an end when the heart muscle starts to contract increasing ventricular pressure above the pressure in the atria and the inflow valve closes. The volume and pressure changes occurring during the heart cycle are depicted in Figure 1.1 (upper panel). A frequently used representation of the heart cycle is the volume-pressure diagram presented in Figure 1.1 (lower panel).

The atria contribute to the ventricular filling process by contracting during the last phase of the diastole, which accounts for about 10–30% of the filling of the ventricle. Figure 1.1 schematically depicts the time course of the pressure and the pressure-volume diagram for the left ventricle at rest.

In addition to the contribution of the atria to the filling process, the following facts are important for a sufficient filling and sufficient ejection at high heart rates.

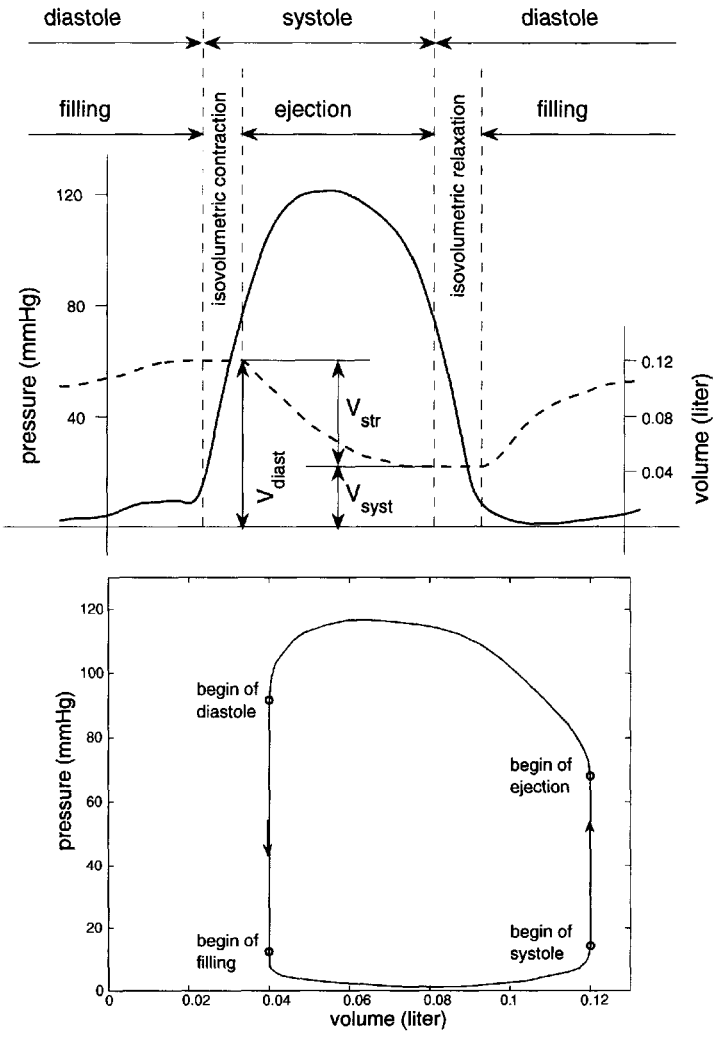

Figure 1.1: Time course of the left ventricular pressure (solid lines) and volume (dashed lines) (upper panel) and corresponding pressure-volume diagram for the left ventricle (lower panel), adapted from Levick (2003).

- Approximately 60% of the stroke volume are ejected during the first quarter of the ejection phase.
- Approximately 80% of the end-diastolic volume is reached during the first quarter of the filling process.

These two facts are reflected by the "volume" curve in the upper panel of Figure 1.1. If we compare, in the upper panel of this figure, the curves for the ventricular pressure and volume at the beginning of the filling process, we can notice that the pressure in the ventricle continues to decrease although the volume in the ventricle rises rapidly. The decrease

in pressure is due to the elastic recoil of the ventricle which causes a suction effect (see Levick, 2003, p. 19).

The mechanism which plays a central role in our modeling of the ventricle function is the so-called Frank–Starling mechanism. This mechanism accounts for the fact that a larger distention of the ventricle at the end of a diastole results in a larger stroke work achieved in the following systole. The (mechanical) stroke work provided by a ventricle during one heart cycle is given by the area inside the corresponding pressure-volume loop in the pressure-volume diagram (see Figure 1.1). Notice that "pressure×volume" has the dimension of work. A consequence of the Frank–Starling mechanism is that, under the same afterload (i.e., the pressure against which the blood has to be ejected), a higher filling pressure for the ventricle causes a higher stroke volume and consequently a higher cardiac output of the ventricle. This is crucial for the synchronization of the pumping performances of the two pumps given by the right heart and the left heart, which are serially connected. Since the right heart and the left heart are beating with the same frequency, a difference in pumping performance can only arise when the stroke volumes of the two ventricles are different. If, for instance, the cardiac output of the left ventricle is larger than that of the right ventricle, then this will result in a shift of blood volume from the pulmonary circuit to the systemic circuit. This in turn increases the pressure in the systemic circuit and decreases it in the pulmonary circuit, thus, as a consequence of the Frank–Starling mechanism, decreasing cardiac output of the left ventricle and increasing cardiac output of the right ventricle, which bring the system back to the original situation. The explanation of the Frank–Starling mechanism is that stretching of the heart muscle fibers increases their sensitivity to Ca^{2+}. For a detailed discussion concerning excitation and contraction of the heart muscle, see (Levick, 2003, Chapter 3).

There are numerous control circuits in the cardiovascular system, which adjust the blood flow in different body regions depending on various demands. There are global and local control loops. In this chapter we consider only local regulatory mechanisms that regulate local blood flow to meet local metabolic demands (see Section 3.1.2). The goal of the global control loops, involving the central nervous system, is to provide overall conditions necessary to sustain the flows controlled by the autoregulatory mechanisms of the various tissues and organs.

One of the most important global control loops, as far as short-term regulation of the cardiovascular system is concerned, is the *baroreceptor loop* (also referred to as *baroreflex control* or just baroreflex). For the basic model discussed in this chapter we will consider only global control by the baroreflex. Other global control loops for the cardiovascular system will be discussed in Subsection 3.1.1. The baroreceptor loop consists of the following main components.

(i) The *baroreceptors*. These are nerve endings, which are mechanoreceptors responding to stretching of the walls of arteries, and thus responding indirectly to pressure changes in the arteries. There are two main locations for baroreceptors: the carotid sinus and the aortic arch (see Figure 3.1). Baroreceptors are stimulated by the magnitude of the pressure (above 60 [mmHg] in the carotid sinus and above 30 [mmHg] in the aortic arch). Baroreceptors are also stimulated by the rate of the pressure increase. Thus, baroreceptors provide, at the same time, information on the mean pressure and on the pulse pressure, i.e., the variation in pressure during a pulse.

Pulse pressure information is important in situations such as moderate hemorrhage where stroke volume and pulse pressure are reduced but mean arterial pressure is almost unchanged.

(ii) The impulse sequences generated by the baroreceptors travel in the glossopharyngeal and vagal nerves to the medulla, where the signals are transformed into signals for the efferent sympathetic and parasympathetic pathways.

(iii) The sympathetic and parasympathetic nerve systems are distributed among various tissues in the body. The sympathetic system innervates the whole heart, whereas the parasympathetic system innervates primarily the sinoatrial node (and the atrioventricular node). Therefore, an increase in sympathetic activity causes, at the same time, an increase in heart rate and in contractile force of the ventricles, whereas a withdrawal of parasympathetic activity increases only heart rate. For a more complete discussion of the effects of the sympathetic and parasympathetic activities on cardiovascular regulation, see Subsection 3.1.1.

1.2 The Basic Model

As in all modeling processes, it is essential to have a clear idea about which part or which aspect of the real system should be the topic of the modeling effort. This is absolutely necessary because the objectives of the modeling effort determine the structure of the model and the mathematical setting. The goal of the modeling process presented in this chapter is to describe the overall reaction of the cardiovascular system under a constant workload over a period of 10–15 minutes. By overall reaction we mean that we are interested only in the time behavior of heart rate and the time course of blood pressure in the arterial and venous parts of the systemic and the pulmonary circuits. We also assume that the workload is sufficiently low so that the metabolic reactions generating the required energy stay in the aerobic regime. We are not interested in details of the blood flow in the arterial tree. Following the general guideline that a model should be as simple as possible and only as complicated as necessary, we can draw the following conclusions from the statement of the modeling objective given above (see also Figure 1.2 for the block diagram of the model).

- We do not distinguish between individual vessels in the arterial and venous parts of the systemic or pulmonary circuits. Instead, we lump them together and consider a single compartment for each of these parts. Moreover, we assume that each compartment can be considered as a vessel with compliant walls that exhibit no resistance to blood flow. That is, we assume that these vessels are only characterized by the pressure in the vessel, which then determines the blood volume in the vessel. For this reason these vessels are called *compliance vessels*.

- The venous and the arterial compartments of the two circuits are connected by the regions which comprise the capillaries, arterioles, and venules of respective circuits. Again, these regions are lumped together into a single vessel, the *systemic peripheral region* and the *pulmonary peripheral region*, which we consider to be pure resistances to blood flow. That is, we assume that these vessels are characterized only by the flow through the vessel. Therefore these vessels are called *resistance vessels*.

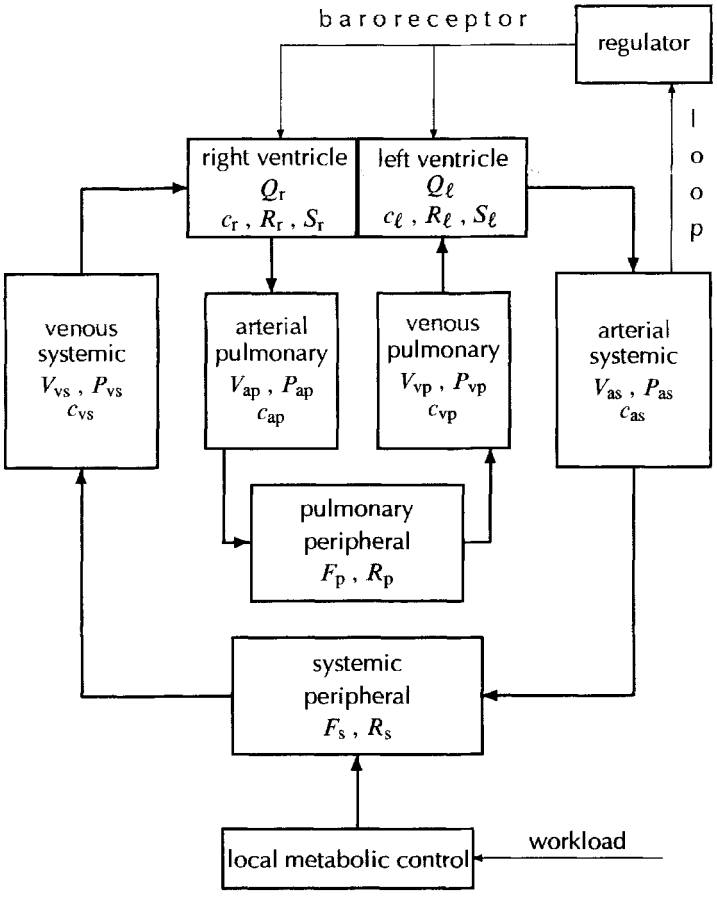

Figure 1.2: Block diagram of the basic cardiovascular model.

- The systemic venous and the pulmonary arterial compartments are connected by the right ventricle, whereas the pulmonary venous and the systemic arterial compartments are connected by the left ventricle. Here, we implicitly assume that the right atrium is a part of the venous systemic compartment and the left atrium is a part of the venous pulmonary compartment.

- We do not consider pulsatility of the blood flow assuming that the time for one heart cycle is short in comparison to the relevant transition times in the system. As a consequence, we consider the mean values of the quantities over one heart cycle instead of the real values.

As mentioned above, we associate with each compartment the pressure P and the volume V of the blood in the compartment. Since these vessels are compliance vessels, we have the relation $V = f(P)$, which, in general, is nonlinear. In order to simplify the following considerations we assume that this relation is linear,

$$V = cP, \tag{1.1}$$

where c is the *compliance* of the compartment. We assume that the compliance of a compartment is constant. With the exception of the systemic arterial compartment, the pressures in the compartments themselves and the pressure variations are sufficiently low in order to justify linearity of the pressure-volume relation (1.1). For the systemic arterial compartment, this may be questionable because of the considerably higher pressure and larger pressure variations there. Moreover, even if we accept that the compliance of the compartment is constant, we should, instead of (1.1), rather assume that

$$V = cP + V_{\mathrm{u}},$$

where V_{u} is the so-called unstressed volume, i.e., the blood volume in the vessel corresponding to zero pressure. We assume here that $V_{\mathrm{u}} = 0$ mainly to avoid the introduction of four additional parameters into the model (the unstressed volumes of the four compartments), which cannot be observed directly. This certainly introduces a modeling error which may not be negligible. A detailed discussion of the pressure-volume relation in vessels with elastic walls can be found in Subsection 4.4.1 (compare also Subsection 3.1.3).

The flow Q_{co} generated by a ventricle, i.e., the *cardiac output* generated by this ventricle, is given by

$$Q_{\mathrm{co}} = HV_{\mathrm{str}}, \tag{1.2}$$

where H denotes the heart rate and V_{str} the *stroke volume*, i.e., the volume of blood ejected by one beat of the ventricle.

The flow F through the peripheral regions of the systemic and pulmonary circuits depends on the pressure in the adjacent compartments and the resistance R against blood flow in the peripheral regions. We simply assume that Ohm's law is valid:

$$F = \frac{1}{R}(P_{\mathrm{a}} - P_{\mathrm{v}}). \tag{1.3}$$

Whenever possible, we adhere to the following notational conventions: the subscripts "a", "v", mean "arterial" and "venous", respectively, whereas the subscripts "s" and "p" stand for "systemic" and "pulmonary," respectively. The subscripts "ℓ" and "r" characterize quantities corresponding to the left heart and the right heart, respectively. The rate of change $\dot{V} = dV/dt$ for the volume V in a compartment is the difference between the flow into and the flow out of the compartment. Together with relation (1.1) we obtain the following equations for the four compartments (see also Grodins, 1963):

$$\begin{aligned} c_{\mathrm{as}}\dot{P}_{\mathrm{as}} &= Q_{\ell} - F_{\mathrm{s}}, \\ c_{\mathrm{vs}}\dot{P}_{\mathrm{vs}} &= F_{\mathrm{s}} - Q_{\mathrm{r}}, \\ c_{\mathrm{ap}}\dot{P}_{\mathrm{ap}} &= Q_{\mathrm{r}} - F_{\mathrm{p}}, \\ c_{\mathrm{vp}}\dot{P}_{\mathrm{vp}} &= F_{\mathrm{p}} - Q_{\ell}. \end{aligned} \tag{1.4}$$

These equations imply that $d(c_{\mathrm{as}}P_{\mathrm{as}} + c_{\mathrm{vs}}P_{\mathrm{vs}} + c_{\mathrm{ap}}P_{\mathrm{ap}} + c_{\mathrm{vp}}P_{\mathrm{vp}})/dt \equiv 0$; i.e., we have

$$c_{\mathrm{as}}P_{\mathrm{as}} + c_{\mathrm{vs}}P_{\mathrm{vs}} + c_{\mathrm{ap}}P_{\mathrm{ap}} + c_{\mathrm{vp}}P_{\mathrm{vp}} \equiv V_{\mathrm{tot}}, \tag{1.5}$$

where V_{tot} denotes the total blood volume, which remains constant. This reflects the assumption that there is no exchange of volume between the cardiovascular system and the interstitium, for instance (compare Subsection 4.5.4). In view of the considered short-time interval (10–15 minutes), this assumption seems to be justified. Using (1.5), we can express one of the pressures as a function of the other pressures. This also shows that we have V_{tot} as a parameter of the model.

Our next task is to express the right and left ventricular outputs, Q_{r}, Q_{ℓ}, as functions of the pressures. For the systemic and pulmonary flows, F_{s}, F_{p}, this is already given by (1.3):

$$\begin{aligned} F_{\text{s}} &= \frac{1}{R_{\text{s}}}(P_{\text{as}} - P_{\text{vs}}), \\ F_{\text{p}} &= \frac{1}{R_{\text{p}}}(P_{\text{ap}} - P_{\text{vp}}). \end{aligned} \tag{1.6}$$

In order to obtain expressions for the left and right ventricular outputs we use (1.2) and consider the two phases of the heart cycle, the systole and the diastole. Besides the stroke volume V_{str}, which is ejected during the systole, we also have to consider two other important volumes, *end-systolic volume* V_{syst} and *end-diastolic volume* V_{dias}. End-systolic volume is the volume remaining in the ventricle after the outflow valve (the aortic valve in the left ventricle and the pulmonary valve in the right ventricle) closes at the end of the systole. End-diastolic volume is the volume in the ventricle at the end of the filling process when the inflow valve (the mitral valve in the left ventricle and the tricuspid valve in the right ventricle) closes. The approach in Grodins (1963) and also in Kappel and Peer (1993) is to consider the filling process in some detail and the ejection process in a more global fashion. Another possibility, which will be presented later (see page 157 ff.), is to consider the ventricle as a vessel with varying compliance or elastance, an inflow valve, and an outflow valve.

To model the filling process, we consider the inflow into the ventricle depending on the pressure difference between the filling pressure and the pressure in the ventricle when the inflow valve is open:

$$\dot{V}(t) = \frac{1}{R}\big(P_{\text{v}}(t) - P(t)\big), \tag{1.7}$$

where $V(t)$ is the volume in the ventricle at time t after the filling process has started, $P(t)$ is the pressure in the ventricle, $P_{\text{v}}(t)$ is the venous filling pressure, which represents the ventricle preload, and R is the total resistance to the inflow into the ventricle. To continue, we assume the following:

- $P_{\text{v}}(t)$ is constant during the diastole, $P_{\text{v}}(t) \equiv P_{\text{v}}$. This assumption is reasonable, because $P_{\text{v}}(t)$ does not vary much at all. We also assume that the arterial pressure P_{a}, which represents the ventricle afterload, remains constant during the systole. Note that the duration of the systole is smaller than the duration of the diastole.

- The end-systolic volume at the end of a heart beat equals the end-systolic volume of the previous heart beat.

- The compliance c of the relaxed ventricle remains constant during the diastole.

For the relaxed ventricle we have the volume-pressure relation

$$V(t) = cP(t) + V_0, \tag{1.8}$$

where V_0 denotes the unstressed volume of the relaxed ventricle. Since the ventricle is a vessel with thick walls, we should assume $V_0 > 0$. We keep $V_0 > 0$ for the moment, but we will set $V_0 = 0$ later. The initial value for (1.7) is given by $V(0) = V_{\text{syst}}$. Using (1.8) in (1.7) and integrating this equation, we obtain

$$V(t) = V_{\text{syst}} e^{-(cR)^{-1}t} + (cP_v + V_0)\big(1 - e^{-(cR)^{-1}t}\big).$$

Let $t_d = t_d(H)$ denote the duration of the filling process. Then we have $V(t_d) = V_{\text{diast}}$, i.e.,

$$V_{\text{diast}} = k(H)V_{\text{syst}} + (cP_v + V_0)a(H), \tag{1.9}$$

where we have set

$$k(H) = e^{-(cR)^{-1}t_d(H)} \quad \text{and} \quad a(H) = 1 - k(H). \tag{1.10}$$

For the duration of the diastole we use the empirical formula

$$t_d = t_d(H) = \frac{1}{H^{1/2}}\Big(\frac{1}{H^{1/2}} - \kappa\Big), \tag{1.11}$$

where κ is in the range of 0.0387–0.0516 when we measure time in minutes.[2] The expression $t_s = \kappa/H^{1/2}$ for the duration t_s of the systole is known as Bazett's formula (Bazett, 1920). Then (1.11) follows from $t_d + t_s = 1/H$.

The stroke volume is given by

$$V_{\text{str}} = V_{\text{diast}} - V_{\text{syst}}. \tag{1.12}$$

We need one more relation between these volumes associated with a ventricle. This relation is provided by the Frank–Starling mechanism discussed in Section 1.1. As a result of this mechanism, a larger distention of the heart, caused by increased filling of the ventricle during diastole, causes an increased force of contraction during the following systole, which we model by the formula

$$V_{\text{str}} = \frac{S}{P_a}\big(V_{\text{diast}} - V_0\big), \tag{1.13}$$

where P_a is the afterload, i.e., the arterial pressure against which the ventricle has to eject, and S is the *contractility* of the ventricle which characterizes the force of contraction of the ventricle. Note that $V_{\text{diast}} - V_0$, and not V_{diast}, is responsible for the distention of the ventricle.

[2] If time was measured in seconds, then the range for κ would be 0.3–0.4.

Equations (1.9), (1.12), and (1.13) constitute a system of linear equations for V_{diast}, V_{syst}, and V_{str}. We obtain

$$V_{\text{str}} = \frac{ca(H)P_{\text{v}}S}{a(H)P_{\text{a}} + k(H)S}, \tag{1.14}$$

$$V_{\text{diast}} = cP_{\text{v}} + V_0 - \frac{ck(H)P_{\text{v}}S}{a(H)P_{\text{a}} + k(H)S}, \tag{1.15}$$

$$V_{\text{syst}} = cP_{\text{v}} + V_0 - \frac{cP_{\text{v}}S}{a(H)P_{\text{a}} + k(H)S}.$$

Obviously we must have

$$V_{\text{str}} \leq V_{\text{diast}},$$

which, in view of (1.14) and (1.15), is equivalent to

$$\big(cP_{\text{v}}a(H) - k(H)V_0\big)S \leq a(H)P_{\text{a}}(cP_{\text{v}} + V_0).$$

Assuming $cP_{\text{v}}a(H) - k(H)V_0 > 0$ or, equivalently,

$$V_0 < \frac{ca(H)P_{\text{v}}}{k(H)},$$

we obtain the inequality

$$S \leq \frac{a(H)(cP_{\text{v}} + V_0)}{a(H)(cP_{\text{v}} + V_0) - V_0}P_{\text{a}}. \tag{1.16}$$

Note that this inequality allows the quotient S/P_{a} to attain values larger than one. In that case we have $V_{\text{syst}} < V_0$ and the end-systolic pressure in the ventricle, according to (1.8), is negative.[3]

Introducing the function

$$f(S, P) := \min\Big(S, \frac{a(H)(cP_{\text{v}} + V_0)}{a(H)(cP_{\text{v}} + V_0) - V_0}P\Big), \quad S \geq 0,$$

we can write (1.14) as

$$V_{\text{str}} = \frac{cP_{\text{v}}a(H)f(S, P_{\text{a}})}{a(H)P_{\text{a}} + k(H)f(S, P_{\text{a}})}, \quad S \geq 0. \tag{1.17}$$

We denote by $k_\ell(H)$ and $a_\ell(H)$, respectively, by $k_{\text{r}}(H)$ and $a_{\text{r}}(H)$, the quantities defined in (1.10), setting $c = c_\ell$ and $R = R_\ell$, respectively, $c = c_{\text{r}}$ and $R = R_{\text{r}}$. Using (1.17) in (1.15) and (1.12), we get the following explicit expressions for the volumes associated with the left and right ventricles:

[3]Note that pressures in the vessels of the cardiovascular system are always pressure differences between the pressure in the vessel and the pressure in the surrounding tissues.

$$
\begin{aligned}
V_{\mathrm{str},\ell} &= \frac{c_\ell P_{\mathrm{vp}} a_\ell(H) f(S_\ell, P_{\mathrm{as}})}{a_\ell(H) P_{\mathrm{as}} + k_\ell(H) f(S_\ell, P_{\mathrm{as}})}, \\
V_{\mathrm{str,r}} &= \frac{c_{\mathrm{r}} P_{\mathrm{vs}} a_{\mathrm{r}}(H) f(S_{\mathrm{r}}, P_{\mathrm{ap}})}{a_{\mathrm{r}}(H) P_{\mathrm{ap}} + k_{\mathrm{r}}(H) f(S_{\mathrm{r}}, P_{\mathrm{ap}})}, \\
V_{\mathrm{diast},\ell} &= \frac{c_\ell a_\ell(H) P_{\mathrm{vp}} P_{\mathrm{as}}}{a_\ell(H) P_{\mathrm{as}} + k_\ell(H) f(S_\ell, P_{\mathrm{as}})}, \\
V_{\mathrm{diast,r}} &= \frac{c_{\mathrm{r}} a_{\mathrm{r}}(H) P_{\mathrm{vs}} P_{\mathrm{ap}}}{a_{\mathrm{r}}(H) P_{\mathrm{ap}} + k_{\mathrm{r}}(H) f(S_{\mathrm{r}}, P_{\mathrm{ap}})}, \\
V_{\mathrm{syst},\ell} &= \frac{c_\ell a_\ell(H) P_{\mathrm{vp}} \big(P_{\mathrm{as}} - f(S_\ell, P_{\mathrm{as}})\big)}{a_\ell(H) P_{\mathrm{as}} + k_\ell(H) f(S_\ell, P_{\mathrm{as}})}, \\
V_{\mathrm{syst,r}} &= \frac{c_{\mathrm{r}} a_{\mathrm{r}}(H) P_{\mathrm{vs}} \big(P_{\mathrm{ap}} - f(S_{\mathrm{r}}, P_{\mathrm{ap}})\big)}{a_{\mathrm{r}}(H) P_{\mathrm{ap}} + k_{\mathrm{r}}(H) f(S_{\mathrm{r}}, P_{\mathrm{ap}})}.
\end{aligned}
\tag{1.18}
$$

In order to simplify our considerations we set $V_0 = 0$ for the rest of this section. For $V_0 = 0$, inequality (1.16) reduces to $S \le P_{\mathrm{a}}$. Consequently, we have $f(S, P) = \min(S, P)$. To simplify matters further, we frequently assume

$$
S_\ell \le P_{\mathrm{as}} \quad \text{and} \quad S_{\mathrm{r}} \le P_{\mathrm{ap}}; \tag{1.19}
$$

i.e., we have $f(S_\ell, P_{\mathrm{as}}) = S_\ell$ and $f(S_{\mathrm{r}}, P_{\mathrm{ap}}) = S_{\mathrm{r}}$. This assumption is justified as long as the workload imposed on the cardiovascular system is not too large.

Equations (1.4) together with (1.6), (1.2), and (1.18) give a nonlinear system of ordinary differential equations, which usually is called Grodins' model of the mechanical part of the cardiovascular system:

$$
\begin{aligned}
c_{\mathrm{as}} \dot{P}_{\mathrm{as}} &= H \frac{c_\ell P_{\mathrm{vp}} a_\ell(H) f(S_\ell, P_{\mathrm{as}})}{a_\ell(H) P_{\mathrm{as}} + k_\ell(H) f(S_\ell, P_{\mathrm{as}})} - \frac{1}{R_{\mathrm{s}}}(P_{\mathrm{as}} - P_{\mathrm{vs}}), \\
c_{\mathrm{vs}} \dot{P}_{\mathrm{vs}} &= \frac{1}{R_{\mathrm{s}}}(P_{\mathrm{as}} - P_{\mathrm{vs}}) - H \frac{c_{\mathrm{r}} P_{\mathrm{vs}} a_{\mathrm{r}}(H) f(S_{\mathrm{r}}, P_{\mathrm{ap}})}{a_{\mathrm{r}}(H) P_{\mathrm{ap}} + k_{\mathrm{r}}(H) f(S_{\mathrm{r}}, P_{\mathrm{ap}})}, \\
c_{\mathrm{ap}} \dot{P}_{\mathrm{ap}} &= H \frac{c_{\mathrm{r}} P_{\mathrm{vs}} a_{\mathrm{r}}(H) f(S_{\mathrm{r}}, P_{\mathrm{ap}})}{a_{\mathrm{r}}(H) P_{\mathrm{ap}} + k_{\mathrm{r}}(H) f(S_{\mathrm{r}}, P_{\mathrm{ap}})} - \frac{1}{R_{\mathrm{p}}}(P_{\mathrm{ap}} - P_{\mathrm{vp}}), \\
c_{\mathrm{vp}} \dot{P}_{\mathrm{vp}} &= \frac{1}{R_{\mathrm{p}}}(P_{\mathrm{ap}} - P_{\mathrm{vp}}) - H \frac{c_\ell P_{\mathrm{vp}} a_\ell(H) f(S_\ell, P_{\mathrm{as}})}{a_\ell(H) P_{\mathrm{as}} + k_\ell(H) f(S_\ell, P_{\mathrm{as}})}.
\end{aligned}
\tag{1.20}
$$

In addition to these differential equations we have also (1.5) which, for given V_{tot}, c_{as}, c_{vs}, c_{ap}, and c_{vp}, defines a hyperplane in $\mathbb{R}^4$, that is invariant for system (1.20); i.e., a solution in this hyperplane at some time stays in it for all future time. Of course, we could also use (1.5) to express one of the pressures by the others and thus reduce system (1.20) to three equations. For instance, we can choose

$$
P_{\mathrm{vp}} = P_{\mathrm{vp}}(P_{\mathrm{as}}, P_{\mathrm{vs}}, P_{\mathrm{ap}}) := \frac{1}{c_{\mathrm{vp}}}\big(V_{\mathrm{tot}} - c_{\mathrm{as}} P_{\mathrm{as}} - c_{\mathrm{vs}} P_{\mathrm{vs}} - c_{\mathrm{ap}} P_{\mathrm{ap}}\big) \tag{1.21}
$$

and take the first three equations of system (1.20) with P_{vp} given by (1.21).

In order to model the reaction of the cardiovascular system under an ergometric workload, we have to include the regulation of the heart rate and the contractilities of the ventricle in response to the workload. Moreover, we also need a submodel for the local metabolic regulation process in the tissues. To keep the model simple we do not model the baroreceptor loop in detail. We shall construct a feedback control, which regulates the heart rate depending on the arterial systemic pressure. Instead of regulating the contractilities directly, we assume that the contractilities vary according to variations in the heart rate. Some motivation for this is provided by the so-called Bowditch effect, which roughly states that a change in heart rate causes a concordant change in the contractilities of both ventricles (Levick, 2003, p. 88). The Bowditch effect may play a role in situations where the heart rate changes rapidly (for instance, because of withdrawal of parasympathetic activity), but sympathetic activity has not yet increased contractilities appropriately. Under an ergometric workload, contractilities of the ventricles are increased or decreased in the same direction as heart rate by sympathetic activity. Since in the basic model we do not model sympathetic and parasympathetic activities directly, we model the variations of the contractilities by the following second-order differential equations:

$$\begin{aligned} \ddot{S}_\ell + \gamma_\ell \dot{S}_\ell + \alpha_\ell S_\ell &= \beta_\ell H, \\ \ddot{S}_r r + \gamma_r \dot{S}_r + \alpha_r S_r &= \beta_r H, \end{aligned} \tag{1.22}$$

where α_ℓ, β_ℓ, γ_ℓ, α_r, β_r, and γ_r are constants, $\alpha_\ell, \alpha_r, \beta_\ell, \beta_r > 0$. This guarantees that the equilibrium values for S_ℓ and S_r vary in the same direction as the equilibrium value for H. It is customary to convert equations such as (1.22) into a system of first-order equations by introducing the state variables $\sigma_\ell = \dot{S}_\ell$ and $\sigma_r = \dot{S}_r$:

$$\begin{aligned} \dot{S}_\ell &= \sigma_\ell, \quad \dot{\sigma}_\ell = -\alpha_\ell S_\ell - \gamma_\ell \sigma_\ell + \beta_\ell H, \\ \dot{S}_r &= \sigma_r, \quad \dot{\sigma}_r = -\alpha_r S_r - \gamma_r \sigma_r + \beta_r H. \end{aligned} \tag{1.23}$$

The purpose of local metabolic control is to increase blood flow to a tissue region in order to increase the O_2 supply for that region according to energy demands. The most efficient way to increase the blood flow in a tissue region locally is to increase the diameter of the arterioles in that region, which results in a decreased resistance to blood flow. Local dilation of the arterioles, in general, is triggered by substances which are set free locally because of increased functional activity of the organ or tissue region (functional activation). This mechanism usually is supported by local metabolic regulation, where by-products of the local metabolism cause dilation of the arterioles. Following Peskin (1981), we assume that

$$R_s = A_{\text{pesk}} C_{v,O_2}, \tag{1.24}$$

where A_{pesk} is a positive constant and C_{v,O_2} is the concentration of O_2 in the venous blood in the capillary region.

Let M_T be the metabolic rate for the tissue region, which is satisfied partially by the O_2 supply provided by the blood flow in the tissue region and partially by an anaerobic energy flow M_b provided by anaerobic biochemical reactions,

$$M_T = F_s(C_{a,O_2} - C_{v,O_2}) + M_b, \tag{1.25}$$

where C_{a,O_2} is the concentration of O_2 in the arterial blood, which is assumed to be constant. The biochemical energy flow is assumed to depend on the rate of the change of C_{v,O_2},

$$M_b = -K \frac{d}{dt} C_{v,O_2}, \tag{1.26}$$

where $K > 0$ is some constant. Differentiating (1.24) and using (1.6), (1.25), and (1.26), we obtain the following differential equation for R_s:

$$\dot{R}_s = \frac{1}{K}\Big(A_{pcsk}\Big(\frac{P_{as} - P_{vs}}{R_s} C_{a,O_2} - M_T\Big) - (P_{as} - P_{vs})\Big). \tag{1.27}$$

In the model for the cardiovascular-respiratory system considered in Chapter (3), the partial O_2 pressure in venous blood is a state variable. Since the O_2 concentration C_{v,O_2} in venous blood is related to the partial O_2 pressure via the dissociation relation (see Subsection 2.2.4), (1.24) is an auxiliary equation for the combined model describing local metabolic control there. However, we can also derive an equation analogous to (1.27) for the combined model (see the discussion on page 127).

In order to model the response of the cardiovascular system to a constant ergometric workload W imposed on a test person on a bicycle ergometer starting at time $t = 0$, we use the following empirical formula for the resulting metabolic rate M_T:

$$M_T = M_0 + \rho W, \tag{1.28}$$

where M_0 is the metabolic rate in the systemic tissue region corresponding to zero workload and ρ is a positive constant.

As already stated above, we assume that the baroreceptor loop is modeled by designing a feedback law which controls the heart rate. Thus, we add the equation

$$\dot{H} = u(t) \tag{1.29}$$

and explain below, how $u(t)$ is constructed as a function of the state variables assuming that we have measurements for P_{as}.

Thus, our model for the cardiovascular system consists of Grodins' model (1.20) together with (1.22) or (1.23) for the contractilities, (1.27) modeling the local metabolic control of resistance, (1.29) describing the control influence. This gives a system of ordinary differential equations in $\mathbb{R}^{10}$ which leaves the hyperplane, given by (1.5), invariant.

We define the state vector,[4]

$$\tilde{x} = \big(P_{as}, P_{vs}, P_{ap}, P_{vp}, S_\ell, \sigma_\ell, S_r, \sigma_r, R_s, H\big)^T \in \mathbb{R}^{10} \tag{1.30}$$

and the parameter vector of the system,

$$p = \big(c_{as}, c_{vs}, c_{ap}, c_{vp}, c_\ell, c_r, V_{tot}, R_p, R_\ell, R_r, \kappa, C_{a,O_2}, K, A_{pcsk}, M_0, \rho, \alpha_\ell, \alpha_r, \beta_\ell, \beta_r, \gamma_\ell, \gamma_r\big)^T \in \mathbb{R}^{20}. \tag{1.31}$$

[4]The state, or more precisely state vector, of a dynamical system at time t carries all information needed to predict the future behavior of the system provided external influences (such as controls or perturbations) on the system are known.

Then we can write (1.20), (1.23), (1.27), and (1.29) as the following system of first-order differential equations:

$$\dot{\tilde{x}}(t) = \mathcal{G}(\tilde{x}(t), p, W, u(t)), \quad t \geq 0. \tag{1.32}$$

The coordinates of $\mathcal{G}$ are given by

$$\begin{aligned}
\mathcal{G}_1 &= \frac{1}{c_{as}}\Big(Q_\ell - \frac{1}{R_s}(P_{as} - P_{vs})\Big),\\
\mathcal{G}_2 &= \frac{1}{c_{vs}}\Big(\frac{1}{R_s}(P_{as} - P_{vs}) - Q_r\Big),\\
\mathcal{G}_3 &= \frac{1}{c_{ap}}\Big(Q_r - \frac{1}{R_p}(P_{ap} - P_{vp})\Big),\\
\mathcal{G}_4 &= \frac{1}{c_{vp}}\Big(\frac{1}{R_p}(P_{ap} - P_{vp}) - Q_\ell\Big),\\
\mathcal{G}_5 &= \sigma_\ell,\\
\mathcal{G}_6 &= -\alpha_\ell S_\ell - \gamma_\ell \sigma_\ell + \beta_\ell H,\\
\mathcal{G}_7 &= \sigma_r,\\
\mathcal{G}_8 &= -\alpha_r S_r - \gamma_r \sigma_r + \beta_r H,\\
\mathcal{G}_9 &= \frac{1}{K}\Big(A_{pcsk}\Big(\frac{P_{as} - P_{vs}}{R_s} C_{a,O_2} - M_T\Big) - (P_{as} - P_{vs})\Big),\\
\mathcal{G}_{10} &= u(t),
\end{aligned}$$

where Q_ℓ and Q_r are given by

$$\begin{aligned}
Q_\ell &= H\frac{c_\ell P_{vp} a_\ell(H) f(S_\ell, P_{as})}{a_\ell(H)P_{as} + k_\ell(H) f(S_\ell, P_{as})},\\
Q_r &= H\frac{c_r P_{vs} a_r(H) f(S_r, P_{ap})}{a_r(H)P_{ap} + k_r(H) f(S_r, P_{ap})}.
\end{aligned}$$

If $S_\ell > P_{as}$, respectively $S_r > P_{ap}$, then the expressions for Q_ℓ, respectively Q_r, simplify to

$$Q_\ell = c_\ell a_\ell(H) H P_{vp}, \quad Q_r = c_r a_r(H) H P_{vs}.$$

As we mentioned above, the hyperplane given by (1.5) is invariant for system (1.32). Therefore, we can reduce the dimension of the system by one: we can replace P_{vp}, for instance, by the expression given in (1.21), so that $P_{vp} = P_{vp}(P_{as}, P_{vs}, P_{ap})$, and eliminate the fourth equation of the system. If one was just interested to solve system (1.32) for given parameters and given control $u(\cdot)$, this reduction would not be necessary, and the solution of (1.32) would automatically stay on the invariant hyperplane. However, the procedure explained in the next section to obtain a stabilizing feedback control requires that we consider only the system on the invariant hyperplane, given by (1.5) (see the discussion following (1.55)). As indicated above we achieve this by eliminating the state variable P_{vp}. For the reduced state

$$x = \big(P_{as}, P_{vs}, P_{ap}, S_\ell, \sigma_\ell, S_r, \sigma_r, R_s, H\big)^\top \in \mathbb{R}^9,$$

we get the system

$$\dot{x}(t) = \mathcal{F}(x(t), p, W, u(t)), \quad t \geq 0. \tag{1.33}$$

The coordinates of $\mathcal{F}$ are given by

$$\begin{aligned}
\mathcal{F}_1 &= \frac{1}{c_{as}}\Big(Q_\ell - \frac{1}{R_s}(P_{as} - P_{vs})\Big),\\
\mathcal{F}_2 &= \frac{1}{c_{vs}}\Big(\frac{1}{R_s}(P_{as} - P_{vs}) - Q_r\Big),\\
\mathcal{F}_3 &= \frac{1}{c_{ap}}\Big(Q_r - \frac{1}{R_p}(P_{ap} - P_{vp}(P_{as}, P_{vs}, P_{ap}))\Big),\\
\mathcal{F}_4 &= \sigma_\ell,\\
\mathcal{F}_5 &= -\alpha_\ell S_\ell - \gamma_\ell \sigma_\ell + \beta_\ell H,\\
\mathcal{F}_6 &= \sigma_r,\\
\mathcal{F}_7 &= -\alpha_r S_r - \gamma_r \sigma_r + \beta_r H,\\
\mathcal{F}_8 &= \frac{1}{K}\Big(A_{pesk}\Big(\frac{P_{as} - P_{vs}}{R_s} C_{a,O_2} - M\Big) - (P_{as} - P_{vs})\Big),\\
\mathcal{F}_9 &= u(t)
\end{aligned} \tag{1.34}$$

with

$$\begin{aligned}
Q_\ell &= H\frac{c_\ell P_{vp}(P_{as}, P_{vs}, P_{ap}) a_\ell(H) f(S_\ell, P_{as})}{a_\ell(H) P_{as} + k_\ell(H) f(S_\ell, P_{as})},\\
Q_r &= H\frac{c_r P_{vs} a_r(H) f(S_r, P_{ap})}{a_r(H) P_{ap} + k_r(H) f(S_r, P_{ap})},
\end{aligned} \tag{1.35}$$

where $P_{vp}(P_{as}, P_{vs}, P_{ap})$ is given by (1.21).

In Table 1.2 we list the parameters of the system and in Table 1.3 we list the state variables and other variables.

1.3 Analysis of the Basic Model

In this section we conduct some mathematical analysis for the basic model introduced in Section 1.2. Among the topics of interest are the following:

- Existence of equilibria.
- Behavior of solutions near an equilibrium.
- Invariance of subsets of the state space with respect to solutions. (A subset of particular interest is the positive cone in the state space, because the state variables in our case have to be positive.)

Parameter	Meaning	Units
c_{as}	Compliance of the arterial systemic compartment	liter/mmHg
c_{vs}	Compliance of the venous systemic compartment	liter/mmHg
c_{ap}	Compliance of the arterial pulmonary compartment	liter/mmHg
c_{vp}	Compliance of the venous pulmonary compartment	liter/mmHg
c_ℓ	Compliance of the relaxed left ventricle	liter/mmHg
c_r	Compliance of the relaxed right ventricle	liter/mmHg
V_{tot}	Total blood volume	liter
R_p	Resistance in the peripheral region of the pulmonary circuit	mmHg min/liter
R_ℓ	Inflow resistance of the left ventricle	mmHg min/liter
R_r	Inflow resistance of the right ventricle	mmHg min/liter
κ	Coefficient in Bazett's formula (see (1.11))	$\text{min}^{1/2}$
C_{a,O_2}	O_2 concentration in arterial systemic blood	1
C_{v,O_2}	O_2 concentration in venous systemic blood	1
K	Constant in the formula for the biochemical energy flow (see (1.26))	liter
A_{pesk}	Constant in the formula relating peripheral systemic resistance and venous O_2 concentration (see (1.24))	mmHg min/liter
M_0	Metabolic rate in the systemic tissue region corresponding to zero workload	liter/min
ρ	Coefficient of W in formula (1.28)	liter/(min Watt)
q_{as}	Weight for P_{as} in the cost functional (1.47)	$\text{min}^{-2}(\text{mmHg})^{-1}$
α_ℓ	Coefficient of S_ℓ in the differential equation for S_ℓ	min^{-2}
α_r	Coefficient of S_r in the differential equation for S_r	min^{-2}
β_ℓ	Coefficient of H in the differential equation for S_ℓ	mmHg/min
β_r	Coefficient of H in the differential equation for S_r	mmHg/min
γ_ℓ	Coefficient of $\dot{S}_\ell$ in the differential equation for S_ℓ	min^{-1}
γ_r	Coefficient of $\dot{S}_r$ in the differential equation for S_r	min^{-1}

Table 1.2: Parameters of the basic model.

Variable	Meaning	Unit
P_{as}	Pressure in the arterial systemic compartment	mmHg
P_{vs}	Pressure in the venous systemic compartment	mmHg
P_{ap}	Pressure in the arterial pulmonary compartment	mmHg
P_{vp}	Pressure in the venous pulmonary compartment	mmHg
S_ℓ	Contractility of the left ventricle	mmHg
S_r	Contractility of the right ventricle	mmHg
R_s	Peripheral resistance in the systemic circuit	mmHg min/liter
H	Heart rate	min^{-1}
$V_{str,\ell}$	Stroke volume of the left ventricle	liter
$V_{str,r}$	Stroke volume of the right ventricle	liter
$V_{diast,\ell}$	End-diastolic volume of the left ventricle	liter
$V_{diast,r}$	End-diastolic volume of the right ventricle	liter
$V_{syst,\ell}$	End-systolic volume of the left ventricle	liter
$V_{syst,r}$	End-systolic volume of the right ventricle	liter
Q_ℓ	Cardiac output of the left ventricle	liter/min
Q_r	Cardiac output of the right ventricle	liter/min

Table 1.3: The state variables and other variables of the model.

1.3.1 Existence of equilibria

In this section we show how to compute the equilibria of our model corresponding to various levels of workload. From (1.29), we see that to achieve equilibrium we must have $u(t) \equiv 0$, which reduces (1.29) to the trivial equation $0 = 0$. Any equilibrium state, $\bar{x} = (\overline{P}_{as}, \ldots, \overline{H})^T$, has to satisfy the nonlinear system we obtain by setting the right-hand sides of the model equations to zero. This gives eight equations for the nine components of the state vector, which shows that we have to expect a one-parameter family of equilibria. As we shall show below we can choose $\overline{H}$ or $\overline{P}_{as}$ as the parameter. In the rest of this section we do not indicate the components of the equilibria by overbars in order to simplify notation. For simplicity, we consider only the case (1.19). The computations for the other cases are quite analogous.

Instead of taking the equations, which we get by setting the right-hand sides of the first three equations in (1.20) to zero, and computing P_{vp} from (1.21), we conclude from (1.4) that

$$Q_\ell = Q_r = F_s = F_p =: F, \tag{1.36}$$

which indicates that we also can use F as a parameter. In addition to (1.4) we have (1.5).

In the following, we shall consider in detail the case where we take either H or F as the parameter for the family of equilibria. In Section A.1 of Appendix A, we shall indicate the computations when P_{as} is taken as the parameter.

From (1.23) we immediately get

$$\begin{aligned} \sigma_\ell = 0, \quad S_\ell &= \frac{\beta_\ell}{\alpha_\ell} H, \\ \sigma_r = 0, \quad S_r &= \frac{\beta_r}{\alpha_r} H. \end{aligned} \tag{1.37}$$

Equations (1.36), together with (1.6), (1.2) (for the left heart and the right heart, respectively), and (1.18), give the following system of equations:

$$P_{as} - P_{vs} = R_s F, \tag{1.38}$$

$$P_{ap} - P_{vp} = R_p F, \tag{1.39}$$

$$HS_\ell \frac{c_\ell a_\ell(H) P_{vp}}{P_{as} a_\ell(H) + S_\ell k_\ell(H)} = F, \tag{1.40}$$

$$HS_r \frac{c_r a_r(H) P_{vs}}{P_{ap} a_r(H) + S_r k_r(H)} = F, \tag{1.41}$$

where we are assuming that $f(S_\ell, P_{as}) = S_\ell$ and $f(S_r, P_{ap}) = S_r$ (compare also (1.19)). Using the abbreviations[5]

$$\begin{aligned} \mu_\ell(H) &= HS_\ell c_\ell a_\ell(H) = \frac{\beta_\ell}{\alpha_\ell} c_\ell a_\ell(H) H^2, \\ \mu_r(H) &= HS_r c_r a_r(H) = \frac{\beta_r}{\alpha_r} c_r a_r(H) H^2, \end{aligned}$$

[5]Note that $\mu_\ell(H)$ and $\mu_r(H)$ have the dimension of flow (with unit liter/min), whereas $\lambda_\ell(H)$ and $\lambda_r(H)$ have the dimension of pressure (with unit mmHg).

$$\lambda_\ell(H) = S_\ell k_\ell(H) = \frac{\beta_\ell}{\alpha_\ell} k_\ell(H) H,$$
$$\lambda_r(H) = S_r k_r(H) = \frac{\beta_r}{\alpha_r} k_r(H) H,$$

we can write (1.38)–(1.41) and (1.5) as

$$\begin{pmatrix} 1 & -1 & 0 & 0 \\ 0 & 0 & 1 & -1 \\ 0 & \mu_r(H) & -a_r(H)F & 0 \\ a_\ell(H)F & 0 & 0 & -\mu_\ell(H) \\ c_{as} & c_{vs} & c_{ap} & c_{vp} \end{pmatrix} \begin{pmatrix} P_{as} \\ P_{vs} \\ P_{ap} \\ P_{vp} \end{pmatrix} = \begin{pmatrix} R_s F \\ R_p F \\ \lambda_r(H)F \\ -\lambda_\ell(H)F \\ V_{tot} \end{pmatrix}, \tag{1.42}$$

which we consider as a linear system for P_{as}, P_{vs}, P_{ap}, and P_{vp}. Setting the right-hand side of (1.27) to zero, we get, using also (1.6),

$$R_s = A_{pesk}\big(C_{a,O_2} - M_T/F\big). \tag{1.43}$$

We solve the first four equations of system (1.42) in order to get P_{as}, P_{vs}, P_{ap}, and P_{vp} as functions of H and F:

$$\begin{aligned}
P_{as} &= \frac{1}{D}\Big(a_r(H)\big(\lambda_\ell(H) + \mu_\ell(H)R_p\big)F^2 + \mu_\ell(H)\big(\lambda_r(H) + \mu_r(H)R_s\big)F\Big), \\
P_{vs} &= \frac{1}{D}\Big(a_\ell(H)a_r(H)R_s F^3 + a_r(H)\big(\lambda_\ell(H) + \mu_\ell(H)R_p\big)F^2 \\
&\qquad + \mu_\ell(H)\lambda_r(H)F\Big), \\
P_{ap} &= \frac{1}{D}\Big(a_\ell(H)\big(\lambda_r(H) + \mu_r(H)R_s\big)F^2 + \mu_r(H)\big(\lambda_\ell(H) + \mu_\ell(H)R_p\big)F\Big), \\
P_{vp} &= \frac{1}{D}\Big(a_\ell(H)a_r(H)R_p F^3 + a_\ell(H)\big(\lambda_r(H) + \mu_r(H)R_s\big)F^2 \\
&\qquad + \mu_r(H)\lambda_\ell(H)F\Big),
\end{aligned} \tag{1.44}$$

where R_s is given by (1.43) and

$$D = \mu_\ell(H)\mu_r(H) - a_\ell(H)a_r(H)F^2. \tag{1.45}$$

The functions $P_{as}(H, F)$, $P_{vs}(H, F)$, $P_{ap}(H, F)$, and $P_{vp}(H, F)$ as given by (1.44) also have to satisfy the fifth equation of the linear system (1.42), which implies

$$c_{as}P_{as}(H, F) + c_{vs}P_{vs}(H, F) + c_{ap}P_{ap}(H, F) + c_{vp}P_{vp}(H, F) = V_{tot}. \tag{1.46}$$

If F is given, then (1.46) is a nonlinear equation for H. On the other hand, if H is given, then (1.46) is a nonlinear equation for F. Once H or F has been computed from (1.46), we get $P_{as}, \ldots, P_{vp}$ from (1.44), R_s from (1.43), and S_ℓ, S_r from (1.37).

In the case when H is given, we want to discuss existence and uniqueness of an equilibrium. Let the function $g = g(F)$ be defined by

$$g(F) = \Big(c_{as}P_{as}(H, F) + c_{vs}P_{vs}(H, F) + c_{ap}P_{ap}(H, F) + c_{vp}P_{vp}(H, F) - V_{tot}\Big)D(H, F),$$

where $D = D(H, F)$ is given by (1.45), $P_{as}(H, F), \ldots, P_{vp}(H, F)$ is given by (1.44), and $R_s = R_s(F)$ by (1.43). Since we must have $R_s > 0$, only $F > F_0$ with

$$F_0 = \frac{M_T}{C_{a,O_2}}$$

makes sense. Let F_1 be the unique positive zero of D; i.e.,

$$F_1 = \sqrt{\frac{\mu_r(H)\mu_\ell(H)}{a_\ell a_r}} = \sqrt{\frac{c_\ell c_r \beta_\ell \beta_r}{\alpha_\ell \alpha_r}}\, H^2.$$

Then it is easy to see that

$$g(F_1) > 0.$$

Also the condition $F_1 > F_0$ must be satisfied. This amounts to

$$H > H_0 := \left(\frac{M_T}{C_{a,O_2}}\left(\frac{\alpha_\ell \alpha_r}{c_\ell c_r \beta_\ell \beta_r}\right)^{1/2}\right)^{1/2}$$

Note that for the pressures themselves we have $\lim_{F \uparrow F_1} P_{as}(H, F) = \cdots = \lim_{F \uparrow F_1} P_{vp}(H, F) = \infty$. Therefore, in case $H > H_0$ the admissible domain for F is the interval (F_0, F_1). For the parameter values given in Table 1.5, we get $H_0 = 16.77$ for the equilibrium "rest" (i.e., for $M = 0.35$) and $H_0 = 30.72$ for the equilibrium "exercise" (i.e., for $M = 0.35 + 0.011 \cdot 75$). The derivative g' is given by

$$\begin{aligned}
g'(F) = {} & c_{as}\Big(2a_r\big(\lambda_\ell(H) + \mu_\ell(H)R_p\big)F + \mu_\ell(H)\lambda_r(H) + \mu_\ell(H)\mu_r(H)A_{pesk}C_{a,O_2}\Big) \\
& + c_{vs}\Big(3a_\ell(H)a_r A_{pesk}\big(C_{a,O_2}F^2 - M_T F\big) + a_\ell(H)a_r A_{pesk}M_T \\
& \qquad + 2a_r\big(\lambda_\ell(H) + \mu_\ell(H)R_p\big)F + \mu_\ell(H)\lambda_r(H)\Big) \\
& + c_{ap}\Big(2a_\ell(H)\big(\lambda_r(H)F + \mu_r(H)A_{pesk}(C_{a,O_2}F - M_T)\big) \\
& \qquad + a_\ell(H)\mu_r(H)A_{pesk}M_T + \mu_r(H)\big(\lambda_\ell(H) + \mu_\ell(H)R_p\big)\Big) \\
& + c_{vp}\Big(3a_\ell(H)a_r R_p F^2 + 2a_\ell(H)\big(\lambda_r(H)F + \mu_r(H)A_{pesk}(C_{a,O_2}F - M_T)\big) \\
& \qquad + a_\ell(H)\mu_r(H)A_{pesk}M_T + \mu_r(H)\lambda_\ell(H)\Big) \\
& + 2V_{tot}a_\ell(H)a_r F.
\end{aligned}$$

From $F > F_0$, i.e., $C_{a,O_2}F > M_T$, we immediately see that $g'(F) > 0$ for $F > F_0$. This proves that (1.46) has at most one solution in (F_0, F_1) for any $H > 0$. If $g(F_0) < 0$, then there exists exactly one solution in (F_0, F_1) and consequently system (1.33) has, for any $H > H_0$, exactly one equilibrium. Using the parameter values given in Table 1.5 and $H^{rest} = 78.85$, respectively, $H^{exer} = 107.4$, we get $g(F_0) = -4.6 \cdot 10^{-6}$, respectively, $g(F_0) = -3.87 \cdot 10^{-6}$.

1.3.2 An invariance property of Grodins' system

In this section, we investigate Grodins' system (1.20) assuming that $H = H(t)$, $S_\ell = S_\ell(t)$, $S_r = S_r(t)$, and $R_s = R_s(t)$ are differentiable functions. We are interested in the positive invariance of the cone

$$\mathcal{K} = \{(P_{as}, P_{vs}, P_{ap}, P_{vp})^T \in \mathbb{R}^4 \mid 0 < P_{vs} < P_{as} \text{ and } 0 < P_{vp} < P_{ap}\},$$

which we consider to be the cone of physiologically meaningful pressures. In addition to $\mathcal{K}$ we also consider the hyperplane $\mathcal{H}$ in $\mathbb{R}^4$ given by

$$\mathcal{H} = \{(P_{as}, P_{vs}, P_{ap}, P_{vp})^T \in \mathbb{R}^4 \mid c_{as}P_{as} + c_{vs}P_{vs} + c_{ap}P_{ap} + c_{vp}P_{vp} = V_{tot}\}.$$

According to (1.5) this hyperplane is invariant with respect to system (1.20); i.e., if a solution of (1.20) is in $\mathcal{H}$ for some t, then it is in $\mathcal{H}$ for all t as long as it exists.

We shall consider system (1.20) for $t \geq 0$ and assume that

(i) $S_\ell(t) > 0$, $S_r(t) > 0$, and $R_s(t) > 0$ for $t \geq 0$;

(ii) $H(t) \in (0, 1/\kappa^2)$ for $t \geq 0$.

The assumption on $H(t)$ implies that $t_d(H(t)) > 0$ for $t \geq 0$ and that the values of $a_\ell(H(t))$, $a_r(H(t))$, $k_\ell(H(t))$, and $k_r(H(t))$ are always in $(0, 1)$. We shall prove the following result:

> *Assume that assumptions* (i) *and* (ii) *hold. Then the set $\mathcal{H} \cap \mathcal{K}$ is positively invariant with respect to system* (1.20)*; i.e., if a solution of system* (1.20) *is in $\mathcal{H} \cap \mathcal{K}$ for some $t_0 \geq 0$, then it is in this set for all $t \geq t_0$ as long as it exists.*

Of course it is sufficient to prove positive invariance of $\mathcal{K}$ with respect to (1.20). Furthermore, without loss of generality, we take $t_0 = 0$. Assume that $\mathcal{K}$ is not positively invariant with respect to (1.20). Then there exist a solution $x(t) = (P_{as}(t), P_{vs}(t), P_{ap}(t), P_{vp}(t))^T$ of (1.20) and a $t_1 > 0$ such that $x(t) \in \mathcal{K}$ for $t \in [0, t_1)$ and $x(t_1) \in \partial\mathcal{K}$. The idea of the proof is to show that there exists an $\epsilon > 0$ such that $x(t) \notin \mathcal{K}$ for $t \in (t_1 - \epsilon, t_1)$, a contradiction which proves the result.

The boundary $\partial\mathcal{K}$ of $\mathcal{K}$ is characterized by inequalities which we obtain from the ones characterizing $\mathcal{K}$ by replacing one or more strict inequalities by an equality. We shall consider the following cases:

(i) $0 = P_{vs} < P_{as}$ and $0 < P_{vp} < P_{ap}$;

(ii) $0 < P_{vs} = P_{as}$ and $0 < P_{vp} < P_{ap}$;

(iii) $0 = P_{vs} = P_{as}$ and $0 < P_{vp} < P_{ap}$;

(iv) $0 = P_{vs} < P_{as}$ and $0 = P_{vp} < P_{ap}$;

(v) $0 = P_{vs} < P_{as}$ and $0 < P_{vp} = P_{ap}$;

(vi) $0 < P_{vs} = P_{as}$ and $0 < P_{vp} = P_{ap}$;

(vii) $0 = P_{vs} = P_{as}$ and $0 = P_{vp} < P_{ap}$;

(viii) $0 = P_{vs} = P_{as}$ and $0 < P_{vp} = P_{ap}$.

The case $P_{as} = P_{vs} = P_{ap} = P_{vp} = 0$ will not be considered, because $0 \notin \mathcal{H}$ in view of $V_{tot} > 0$. The missing cases are obtained from cases (i)–(viii) by interchanging P_{as} with P_{ap} and P_{vs} with P_{vp}. By symmetry of system (1.20), with respect to this change

the proofs for these missing cases are completely analogous to the ones for cases (i)–(viii). It is also clear that if an inequality is true for t_1, then it is also true for t in a neighborhood of t_1.

Case (i). $P_{vs}(t_1) = 0$ implies $Q_r(t_1) = 0$ and consequently $\dot{P}_{vs}(t_1) = F_s(t_1)/c_{vs} = P_{as}(t_1)/(c_{vs}R_s(t_1)) > 0$. This implies $P_{vs}(t) < 0$, i.e., $x(t) \notin \overline{K}$, for $t \in (t_1 - \epsilon, t_1)$ with some $\epsilon > 0$.

Case (ii). In this case we have $F_s(t_1) = 0$ and consequently $\dot{P}_{as}(t_1) = Q_\ell(t_1)/c_{as}$ and $\dot{P}_{vs}(t_1) = -Q_r(t_1)/c_{vs}$. We have $f(S_\ell(t_1), P_{as}(t_1)) > 0$ and $f(S_r(t_1), P_{ap}(t_1)) > 0$. Therefore, $P_{vs}(t_1) > 0$ and $P_{vp}(t_1) > 0$ implies $Q_r(t_1) > 0$ and $Q_\ell(t_1) > 0$. This proves $\dot{P}_{as}(t_1) - \dot{P}_{vs}(t_1) > 0$ and consequently $P_{as}(t) - P_{vs}(t) < 0$, i.e., $x(t) \notin \overline{K}$, for $t \in (t_1 - \epsilon, t_1)$ with some $\epsilon > 0$.

Case (iii). We get $Q_r(t_1) = F_s(t_1) = 0$ and $\dot{P}_{vs}(t_1) = 0$. In view of $f(S_r(t_1), P_{ap}(t_1)) > 0$ and $P_{vp}(t_1) > 0$, we get $\dot{P}_{as}(t_1) = Q_\ell(t_1)/c_{as} > 0$. This implies $\dot{P}_{as}(t_1) - \dot{P}_{vs}(t_1) > 0$ and we get a contradiction as in the previous case.

Cases (iv) *and* (v). We only observe that $0 = P_{vs}(t_1) < P_{as}(t_1)$ and argue as in Case (i).

Case (vi). We can proceed as in Case (ii).

Case (vii). We have $Q_r(t_1) = Q_\ell(t_1) = F_s(t_1) = 0$ and $F_p(t_1) > 0$. This implies $\dot{P}_{vp}(t_1) > 0$ and consequently $P_{vp}(t) < 0$, i.e., $x(t) \notin \overline{K}$, for $t \in (t_1 - \epsilon, t_1)$ with some $\epsilon > 0$.

Case (viii). We have $Q_r(t_1) = F_s(t_1) = F_p(t_1) = 0$. From $S_\ell(t_1) > P_{as}(t_1) = 0$, we get $S_\ell(t) > P_{as}(t)$ for $t \in (t_1 - \epsilon, t_1)$ with some $\epsilon > 0$. This implies $f(S_\ell(t), P_{as}(t)) = P_{as}(t) > 0$ for $t \in (t_1 - \epsilon, t_1)$. Thus we have $Q_\ell(t) = c_\ell a_\ell(H(t))H(t)P_{vp}(t)$, $t \in (t_1 - \epsilon, r_1)$. By continuity, this implies $Q_\ell(t_1) = c_\ell a_\ell(H(t_1))H(t_1)P_{vp}(t_1) > 0$ and consequently $\dot{P}_{as}(t_1) = Q_\ell(t_1)/c_{as} > 0$. Again we get the contradiction $P_{as}(t) < 0$, i.e., $x(t) \notin \overline{K}$, for $t \in (t_1 - \epsilon, t_1)$ with some $\epsilon > 0$.

1.4 The Linear-Quadratic Regulator Problem

The control $u(t)$ in (1.29) represents the baroreceptor loop. This loop includes the action of the baroreceptors, which measure P_{as}, and the generation of the control signals in the medulla, which are transmitted by the autonomic nervous system. This loop also includes the action of these signals on the pacemaker cells in the sine node in order to change the heart frequency. In this chapter, we neglect the fact that these control signals also influence the systemic peripheral resistance, the compliance of the venous systemic compartment, and directly influence the contractilities of the ventricles, which we assume to be controlled indirectly via the heart frequency (see (1.22)). Since we do not know with sufficient detail how the signals coming from the baroreceptors are transformed in the medulla into the signals transmitted by the sympathetic and parasympathetic nervous system, we base our approach on optimal control theory in order to construct a stabilizing feedback control which drives the system from one equilibrium state to another.

In particular, we consider a situation where the cardiovascular system transitions from the equilibrium state x^{rest} corresponding to zero workload, $M_T = M_T^{rest} = M_0$, to

the equilibrium state x^{exer} corresponding to the imposed constant workload W^{exer}, $M_{\text{T}} = M_{\text{T}}^{\text{exer}} = M_0 + \rho W^{\text{exer}}$. We assume that the control $u(t)$ is chosen such that the quadratic cost functional

$$J(u(\cdot), x^{\text{rest}}) = \int_0^\infty \left(q_{\text{as}}^2 (P_{\text{as}}(t) - P_{\text{as}}^{\text{exer}})^2 + u(t)^2\right) dt \tag{1.47}$$

is minimized. Here $P_{\text{as}}(t)$ is the first component of the solution $x(t)$ of the model equations (1.33) with initial condition

$$x(0) = x^{\text{rest}}$$

and $W = W^{\text{exer}}$. The positive constant q_{as}^2 is a weighting factor. The cost functional penalizes deviations of the arterial systemic pressure from the equilibrium value and large values of the control function, i.e., of $\dot{H}(t)$. That only the first component P_{as} of the state vector is included the cost functional reflects the assumption that only this component is sensed in the system.

In addition to system (1.33), we have the output equation

$$y(t) = q_{\text{as}}\left(P_{\text{as}}(t) - P_{\text{as}}^{\text{exer}}\right) = \left(q_{\text{as}}, 0, \ldots, 0\right)\left(x(t) - x^{\text{exer}}\right), \quad t \geq 0.$$

In view of this equation the cost functional (1.47) can be written as

$$J(u(\cdot), x^{\text{rest}}) = \int_0^\infty \left(y(t)^2 + u(t)^2\right) dt. \tag{1.48}$$

Optimality of the control is not the main point here, but rather obtaining a stabilizing control, i.e., a control which steers the system to the equilibrium x^{exer}. Because of the inherent modeling errors, an optimal control for the model system would not be an optimal control for the real cardiovascular system in general. Having this in mind, we introduce the transformation $\xi(t) = x(t) - x^{\text{exer}}$ and linearize the model equations around $\xi = 0$, which gives the linear system

$$\begin{aligned} \dot{\xi} &= A\xi + Bu(t), \quad t \geq 0, \\ \xi(0) &= x^{\text{rest}} - x^{\text{exer}}, \end{aligned} \tag{1.49}$$

where

$$\begin{aligned} A &= \frac{\partial \mathcal{F}}{\partial x}\left(x^{\text{exer}}, p, W^{\text{exer}}, 0\right) \in \mathbb{R}^{9\times 9}, \\ B &= \left(0, \ldots, 0, 1\right)^{\mathsf{T}} \in \mathbb{R}^9. \end{aligned}$$

In Section A.2 of Appendix A, we provide formulas for the elements of the matrix A. Under the transformation $x \to \xi$ the cost functional J takes the form

$$J(u(\cdot), x^{\text{rest}} - x^{\text{exer}}) = \int_0^\infty \left(\eta(t)^2 + u(t)^2\right) dt, \tag{1.50}$$

where

$$\eta(t) = C\xi(t), \quad t \geq 0, \tag{1.51}$$

with $C = (q_{as}, 0, \ldots, 0)$, and $\xi(t)$ is the solution of the initial value problem (1.49) with the given control $u(t)$. The linear-quadratic regulator problem for the linear system (1.49), (1.51) with the quadratic cost functional (1.50) (hence the name linear-quadratic regulator problem) requires that we find a function $\hat{u} \in L^2(0, \infty; \mathbb{R})$ such that

$$J(\hat{u}, x^{\text{rest}} - x^{\text{exer}}) = \min_{u \in L^2(0,\infty;\mathbb{R})} J(u, x^{\text{rest}} - x^{\text{exer}}).$$

From control theory (see, for instance, Kwakernaak and Sivan, 1972; Knobloch and Kwakernaak, 1985), we know that the solution of the linear-quadratic regulator problem is given by a linear feedback law; i.e., we have

$$\hat{u}(t) = K\xi^*(t), \quad t \geq 0, \tag{1.52}$$

where $\xi^*(t)$ is the solution of the closed-loop system

$$\dot{\xi}(t) = (A + BK)\xi(t), \quad t \geq 0, \qquad \xi(0) = x^{\text{rest}} - x^{\text{exer}}.$$

The feedback matrix K is given as $K = -B^{\mathsf{T}}X \in \mathbb{R}^{1\times 9}$ and X is the solution of the Riccati matrix equation

$$XA + A^{\mathsf{T}}X - XBB^{\mathsf{T}}X + C^{\mathsf{T}}C = 0. \tag{1.53}$$

The Riccati equation (1.53) has a unique positive definite solution X if the pair (A, B) is stabilizable and the pair (C, A) is detectable. Stronger conditions are controllability of (A, B) and observability of (C, A), which require

$$\operatorname{rank}\left(B, AB, \ldots, A^8B\right) = 9 \quad \text{and} \quad \operatorname{rank}\left(C^{\mathsf{T}}, A^{\mathsf{T}}C^{\mathsf{T}}, \ldots, \left(A^{\mathsf{T}}\right)^8 C^{\mathsf{T}}\right) = 9.$$

The feedback law (1.52) in the original coordinates is

$$u^*(t) = K(x^*(t) - x^{\text{exer}}), \quad t \geq 0, \tag{1.54}$$

and it provides the optimal control for the linearized system $\dot{x}(t) = A(x(t) - x^{\text{exer}}) + Bu(t)$ minimizing the cost functional (1.48) among all $u \in L^2(0, \infty; \mathbb{R})$. For the nonlinear system (1.33), $u^*(t)$ given by (1.54) (now $x^*(t)$ is the solution of the closed-loop system $\dot{x} = \mathcal{F}(x(t), p, W^{\text{exer}}, K(x^* - x^{\text{exer}}))$, $x(0) = x^{\text{rest}}$) is also a stabilizing control provided that $\|x^*(t) - x^{\text{exer}}\|$ and $|u^*(t)|$ are small enough (see Russell, 1979). This is another reason to assume that the imposed workload W^{exer} has to be sufficiently small. System (1.33), with the feedback control (1.54), gives the closed-loop system

$$\begin{aligned} &\dot{x}(t) = \mathcal{F}\big(x(t), p, W^{\text{exer}}, K(x(t) - x^{\text{exer}})\big), \quad t \geq 0, \\ &x(0) = x^{\text{rest}}. \end{aligned} \tag{1.55}$$

If we did the computations—which give the feedback law for the reduced system (1.33)—for the original system (1.32), then the corresponding Riccati equation could not have a unique positive definite solution, and the solution procedure would break down. Indeed, if the Riccati equation had a unique positive definite solution $\tilde{X} \in \mathbb{R}^{10\times 10}$, then the feedback control $u(t) = -\tilde{B}^{\mathsf{T}}\tilde{X}\tilde{x}(t)$, where $\tilde{B} = \operatorname{col}(0, \ldots, 0, 1) \in \mathbb{R}^{10}$, would be a stabilizing control for the linearized system $\dot{\tilde{\xi}}(t) = \tilde{A}\tilde{\xi}(t) + \tilde{B}u(t)$ corresponding to (1.32).

The matrix $\tilde{A}$ is the Jacobian $(\partial\mathcal{G}/\partial\tilde{x})(\tilde{x}^{\text{excr}}, p, W^{\text{excr}}, 0)$. Invariance of the hyperplane (1.5) for system (1.32) means that $w^{\mathsf{T}}\mathcal{G}(\tilde{x}, p, W^{\text{excr}}, 0) = 0$ for all $\tilde{x} \in \mathbb{R}^{10}$, where $w = \text{col}(c_{\text{as}}, c_{\text{vs}}, c_{\text{ap}}, c_{\text{vp}}, 0, \ldots, 0) \in \mathbb{R}^{10}$. This implies $w^{\mathsf{T}}\tilde{A} = 0$. Since we also have $w^{\mathsf{T}}\tilde{B} = 0$, we get

$$w^{\mathsf{T}}\big(\tilde{A} - \tilde{B}\tilde{B}^{\mathsf{T}}\tilde{X}\big) = 0;$$

i.e., the closed-loop system has zero as an eigenvalue and thus cannot be asymptotically stable. This contradiction shows that the Riccati equation in this case cannot have a unique positive definite solution.

The feedback laws (1.52) and (1.54) are not realistic in the sense that they require knowledge of $\xi(t)$ in order to get the control $u(t)$. However, only information on the first component of $\xi(t)$ (i.e., information on P_{as}) is transmitted to the controller in the medulla. The question arises of whether we can reconstruct the full state $\xi(t)$ of system (1.49) from observations of the first component over some time interval. Under the assumptions stated above the answer to this question is "yes" and an estimate $\hat{\xi}(t)$ of the state $\xi(t)$ is obtained as the solution of the dynamical observer equation (see, for instance, Kwakernaak and Sivan, 1972; Knobloch and Kwakernaak, 1985)

$$\begin{aligned}
&\frac{d}{dt}\hat{\xi} = (A + BK)\hat{\xi} + LC(\xi - \hat{\xi}), \quad t \geq 0,\\
&\hat{\xi}(0) = x^{\text{rest}} - x^{\text{excr}}.
\end{aligned}$$

We see that the dynamical observer (also called Luenberger observer) is a model of the original closed-loop system, whose input is the difference between the measured components of the state of system (1.49) and of the estimate for this state. The input matrix L for the dynamical observer is given by $L = YC^{\mathsf{T}}$, where Y is the solution of the following dual matrix Riccati equation:

$$YA^{\mathsf{T}} + AY - YC^{\mathsf{T}}CY + BB^{\mathsf{T}} = 0. \tag{1.56}$$

In the control laws (1.52) and (1.54), we now use the estimates $\hat{\xi}(t)$ and $\hat{x}(t) = \hat{\xi}(t) + x^{\text{excr}}$ instead of the states $\xi(t)$ and $x(t)$. This finally gives the following closed-loop system with dynamical observer as the complete closed-loop model for the cardiovascular system:

$$\begin{aligned}
&\dot{x}(t) = \mathcal{F}\big(x(t), p, W^{\text{excr}}, K(\hat{x}(t) - x^{\text{excr}})\big), \quad t \geq 0,\\
&\dot{\hat{x}}(t) = (A + BK)(\hat{x}(t) - x^{\text{excr}}) + LC(x(t) - \hat{x}(t)), \quad t \geq 0,\\
&x(0) = \hat{x}(0) = x^{\text{rest}}.
\end{aligned} \tag{1.57}$$

The block diagram for this system is shown in Figure 1.3.

1.5 The Bicycle Ergometer Test

As already mentioned, the goal of the modeling process described in the previous sections is to simulate the reaction of the cardiovascular system under a constant ergometric workload with special emphasis on the role played by the baroreceptor loop. We will now consider

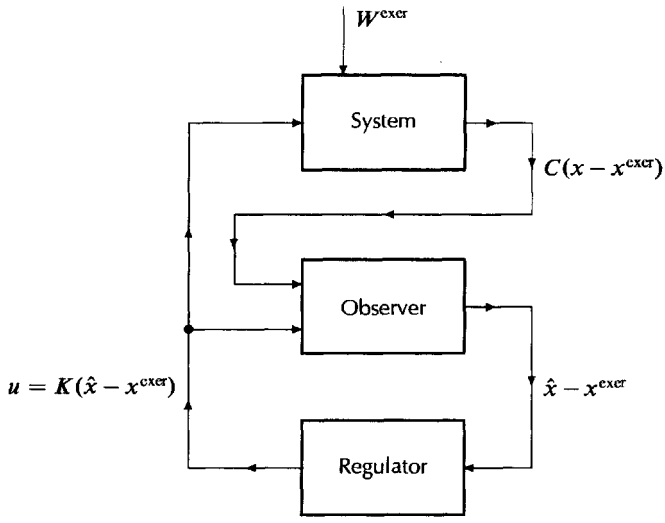

Figure 1.3: The complete closed-loop model for the cardiovascular system.

model validation based on the data obtained from bicycle ergometer tests with test persons in an upright sitting position. Data recordings began 10 minutes before the exercise phase started. The workload W^{exer} for the exercise phase, which also lasted for 10 minutes, was constant. In order to meet the assumptions of the modeling process, a rather low workload was chosen,

$$W^{exer} = 75\,[\text{Watt}].$$

Initially, only measurements for the heart rate H and the arterial systemic pressure P_{as} were made. These measurements were taken every 2 seconds with an Ohmeda 2300 Finapres Continuous NIBP Monitor during the whole period of 20 minutes (10 minutes rest phase and 10 minutes exercise phase):

$$\eta_i \sim H(t_i),\ \xi_i \sim P_{as}(t_i), \quad i = N_{start}, \ldots, N_{end},$$

where $t_i = i/30\,[\text{min}]$, $N_{start} = -N_{end}$, and $N_{end} = 30 \cdot 10 = 300$. The exercise phase starts at $t_0 = 0$. We set $t_{end} = t_{N_{end}} = 10\,[\text{min}]$.

At a later stage of the tests we also obtained measurements for the cardiac output Q_ℓ of the left ventricle using Doppler echocardiography. With the echocardiographic system Vingmed CFM 800 we obtained measurements every 30 seconds on average,

$$\zeta_j \sim Q_\ell(\tilde{t}_j), \quad j = \tilde{N}_{start}, \ldots, \tilde{N}_{end},$$

where $-10\,[\text{min}] \le \tilde{t}_i < \tilde{t}_j \le 10\,[\text{min}]$ for $i < j$. Naturally we tried to get more measurements during the exercise phase. Typically we had $\tilde{N}_{start} = -4$ and $\tilde{N}_{end} = 20$, $\tilde{t}_0$ being the first positive time instant, i.e., the first measurement in the exercise phase occurred at $\tilde{t}_0$. Using two-dimensional (2D) echocardiography we got also reliable measurements for $V_{diast,\ell}$ and $V_{syst,\ell}$ for the equilibrium states "rest" and "exercise."

The method of Doppler echocardiographic measurements for the cardiac output Q_ℓ of the left ventricle is based on the relation

$$V_{\mathrm{str},\ell} = A \cdot \mathrm{VTI}, \tag{1.58}$$

where, at some section of the aorta, A is the area of the cross section and VTI is the so called velocity-time integral corresponding to one systole, i.e.,

$$\mathrm{VTI} = \int_0^{t_{\mathrm{systole}}} \bar{v}(t)\, dt,$$

where $\bar{v}(t)$ is the average flow velocity over the cross section at time t. Doppler echocardiographic devices, as for instance the Vingmed CFM 800 system, determine $\bar{v}(t)$ by directly measuring the velocity of the red blood cells relative to the sonar head of the device (using the Doppler effect) and then determine the VTI by numerical integration. In order that the Doppler echocardiographic measurements give a sufficiently good approximation for $\bar{v}(t)$, the following requirements have to be satisfied (see Fehske, 1988):

- The axis of the sonar head has to be orthogonal to the cross section of the aorta, where the average flow velocity is determined.
- The velocity profile at the cross section has to be flat, which means that the cross section has to be close to the point where the aorta enters the left ventricle.

The second requirement may rule out test persons, who have a very steep position of the axis of their heart, but is necessary in view of formula (1.58) because the area A of the cross section has to stay almost constant during the systole (compare Christie et al., 1987). Both requirements imply that the measurements have to be done by hand by an experienced cardiologist. It is also clear that the time interval between measurements for Q_ℓ will be rather large in comparison to the measurements for H and P_{as}.

In order to obtain the area A of the cross section, we use the fact that at the point of measurement, the cross section is well approximated by a circle of some diameter d, i.e.,

$$A = \frac{1}{4} d^2 \pi.$$

This diameter is determined a priori by careful 2D echocardiographic measurements (using the leading-edge method, for instance).

1.6 Parameter Identification

The model for the cardiovascular system developed in Sections (1.2)–(1.4) involves a rather large number of parameters. The values for only a few of these parameters can be obtained a priori. The majority of the parameters must be determined by parameter identification procedures using the measurements obtained from bicycle ergometer tests (see Section 1.5, for instance). In order to avoid severe computational difficulties, we have to keep the number of these parameters as small as possible.

1.6.1 A priori determined parameters

(a) *The total blood volume* V_{tot}. The total blood volume V_{tot} (in cm^3) can be expressed in terms of the body surface s (in m^2) as follows (Altman and Dittmer, 1971, p. 376 ff.):

$$V_{\text{tot}} = 3,290s - 1,229.$$

For the body surface s (in m^2) we have Du Bois' formula (Keidl, 1985, p. 377)

$$s = 0.007184w^{0.425}h^{0.725},$$

where w is the weight (in kg) and h the height (in cm). Compare also the discussion in Subsection 4.2.3 and equation (4.2). For a person with $w = 78$ [kg] and $h = 172$ [cm] we get $V_{\text{tot}} = 5.058$ [liter].

(b) *The compliances of the compartments of the systemic and the pulmonary circuit.* In order to determine the compliances, we used data available in the literature (Keidl, 1985; Despopoulos and Silbernagl, 1991; Grodins, 1959; Burton, 1969) to estimate the distribution of stressed blood volume in the four compartments:

Compartment	Blood volume
Arterial systemic	$0.212\,V_{\text{tot}}$
Venous systemic	$0.514\,V_{\text{tot}}$
Arterial pulmonary	$0.107\,V_{\text{tot}}$
Venous pulmonary	$0.167\,V_{\text{tot}}$

The bicycle ergometer data give (see Section 1.5)

$$P_{\text{as}}^{\text{rest}} = \frac{1}{N_1}\sum_{i=0}^{N_1-1}\xi_i \quad [\text{mmHg}]. \tag{1.59}$$

For the other pressures (in mmHg) we take the nominal values

$$P_{\text{vs}}^{\text{rest}} = 4, \quad P_{\text{ap}}^{\text{rest}} = 15 \quad \text{and} \quad P_{\text{vp}}^{\text{rest}} = 6.$$

Using (1.1), we obtain the following expressions for the compliances:

$$c_{\text{as}} = \frac{0.212}{P_{\text{as}}^{\text{rest}}}V_{\text{tot}}, \quad c_{\text{vs}} = \frac{0.514}{4}V_{\text{tot}}, \quad c_{\text{ap}} = \frac{0.107}{15}V_{\text{tot}}, \quad c_{\text{vp}} = \frac{0.167}{6}V_{\text{tot}}. \tag{1.60}$$

(c) *The constant* κ *in* (1.11). If echocardiographic measurements are available, one easily gets measurements for the duration t_d of the diastole and for the duration $t_c = 1/H$ of the heart cycle. Let $t_{d,i}$ and $t_{c,i}$, $i = 1, \ldots, k$, be the corresponding measurements. Then we obtain from Bazett's formula (see the paragraph following (1.11)) the following least squares estimate for κ:

$$\kappa = \sum_{i=1}^{k}(t_{c,i} - t_{d,i})t_{c,i}^{1/2} \Big/ \sum_{i=1}^{k} t_{c,i}.$$

Without echocardiographic measurements we usually take $\kappa = 0.0516$.[6]

(d) *The constants M_0 and ρ in* (1.28). Equation (1.28) is an empirical regression formula for the total metabolic rate in dependence on the workload imposed on the test person. In general we take $M_0 = 0.35$ [liter/min]. For a test person in average physical condition we take $\rho = 0.011$ [liter min^{-1} Watt^{-1}].

(e) *The arterial O_2 concentration.* For the ergometric workload levels considered in our tests, we can assume that the oxygenation of blood in the alveoli is maximal; i.e., the O_2 concentration in arterial blood is equilibrated with the O_2 concentration in alveolar air. This means we can take $C_{a,O_2} = 0.2$.

(f) *The constant β_ℓ in the first equation of* (1.22). In case echocardiographic measurements are available, for instance, during the rest phase, we can determine measurements for $V^{\text{rest}}_{\text{diast},\ell}$ and $V^{\text{rest}}_{\text{syst},\ell}$. From (1.13) (with $V_0 = 0$) we get

$$S^{\text{rest}}_\ell = \lambda P^{\text{rest}}_{\text{as}}, \quad \text{where } \lambda = \frac{V^{\text{rest}}_{\text{diast},\ell} - V^{\text{rest}}_{\text{syst},\ell}}{V^{\text{rest}}_{\text{diast},\ell}}. \tag{1.61}$$

For the computation of the equilibrium x^{rest} (given H^{rest}) we use (1.61) instead of the first equation in (1.37). From (1.40) we get

$$P^{\text{rest}}_{\text{vp}} = \frac{a_\ell(H^{\text{rest}}) + \lambda k_\ell(H^{\text{rest}})}{\lambda c_\ell a_\ell(H^{\text{rest}}) H^{\text{rest}}} F^{\text{rest}}.$$

Equations (1.38), (1.39), and (1.41) imply

$$\begin{aligned}
P^{\text{rest}}_{\text{vs}} &= \frac{1}{\mu_{\text{r}}(H^{\text{rest}})}\Big(\lambda_{\text{r}}(H^{\text{rest}})F^{\text{rest}} \\
&\qquad + a_{\text{r}}(H^{\text{rest}})(F^{\text{rest}})^2\Big(R_{\text{p}} + \frac{a_\ell(H^{\text{rest}}) + \lambda k_\ell(H^{\text{rest}})}{\lambda c_\ell a_\ell(H^{\text{rest}}) H^{\text{rest}}}\Big)\Big), \\
P^{\text{rest}}_{\text{as}} &= A_{\text{pesk}}(C_{a,O_2} F^{\text{rest}} - M^{\text{rest}}_{\text{T}}) + P^{\text{rest}}_{\text{vs}}, \\
P^{\text{rest}}_{\text{ap}} &= P^{\text{rest}}_{\text{vp}} + R_{\text{p}} F^{\text{rest}}.
\end{aligned}$$

Equation (1.46) finally gives a nonlinear equation for F^{rest}:

$$c_{\text{as}} A_{\text{pesk}}(C_{a,O_2} F^{\text{rest}} - M^{\text{rest}}_{\text{T}}) + (c_{\text{as}} + c_{\text{vs}}) P^{\text{rest}}_{\text{vs}} + c_{\text{ap}} R_{\text{p}} F^{\text{rest}} + (c_{\text{ap}} + c_{\text{vp}}) P^{\text{rest}}_{\text{vp}} = V_{\text{tot}}.$$

When we have determined F^{rest} from this equation, we obtain $P^{\text{rest}}_{\text{as}}$, $P^{\text{rest}}_{\text{vs}}$, $P^{\text{rest}}_{\text{ap}}$, and $P^{\text{rest}}_{\text{vp}}$ from the equations given above and $R^{\text{rest}}_{\text{s}}$ from

$$R^{\text{rest}}_{\text{s}} = \big(P^{\text{rest}}_{\text{as}} - P^{\text{rest}}_{\text{vs}}\big)/F^{\text{rest}}.$$

Then we obtain S^{rest}_ℓ from (1.61), and (1.37) can be used to express β_ℓ in terms of α_ℓ:

$$\beta_\ell = \frac{S^{\text{rest}}_\ell}{H^{\text{rest}}} \alpha_\ell;$$

i.e., β_ℓ can be eliminated from the set of parameters which have to be identified provided we have echocardiographic measurements for $V^{\text{rest}}_{\text{diast},\ell}$ and $V^{\text{rest}}_{\text{syst},\ell}$.

[6] If time is measured in seconds, then the corresponding value is $\kappa = 0.4$.

1.6.2 The output least-squares formulation of the parameter identification problem

If we utilize all possibilities for determining parameters a priori described above, the following 13 parameters still have to be determined:

$$c_\ell,\ c_r,\ R_\ell,\ R_r,\ R_p,\ K,\ A_{pesk},\ \alpha_\ell,\ \alpha_r,\ \beta_r,\ \gamma_\ell,\ \gamma_r,\ q_{as}.$$

Note that the solutions of the model equations also depend on q_{as}, the weight factor in the cost functional (1.47). If no echocardiographic measurements are available the above list of parameters has to include β_ℓ also. In our simulations and our efforts to validate the model, it turned out that the results could be improved considerably by admitting different values for the parameters R_p and A_{pesk} during the phases "rest" and "exercise." This is a strong indication that R_p and A_{pesk} in fact are functions of the state variables of the system. Thus, the vector q of all those parameters which cannot be determined a priori is given by

$$q = \left(c_\ell, c_r, R_\ell, R_r, R_p^{rest}, R_p^{exer}, K, A_{pesk}^{rest}, A_{pesk}^{exer}, \alpha_\ell, \alpha_r, \beta_r, \gamma_\ell, \gamma_r, q_{as}\right)^T \in \mathbb{R}^{15}$$

in case β_ℓ is determined a priori and

$$q = \left(c_\ell, c_r, R_\ell, R_r, R_p^{rest}, R_p^{exer}, K, A_{pesk}^{rest}, A_{pesk}^{exer}, \alpha_\ell, \alpha_r, \beta_\ell, \beta_r, \gamma_\ell, \gamma_r, q_{as}\right)^T \in \mathbb{R}^{16}$$

otherwise. Correspondingly, we have to distinguish two parameter vectors p^{rest} and p^{exer}. The vector p^{rest} is the vector p given by (1.31) with $R_p = R_p^{rest}$, $A_{pesk} = A_{pesk}^{rest}$, whereas p^{exer} is p with $R_p = R_p^{exer}$, $A_{pesk} = A_{pesk}^{exer}$. The measurable output of the system is considered to be a function of q,

$$y(t;q) = \left(P_{as}(t;q), H(t;q), Q_\ell(t;q)\right), \text{ respectively, } y(t;q) = \left(P_{as}(t;q), H(t;q)\right).$$

The parameter estimate $\hat{q}$ is obtained as the solution of the following optimization problem, which is commonly known as the output least-squares (OLS) formulation of the parameter identification problem (compare Figure 1.4):

(OLS)

Let $\mathcal{Q}$ be the set of admissible parameters. Find $\hat{q} \in \mathcal{Q}$ such that

$$G(\hat{q}) = \min_{q \in \mathcal{Q}} G(q),$$

where

$$\begin{aligned} G(q) = {} & a_1^{rest} \sum_{i=N_{start}}^{-1} \left(P_{as}^{rest}(q) - \xi_i\right)^2 + a_1^{exer} \sum_{i=0}^{N_{end}} \left(P_{as}(t_i;q) - \xi_i\right)^2 \\ & + a_2^{exer} \sum_{i=0}^{N_{end}} \left(H(t_i;q) - \eta_i\right)^2 \\ & + a_3^{rest} \sum_{i=\tilde{N}_{start}}^{-1} \left(Q_\ell^{rest}(q) - \zeta_i\right)^2 + a_3^{exer} \sum_{i=0}^{\tilde{N}_{end}} \left(Q_\ell(\tilde{t}_i;q) - \zeta_i\right)^2. \end{aligned}$$

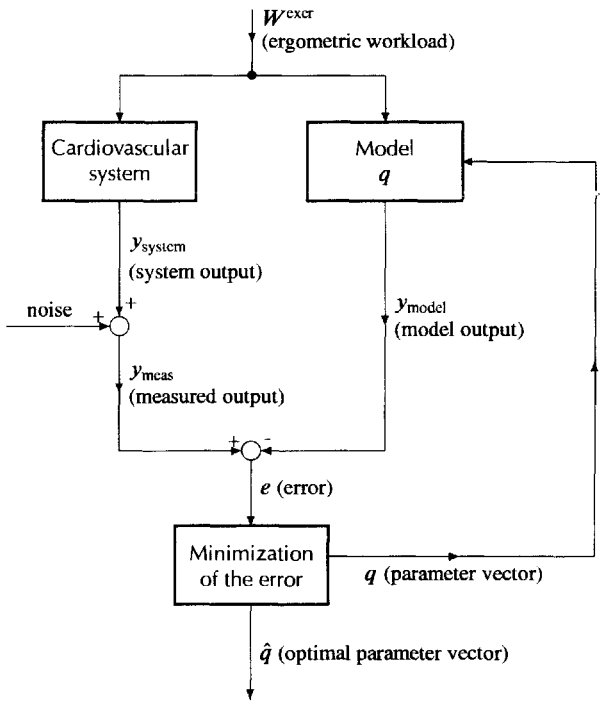

Figure 1.4: Flow chart for the parameter identification problem.

The weighting factors a_1^{rest}, a_1^{exer}, a_2^{exer}, a_3^{rest}, and a_3^{exer} may be chosen according to the relative numbers of measurements available for the components of the measurable output and may also reflect information on the reliability of the measurements. The measurements η_i, $i = N_{start}, \ldots, -1$, for H do not appear in the cost functional G, because these values are used to define H^{rest} (as arithmetic mean of these measurements). If no data for the cardiac output of the left ventricle are available or we do not use such measurements, we set $a_3^{rest} = a_3^{exer} = 0$.

We now summarize the main steps for solving the parameter identification problem.

(a) Given data:

(i) Time intervals for the rest phase and for the exercise phase

$$[t_{start}, 0] \quad \text{and} \quad [0, t_{end}].$$

We usually have $t_{start} = -10$ [min] and $t_{end} = 10$ [min] (compare Section 1.5).

(ii) $W^{rest} = 0$ and W^{exer}. Usually we have $W^{exer} = 75$ [Watt].

(iii) Components of p^{rest} and p^{exer}, which are not contained in q (see Subsection 1.6.1).

(iv) Measurements ξ_i, η_i, and ζ_j for $P_{as}(t_i)$, $H(t_i)$, and $Q_\ell(\tilde{t}_j)$, $i = N_{start}, \ldots, N_{end}$, $j = \tilde{N}_{start}, \ldots, \tilde{N}_{end}$.

(v) The weighting factors a_1^{rest}, a_1^{exer}, a_2^{exer}, a_3^{rest} and a_3^{exer}.

(b) Steps of the algorithm:

Step 1: Compute

$$H^{\text{rest}} = \frac{1}{-N_{\text{start}} + 1} \sum_{i=N_{\text{start}}}^{-1} \eta_i,$$

$$H^{\text{exer}} = \frac{1}{N_{\text{end}} - N_1 + 1} \sum_{i=N_1}^{N_{\text{end}}} \eta_i,$$

where N_1 is determined by $t_{N_1-1} < 3$ [min] and $t_{N_1} \geq 3$ min. Note that after the first three minutes of the exercise phase the data indicate that the system has already reached a new equilibrium state. Furthermore, we choose the set of admissible parameters $\mathcal{Q}$. In general, we just take the positive cone in $\mathbb{R}^{15}$ and $\mathbb{R}^{16}$, respectively, for $\mathcal{Q}$; i.e., we only require that all parameters are positive.

Step 2: Choose a starting value $q_0 \in \mathcal{Q}$ for the optimization algorithm.

Step 3: Given $q \in \mathcal{Q}$, compute p^{rest} and p^{exer}.

Step 4: Compute the two equilibrium states $x^{\text{rest}} = x^{\text{rest}}\big(H^{\text{rest}}, W^{\text{rest}}, p^{\text{rest}}\big)$ and $x^{\text{exer}} = x^{\text{exer}}\big(H^{\text{exer}}, W^{\text{exer}}, p^{\text{exer}}\big)$ (compare Subsection 1.3.1).

Step 5: Compute the Jacobian

$$A = \frac{\partial \mathcal{F}}{\partial x}\big(x^{\text{exer}}, p^{\text{exer}}, W^{\text{exer}}, 0\big)$$

using the formulas given in Section A.2 of Appendix A.

Step 6: Solve the Riccati equations (1.53), (1.56) and compute

$$K = -B^{\mathsf{T}}X \quad \text{and} \quad L = YC^{\mathsf{T}}.$$

Step 7: Solve system (1.57) on $[0, t_{\text{end}}]$ and compute $P_{\text{as}}(t_i)$, $H(t_i)$, $i = 0, \ldots, N_{\text{end}}$, and $Q_\ell(\tilde{t}_j)$, $j = 0, \ldots, \tilde{N}_{\text{end}}$ (in case we have measurements for Q_ℓ).

Step 8: Compute $G(q)$ and check if the stopping criterion for the optimization algorithm is satisfied. If this is the case, set $\hat{q} = q$, otherwise continue with the next step.

Step 9: Update q according to the optimization algorithm and go to Step 3.

If we do not use the dynamical observer, then instead of Steps 6 and 7 we have to use the following steps:

Step 6a: Solve the Riccati equation (1.53) and compute

$$K = -B^{\mathsf{T}}X.$$

Step 7a: Solve system (1.55) on $[0, t_{\text{end}}]$ and compute $P_{\text{as}}(t_i)$, $H(t_i)$, $i = 0, \ldots, N_{\text{end}}$, and $Q_\ell(\tilde{t}_j)$, $j = 0, \ldots, \tilde{N}_{\text{end}}$ (in case we have measurements for Q_ℓ).

1.7 Numerical Results

In this section we present some of our results concerning the parameter identification based on the bicycle ergometer test. We also report our experiences concerning the numerical computations.

1.7.1 Parameter identification

The bicycle ergometer tests were conducted as described in Section 1.5 and we present here the results for the case when we also had echocardiographic measurements for the left cardiac output.

The data for P_{as}, H, and Q_ℓ are presented in Figures 1.5 and 1.6 (dashed lines). Using the data listed in Table 1.4, we obtain (see Subsection 1.6.1)

$$V_{\text{tot}} = 5.058\,[\text{liter}]$$

and (see (1.59) and (1.60))

$$P_{\text{as}}^{\text{exer}} = 105.55\,[\text{mmHg}]$$

as well as

$$c_{\text{as}} = 0.01016, \quad c_{\text{vs}} = 0.64995, \quad c_{\text{ap}} = 0.03608, \quad c_{\text{vp}} = 0.14078\,[\text{liter/mmHg}].$$

Furthermore, according to Subsection 1.6.1 we have

$$\kappa = 0.0516\,[\text{min}^{1/2}], \quad M_0 = 0.35\,[\text{liter/min}],$$
$$\rho = 0.011\,[\text{liter min}^{-1}\text{Watt}^{-1}], \quad C_{a,O_2} = 0.2.$$

Our choice for the weights $a_1^{\text{rest}}, \ldots, a_3^{\text{exer}}$ reflects the number of measurements and the reliability of the measurements:

$$a_1^{\text{rest}} = 33.11, \quad a_1^{\text{exer}} = 3.30, \quad a_2^{\text{exer}} = 5.87, \quad a_3^{\text{rest}} = 5 \cdot 10^4, \quad a_3^{\text{exer}} = 10^4.$$

We used the OLS formulation of the parameter identification problem as described in Subsection 1.6.2. For the minimization of the cost functional $G(q)$ we used the Minpack implementation LMDIF1, respectively, LMDER1, of the Levenberg–Marquardt algorithm. In Table 1.5 we present in the second column the results obtained by using only measurements for P_{as} and H, whereas in the third column we see the results obtained by using measurements for Q_ℓ also. Note that in this case β_ℓ is not an identified parameter but is calculated according to Subsection 1.6.1. In Figure 1.5, we depict the measurements for P_{as}, H, and Q_ℓ and the model output for these variables taking the parameter values of the second column in Table 1.5. Note also that the measurements for Q_ℓ are not used for the parameter identification in this case, but are used only for comparison with the model output for Q_ℓ.

In Figure 1.6, we again depict the measurements for P_{as}, H, and Q_ℓ and the model output for these variables obtained with the parameter values of the third column in Table 1.5. However, this time the measurements for Q_ℓ were used for parameter identification. Therefore, it is not surprising that the approximation of the data for Q_ℓ is much better compared to the case depicted in Figure 1.5. Finally, in Figure 1.7 we present the results analogous to those in Figure 1.6 but using the nonlinear feedback law presented in Appendix B.

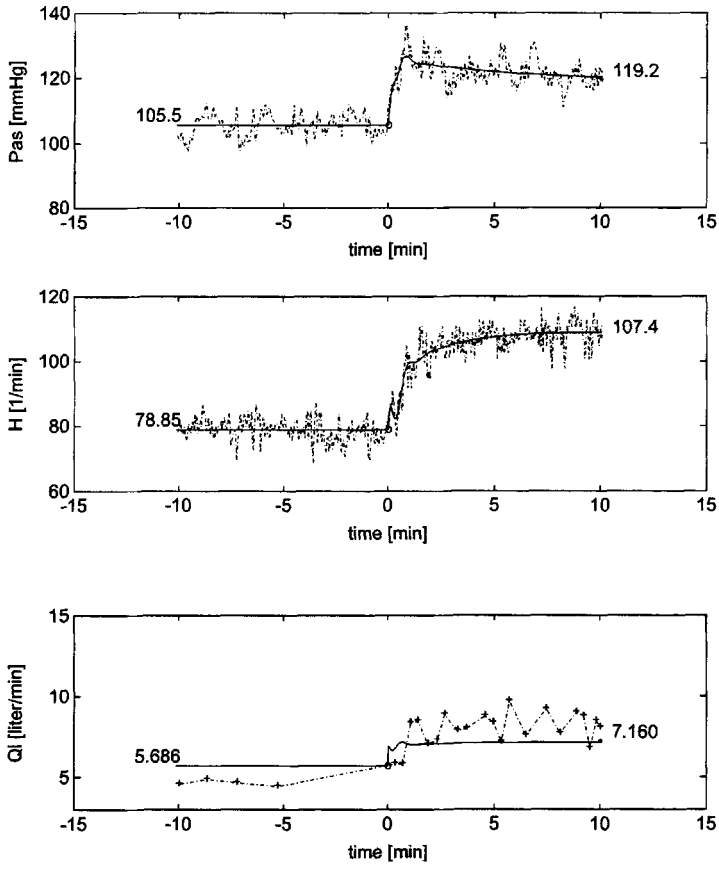

Figure 1.5: Measurements (dash-dotted lines) for P_{as}, H, Q_ℓ and model output (solid lines) using parameters obtained from parameter identification using P_{as} and H only.

1.7.2 Gradient computations

Implementations of optimization algorithms, which use gradient information, usually approximate derivatives by forward or central difference quotients. An example is the Minpack routine LMDIF1. There the step size δ_j for the forward difference quotient approximating $(\partial/\partial q_j)(q^0)$ is chosen according to

$$\delta_j = \epsilon_m^{1/2}|q_j^0|,$$

where ϵ_m is the smallest nonzero machine number. In case of the workstation HP 9000-735 which was used for the computations, we have

$$\epsilon_m = 0.22204460449250313 \cdot 10^{-15}.$$

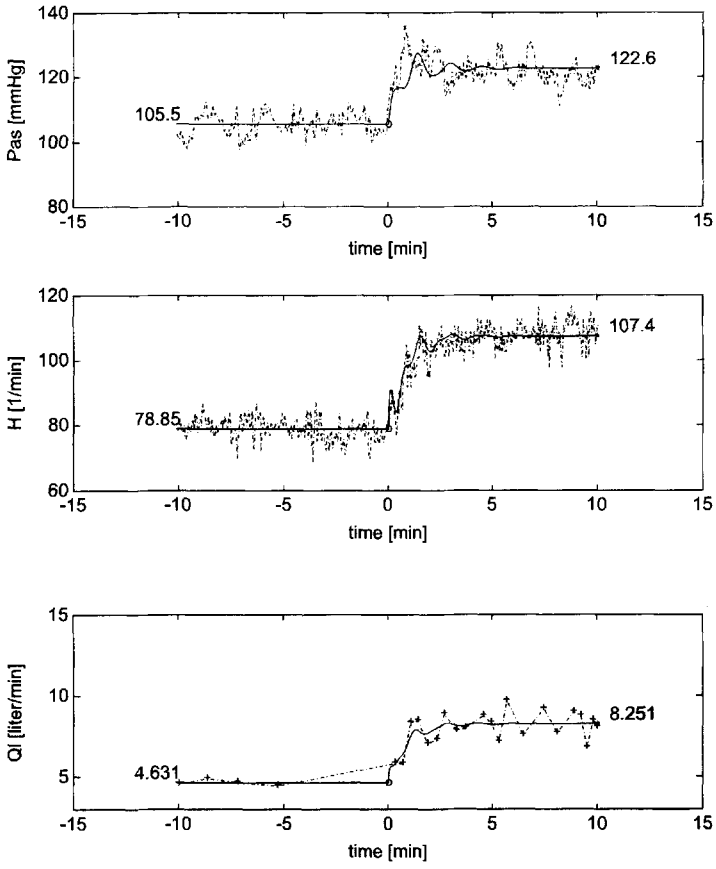

Figure 1.6: Measurements (dash-dotted lines) for P_{as}, H, Q_ℓ, and model output (solid lines) using parameters obtained from parameter identification using P_{as}, H, and Q_ℓ.

For $j = 7$, i.e., $q_7 = \alpha_\ell$, we get for q^0, given by the last column in Table 1.5, the step size

$$\delta_7 = 4.707579608146 \cdot 10^{-7}.$$

In Figure 1.8 we present a plot of

$$\alpha_\ell \to G(q_1^0, \ldots, q_6^0, \alpha_\ell, q_8^0, \ldots, q_{15}^0) \quad \text{for } \alpha_\ell \in [31.592008462, 31.592055067].$$

Furthermore, we depict the "tangents" at the point $\alpha_\ell = q_7^0$ obtained by forward, respectively, central, differences and by solving the variational equations, which give the exact gradients. We can see that the gradient approximations obtained by forward or central differences are far off from the real gradient. On the other hand, we see that the "analytically" computed gradient gives a very precise approximation. A behavior similar to that described above was observed for the parameters γ_r, γ_ℓ, K, and q_{as}. The explanation for

Height of the test person	h	172 [cm]
Weight of the test person	w	78 [kg]
Diameter of the aorta	D	2.1 [cm]
End-diastolic volume	$V^{\text{rest}}_{\text{diast},\ell}$	0.08 [liter]
	$V^{\text{exer}}_{\text{diast},\ell}$	0.102 [liter]
End-systolic volume	$V^{\text{rest}}_{\text{syst},\ell}$	0.031 [liter]
	$V^{\text{exer}}_{\text{syst},\ell}$	0.028 [liter]
Ejection fraction	$\lambda^{\text{rest}}_{\ell}$	0.6125
	$\lambda^{\text{exer}}_{\ell}$	0.7255

Table 1.4: Height and weight of the test person; 2D echocardiographic data.

Parameter	Without Q_ℓ measurements	With Q_ℓ measurements	With Q_ℓ measurements, "exact" gradients
c_ℓ	0.014621	0.023052	0.022054
c_r	0.031433	0.044131	0.044326
R_ℓ	0.073	0.267	0.243
R_r	0.225	0.0417	0.0567
R_p^{rest}	0.9	1.5	1.6
R_p^{exer}	0.04	0.32	0.32
K	66.1213	16.0376	15.9591
$A_{\text{pcsk}}^{\text{rest}}$	128	178	178
$A_{\text{pcsk}}^{\text{exer}}$	446	254	254
α_ℓ	25.459	30.559	31.592
α_r	10.388	28.679	28.342
β_ℓ	32.686	25.065	25.065
β_r	1.011	1.413	1.416
γ_ℓ	−2.859	−1.674	−1.332
γ_r	93.240	−1.861	−2.045
q_{as}	24.200	163.047	133.223

Table 1.5: Results of parameter identification with measurements for P_{as} and H as well as with measurements for P_{as}, H, and Q_ℓ (only values are given; for units see Table 1.2).

this behavior is that the numerical algorithm for computing the values of G is rather complicated and therefore rounding errors may accumulate. When the curve which has to be approximated is rather steep, then we still can get a reasonable approximation of gradients by forward or central differences. However, if the curve is already rather flat, then the gradients computed via finite differences can be completely wrong. For some parameters, gradient approximations by finite differences may give very good results also in regions where the curve is already rather flat. As an example, we present the analogous graphs for the parameter $q_2 = c_r$ in Figure 1.9.

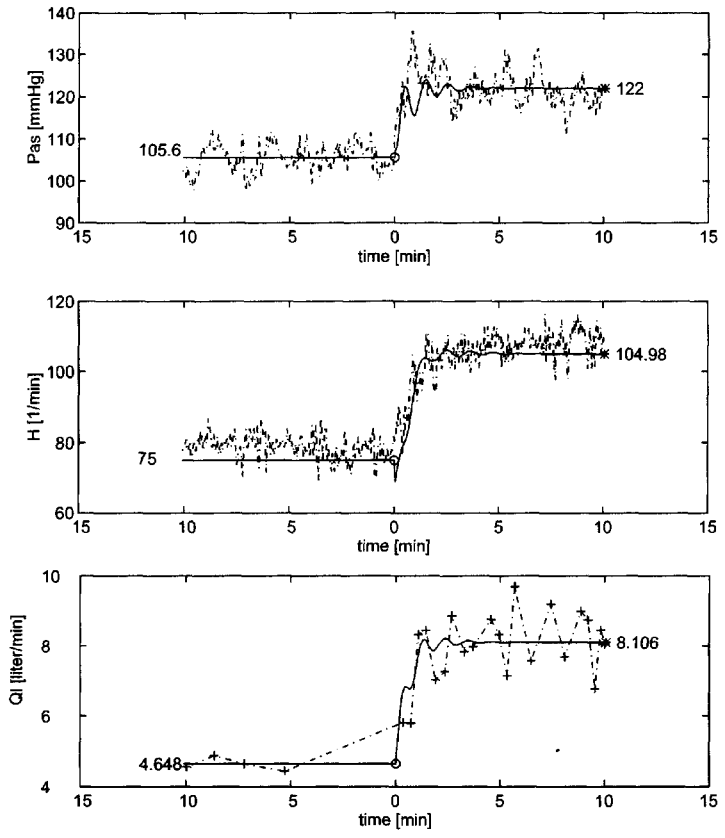

Figure 1.7: Same measurements as in Figure 1.6 but with a nonlinear feedback law.

1.7.3 Sensitivity analysis

Classical sensitivities

When the basic model was validated using data obtained from bicycle ergometer tests, only the 15, respectively, 16, parameters contained in the vector q (see the beginning of Subsection 1.6.2) were determined by solving the parameter identification problem using the OLS formulation as described in Section 1.6.2. The other parameters were determined a priori (see Subsection 1.6.1). These parameters included the compliances c_{as}, c_{vs}, c_{ap}, c_{vp}, and the total blood volume V_{tot}. In order to decide if one or more of these parameters should also be determined via parameter estimation using data from bicycle ergometer tests, one can explore the sensitivities of the model outputs P_{as}, H, and Q_ℓ with respect to these parameters as given in Figure 1.10. From these figures we conclude that at least V_{tot} should be included in the parameter vector q in order to be determined via parameter estimation from the data. It is important to base such decisions on the sensitivities, as defined in Section A.3 of Appendix A, and not on the derivatives of the measured outputs with respect to the parameters. Comparing Figure 1.10 with Figure 1.11, we see that the derivatives may lead to wrong conclusions regarding the degree of dependence on the various parameters.

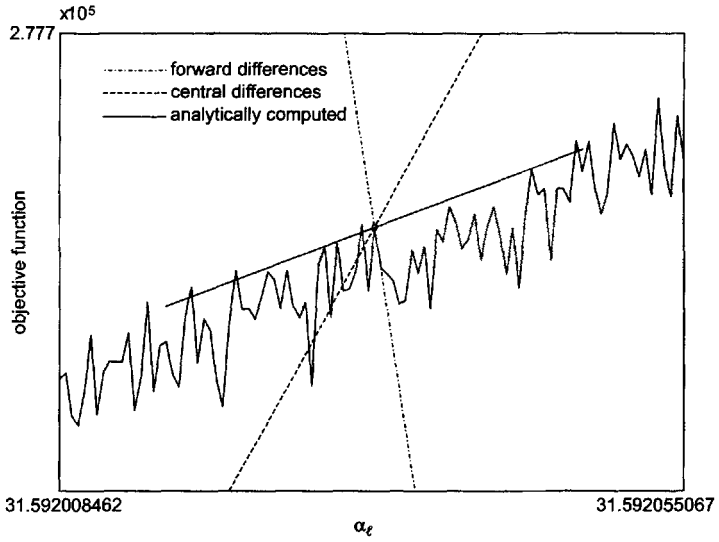

Figure 1.8: Graph of $\alpha_\ell \to G(q_1^0, \ldots, q_6^0, \alpha_\ell, q_8^0, \ldots, q_{15}^0)$ drawn with the step size used for difference approximations of derivatives; q^0 is the parameter vector given in the fourth column of Table 1.5.

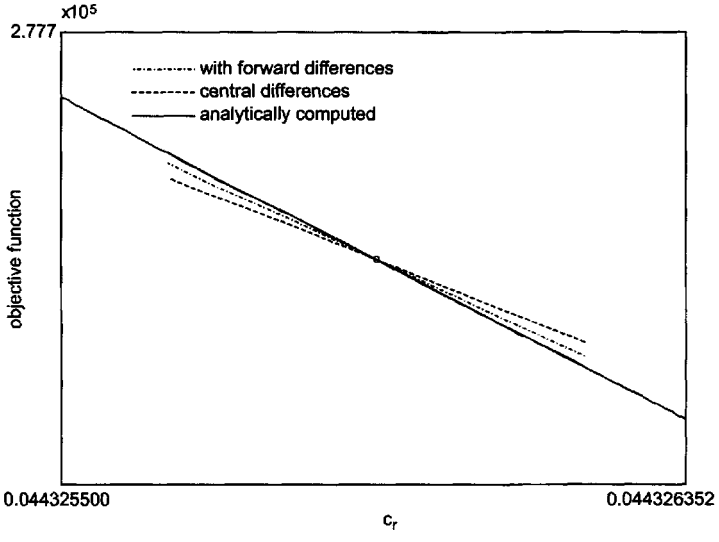

Figure 1.9: Graph of $c_r \to G(q_1^0, c_r, q_3^0, \ldots, q_{15}^0)$ drawn with the step size used for difference approximations of derivatives;q^0 is the parameter vector given in the fourth column of Table 1.5.

Generalized sensitivities

Generalized sensitivities, as introduced in Section A.4 of Appendix A, provide essentially two types of information concerning the dependence of parameter estimates on the measurements of an output variable:

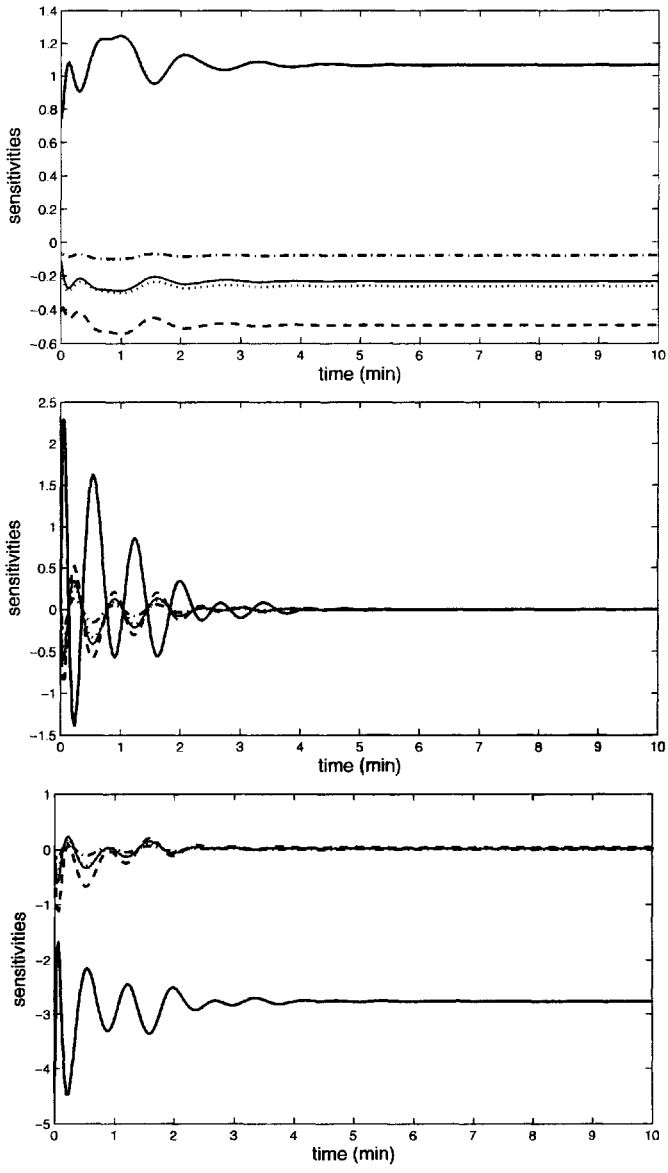

Figure 1.10: Classical sensitivities of P_{as} (upper panel), H (middle panel), and Q_ℓ (lower panel) with respect to c_{as} (dotted lines), c_{vs} (dashed lines), c_{ap} (dash-dotted lines), c_{vp} (solid, thin lines), and V_{tot} (solid, thick lines).

(a) Information on the correlation between parameters with respect to measurements for a specific output variable of the system. Oscillatory and nonmonotonic behavior of the generalized sensitivities indicates a strong correlation between the parameters. A more or less monotonic increase of the generalized sensitivity function from 0 to 1 indicates little correlation between the parameters.

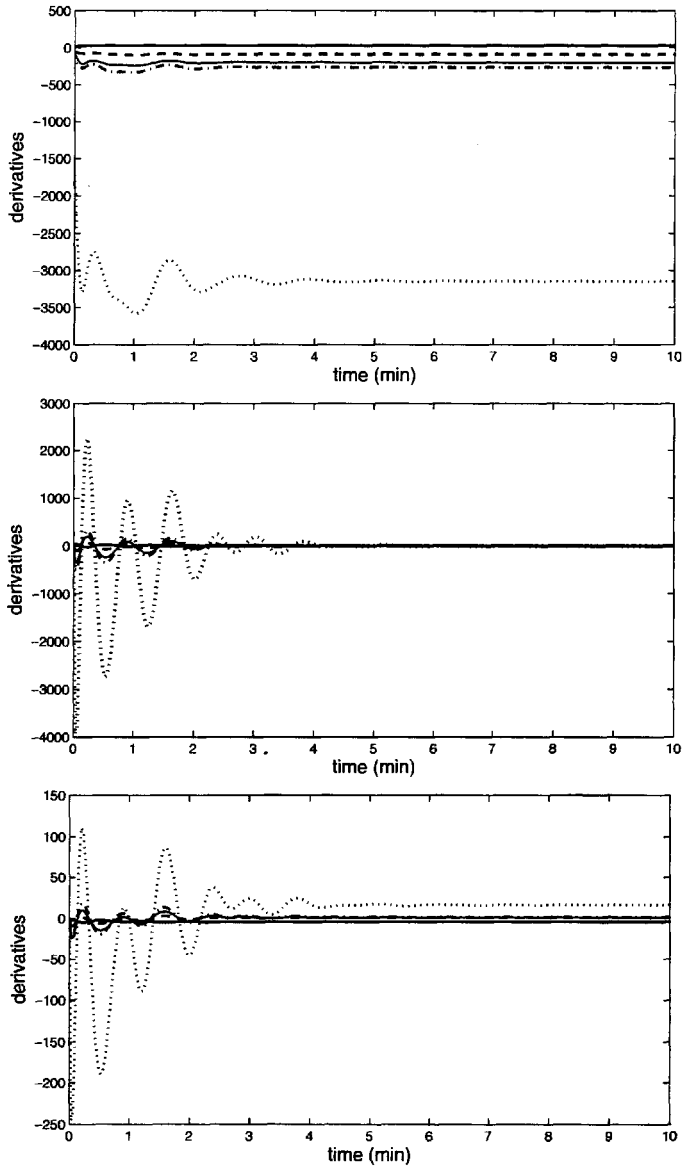

Figure 1.11: Derivatives of P_{as} (upper panel), H (middle panel), and Q_ℓ (lower panel) with respect to c_{as} (dotted lines), c_{vs} (dashed lines), c_{ap} (dash-dotted lines), c_{vp} (solid, thin lines), and V_{tot} (solid, thick lines).

(b) Information on the relative content of information carried by the measurements at different times for the parameters. If the generalized sensitivity function for a parameter is monotonically increasing, then those measurements taken in that time interval, where the generalized sensitivity function essentially increases from 0 to 1, provide all the information on the parameter, whereas the measurements taken outside that interval are more or less irrelevant for the parameter.

If we just take one parameter, then the sensitivity function is necessarily monotonically increasing and shows the information as described above under item (b). From Figure 1.12, we see that information content for c_{as} of the measurements for P_{as} is uniformly

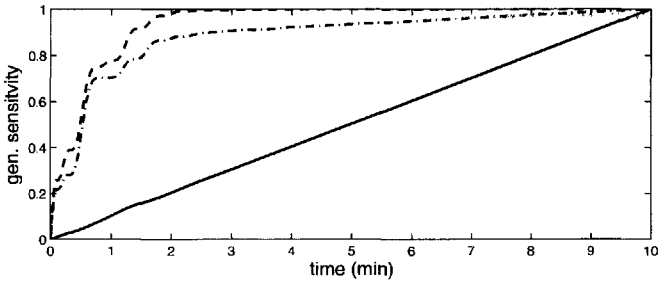

Figure 1.12: Generalized sensitivities of c_{as} as the only parameter for P_{as} (solid line), for H (dashed line), and for Q_ℓ (dash-dotted line).

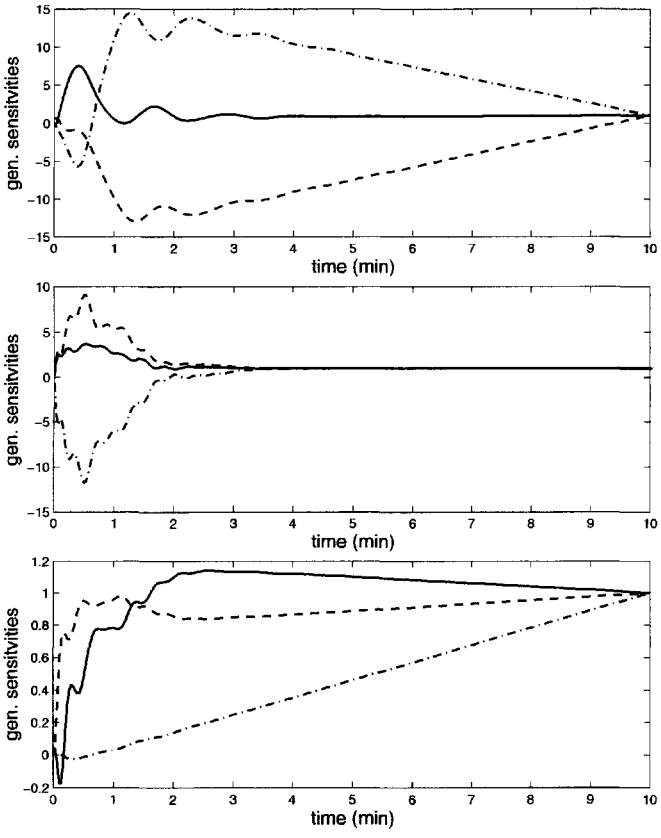

Figure 1.13: Generalized sensitivities of c_{as} (solid lines), c_{vs} (dashed lines), and V_{tot} (dash-dotted lines) with respect to P_{as} (upper panel), H (middle panel), and Q_ℓ (lower panel).

distributed on the whole interval [0, 10] (solid line), only the measurements for H on the interval [0, 2] are relevant for c_{as} (dashed line), whereas the measurements for Q_ℓ on the entire time interval carry information on c_{as}. However, measurements on the interval [0, 2] are more important than the rest of the measurements on [3, 10] (dash-dotted line).

If we consider more than one parameter simultaneously, then information according to item (a) from above is also provided by the generalized sensitivity functions. As an example, we consider the generalized sensitivity functions for the compliances c_{as}, c_{vs} together with the total blood volume V_{tot} as depicted in Figure 1.13. The upper and middle panels show that the parameters are rather strongly correlated with respect to measurements for P_{as} and H, whereas from the lower panel we conclude that V_{tot} is uncorrelated to the other two parameters with respect to measurements for Q_ℓ. The compliances are correlated with respect to measurements for Q_ℓ, but much less than with respect to measurements for P_{as} or H. If we consider the three parameters α_ℓ, α_r, and γ_ℓ we have a similar situation. Figure 1.14 shows that α_ℓ and α_r are strongly correlated with respect to measurements for P_{as}, whereas γ_ℓ is uncorrelated (upper panel). With respect to measurements for H all

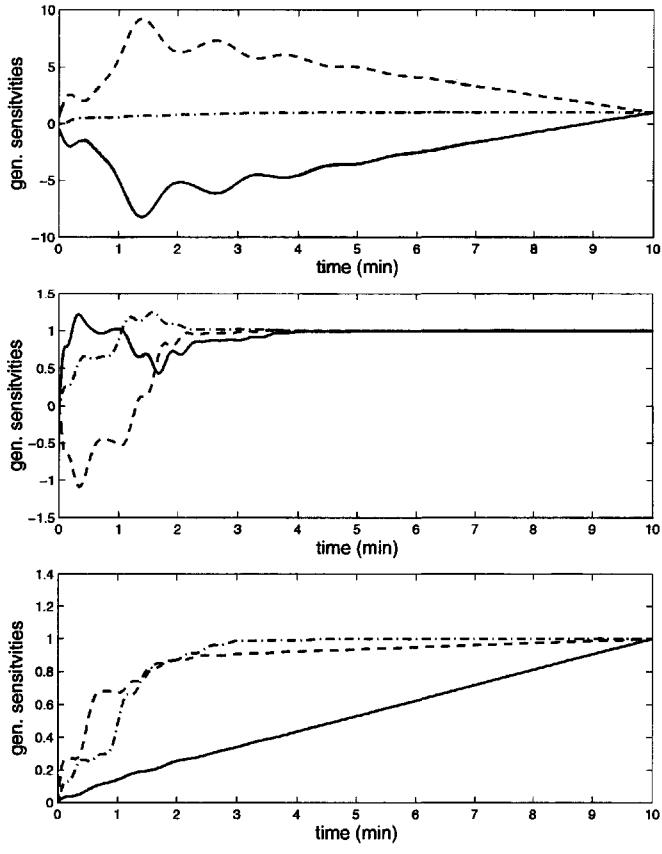

Figure 1.14: Generalized sensitivities of α_ℓ (solid lines), α_r (dashed lines), and γ_ℓ (dash-dotted lines) with respect to P_{as} (upper panel), H (middle panel), and Q_ℓ (lower panel).

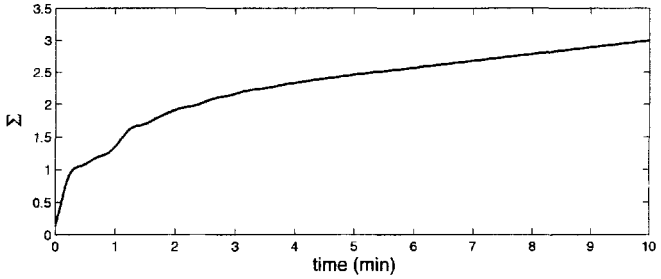

Figure 1.15: Sum of generalized sensitivities of α_ℓ, α_r, and γ_ℓ with respect to measurements for P_{as}.

three parameters are correlated, but γ_ℓ is considerably less correlated (middle panel). All the three parameters are rather uncorrelated with respect to measurements of Q_ℓ (lower panel).

Finally, we depict in Figure 1.15 the sum of the generalized sensitivities of the parameters α_ℓ, α_r, and γ_ℓ with respect to measurements for P_{as}. According to Remark 2 in Section A.4 of Appendix A this sum has to be monotonically increasing.

This page intentionally left blank

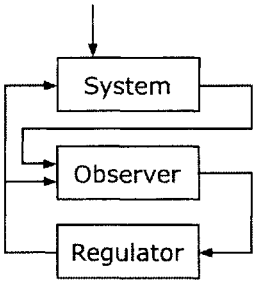

Chapter 2

Respiratory Modeling

In this chapter we will consider models for the respiratory control system, the basic components of which have been extensively studied. Research in this field is continuing at a fast pace and it is difficult to keep abreast of all important developments and advances. For a comprehensive review of the history of respiratory models, we refer the interested reader to the paper by Khoo and Yamashiro (1989) and the books by Fishman, Cherniack, and Widdicombe (1986) and by Swanson, Grodins, and Hughson (1990).

One of the earliest significant works on the respiratory control system dates back to 1905 when Haldane and Priestley (1905) discussed the negative feedback feature of ventilation control and CO_2 regulation. Since then a number of seminal models has been proposed. The multiple factor theory of ventilation control introduced by Gray (1946) represents an important early quantitative model of the respiratory system which greatly influenced research on this subject. However, his theory did not incorporate interaction between hypoxic and hypercapnic response components (Cunningham, Robbins, and Wolff, 1986).[7]

In the early 1950s, when a large part of classical control theory was developed, Grodins et al. (1954) proposed the first control-based dynamical model of CO_2 regulation. Subsequent work includes the model proposed by Horgan and Lange (1963) which incorporated transport delays involving a Gray-type controller. This model was able to produce Cheyne–Stokes respiration but could mimic certain respiratory responses only when unphysiologically large time delays were employed. Milhorn et al. (1965) introduced a model that included cerebral blood flow and a Gray-type controller responsive to P_{CO_2} in the brain and P_{a,O_2} in the arteries. Even with these additional elements, the model could not faithfully reproduce observed responses to step changes in CO_2 (Khoo and Yamashiro, 1989). About the same time, Longobardo, Cherniack, and Fishman (1966) included a Lloyd-and-Cunningham-type controller involving, among other features, a multiplicative interaction of O_2 and CO_2 control influences (Lloyd and Cunningham, 1963). Their model could simulate Cheyne–Stokes respiration under various conditions such as congestive heart failure, but their predictions required a large initial disturbance in ventilation. In 1967, Grodins, Buell, and Bart (1967) extended their 1954 model to include

[7]Hypoxia describes a state where P_{a,O_2} is decreased, whereas hypercapnia is a state with elevated P_{a,CO_2} level.

variable delays, cerebral blood flow, and a cerebral spinal fluid (CSF) compartment reflecting the influence of H^+ concentration in CSF on ventilation.

During the 1980s, with the advancement of computer simulations, a number of important models were developed. Longobardo et al. (1982) introduced a model of the transition to the sleep state including a representation of sleep apnea. At the same time, Khoo et al. (1982) developed a model in the same family as the Longobardo model to study the stability properties of the respiratory control system. This model was later extended in 1991 to simulate respiration during sleep (Khoo, Gottschalk, and Pack, 1991). It should be mentioned that all of these models are primarily concerned with chemical control of minute ventilation and not with the specific details of the respiratory cycle.

More recently, Batzel and Tran (2000a) extended the models presented in Khoo et al. (1982) and Khoo, Gottschalk, and Pack (1991) by including variable cardiac output (thereby introducing state-dependent delays in the feedback control loop) and infant sleep respiratory patterns such as obstructive apnea and central apnea (which may play a role in connection with sudden infant death syndrome (SIDS)). Numerical simulations were performed with this model to study the stability characteristics of the feedback control system including events of periodic breathing (PB), Cheyne–Stokes respiration (CSR) and apnea as they occur during the transition to quiet (non-REM) sleep in infants of age three to four months. This model was too complicated for a comprehensive analytical stability analysis. Subsequently, Batzel and Tran (2000b, 2000c) introduced two simplified mathematical models and an analysis was performed to understand how the delay inherent in the respiratory control system affects its stability as well as to analyze how elements of physiological control (such as ventilation rate and controller gain) influence stability. Other recent works by Ursino et al. (2001a, 2001b) present a mathematical model of the human respiratory control system consisting of three compartments for gas storage and exchange (lung, brain, and body tissues). The model focuses on the interactions between ventilation and cardiovascular regulation, and between the controller and metabolism in response to hypoxia and hypercapnia. Many other models have been developed, some of which are discussed in the following sections.

2.1 Respiratory Control Physiology

The respiratory system acts in conjunction with the cardiovascular system to deliver O_2 and nutrients required for metabolism and to remove CO_2 which, in this context, is a waste product of metabolism.

Respiration refers to the entire process involved in the exchange of O_2 and CO_2 between the environment and the cells of the body. This includes ventilation (breathing), diffusion of gases in the alveoli, transport of O_2 and CO_2 by the circulatory system, internal respiration (exchange of gases between cells and capillary blood), and cellular respiration (the metabolic processes involving O_2 and CO_2 in the cell).

2.1.1 General features of respiration

Ventilation refers to the rate at which air is moved into the lungs. As metabolic demands vary, so do the utilization of O_2 and the production of CO_2, and the respiratory system must respond to these varying demands. One mechanism available is the feedback control loop, which monitors blood levels of O_2 and CO_2 and varies the level of ventilation in response

to deviations in the levels of these blood gases so as to maintain the stability of the system. This mechanism is referred to as *chemical control of ventilation*. This system operates during periods of rest in the absence of voluntary changes in ventilation, and during sleep.

This is not the only mechanism that regulates ventilation. For example, during exercise, ventilation rises dramatically to respond to greatly increased metabolic demands, but O_2 and CO_2 levels are nearly unchanged from their levels at rest. This implies the existence of another mechanism that does not depend on measured deviations in the levels of these blood gases. This mechanism is not well understood and may involve some form of feedforward mechanism or learned response. Cardiovascular-respiratory function during exercise in general and ventilation control during exercise in particular are currently under active investigation. See, as two examples, Rowell (2004) and Helbling et al. (1997) and the discussion on page 123.

It is also clear that cardiac output and ventilation must be coordinated to some degree, so that efficient loading and unloading of blood gases can be achieved. This coordination includes aspects of ventilation-perfusion matching, synchronization of heart rate and ventilation, the influence of blood gases on cardiovascular function, and other areas which are being actively investigated with potentially important medical applications.

In this chapter, we will focus on modeling and applications of the chemical feedback control system. In any feedback control system, it is necessary to have some means to monitor the state of the system and vary the behavior of the system so as to counteract deviations from steady state operation or to maintain some defined tracking of the system.

The ventilation rate is varied to influence the key quantities of O_2 and CO_2. There are two sensory sites where the blood levels of O_2 and CO_2 are monitored. This information is fed back to the central respiratory center influencing ventilation. In the setting of mathematical control theory, ventilation is referred to as the control function and O_2 and CO_2 are the controlled variables. The ventilatory control system acts to maintain steady state function of the respiratory system by altering ventilation so as to return the system to steady state levels of O_2 and CO_2 after perturbations. Ventilation is determined by the rate and depth of breathing and has the dimension of flow. Minute ventilation, denoted by $\dot{V}_E$, refers to this flow when we use the units liters per minute. Minute ventilation characterizes the average flow of air through the lungs and can be thought as either the inspiratory or expiratory flow.

Exchange of CO_2 and O_2 in the lungs is by passive diffusion, hence, efficient exchange depends on maintaining effective diffusion gradients which can be influenced only by how quickly air is renewed in the alveoli (i.e., alveolar ventilation, $\dot{V}_A$).

Typically, respiratory physiology utilizes partial pressure units for O_2 and CO_2 in both gas and blood phases, with partial pressures denoted by P_{O_2} and P_{CO_2}, respectively. Partial pressures are clearly the right quantities when discussing the gas phase in the lungs and alveoli. In the blood phase, partial pressure is a measure of gas concentration in the blood (for more details see Subsection 2.1.4).

2.1.2 The chemical control system for ventilation

The essential features of the chemical control system in humans are illustrated in Figures 2.1 and 2.2. There are two sensory mechanisms for monitoring systemic blood gas levels and these are illustrated in Figure 2.1.

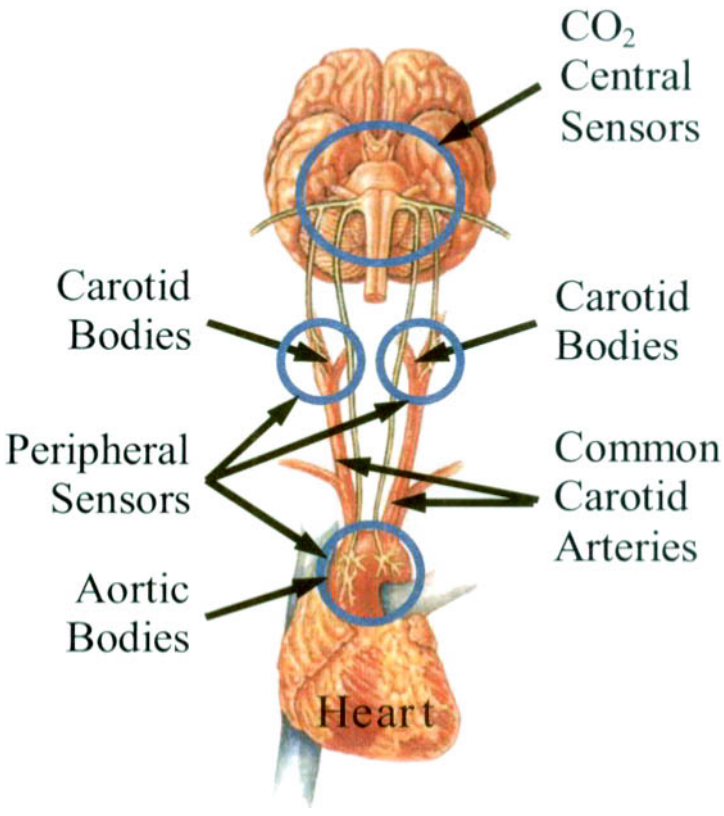

Figure 2.1: Peripheral and central sensory sites.

Chemoreceptors for CO_2 and O_2 are found in the carotid bodies located at the carotid sinuses and also in the aortic bodies near the ascending aorta. These sensors measure systemic arterial levels of these gases and are referred to collectively as the peripheral sensory system. It appears that the carotid bodies are the primary determiners of response, and aortic influence becomes important when carotid response is lacking (Prabhakar and Peng, 2004). Hence, we will be primarily concerned with the sensory loop involving the carotid bodies. CO_2 level in brain tissue is also measured by what is referred to as the central sensory system. Information from both these sensory sites is collected, integrated, and translated into a ventilatory drive signal by the respiratory controller (referred to as the respiratory center) located in the medulla and pons. This ventilatory drive is transmitted to the respiratory (primarily inspiratory) muscles to modulate breathing. The interaction of the sensors, respiratory center, and lung action constitutes a negative feedback loop whose primary components are illustrated in Figure 2.2. Based on information transmitted from the sensors regarding variations in blood gases, the respiratory center responds with changes in ventilation so as to restore the steady state of the system. The two sensory systems influence

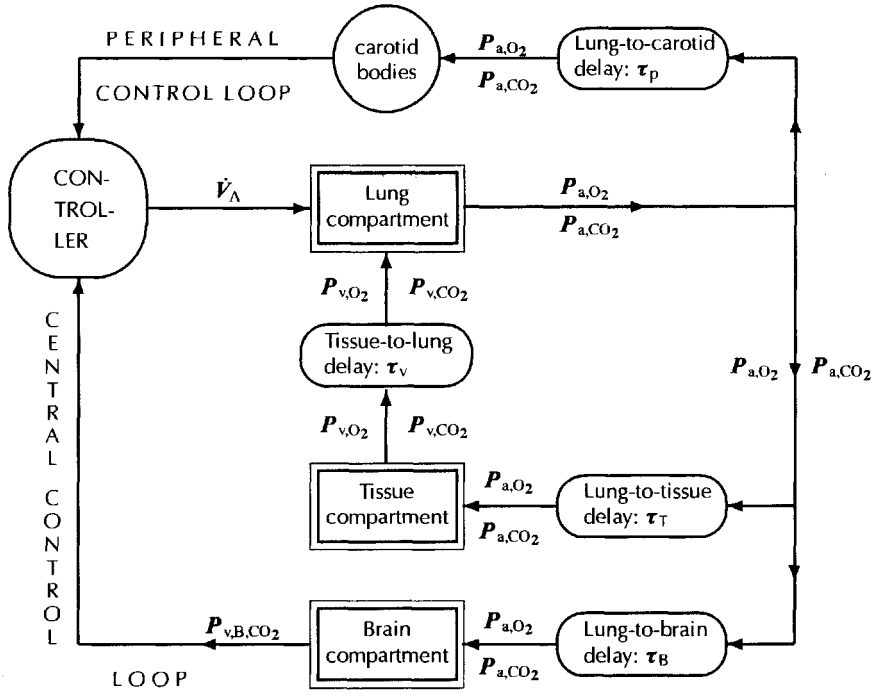

Figure 2.2: Delays and control loops in the respiratory system.

the overall ventilatory response differently, and hence the peripheral and central influences on ventilation are often referred to as the peripheral and central controllers, respectively.

Interaction of peripheral and central controllers

Extensive steady state and dynamic experimental research has been carried out to discover the factors which influence ventilation and to distinguish the influence of the central and peripheral sensory information on ventilation (see, for example, Cunningham, Robbins, and Wolff, 1986). A number of models have been suggested to capture the overall function of ventilatory chemical control.

One of the earliest models of chemical control was provided by Gray (1946) who postulated an independent and additive influence of CO_2, O_2, and pH. This approach greatly influenced the work of other early researchers in this area. As research progressed, Lloyd and Cunningham (1963) were led to postulate a multiplicative interaction of arterial CO_2 and O_2. A number of models have since been proposed which combined multiplicative and additive elements drawn from these early models. For example, Longobardo, Cherniack, and Fishman (1966) included only a multiplicative interaction of the Lloyd-and-Cunningham-type, while Duffin (1972) incorporated a similar relation but only in the peripheral control while assuming an additive delayed CO_2 response for the central control.

The overall picture which has emerged for the response of the respiratory center to changes in CO_2 and O_2 is reasonably represented by an additive interaction of the

peripheral and central controls with a multiplicative interaction between CO_2 and O_2 in the peripheral control (compare discussions in Cunningham, Cherniack, and Fishman, 1986; Duffin, 2005). The central chemosensors are the primary sensors for CO_2, while the peripheral sensors are the primary sensors for O_2 (Lahiri and Forster II, 2003) although new information indicating a higher degree of complexity in the respiratory sensory system is continually emerging. At normal O_2 levels (normoxia), the total ventilatory response is primarily determined by CO_2. There is significant individual variation in the proportional levels of central and peripheral ventilatory drive (Mohan and Duffin, 1997) and we will assume in our modeling that the central control contributes 70–80% of total drive at normoxia (see, for example, Khoo, Gottschalk, and Pack, 1991).

The central controller responds in a broad sense to brain CO_2. This response includes pathways involving H^+ ions and changes in pH in brain tissue including interactions with CSF. The relation between CO_2 and H^+ ions can be seen in (2.3) below. A detailed picture reflecting which cells, sites, and mechanisms are involved in the central control is only now beginning to emerge as can be seen in Nattie (1999), Ballantyne and Scheid (2001), Feldman, Mitchell, and Nattie (2003), and Mulkey et al. (2004). It appears that the central sensory sites are broadly distributed and may involve intracellular and extracellular responses to pH and perhaps a component involving a direct response to CO_2. The reasons for such a complex situation may be the need to sense both the levels of ventilation to match metabolic demands and the the appropriate pH levels to be maintained. The accumulation of various mechanisms may also be explained by a sequence of evolutionary adaptations that have accumulated during periods of changing environmental conditions (see, e.g., Nattie, 1999).

The peripheral controller responds to both CO_2 and O_2. The signal that emerges from the peripheral chemosensors, representing the integrated influence of CO_2 and O_2, reflects a multiplicative interaction of the two gases. Furthermore, the O_2 factor incorporates a nonlinear O_2 response which becomes significant only during a significant drop in O_2 levels, less than 70 [mmHg] (near hypoxic condition). The hypoxic stimulus appears to involve O_2 stimulating the release of neurotransmitters by glomus cells in the carotid bodies (Prabhakar and Peng, 2004). The mode of CO_2 stimulation at the peripheral sensors most likely involves intracellular H^+ ion formation. As CO_2 rises, H^+ ion concentration rises, and this pH reduction in the glomus cells or associated nerve endings of the carotid body triggers neuronal activity (Lahiri and Forster II, 2003).

The blood gases need to be transported a physical distance from the lungs (where gas levels are varied) to the sensory sites (where blood gas levels are measured). This introduces delays in the feedback loops which can affect the stability of the system. These transport delays depend on the blood flows in, for instance, Q_{co} in the aorta or F_B in the carotid artery leading to the brain and the volume of the relevant vasculature which connects the lungs and sensors. Since the delays depend also on the past history of these flows (which are in turn determined by the past state of the system), the delays are state dependent. These delays and their relations to the respiratory control system are illustrated in Figures 2.2 and 2.4. Further analysis of these delays and their role in the stability of the system is given in Section 2.3.

It is interesting to note that the respiratory chemoreceptors in the carotid sinuses are located near the carotid bodies baroreceptors which monitor the arterial blood pressure (similar to aortic sensors). Indeed, the cardiovascular and respiratory systems interact in a

number of ways that will be further discussed in Chapter 3. We mention here the influence of blood gas levels of CO_2 and O_2 on local vascular resistance and on Q_{co}, noting that metabolic effects can influence longer-term control of blood pressure as well. Conversely, as just mentioned, Q_{co} and F_B influence respiratory negative feedback loops via transport delays inherent during the movement of blood gases to the sensory sites located a physical distance from the lungs.

Respiratory center

The respiratory center has three main functions: (a) processing information sent from chemosensors, pulmonary receptors, and higher brain centers; (b) generating a central respiratory pattern based on that information; (c) sending out nerve impulses to stimulate the respiratory muscles to generate that respiratory pattern.

A single breath involves inspiration and expiration. Because the respiratory quotient RQ (i.e., the ratio of CO_2 production to O_2 consumption) varies depending on the type of substrates metabolized (for carbohydrate RQ = 1.0; for fat RQ = 0.70; for protein RQ = 0.80), expiratory ventilation is slightly lower than inspiratory ventilation for the usual mixture of substrates. We will ignore this difference and equate the two in our discussion.

The volume of air in a single inspiration (or expiration) is referred to as tidal volume V_T. Inspiration is the more active process (involving the diaphragm and rib cage muscles to lower the intrapleural pressure in the lungs) and it takes up about 35–40% of the time of a breath. Total minute ventilation (liters inhaled per minute), denoted by $\dot{V}_E$, depends on the rate and depth of breathing:

$$\dot{V}_E = V_T f_v, \tag{2.1}$$

where f_v represents the frequency of breaths per minute and V_T is given in liters per breath (about 0.5 liters for an adult). Different combinations of frequency and tidal volume can produce the same net $\dot{V}_E$ (but different alveolon ventilation ($\dot{V}_A$) as discussed in Subsection 2.2.6).

The respiratory center generates the pattern of depth and rate of breathing. The pattern of breathing is produced by the superposition of at least two pattern sources. A basic respiratory rhythm is contributed by a primary central rhythm generator, and this rhythm is then altered, based on incoming sensory information.

The respiratory center consists essentially of three cell groups located in the pons and medulla: the dorsal respiratory group, the ventral respiratory group, and the pontine respiratory group. These groups interact to generate rhythm, integrate chemosensor information to respond to metabolic requirements, generate the motor output to respiratory motorneurons, and influence the patency (dilation) of the upper airway muscles as well. For further details, see Duffin (2004) and Smith et al. (2000).

While much has been learned on the neurological level about the respiratory center, functional questions, such as how $\dot{V}_E$ is partitioned into combinations of rate and depth of breathing, have been less well resolved. Certainly, the goal of minimizing the work of breathing may be an important factor in determining the pattern of breathing.

2.1.3 Structural features of ventilation

The structural features of the ventilatory system play an important role in the efficiency of the control of ventilation. Air passes from the nose and mouth through the larynx and

pharynx (these last two elements are referred to as the upper airways), and then through a branching tree of conductive tubes (airways) ending in the alveoli which are small air sacs whose thin walls are surrounded by an intricate capillary sheath. Exchange of gases occur at the alveolar-capillary boundary.

The branching process incorporates approximately 23 levels of branches terminating in alveolar sacs. This allows for the placement of between 274 to 790 million alveoli (Ochs et al., 2004) with a mean number of about 480 million alveoli and a surface interface with ambient air on the order of 130 square meters (Weibel and Hoppeler, 2004) (easily the largest interface with the environment). Such a structure would be mechanically unstable if the alveoli were not lined with a surfactant that helps to keep the alveoli open. The terminal alveoli, and several of the lowest conducting branches (alveolar ducts and respiratory bronchioles) containing alveoli, allow for the diffusion of blood gases but the higher branches do not. The diffusion process is promoted not only by the thinness of the alveolar-capillary boundary, but also by the great extent to which the alveoli are intertwined with capillaries. The total volume of those higher branching conducting airways, which do not contribute to gas exchange, is referred to as the *anatomical ventilatory dead space*. At the beginning of each breath, part of the fresh inspired air is maintained in the anatomical dead space, and at the end of each breath a part of the alveolar-capillary equilibrated air is retained in this dead space. This structural feature, together with the *alveolar dead space* consisting of those alveoli which do not effectively exchange blood gases because of malfunction, dampens the net responsiveness of ventilation in responding to changing demands for the exchange of blood gases. The alveolar dead space can be partly compensated for by the tendency for vasoconstriction in areas of underventilation (hypoxic pulmonary vasoconstriction), while the anatomical dead space cannot. The relation describing the net action of ventilation is given by

$$\dot{V}_A = \dot{V}_E - \dot{V}_D,$$

where $\dot{V}_E$ represents minute ventilation (liters inhaled per minute), $\dot{V}_A$ represents the alveolar or effective ventilation, and $\dot{V}_D$ represents the total dead space ventilation. Thus it is $\dot{V}_A$ that really counts in respiratory function.

As mentioned above, the efficiency of the exchange of CO_2 and O_2 in the lungs depends upon maintaining effective diffusion gradients since the exchange is carried out by passive diffusion. CO_2 diffuses much more easily (about 20 times more easily) than O_2 across the alveolar-capillary boundary. Hence, under normal circumstances, the alveolar, capillary, and systemic arterial partial pressures of CO_2 can be essentially identified (Koulouris et al., 2001). Because of the lower efficiency of O_2 diffusion and other factors (Spanoudaki and Myrianthefs, 2004), there is an alveolar-arterial gradient of about 3–6 [mmHg]. This gradient varies with age and other factors and can become significant as a result of certain lung diseases. Ventilation-perfusion matching, denoted by $\dot{V}_A/Q_{co}$, refers to the degree to which an alveolar region is sufficiently perfused with capillary blood so as to efficiently use the available alveolar air. For the lungs as a whole, this represents the matching of total alveolar ventilation $\dot{V}_A$ to total blood flow through the lungs (equal to Q_{co}). The upper regions of the lungs are both underperfused and underventilated due to hydrostatic gravitational effects, but less underventilated than underperfused (higher $\dot{V}_A/Q_{co}$). Hence, there is a mismatch. As one proceeds down the lungs, the influences of gravity and other factors increase the degree of both ventilation and perfusion, but not at the

same rate, causing the lower regions to become overperfused (lower $\dot{V}_A/Q_{co}$). There is a crossing point at which the ideal ventilation-perfusion is perfectly matched. There are certain medical conditions in which such influences have important consequences (see, e.g., Loeppky et al., 2005), but normally, the degree of $\dot{V}_A/Q_{co}$ matching ensures efficient use of alveolar ventilation. As a result of the structural features described above, under normal circumstances, the loading of O_2 and unloading of CO_2 in the lungs is so efficient that the process of equilibration in each red blood cell is completed long before the cell passes out of the pulmonary capillary bed, which ensures that even during exercise when the transit time is greatly reduced, metabolic requirements can be met.

The modeling focus in this book does not require implementing detailed features of lung structure and function. Such features can be important in certain clinical applications such as modeling respiratory function during anesthesia. See, for example, Ottesen, Olufsen, and Larsen (2004).

2.1.4 Blood gas transport

The loading and unloading of blood gases for transport to and from the lungs by the blood depends on a number of important and complex mechanisms. The specific features differ for O_2 and CO_2 and some of these features are discussed below. The partial pressure unit for a gas contained in body tissue fluid and blood is another measure of concentration, drawing the motivation for its use from Henry's law for gas equilibrated with a fluid. This law states that the amount of the gas in a fluid is directly proportional to the partial pressure of the gas above the fluid (in the equilibrium state). Solutions which satisfy this law are called simple solutions.

Due to a number of chemical mechanisms and the presence of hemoglobin (Hb), the carrying capacity of blood for O_2 and CO_2 is higher than it would be if the gases were simply dissolved in blood. As O_2 enters the blood in a dissolved state, it is quickly taken up by Hb, allowing for further O_2 to dissolve, and thereby greatly increasing the blood carrying capacity of O_2.

Similarly, at the alveolar-capillary boundary, CO_2 is also first dissolved in the capillary blood as a simple solution. Much of this CO_2 is taken out of the simple solution and stored in alternate forms (primarily bicarbonate), as described below, leaving room for further CO_2 to dissolve. Dissociation relations have been derived which relate the total concentration of these blood gases to the equivalent partial pressure that would produce these concentrations in a simple solution.

O_2 transport

For normal initial alveolar-capillary O_2 partial pressure gradients (i.e., $\Delta P_{O_2} = 60$ [mmHg]), O_2 equilibration requires about 0.25 seconds. Pulmonary capillary blood remains in contact with alveoli for about 0.75 seconds as it passes through the pulmonary capillaries, and hence complete O_2 equilibration is normally achieved. Because of the presence of Hb, O_2 in blood is not carried merely in a simple solution. Consequently, the O_2 dissociation curve which plots O_2 concentration versus O_2 partial pressure is S-shaped (increasing to the right), flattening out as it approaches the maximum carrying capacity. The concentration–partial pressure relation takes the form (Revow et al., 1989)

$$C_{O_2} = a_o \left(1 - e^{-b_o P_{O_2}}\right)^{c_o}, \tag{2.2}$$

where a_o, b_o, and c_o are positive constants. Moreover, C_{O_2} represents O_2 concentration and P_{O_2} represents O_2 partial pressure. The constants a_o and b_o are varied in the dissociation curve to reflect changes in the O_2 affinity to Hb that arise with the change in age or physical condition. The standard value for c_o is $c_o = 2$, which is also used for the curves in Figure 2.3. The quantity of O_2 saturation, denoted by S_{a,O_2}, is another measure of the O_2 carrying capacity of blood. It characterizes the percentage of utilized Hb carrying capacity,

$$S_{a,O_2} = \frac{[\text{Hb}]_{O_2}}{[\text{Hb}]_{\text{total}}} \times 100.$$

When S_{a,O_2} is plotted as a function of partial pressure, a similar S-shaped curve is found which flattens out as S_{a,O_2} approaches 100%. The O_2 dissociation curve varies depending on the age and physical condition of the individual. At birth and during the first months of life, infant blood contains primarily fetal Hb (see discussion on page 98) which is slowly replaced by adult Hb, a process that is essentially completed in the first year. The change in proportion of fetal to adult Hb (along with certain other changes) alters the dissociation curve as depicted in Figure 2.3, where the parameters a_o, b_o, and c_o are chosen as reported in Revow et al. (1989). Further details can also be found in Delivoria-Papadopoulos and DiGiacomo (1992).

CO_2 transport

For CO_2, although the initial partial pressure gradient at the alveolar-capillary boundary is lower ($\Delta P_{CO_2} = 6$[mmHg]) than for O_2, the increased solubility of CO_2 means that

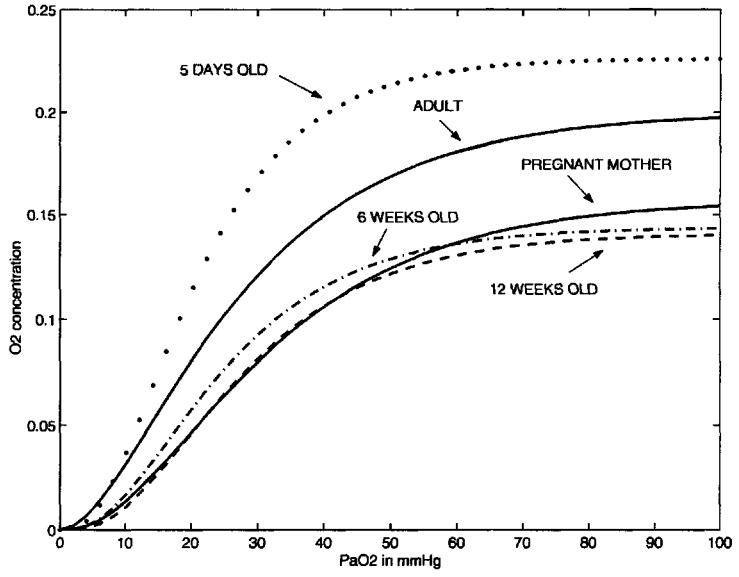

Figure 2.3: Fetal to adult O_2 dissociation curves.

complete equilibration of alveolar and capillary blood is nearly always achieved. CO_2 is transported in several ways: it can be dissolved as a physical solution, combined with Hb and proteins, transported as carbonic acid formed in the reaction described by the left side of (2.3), or transported as bicarbonate ions formed as in the right-hand side of (2.3),

$$H_2O + CO_2 \leftrightarrows H_2CO_3 \leftrightarrows H^+ + HCO_3^-. \tag{2.3}$$

It is important to note that (2.3) exhibits the close connection between CO_2 and hydrogen ions H^+ in solution. The pH value is the negative logarithm of the concentration of H^+ and is a measure for the acid-base balance, a key factor in metabolism. Clearly, ventilation which eliminates CO_2 from the blood can influence the pH level by shifting the direction of the above reaction. Indeed, hyperventilation due to hypoxia that occurs at high altitude can create acid-base imbalance and respiratory alkalosis (Samaja, 1997) as a result of excessive loss of CO_2. This, together with reduced central control CO_2 stimulation, can create an upper bound on effective ventilatory response to hypoxia (Samaja, 1997). The CO_2 dissociation plot of concentration as a function of partial pressure is nearly linear (increasing to the right) in the normal physiological range and can be expressed as

$$C_{CO_2} = K_{CO_2} P_{a,CO_2} + k_{CO_2}. \tag{2.4}$$

Arterial CO_2 partial pressure P_{a,CO_2} is about 40 [mmHg], while interstitial CO_2 partial pressure P_{T,CO_2} is 45–50 [mmHg], thus allowing for efficient equilibration of interstitial CO_2 with venous blood CO_2. At the alveolar-capillary boundary, venous blood eliminates sufficient CO_2 to restore the alveolar-arterial P_{a,CO_2} level to 40 [mmHg].

Bohr and Haldane effects

Recall that dissociation relations have been developed for CO_2 and O_2, which relate the total concentration of these blood gases to an equivalent partial pressure acting in a simple solution. The presence of CO_2 in the blood influences the binding of O_2 to Hb. An important feature of this effect is that the reduction in CO_2 concentration that occurs as blood passes through the lungs promotes O_2 binding (shifting the O_2 dissociation curve to the left), while the increase in CO_2 that occurs in the tissues has the opposite effect, promoting O_2 unloading. This phenomenon is referred to as the Bohr effect.

The level of O_2 bound to Hb in turns affects the level of CO_2 concentration in the blood. As Hb becomes deoxygenated, there is room for CO_2-related compounds (carbamino compounds) to attach to Hb. H^+ also has room to bind with Hb, thus shifting the reaction in (2.3) to the right and allowing for increased formation of carbonic acid. The net result is that a reduction in O_2 raises the carrying capacity of blood for CO_2 (shifting the CO_2 dissociation curve to the left). An increase in O_2 binding has the opposite effect and its influence on carrying capacity of blood for CO_2 is referred to as the Haldane effect. Clearly, the complimentary actions of the Bohr and Hadane effects promote the loading and unloading of blood gases in the lungs and other tissues.

Ideal gas law

In respiratory physiology, experimental results and physiological parameters are reported under a variety of conditions. To understand how to match up various experimental conditions, we need to review some elements of the ideal gas law.

An ideal gas is a gas consisting of atoms and molecules that essentially are points (taking up negligible space), interacting elastically according to kinetic laws, and is characterizable by the three states of temperature T, pressure P, and volume V. Many gases, including gases associated with ventilation, approximate these conditions.

The ideal gas law is a consequence of experimental observations encapsulated in Boyle's law and Charles's law. Combining the observations of these laws, we have

$$PV = KT,$$

where K represents a fixed constant. Holding T fixed the equation states that P and V are inversely proportional (Boyle's law), while holding P fixed implies that T and V are directly proportional (Charles's law). Regularizing units so that we may relate volume to mass (Avogadro's law), we may state the ideal gas law in its usual form

$$PV = nRT, \tag{2.5}$$

where R is the universal gas constant[8] and n the number of moles of the gas. For the same quantity n (in moles) of an ideal gas and any two different configurations, P_i, T_i, and V_i, $i = 1, 2$, for pressure, temperature, and volume, we get from (2.5)

$$\frac{P_1 V_1}{T_1} = \frac{P_2 V_2}{T_2}. \tag{2.6}$$

We could also say that a fixed molar quantity n of an ideal gas varies its volumes depending on the values of pressure and temperature. Given the idealized nature of an ideal gas, we can combine several different such gases, where each holds at the same volume V and behaves independently of the others, leading to the combined gas relation (using (2.5))

$$P_{\text{tot}} V = (n_1 + n_2 + n_3 + \cdots + n_k) RT, \tag{2.7}$$

where n_i represents the molar quantity of the ith gas and P_{tot} is the sum of pressures. Dividing (2.7) by V reveals that we have summed up k independent pressures. Each pressure expression

$$P_i = \frac{n_i RT}{V} \tag{2.8}$$

defines the partial pressure of the ith gas component and is the pressure that would be associated with that gas component if it occupied the entire volume V alone.

This leads directly to the expression of Dalton's law, which states that the total pressure of a mixed gas is the sum of all the individual (partial) pressures of the independent gas components. Dividing the corresponding sides of (2.8) by (2.7) and simplifying allows us to state that

$$P_i = F_i P_{\text{tot}}, \tag{2.9}$$

[8] $R = 8.31$ [J/(°K mol)].

where F_i is the molar fraction of the ith gas. In other words, each individual gas pressure contributes a partial pressure P_i in proportion to its molar fraction F_i of the total molar volume of the combined gas. Note also that for fixed pressure and temperature, we have (Avogadro's law) that the molar and volume fractions of a gas constituent are the same.

We can use these relations to relate experimental values that have been measured under different conditions. Two of the most common types of conditions are

- BTPS (body temperature and ambient pressure, water saturated), where $T = 37°\,\mathrm{C} = 310°\,\mathrm{K}$, P = ambient pressure P_{amb}, and $P_{\mathrm{H_2O}} = 47\,\mathrm{mmHg}$.
- STPD (standard temperature and pressure, dry), where $T = 0°\,\mathrm{C} = 273°\,\mathrm{K}$, P= sea level barometric pressure $P_0 = 760\,\mathrm{mmHg}$, and $P_{\mathrm{H_2O}} = 0\,\mathrm{mmHg}$.

For example, as air enters the respiratory passages, it is warmed to body temperature, and water vapor is introduced from the fluids found on the respiratory airway surfaces. By the time the air enters the alveoli, it has become fully saturated with water vapor at 47 [mmHg] while maintaining the same total pressure (which must be the same inside and outside the body). Hence, ventilatory flows and volumes are most easily reported in BTPS units. On the other hand, metabolic quantities and blood phase values are usually given in STPD units, allowing for standardized measurements. Hence, in mass balance equations involving both blood phase and gas phase quantities (and parameters), a conversion factor relating BTPS and STPD must be included. This conversion is based on the formulation of the ideal gas law given in (2.6), that is,

$$\frac{760\,V_{\mathrm{STPD}}}{273} = \frac{(P_{\mathrm{amb}} - 47)\,V_{\mathrm{BTPS}}}{310}.$$

In the above equation, we are correcting for the added water vapor before making the conversion given that the reference fractional values of component gases in air are normally given for dry air. Water vapor acts as an ideal gas in some ways, but the quantity of water vapor that can be held in air changes with temperature, distorting the normal ideal gas law relation. This is why constituent gas volume reference fractions are usually given for dry air. Solving for V_{BTPS} in terms of V_{STPD} gives

$$V_{\mathrm{BTPS}} = \frac{863}{(P_{\mathrm{amb}} - 47)}\,V_{\mathrm{STPD}}, \tag{2.10}$$

which indicates that the V_{BTPS} is approximately 1.2 times larger than V_{STPD} at sea level, where $P_{\mathrm{amb}} = 760$.

2.1.5 Respiratory control stresses and problems

Obviously, given the complicated interdependencies of the various mechanisms involved in respiratory function, there are many avenues by which dysfunction can be introduced. Smoking-related alveolar dysfunction and other forms of COPD (chronic obstructive pulmonary disease) introduce problems with ventilation-perfusion matching and efficient respiratory function. These problems could be generically modeled as increases in physiological dead space (sums of anatomical and alveolar dead spaces).

Rather than focusing on dysfunction caused by disease-related anatomical changes, in the modeling applications to follow, we wish to consider problems related to the control of respiration and to consider the mathematical and physiological issues related to the stability of the system. There are a number of areas in which natural changes induce problems for the stable control of the system.

One key area is the phenomenon of apnea or cessation of ventilatory flow. This can be caused by either a blockage in air flow or a loss of breath drive. The former is termed obstructive apnea (OA) and the latter central apnea (CA). Especially during sleep, when muscle tone is reduced, the upper airways (pharynx and larynx) are susceptible to partial or total collapse, and hence air flow obstruction. The total blockage of airflow during sleep is termed obstructive sleep apnea (OSA). Even partial obstruction creates difficulties for stable control. Furthermore, the reduction in muscle tone during sleep can also reduce the responsiveness of the ventilatory muscles, and this can attenuate the influence of any control response.

Such changes in control responsiveness to the state of the system during sleep, combined with delays in the feedback loops, may also result in inappropriate or out-of-phase respiratory control action, which can result in a loss of ventilatory drive and cessation of breathing. When this occurs during sleep, it is termed central sleep apnea (CSA). Reduced cardiac output (such as during CHF), which lengthens the feedback delay, can also contribute to system instability. Furthermore, cardiovascular disease, including heart failure (HF) and OSA, are linked (Hamilton, Solin, and Naughton, 2004; Hoffmann et al., 2004). Such issues, discussed further below, have clinical importance.

We mention also the lung inflation/deflation reflex (often referred to as the Hering–Breuer reflex), which depends on lung stretch receptors that provide information on the degree of lung expansion or contraction. This reflex may play some role in the pattern of inspiration and expiration in humans, but it is usually activated in adults only after thresholds beyond the usual tidal volume variations. However, in newborns this reflex may play a more important role in regulating lung volume, and sleep state may influence its action (see, for example, Hand et al., 2004).

2.1.6 Approaches to modeling respiratory control

A number of historically important modeling attempts were mentioned in the introduction to this chapter. Modeling efforts can be classified in several ways: models that seek to study particular aspects of respiration to reduce the model to the simplest configuration consistent with the problem (minimal models); models that attempt to include all relevant known physiological features connected to the problem (intermediate models); and models that seek to map the current state of knowledge about the system as a whole (comprehensive models).

A major focus of research (which has many clinical applications) has been the control of ventilation, and in particular the study of the stability of the control system. We will provide examples of such (intermediate) models and their clinical significance in Section 2.4. Examples of minimal models of respiratory control include Glass and Mackey (1979), Carley and Shannon (1988), and Cleave et al. (1986), which were used to examine the stability properties of respiratory control, including the conditions for PB and the existence of Hopf bifurcations in the transition to unstable behavior. Such simplified models are

designed to test certain hypotheses about respiratory control function or to provide proof of concept. But such models do not include sufficient physiological details needed to study the interaction of various processes or, in general, to be applied to clinical situations. In the minimal models cited above, the goal was to consider influences of blood gases on total averaged ventilation as measured by minute ventilation, and thus these models ignored the details of the discrete process of individual breath-to-breath action as well as the influence of anatomical and physiological features, all of which can play significant roles in, for instance, OA.

Examples of intermediate models which are able to provide clinically usable insight include the work on modeling instability during sleep by Khoo, Gottschalk, and Pack (1991) and Longobardo, Cherniack, and Fishman (1989). We will now consider in detail an intermediate compartment model that takes into account numerous physiological features of respiratory control.

2.2 Respiratory Control Model

A survey of the modeling literature reveals that the majority of the models describe the respiratory system in terms of compartmental models (see, for example, Khoo et al., 1982; Batzel and Tran, 2000a). By a compartmental model we mean a model consisting of elements (compartments) that represent homogenous tissues or discrete organs for which state variables are assumed well mixed and no internal structure is assumed. The differential equation, describing the rate of change of a substance in a compartment, is based on a perfusion-limited model, or equivalently, a flow-limited model of disposition, and is derived from the mass conservation principle. That is, the rate of change of the substance in the compartment equals the total flow into the compartment minus the total flow out of the compartment. Another approach for modeling the respiratory system is to concentrate on the function of specific subsystems such as the lungs. In particular, several models exist in the literature which use an electrical circuit analogue to represent the pressure and airflows in the lungs (see Rideout, 1991). In these models, capacitors, resistors, inductors, and diodes are used to represent compliance, resistance, inertia, and valves, respectively.

As is appropriate to any discussion of mathematical modeling of complex systems, such as the respiratory control system, a balance must be maintained between complexity and simplicity. The models must be of high fidelity to accurately describe the mechanisms and the dynamics of the underlying process. On the other hand, reasonable assumptions and simplifications must be made, so that the mathematical models are tractable at least from a computational point of view. In this section, we will discuss a mathematical model for the respiratory control system as described in (Batzel and Tran, 2000a). This physiologically based model, which is proposed by Khoo, Gottschalk, and Pack (1991), consists of three compartments (the lungs, the brain, and the body tissues) for blood gas exchange and storage. The brain compartment is necessary to allow tracking of cerebral CO_2, which provides input to the central controller in the brain. Together, the central and peripheral controllers constitute the ventilation control system (see Section 2.1 for additional discussions).

The model consists of five state variables representing the partial pressures (or concentrations) of the blood gases, CO_2 and O_2 in the lungs and tissues, and CO_2 in the brain. Since a cardiovascular submodel is not included, cardiac output Q_{co} and blood flows F_s and F_p are equated. Alveolar partial pressures are equated with systemic arterial partial

pressures, and tissue concentrations with systemic venous partial pressures. We will use, as state variables, symbols which emphasize the systemic arterial (high O_2 and low CO_2) levels and systemic venous (high CO_2 and low O_2) levels (see below).

We begin the model development by making the following assumptions.

(i) Temperature in the body, humidity in the body, and ambient pressure are constant.

(ii) Arterial and alveolar CO_2 are assumed equal, while a small O_2 alveolar-arterial gradient is included where noted. Also, tissues and venous blood gases are in equilibrium.

(iii) The alveoli and pulmonary capillary spaces are two well-mixed interfaced compartments with detailed structure and flows omitted.

(iv) Gas exchange is by diffusion (recalling that the alveolar space represents a very large surface area and the blood gas barrier between the alveoli and intertwined capillaries is extremely thin, allowing for efficient diffusion of gases in both directions).

(v) The central sensor responds to cerebral CO_2 partial pressure (detailed aspects of mechanisms involving H^+, pH, and CSF involvement are subsumed under the net general response to the level of CO_2).

(vi) The left and right lungs behave alike and airflows are the same in each lung.

(vii) The effective ventilatory flow is 0.70 of the total minute volume.

(viii) Intercardiac shunting (about 2%) is negligible.

In the following, we will describe the three compartments that constitute the model for the respiration control system.

2.2.1 The lung compartment

As discussed earlier, the convenience of compartmentalization is that it leads directly to a set of dynamical equations based on simple balance relations. This can be stated simply as

$$\begin{aligned}\text{change in compartment } j \;=\; &(\text{sum of all transfers into compartment } j)\\ &-(\text{sum of all transfers out of compartment } j)\\ &+(\text{creation within compartment } j)\\ &-(\text{destruction within compartment } j).\end{aligned}$$

From the schematic diagram of the respiratory control system depicted in Figure 2.2, one can immediately write the dynamical equations for the lung compartment by writing the mass balance equations for the rate of change of the lung CO_2 and O_2 volumes. That is,

$$\begin{aligned}V_{A,CO_2}\dot{F}_{A,CO_2} &= F_p\left(C_{v,CO_2} - C_{a,CO_2}\right) + \dot{V}_A\left(F_{i,CO_2} - F_{A,CO_2}\right),\\ V_{A,O_2}\dot{F}_{A,O_2} &= F_p\left(C_{v,O_2} - C_{a,O_2}\right) + \dot{V}_A\left(F_{i,O_2} - F_{A,O_2}\right),\end{aligned} \tag{2.11}$$

where F_{A,CO_2}, respectively, F_{A,O_2}, is the fractional concentration of CO_2, respectively, of O_2, in the lung compartment (i.e., in the alveolar region), F_{i,CO_2} and F_{i,O_2} are the analogous quantities for inspired air, F_p is the pulmonary blood flow, C_{v,CO_2} refers to the (high) venous blood concentration of CO_2 coming from the tissue compartment, and C_{a,CO_2} refers to the (low) concentration of CO_2 remaining in the blood after lung unloading, which will also be the concentration of the arterial blood flowing to the tissue compartment. Moreover, V_{A,CO_2} denotes the effective CO_2 volume in the lung compartment, whereas V_{A,O_2} is the analogous quantity for O_2. The first term on the right-hand sides of both equations accounts for the net change in CO_2, respectively, O_2, concentration due to gas transport by blood flow. The second term on the right-hand sides of both equations accounts for the net change in CO_2, respectively, O_2, concentration due to alveolar ventilation. The sum of the two terms gives the total change in alveolar CO_2, respectively, O_2, concentration.

Distinction is made between V_{A,CO_2} and V_{A,O_2}. While V_{A,O_2} is essentially the same as the actual gas volume in the lungs, V_{A,CO_2} is distinctively larger because CO_2 (which as we have noted passes easily into solution) dissolves into lung tissue and fluid, which represent a storage volume of the gas in addition to the lung volume. See, for example, the values provided in Khoo et al. (1982). Also note that the above relations must be in BTPS, STPD, or other units. Typically ventilation values, volumes, and parameters are given in BTPS units, while blood gases concentrations are given in STPD units (as are the metabolic rates which appear in the tissue compartment equations (2.13) below). We match up the units by using (2.10) to convert the concentration terms in (2.11) (given in STPD) to BTPS. To derive the final form of the lung compartment equations of the model, we next substitute the following relations (of the form found in (2.9)) into (2.11):

$$\begin{aligned} P_{A,CO_2} &= F_{A,CO_2}(P_{amb} - 47), \\ P_{A,O_2} &= F_{A,O_2}(P_{amb} - 47), \\ P_{i,CO_2} &= F_{i,CO_2}(P_{amb} - 47), \\ P_{i,O_2} &= F_{i,O_2}(P_{amb} - 47). \end{aligned}$$

We set $P_{amb} = 760$ for sea level pressure.

Lastly, according to assumption (ii) above, we make use of two simplifying assumptions: $P_{A,CO_2} = P_{a,CO_2}$ and $P_{A,O_2} = P_{a,O_2}$. We arrive at the following lung compartment model equations:

$$\begin{aligned} V_{A,CO_2}\dot{P}_{a,CO_2} &= 863F_p\left(C_{v,CO_2} - C_{a,CO_2}\right) + \dot{V}_A\left(P_{i,CO_2} - P_{a,CO_2}\right), \\ V_{A,O_2}\dot{P}_{a,O_2} &= 863F_p\left(C_{v,O_2} - C_{a,O_2}\right) + \dot{V}_A\left(P_{i,O_2} - P_{a,O_2}\right). \end{aligned} \tag{2.12}$$

We emphasize again, for clarity and future reference when we combine the cardiovascular and respiratory models, that in this respiratory model setting we identify concentrations of blood gases in venous blood coming from the tissues with gas concentrations in pulmonary arterial blood. Likewise, gas concentrations in systemic arterial blood are identified with those in pulmonary venous blood. Furthermore, in this setting, where we do not include left and right hearts, we make the identification

$$F_p = F_s = Q_{co},$$

where Q_{co} represents cardiac output. In the tables in this chapter we report the value Q_{co}, but in the next chapter we will include separate pulmonary and systemic flows.

2.2.2 The tissue compartment

The tissue compartment in the model presented here is a lumped compartment including all tissue (including brain tissue) metabolic activities. The equations are derived in a similar fashion to those developed for the lung compartment. Mass balance equations reflect the production and removal of CO_2 and the delivery and uptake of O_2 in the tissue compartment, related to the processes that sustain metabolic activity. Because the diffusion process between capillary and cell is rapid, we are justified in assuming that the tissue and venous blood gas levels are equilibrated (see also the above list of assumptions):

$$C_{T,CO_2} = C_{v,CO_2},$$
$$C_{T,O_2} = C_{v,O_2}.$$

Consequently, the equations governing the exchange of gases in the tissue compartment are given by

$$\begin{aligned} V_{T,CO_2}\dot{C}_{v,CO_2} &= MR_{CO_2} + F_s\left(C_{a,CO_2} - C_{v,CO_2}\right), \\ V_{T,O_2}\dot{C}_{v,O_2} &= -MR_{O_2} + F_s\left(C_{a,O_2} - C_{v,O_2}\right). \end{aligned} \tag{2.13}$$

The left-hand sides of these equations represent the change in CO_2 volume, respectively, O_2, in the tissue compartment. The change in CO_2 volume in the tissue compartment is calculated by multiplying the fixed effective CO_2 volume V_{T,CO_2} with the change in CO_2 concentration C_{v,CO_2}. The change in O_2 volume is calculated analogously. The right-hand sides of equations (2.13) describe the net volume changes in terms of the metabolic production of CO_2, denoted by MR_{CO_2}, and its removal described by the net change in the arterial and venous blood CO_2 concentrations, denoted, respectively, by C_{a,CO_2} and C_{v,CO_2}, for the blood flowing through the tissues. The net volume change is found by multiplying concentrations by the tissue (systemic) blood flow F_s. Analogous considerations for the change in O_2 volume lead to the second equation in (2.13).

2.2.3 The brain compartment

In this model, brain tissue is lumped into the general tissue compartment. It would be easy to subdivide the general tissue compartment into brain tissue and nonbrain tissue compartments (see, e.g., Grodins, Buell, and Bart, 1967) and, likewise to subdivide general tissue blood flow F_s into cerebral and noncerebral blood flows. However, for our purposes, we need only track brain CO_2 levels, needed as input to the central ventilatory control. We can do this with the following relation:

$$V_{B,CO_2}\dot{C}_{v,B,CO_2} = MR_{B,CO_2} + F_B\left(C_{a,CO_2} - C_{v,B,CO_2}\right),$$

where V_{B,CO_2} denotes the fixed effective in volume of CO_2 brain tissue compartment, MR_{B,CO_2} represents brain CO_2 metabolic production, F_B denotes cerebral blood flow (CBF), and C_{v,B,CO_2} denotes CO_2 concentration in the venous blood leaving the brain compartment. This relation follows analogously from the mass balance relations for the general tissue compartment and from the assumption that CO_2 concentrations in brain tissue and brain venous blood are equilibrated. That is,

$$C_{B,CO_2} = C_{v,B,CO_2},$$

where C_{B,CO_2} represents the concentration of CO_2 in brain tissue. Given that proper brain function is vital, brain metabolic activity and CBF tend to be tightly regulated and the subsystem is, to a large extent, isolated from outside effects. Thus we assume F_B to be constant. This simplification is reasonable except under special conditions such as excessive hypercapnia. Models for the dependence of CBF on CO_2 levels, such as those found in Fincham and Tehrani (1983b), can be included in the model, along with subdivision of the tissue compartment into brain and nonbrain tissue, if the level of modeling or physiological conditions warrant.

2.2.4 Dissociation relations

Dissociation formulas are used to relate concentrations to partial pressures. For O_2, the relation takes the form presented in (2.2). The parameters in this relation change depending on age and physiological condition. For CO_2, a linear relation, as given by (2.4), is reasonable over the physiologically reasonable range of values for CO_2.

2.2.5 State delays

Having set up the mass balance equations, we must now take into account the fact that arterial and venous concentrations are transported by finite blood flows, and hence transport delays must be included in the model equations. These delays are depicted in Figure 2.2. For example, in the first equation of (2.14), we are considering the drop in CO_2 concentration as the venous blood passes through the lungs coming from the tissue compartment and exiting as the arterial concentration heading to the tissue compartment. The exchange in the lungs at time t involves venous blood that was in the tissue compartment at an earlier time, since the blood flow had to transport the venous or tissue concentration (recall that we equate these quantities) from the tissue compartment to the lungs (which takes some finite time $\tau_v > 0$). Hence, we have to evaluate C_{v,CO_2} in (2.12) at time $t - \tau_v$. Thus the venous-arterial CO_2 gradient in the lung takes the form

$$C_{v,CO_2}(t - \tau_v) - C_{a,CO_2}(t)$$

in (2.12). The value for τ_v depends on the blood flow F and the vascular geometry of the path from the tissue region to the lungs.

Similar considerations are used to incorporate the other delays depicted in Figure 2.2. This leads to the following system of delay equations:

$$\begin{aligned}
V_{A,CO_2}\dot{P}_{a,CO_2}(t) &= 863F_p\left(C_{v,CO_2}(t-\tau_v) - C_{a,CO_2}(t)\right) \\
&\qquad + \dot{V}_A\left(P_{i,CO_2} - P_{a,CO_2}(t)\right), \\
V_{A,O_2}\dot{P}_{a,O_2}(t) &= 863F_p\left(C_{v,O_2}(t-\tau_v) - C_{a,O_2}(t)\right) \\
&\qquad + \dot{V}_A\left(P_{i,O_2} - P_{a,O_2}(t)\right), \\
V_{T,CO_2}\dot{C}_{v,CO_2}(t) &= MR_{CO_2} + F_s\left(C_{a,CO_2}(t-\tau_T) - C_{v,CO_2}(t)\right), \\
V_{T,O_2}\dot{C}_{v,O_2}(t) &= -MR_{O_2} + F_s\left(C_{a,O_2}(t-\tau_T) - C_{v,O_2}(t)\right), \\
V_{B,CO_2}\dot{C}_{v,B,CO_2}(t) &= MR_{B,CO_2} + F_B\left(C_{a,CO_2}(t-\tau_B) - C_{v,B,CO_2}(t)\right).
\end{aligned} \tag{2.14}$$

Further discussion on the nature of the delays in the system and their relation to stability is given in Section 2.3.

2.2.6 Empirical control equation

From the discussion in Subsections 2.1.2 and 2.1.4, it is clear that there is a close connection between CO_2 and H^+ in the processes controlling ventilation (see also Lahiri and Forster II, 2003). The pathways by which CO_2 and H^+ interact to stimulate the peripheral and central chemosensors are complex. For our modeling purposes, when we speak of the influence of CO_2 on ventilation, we are in fact discussing the net effect, omitting the details on the chemical and cellular levels.

A relationship describing the dependence of minute ventilation $\dot{V}_E$ on P_{a,CO_2}, P_{a,O_2}, and P_{v,B,CO_2} is given by

$$\begin{aligned}\dot{V}_E = {} & G_P e^{-0.05 P_{a,O_2}(t-\tau_p)} \max\bigl(0,\, P_{a,CO_2}(t-\tau_p) - I_P\bigr) \\ & + G_C \max\Bigl(0,\, P_{v,B,CO_2}(t) - \frac{M R_{B,CO_2}}{K_{CO_2} F_B} - I_C\Bigr).\end{aligned} \tag{2.15}$$

The first term in (2.15) describes the effect of the blood gases P_{a,CO_2} and P_{a,O_2} on ventilation, as sensed by peripheral sensors located in the carotid artery. This effect will be referred to as the peripheral control ($\dot{V}_P$). The second term describes the effect of P_{v,B,CO_2} on ventilation and will be referred to as the central control ($\dot{V}_C$). This expression for ventilation, taken from Khoo et al. (1982), is based on experimental observations as in Cunningham, Robbins, and Wolff (1986). A transport delay τ_p between the lungs and peripheral control appears in this equation. The parameters G_P and G_C represent the peripheral and central controller gains, respectively. These gains influence the responsiveness of the control system to changes in sensory information provided by the peripheral and central respiratory sensors. The parameters I_C and I_P denote cutoff thresholds, so that the respective ventilation terms become zero when the quantities fall below these thresholds. Ventilatory dead space effects can be accounted for by defining the relation

$$\dot{V}_A = E_F \dot{V}_E, \tag{2.16}$$

where $\dot{V}_A$ is the alveolar ventilation, which reflects, the air volume involved in effective gas exchange, and E_F is a constant smaller than 1. In this way, total minute ventilation is reduced by a fixed percentage of dead space, which amounts to modeling the change in ventilation as a change in rate of breathing. This, in essence, represents a scale reduction in the control gains G_C and G_P, which is reasonable since the dead space reduces the effectiveness of breathing (see, e.g., Batzel and Tran, 2000a). A second way to account for the dead space is described by

$$\dot{V}_A = \dot{V}_E - \dot{V}_D. \tag{2.17}$$

In this relation a fixed quantity $\dot{V}_D$ is subtracted from $\dot{V}_E$. As this reflects a fixed dead space independent of the increases and decreases in $\dot{V}_E$, the relation implies that ventilation is changed by altering the depth of breathing. The above expressions describe the basic features of respiratory control.

Alternate formulas can be used to refine these features. For example, we can derive a ventilation model that changes the total minute ventilation by changing both the rate and

depth of breathing as is most commonly the case in humans. Also, using the formula given by Severinghaus (1979) to relate P_{a,O_2} and O_2 saturation

$$S_{a,O_2} = 100\left(1 - 2.4e^{-0.05P_{a,O_2}}\right), \tag{2.18}$$

we can relate ventilation to O_2 saturation using the following formula which also incorporates a small fixed peripheral drive at 100% saturation:

$$\begin{aligned}\dot{V}_E = {} & G_P\left(102.4 - S_{a,O_2}(t-\tau_p)\right)\max\left(0,\, P_{a,CO_2}(t-\tau_p) - I_P\right) \\ & + G_C\max\left(0,\, P_{v,B,CO_2}(t) - \frac{MR_{B,CO_2}}{K_{CO_2}F_B} - I_C\right).\end{aligned} \tag{2.19}$$

Obviously, in this last formula, the value of control gain parameter G_P must be adjusted from that given in (2.15). Both formulas (2.15) and (2.18) are used in simulations, and this is noted in the relevant tables. These controls represent a compromise between the requirement of sufficient complexity, to allow for the representation of important features of the control system, and the constraint of being simple enough to allow for analytic treatment. This is always one of the issues (along with issues of model identifiability and parameter estimation) to be considered in devising a modeling approach.

As mentioned in Section 2.1, much research has been done on clarifying the nature of ventilatory control, and other forms for the control relation have been proposed. See, for example, the controls suggested in Fincham and Tehrani (1983a), Longobardo et al. (1982), and Duffin (2005).

2.2.7 Minute ventilation and tidal volume

A first approximation of tidal volume behavior can be included by considering the details associated with a single breath. During inspiration, leftover exhaled air remaining in the dead space of the lungs (the branching conducting tubes which do not exchange gases) is included in the inflowing alveolar air (approximately 150 [ml] for an adult). Thus, in terms of a time profile, the first segment of inspired air does not have the same CO_2 and O_2 concentration profile as fresh air. As inspiration continues and more fresh air enters the alveoli, the overall alveolar gas content approaches closer to that of normal air. Clearly, also expired air provides a different concentration profile of CO_2 and O_2 compared to fresh air, and little gas exchange occurs during expiration. Hence, the effective time frame for blood gas transfer is only part of the overall duration of a breath. This can be simply implemented by partitioning the time of a breath and replacing $\dot{V}_A$ on each breath interval with a value V_{eff} as follows. During the first segment of inspiration (until the air in the dead space has passed into the lungs), $\dot{V}_{eff}$ should be a reduced level of $\dot{V}_A$. During the remaining segment of inspiration, $\dot{V}_{eff}$ should equal the $\dot{V}_A$ representing the inflow of normal gas concentrations. Finally, during expiration $\dot{V}_{eff}$ will again be a reduced level of $\dot{V}_A$. Furthermore, V_{A,CO_2} and V_{A,O_2} are varied during inspiration and expiration, depending on $\dot{V}_E$. See Khoo and Kronauer (1983) for a discussion of such an approach. Note that the actual chemical drive in the model will be proportionally larger to force the flow of fresh air through the lung compartment during the fresh air phase of inspiration (a factor of about 2.5). For other approaches to modeling breath-to-breath behavior, see Saunders, Bali, and Carson (1980).

A small alveolar-arterial O_2 gradient can be introduced by reducing P_{i,O_2} by the desired amount.

2.2.8 Cardiac output and CBF

In this chapter, we are focusing on the respiratory control system. The implementation of CVS mechanisms which alter Q_{co} were discussed in Chapter 1 and will be further developed in Chapter 3 along with mechanisms that influence F_B. However, as discussed in Subsection 3.1.4, Q_{co} and F_B are also influenced by blood gases, and this dependency is reflected in data from sources such as Richardson, Wasserman, and Patterson, Jr. (1961). A model based on numerical interpolation of such data, reflecting the dependency of Q_{co} on arterial blood gas pressures P_{a,CO_2} and P_{a,O_2} but not based on physiological mechanisms, has been devised by Fincham and Tehrani (1983b). A similar model for F_B dependent on P_{v,B,CO_2}, discussed in Khoo (1989), is based on information such as that provided in Lambertsen (1980). The models predict variations in these blood flows from reference levels as blood gas levels change. While the interaction of blood gas levels with CVS function is in reality much more complicated, and the dynamics is somewhat slower, these simple models can be used to exhibit the elements involved in determining transport delays.

As we are interested in studying individual physiological effects, the flows F_B and Q_{co} are, in general, explicitly given as functions of time or assumed constant. We implement the dependence of F_B and Q_{co} on blood gases in the CHF case (scaling for reduced Q_{co}) in Subsection 2.4.3 and provide calculated values for the various transport delays. Further discussion on this can be found in Subsection 2.3.1.

2.3 Stability of Respiratory Control

2.3.1 Computation of the delays

The transport delays discussed in Subsection 2.2.5 were described as dependent on both the flows that fill the related vascular volumes through which the flows travel and the size of these vascular volumes. We assume the flow dynamics to be that of an incompressible fluid. For the arterial vascular elements, we assume that they are rigid so that changes of flow in time will be simultaneous at all parts of the vascular elements. The venous vascular elements are much more compliant, and this leads to more complicated mechanisms for determining the transport delay from the tissue compartment to the lung compartment.

For simplicity, we consider first the lung-to-brain path. The delay components determining the net lung-to-brain delay are depicted in Figure 2.4. A bolus of blood volume at the lungs will be transported to the left heart, then through a section of the aorta (where flow is specified by Q_{co}), and finally through the carotid arteries (where the flow is given by F_B) to the sensory site in the brain. To motivate the idea for computing the delay, let us assume that a weightless elastic membrane is pushed along the vascular path by the blood flow and extends always over the total cross section, thus preventing any flow around the membrane. Then the time it takes for this membrane, starting at the lungs, to reach the brain will be the time it takes to fill the volume of the vascular path from lung to brain.

The time τ it takes a bolus of blood, which starts at the origin of the carotid artery at time $t - \tau$, to reach the sensory site in the brain at time t has to satisfy the condition

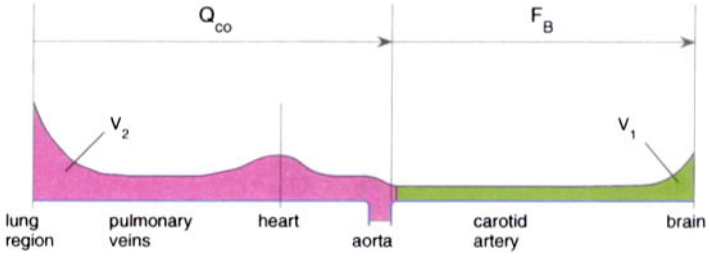

Figure 2.4: Computation of transport delays.

$$\int_{t-\tau}^{t} F_B(s)\,ds = \int_{-\tau}^{0} F_B(t+s)\,ds = V_1,$$

where V_1 is the volume of the vasculature connecting the origin of the carotid artery with the sensory site in the brain. Adopting the notation for the past history of a function introduced in Section C.1 in Appendix C, we can write this as

$$\int_{-\tau}^{0} (F_B)_t(s)\,ds = V_1. \tag{2.20}$$

Next, we have to compute τ_B such that a bolus of blood leaving the lung at time $t - \tau_B$ reaches the origin of the carotid artery at time $t - \tau$. This time τ_B is determined by

$$\int_{t-\tau_B}^{t-\tau} Q_{co}(s)\,ds = \int_{-\tau_B}^{-\tau} Q_{co}(t+s)\,ds = V_2,$$

where V_2 is the volume of the vasculature connecting the lung with the origin of the carotid artery (which comprises pulmonary veins, the left heart, and a small section of the aorta). This can be written as

$$\int_{-\tau_B}^{-\tau} (Q_{co})_t(s)\,ds = V_2. \tag{2.21}$$

A bolus of blood leaving the lung region at a time different from $t - \tau_B$ cannot reach the sensory site in the brain at time t, which shows that τ_B is a point delay (and not a distributed delay).

From the discussion in Subsection 2.2.8, it can be seen that F_B and Q_{co} are related to the present and past values of the blood gas concentrations, and thus to the state of the system (see Section C.1 of Appendix C for the definition of the state of a delay differential equation). This relation relating the flows F_B and Q_{co} to the blood gas concentrations is very complex, but it can be represented by an empirical relation obtained from previous data (see Fincham and Tehrani (1983b) for details). In the discussion of the cardiovascular-respiratory system (CVRS) in Chapter 3, the dependence of the flows on blood gas concentration is further examined (see Subsection 3.1.4). Consequently, τ_B, defined by conditions (2.20) and (2.21), is a function of the state x_t,

$$\tau_B = \tau_B(x_t);$$

i.e., the length of this delay at any time t depends on the present and past behaviors of the system. For simplicity, in many situations F_B and Q_{co} are assumed to be explicitly given functions of time. Then conditions (2.20) and (2.21) imply that also τ_B is a fixed function of time, $\tau_B = \tau_B(t)$. If F_B and Q_{co} are constant, then τ_B is given by

$$\tau_B = \frac{V_1}{F_B} + \frac{V_2}{Q_{co}}.$$

If $f_0 > 0$ is a lower bound for the flows F_B, Q_{co}, then we have the estimate $\tau_B \geq (V_1 + V_2)/f_0$. In modeling CHF in Subsection 2.4.3, we implement the dependence of F_B and Q_{co} on the blood gases, CO_2 and O_2, as described in Subsection 2.2.8, and calculate the delay τ_B as explained above.

Analogous statements are true for the delays τ_p, τ_v, and τ_T. In the case of τ_v, conditions (2.21) should be replaced with more complicated ones, which include the effects of the considerably larger compliance of the venous vasculature which cannot be neglected. In particular, it cannot be assumed that at a fixed time t the flow is constant along segments of the connecting vasculature.

Sample values for the various transport delays can be found in Grodins, Buell, and Bart (1967), Khoo et al. (1982), and Batzel and Tran (2000c), with a range of 6–10 seconds for the lung-to-carotid delay τ_p (Lorenzi-Filho et al., 1999). In general, our values for the delays (see the tables in Section 2.4) are compromises between the values reported in the literature. The lung-to-brain delay τ_B is set to a slightly larger value, as given in Grodins, Buell, and Bart (1967), Khoo et al. (1982), and Khoo (2000), although the overall effective dynamics of central response may be longer (see, for example, Yang and Khoo, 1994; Lorenzi-Filho et al., 1999). Values for τ_T, τ_v are similar to those given in Grodins, Buell, and Bart (1967). When variable cardiac output is simulated, delays are calculated, as explained above, using vascular volume quantities similar to those given in Grodins, Buell, and Bart (1967).

2.3.2 Stability and delays

For the remainder of this section we will consider the effect of the delays, which are inherent in the respiratory control system, on the stability of the system (see Appendix C for a brief overview of the stability theory for linear delay differential equations). In addition, we will analyze some of the structure of the physiological control to see how this structure works to maintain stability.

This control takes the form of a negative feedback loop, as discussed in Subsection 2.1.2. That is to say, the control response is varied based on the state of the system, acting to stabilize the system around a fixed steady state as illustrated in Figure 2.5. In this figure we consider only the P_{a,CO_2} sensory component. The decrease in ventilation raises P_{a,CO_2}, which is detected at the two sensory sites, and this information is communicated to the central processor (respiratory center). The increase in P_{a,CO_2} is translated by the central processor into signals that activate the respiratory muscles, increasing ventilation and lowering the P_{a,CO_2} level. This process continues until P_{a,CO_2} is returned to the steady state of the system. Because of the transport delays from lung to sensor previously discussed, the control response to the delayed sensed state of the system may no longer be the appropriate response to the current state of the system and instability can result. We should note that

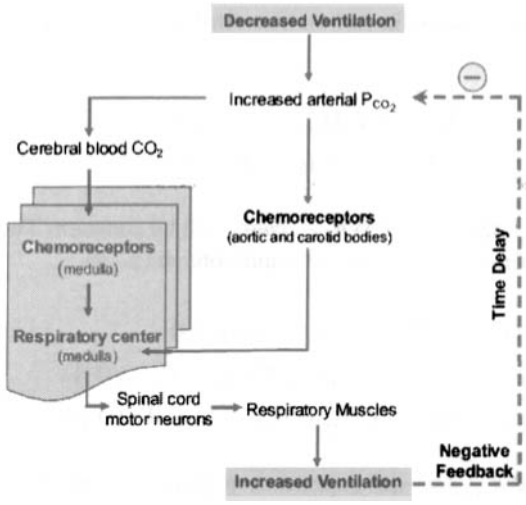

Figure 2.5: Negative feedback loop for an increase in CO_2.

there are also delays in transferring the sensory information to the central processor and in activating the lung muscles, but these neurological delays are generally much shorter than the transport delays determined by blood flow.

The mathematical model for the respiratory control system described in Section 2.2 is too complex for a rigorous analytical study of the effect of delay on stability. In this section, we simplify the model presented in Section 2.2 to the point where it has only the two state variables P_{a,CO_2} and P_{a,O_2}. We make the following simplifying assumptions:

(a) P_{v,CO_2} and P_{v,O_2} are constant.

(b) F_p is constant.

(c) The variations of P_{a,O_2} are small enough, so that we can approximate the dissociation curve (2.2) by a linear function,

$$C_{a,O_2} = B_a + m_a P_{a,O_2}, \quad C_{v,O_2} = B_v + m_v P_{v,O_2} \tag{2.22}$$

with some constants $m_a > 0$, $m_v > 0$, B_a, and B_v.

(d) Only the peripheral control loop is modeled, i.e., $G_C = 0$ in (2.15).

(e) Breath-to-breath changes are not modeled (constant flow model).

Assumption (a) is fairly reasonable even if other variables are oscillating (compare the figures in Section 2.4 representing the variations in the partial pressures of the blood gases). In view of assumption (b), the delay τ_p is constant. This is the only delay present in the reduced system, because τ_T in (2.14) is associated only with the quantities C_{v,CO_2} and C_{v,O_2}, which in view of assumption (a) are constant. Since, by assumption (d), we have $G_C = 0$, the partial pressure P_{v,B,CO_2}, respectively, the concentration C_{v,B,CO_2}, is not needed; i.e., we

can eliminate the last equation in (2.14). The third and fourth equations in (2.14) reduce to the relations

$$\begin{aligned} MR_{CO_2} + F_s\big(C_{a,CO_2}(t-\tau_T) - C_{v,CO_2}\big) &= 0, \\ -MR_{O_2} + F_s\big(C_{a,O_2}(t-\tau_T) - C_{v,O_2}\big) &= 0, \end{aligned}$$

which imply that F_s, MR_{O_2}, and MR_{CO_2} cannot all be constant. The concentrations C_{a,CO_2} and C_{a,O_2} are determined by the first two equations in (2.14),

$$\begin{aligned} V_{A,CO_2}\dot{P}_{a,CO_2}(t) &= 863F_p\big(C_{v,CO_2} - C_{a,CO_2}(t)\big) \\ &\quad + \dot{V}_A(t)\big(P_{i,CO_2} - P_{a,CO_2}(t)\big), \\ V_{A,O_2}\dot{P}_{a,O_2}(t) &= 863F_p\big(C_{v,O_2} - C_{a,O_2}(t)\big) + \dot{V}_A(t)\big(P_{i,O_2} - P_{a,O_2}(t)\big), \end{aligned} \tag{2.23}$$

where $C_{a,CO_2}(t)$ and $C_{a,O_2}(t)$ are expressed, respectively, by $P_{a,CO_2}(t)$, and $P_{a,O_2}(t)$ via (2.22). The ventilation $\dot{V}_A(t)$ is given by

$$\dot{V}_A(t) = E_F G_P e^{-0.05P_{a,O_2}(t-\tau_p)} \max\big(0,\, P_{a,CO_2}(t-\tau_p) - I_P\big).$$

We set $X(t) = P_{a,CO_2}(t)$, $Y(t) = P_{a,O_2}(t)$, $\tilde{V}(X,Y) = e^{-0.05Y}\max(0, X - I_P)$, and $\tau = \tau_p$. Easy computations show that, with these substitutions, system (2.23) takes the form

$$\begin{aligned} \dot{X}(t) &= K_1\big(K_2 - X(t)\big) - K_3\tilde{V}\big(X(t-\tau), Y(t-\tau)\big)\big(X(t) - P_{i,CO_2}\big), \\ \dot{Y}(t) &= K_4\big(K_5 - K_6Y(t) - K_7\big) + K_8\tilde{V}\big(X(t-\tau), Y(t-\tau)\big)\big(P_{i,O_2} - Y(t)\big), \end{aligned} \tag{2.24}$$

where

$$\begin{aligned} K_1 &= \frac{863F_pK_{CO_2}}{V_{A,CO_2}} > 0, \quad K_2 = P_{v,CO_2} > 0, \quad K_3 = \frac{E_FG_P}{V_{A,CO_2}} > 0, \\ K_4 &= \frac{863F_p}{V_{A,O_2}} > 0, \quad K_5 = m_vP_{v,O_2} + B_v > 0, \quad K_6 = m_a > 0, \\ K_7 &= B_a, \quad K_8 = \frac{E_FG_P}{V_{A,O_2}} > 0. \end{aligned}$$

It is easy to see that $\tilde{V}(X,Y)$ is increasing in X and decreasing in Y. In ambient air, P_{i,CO_2} is very small, so we assume henceforth that $P_{i,CO_2} = 0$. With the change of variables

$$x(t) = X(t), \quad y(t) = P_{i,O_2} - Y(t),$$

system (2.24) is transformed into

$$\begin{aligned} \dot{x}(t) &= a_1 - a_2x(t) - a_3V(x(t-\tau), y(t-\tau))x(t), \\ \dot{y}(t) &= b_1 - b_2y(t) - b_3V(x(t-\tau), y(t-\tau))y(t), \end{aligned} \tag{2.25}$$

where

$$a_1 = \frac{863 F_p K_{CO_2}}{V_{A,CO_2}} P_{v,CO_2}, \quad a_2 = \frac{863 F_p K_{CO_2}}{V_{A,CO_2}}, \quad a_3 = \frac{E_F G_P}{V_{A,CO_2}} e^{-0.05 P_{i,O_2}},$$

$$b_1 = \frac{863 F_p}{V_{A,O_2}} (m_a P_{i,O_2} + B_a - m_v P_{v,O_2} - B_v),$$

$$b_2 = \frac{863 F_p m_a}{V_{A,O_2}}, \quad b_3 = \frac{E_F G_P}{V_{A,O_2}} e^{-0.05 P_{i,O_2}},$$

and $V(x, y) = (x - I_P)e^{0.05y}$. All these constants are positive. For b_1 this follows from the fact that the expression in brackets is the difference between the O_2 concentration C_{I,O_2} in arterial blood, which corresponds to the partial O_2 pressure in inhaled air, and the O_2 concentration in venous blood (compare (2.22)). Since $P_{I,O_2} > P_{a,O_2}$, this difference is certainly larger than $C_{a,O_2} - C_{v,O_2} > 0$. Positivity of the other constants is obvious. The function V has the following properties:

(i) $V(x, y)$ is increasing in x and y;

(ii) $V(I_P, y) = 0$ for all y;

(iii) V is differentiable for $x \neq I_P$ with $V_x > 0$, $V_y > 0$ for $x > I_P$ and $y > 0$.

The above nonlinear system of delay equations (2.25) is of the form

$$\dot{x}(t) = f(x_t),$$

where $f : C([-\tau, 0], \mathbb{R}^2) \to \mathbb{R}^2$. We first observe, from Section C.1 of Appendix C, that system (2.25), with the initial condition $(0, \phi) \in \mathbb{R} \times C([-\tau, 0], \mathbb{R}^2)$, has a unique solution. We are interested in the equilibria of the system and the local stability properties of these equilibria. In Batzel and Tran (2000b), it was shown that system (2.25) has a unique equilibrium $(\bar{x}, \bar{y})$ with $\bar{x} > I_P$ and $\bar{y} > 0$. In order to see this, we start with the equations

$$a_1 - a_2 x - a_3 x V(x, y) = 0 \quad \text{and} \quad b_1 - b_2 x - b_3 x V(x, y) = 0,$$

which imply

$$x = \frac{a_1}{a_2 + a_3 V(x, y)}, \quad y = \frac{b_1}{b_2 + b_3 V(x, y)}. \tag{2.26}$$

Using these expressions in $V(x, y) = (x - I_P)e^{0.05y}$, we obtain an equation for the equilibrium value of V,

$$V = \left(\frac{a_1}{a_2 + a_3 V} - I_P\right) \exp\left(\frac{0.05 b_1}{b_2 + b_3 V}\right) \tag{2.27}$$

or, equivalently,

$$g(V) := \frac{a_1}{a_2 + a_3 V} = I_P + V \exp\left(-\frac{0.05 b_1}{b_2 + b_3 V}\right) =: h(V).$$

We see that $g(\cdot)$ is strictly decreasing for $V \geq 0$ with $g(0) = a_1/a_2 = P_{v,CO_2}$ and $\lim_{V\to\infty} g(V) = 0$, whereas $h(\cdot)$ is strictly increasing for $V \geq 0$ with $h(0) = I_P$ and $\lim_{V\to\infty} h(V) = \infty$. Assuming that

$$P_{v,CO_2} > I_P,$$

(2.27) has a unique solution $\bar{V} > 0$. Then we get from (2.26) the unique equilibrium

$$\bar{x} = \frac{a_1}{a_2 + a_3\bar{V}}, \quad \bar{y} = \frac{b_1}{b_2 + b_3\bar{V}}.$$

In order to investigate the local stability properties of this equilibrium for system (2.25), we first introduce two new variables,

$$\xi(t) = x(t) - \bar{x},$$
$$\eta(t) = y(t) - \bar{y},$$

and linearize the resulting system around $\xi = 0, \eta = 0$,

$$\frac{d}{dt}\begin{pmatrix}\xi(t)\\ \eta(t)\end{pmatrix} = A\begin{pmatrix}\xi(t)\\ \eta(t)\end{pmatrix} + B\begin{pmatrix}\xi(t-\tau)\\ \eta(t-\tau)\end{pmatrix}, \tag{2.28}$$

where

$$A = \begin{pmatrix}-a_2 - a_3\bar{V} & 0\\ 0 & -b_2 - b_3\bar{V}\end{pmatrix}, \quad B = \begin{pmatrix}-a_3\bar{x}\bar{V}_x & -a_3\bar{x}\bar{V}_y\\ -b_3\bar{y}\bar{V}_x & -b_3\bar{y}\bar{V}_y\end{pmatrix}$$

and $\bar{V} = V(\bar{x}, \bar{y})$, $\bar{V}_x = V_x(\bar{x}, \bar{y})$, and $\bar{V}_y = V_y(\bar{x}, \bar{y})$. The characteristic equation for system (2.28) is given by $\det \Delta(\lambda, \tau) = 0$, where $\Delta(\lambda, \tau) = \lambda I - A - B^{-\lambda\tau}$ (see Section C.3 in Appendix C). Simple computations show that

$$\chi(\lambda, \tau) := \det \Delta(\lambda, \tau) = P(\lambda) + Q(\lambda)e^{-\tau\lambda},$$

where

$$P(\lambda) = \lambda^2 + (A_1 + B_1)\lambda + A_1B_1,$$
$$Q(\lambda) = (A_2 + B_2)\lambda + A_1B_2 + A_2B_1$$

with

$$A_1 = a_2 + a_3\bar{V}, \quad B_1 = b_2 + b_3\bar{V},$$
$$A_2 = a_3\bar{x}\bar{V}_x, \quad B_2 = b_3\bar{y}\bar{V}_y.$$

In case $\tau = 0$, we have $\chi(\lambda, 0) = P(\lambda) + Q(\lambda)$, which is a quadratic polynomial with positive coefficients. Consequently, all the zeros of the characteristic equation have negative real parts. Therefore system (2.25) with $\tau = 0$ is asymptotically stable.

For a simpler model analyzed in Cooke and Turi (1994), stability criteria based on the relation between the value $\bar{V}$ and the value $\bar{x}\bar{V}_x + \bar{y}\bar{V}_y$ were obtained. We shall present the stability results for (2.28) and the main ideas behind the proof. For a thorough analysis we refer the reader to Batzel and Tran (2000b). The considerations there are based on ideas

presented in Cooke and Turi (1994) (see also Cooke and van den Driessche, 1986; Boese, 1998).

We first observe that the roots of $\chi(\lambda, \tau) = \det \Delta(\lambda, \tau)$ depend continuously on τ in the following sense: if λ_0 is a root of multiplicity k of $\chi(\lambda, \tau_0)$, then for any $\epsilon > 0$ such that there is no other zeros in $|\lambda - \lambda_0| < \epsilon$, there exists a $\delta > 0$ such that $|\tau - \tau_0| < \delta$ implies that there exist k, not necessarily distinct, roots $\lambda_1, \ldots, \lambda_k$ of $\chi(\lambda, \tau)$ with $|\lambda_i - \lambda_0| < \epsilon$, $i = 1, \ldots, k$. If λ_0 is a simple root, i.e., $k = 1$, then we can define a mapping $\tau \to \lambda(\tau)$ from a neighborhood of τ_0 into a neighborhood of λ_0 with the property $\chi(\lambda(\tau), \tau) = 0$. These results follow by a straightforward application of Rouché's theorem (for a proof, see, for instance, Dieudonné, 1960). If λ_0 is a simple root, then the mapping $\tau \to \lambda(\tau)$ is also differentiable in a neighborhood of τ_0. This follows from the implicit function theorem applied to $\chi(\lambda(\tau), \tau) \equiv 0$, because $(\partial\chi/\partial\lambda)(\lambda_0, \tau_0) \neq 0$ since λ_0 is a simple root of $\chi(\lambda, \tau_0)$. By differentiation with respect to τ, we get

$$\lambda'(\tau) = -\frac{\partial \chi}{\partial \tau}(\lambda(\tau), \tau)\Big(\frac{\partial \chi}{\partial \lambda}(\lambda(\tau), \tau)\Big)^{-1}.$$

Since the system is asymptotically stable for $\tau = 0$, we investigate whether eigenvalues can cross the imaginary axis from left to right if $\tau > 0$. This is the only possibility of getting eigenvalues with positive real parts, because the modulus of all eigenvalues with positive real parts is bounded by a constant independent of the delays (see Section C.3 in Appendix C). Thus, we have to investigate the possibility of having eigenvalues on the imaginary axis.

From $\chi(0, \tau) = P(0) + Q(0) = A_1 B_1 + A_1 B_2 + A_2 B_1 > 0$ for $\tau \geq 0$, it is clear that $\lambda = 0$ is never an eigenvalue. Therefore, only eigenvalues of the form $\pm i\omega$ with $\omega \neq 0$ are possible on the imaginary axis. The following result characterizes the existence of such eigenvalues.

For $\omega_0 \in \mathbb{R}$, the following two statements are equivalent:

(i) *We have $\chi(i\omega_0, \tau) = 0$ for some $\tau > 0$;*

(ii) *$F(\omega_0) = 0$, where*

$$F(\omega) = |P(i\omega)|^2 - |Q(i\omega)|^2, \quad \omega \in \mathbb{R}.$$

If (i), *or equivalently* (ii), *is true, then there exists a sequence $\tau_k = \tau_0 + 2k\pi/\omega_0$, $k = 0, 1, \ldots$, with $\tau_0\omega_0 \in (0, 2\pi)$ such that $\chi(i\omega_0, \tau_k) = 0$.*

We first prove that (i) implies (ii). Let $\chi(i\omega_0, \tau) = 0$, i.e.,

$$P(i\omega_0) = -Q(i\omega_0)e^{-i\omega_0\tau}.$$

Taking absolute values and the square on both sides, we obtain

$$|P(i\omega_0)|^2 = |Q(i\omega_0)|^2;$$

i.e., we have $F(\omega_0) = 0$.

Assume now that $F(\omega_0) = 0$ or, equivalently, $|P(i\omega_0)| = |Q(i\omega_0)|$. This shows that either $P(i\omega_0) = Q(i\omega_0) = 0$ or $P(i\omega_0) \neq 0$ and $Q(i\omega_0) \neq 0$. The first alternative

would imply $\chi(i\omega_0, 0) = 0$, a contradiction to the fact that $\chi(\lambda, 0)$ has only roots with negative real parts. Therefore, we have $|P(i\omega_0)|/|Q(i\omega_0)| = 1$. In polar coordinates, we have the representation

$$-\frac{P(i\omega_0)}{Q(i\omega_0)} = e^{i\alpha} \tag{2.29}$$

with some real constant $\alpha \in (0, 2\pi)$. Note that $\alpha = 0$ is not possible because this would imply $\chi(i\omega_0, 0) = P(i\omega_0) + Q(i\omega_0) = 0$. If we choose

$$\tau_0 = \frac{\alpha}{\omega_0},$$

then we have $\omega_0\tau_0 \in (0, 2\pi)$. For $\tau_k = \tau_0 + 2k\pi/\omega_0$, $k = 0, 1, \ldots$, we get

$$-\frac{P(i\omega_0)}{Q(i\omega_0)} = e^{-i\omega_0\tau_0} = e^{-i\omega_0\tau_k},$$

and consequently $\chi(i\omega_0, \tau_k) = P(i\omega_0) + Q(i\omega_0)e^{-i\omega_0\tau_k} = 0, k = 0, 1, \ldots$.

If $i\omega_0$, with $\omega_0 \in \mathbb{R}$ and $\omega_0 \neq 0$, is a simple root of $\chi(\lambda, \tau_0)$, then the sign of $\operatorname{Re}\lambda'(\tau_0)$ reveals that the root $\lambda(\tau)$ moves from the left half plane into the right half plane or vice versa when τ increases through τ_0. The following result shows that it is enough to investigate the function F (for a proof see Boese, 1998):

Let $\omega_0 \in \mathbb{R}$ be a root of F and let $(\tau_k)_{k=0,1,\ldots}$ be the sequence such that $i\omega_0$ is a root of $\chi(\lambda, \tau_k)$, $k = 0, 1, \ldots$. Then ω_0 is a simple root of F if and only if $i\omega_0$ is a simple root for all $\chi(\cdot, \tau_k)$. Moreover, we have

$$\operatorname{sign}\left(\operatorname{Re}\lambda'(\tau)\,|_{t=\tau_k}\right) = \operatorname{sign}\left(\omega_0 F'(\omega_0)\right), \quad k = 0, 1, \ldots.$$

Simple computations show that

$$F(\omega) = \omega^4 + k_1\omega^2 + k_2,$$

where

$$k_1 = A_1^2 + B_1^2 - (A_2 + B_2)^2, \quad k_2 = A_1^2 B_1^2 - (A_1 B_2 + A_2 B_1)^2.$$

If F does not have a real root, then there cannot be a crossing of the imaginary axis by eigenvalues of the linearized system (2.28) into the right half plane, so that the equilibrium $(\bar{x}, \bar{y})$ of system (2.25) has to be asymptotically stable for all τ. Obviously, it is sufficient to discuss the positive roots of the quadratic polynomial $\hat{F}(v)$ given by $\hat{F}(v) = v^2 + k_1 v + k_2$. We also note that

$$\operatorname{sign}\left(\omega_0 F'(\omega_0)\right) = \operatorname{sign}\hat{F}'(\omega_0^2).$$

We have the following alternatives for the zeros of $\hat{F}$:

Case 1. $k_1 \geq 0$ and $k_2 \geq 0$:	$\hat{F}$ has no positive root.
Case 2. $k_1 < 0$ and $k_2 > \frac{k_1^2}{4}$:	$\hat{F}$ has no positive root.
Case 3. $k_1 \geq 0$ and $k_2 < 0$:	$\hat{F}$ has exactly one positive root.
Case 4. $k_1 < 0$ and $k_2 \leq 0$:	$\hat{F}$ has exactly one positive root.
Case 5. $k_1 < 0$ and $0 < k_2 < \frac{k_1^2}{4}$:	$\hat{F}$ has two positive roots.
Case 6. $k_1 < 0$ and $k_2 = \frac{k_1^2}{4}$:	$\hat{F}$ has a positive double root.

If $\hat{F}$ has exactly one positive root $v_0 = \omega_0^2$, then $\hat{F}'(v_0) > 0$ and consequently $F'(\pm i\omega_0) > 0$. If $0 < v_1 = \omega_1^2 < v_2 = \omega_2^2$ are two positive roots, then $\hat{F}'(v_1) < 0$ and $\hat{F}'(v_2) > 0$, which implies $F'(\pm i\omega_1) < 0$ and $F'(\pm i\omega_2) > 0$.

We have the following stability properties of the equilibrium $(\bar{x}, \bar{y})$ of system (2.25):

(a) *In Cases* 1 *and* 2, *the equilibrium* $(\bar{x}, \bar{y})$ *is asymptotically stable for all* $\tau \geq 0$.

(b) *In Cases* 3 *and* 4, *let* v_0 *be the only positive zero of the polynomial* $\hat{F}$. *We set* $\omega_0 = +\sqrt{v_0}$ *and* $\tau_0 = \alpha/\omega_0$, *where* α *is defined in* (2.29). *Then the equilibrium* $(\bar{x}, \bar{y})$ *is asymptotically stable for* $0 \leq \tau < \tau_0$ *and unstable for* $\tau > \tau_0$.

(c) *In Case* 5, *let* v_1 *and* v_2, *where* $0 < v_1 < v_2$, *be the positive zeros of the polynomial* $\hat{F}$. *With* $\omega_1 = +\sqrt{v_1}$, $\omega_2 = +\sqrt{v_2}$, *we define*

$$\tau_k = \frac{\alpha + 2k\pi}{\omega_1}, \quad \sigma_k = \frac{\alpha + 2k\pi}{\omega_2}, \quad k = 0, 1, \ldots .$$

Let k_0 *be the smallest integer satisfying*

$$k_0 \geq \frac{\omega_2}{\omega_2 - \omega_1} - \frac{\alpha}{2\pi} > 0. \tag{2.30}$$

Then, we have $\sigma_{k-1} \leq \tau_{k-1} < \sigma_k$ *for* $k = 1, \ldots, k_0 - 1$. *The equilibrium* $(\bar{x}, \bar{y})$ *is asymptotically stable for* $0 \leq \tau < \sigma_0$ *and* $\sigma_{k-1} < \tau < \sigma_k$, $k = 0, \ldots, k_0 - 1$, *whereas it is unstable for* $\sigma_k < \tau < \tau_k$ *and* $\tau > \sigma_{k_0-1}$.

We did not include a statement on the stability behavior of the equilibrium corresponding to Case 6, because this would require additional considerations beyond the scope of the theory provided here.

Statement (a) is clear, because no eigenvalue can move from the left half plane into the right half plane as τ increases. If there exists exactly one positive root of $\hat{F}$, then at each τ_k a pair of conjugate complex eigenvalues moves from the left into the right half plane. Therefore, for $\tau > \tau_0$, there is at least one pair of eigenvalues in the right half plane, whereas for $\tau < \tau_0$, there are no eigenvalues in the right half plane.

In order to prove statement (c), we first observe that (2.30) is equivalent to

$$\sigma_{k_0} \leq \tau_{k_0-1}.$$

Moreover, we have $\omega_2(\omega_2 - \omega_1)^{-1} - \alpha(2\pi)^{-1} > (1 - \omega_1/\omega_2)^{-1} - 1 > 0$. Thus we have $k_0 \geq 1$. Furthermore, in view of $2\pi/\omega_2 < 2\pi/\omega_1$ we get, by induction, $\sigma_k < \tau_{k-1}$, $k = k_0, k_0 + 1, \ldots$. By definition of k_0, we have $\sigma_0 < \tau_0 < \sigma_2 < \cdots < \sigma_{k_0-2} < \tau_{k_0-2} < \sigma_{k_0-1}$. Since at each σ_k a pair of eigenvalues moves into the right half plane and for each τ_k a pair of eigenvalues moves from the right into the left half plane, it is clear that the τ-intervals, where the equilibrium $(\bar{x}, \bar{y})$ is asymptotically stable, respectively, unstable, alternate up to $(\sigma_{k_0-1}, \sigma_{k_0})$. But at σ_{k_0} another pair of eigenvalues moves into the right half plane before, respectively, at the same moment, a pair moves back into the left half plane at τ_{k_0-1}. Therefore, for $\tau > \sigma_{k_0-1}$, there is always at least one pair of eigenvalues in the right half plane. Thus the equilibrium $(\bar{x}, \bar{y})$ is unstable for $\tau > \sigma_{k_0-1}$.

In order to formulate stability criteria in terms of the constants A_i, B_i, $i = 1, 2$, one should observe that these constants are positive and therefore the inequalities $k_2 < 0$, $k_2 > 0$, etc. are equivalent to $A_1B_1 < A_1B_2 + A_2B_1$, $A_1B_1 > A_1B_2 + A_2B_1$, etc. From Cases 1, 3, and 4, we get immediately the following statements.

(i) *If* $A_1B_1 - (A_1B_2 + A_2B_1) \geq 0$ *and* $A_1^2 + B_1^2 - (A_2 + B_2)^2 = k_1 \geq 0$, *then the equilibrium* $(\bar{x}, \bar{y})$ *of system* (2.25) *is asymptotically stable for all constant delays* $\tau \geq 0$.

(ii) *If* $A_1B_1 - (A_1B_2 + A_2B_1) < 0$ *and* $A_1^2 + B_1^2 - (A_2 + B_2)^2 = k_1 \geq 0$ *or if* $A_1B_1 - (A_1B_2 + A_2B_1) \leq 0$ *and* $A_1^2 + B_1^2 - (A_2 + B_2)^2 = k_1 < 0$, *then there exists a* $\tau_0 > 0$ *such that the equilibrium* $(\bar{x}, \bar{y})$ *of system* (2.25) *is asymptotically stable for* $\tau < \tau_0$ *and unstable for* $\tau > \tau_0$.

Another criterion for asymptotic stability for all $\tau \geq 0$ was given in Batzel and Tran (2000b).

If $\bar{V} \geq \bar{x}\bar{V}_x + \bar{y}\bar{V}_y$, *then the equilibrium* $(\bar{x}, \bar{y})$ *of system* (2.25) *is asymptotically stable for all constant delays* $\tau \geq 0$.

To verify the above stability criteria, we carry out numerical simulations with the simplified 2D state space model (2.23). The initial conditions were chosen to be small offsets from the steady state values. The steady state values together with other parameter values that were used in the numerical simulations are given in Table 2.1. In the table we also give the nominal delay time τ, as defined by the pulmonary blood flow F_p, and the multiplier μ_0 by which the nominal delay has to be multiplied in order to obtain the limiting delay τ_0 where instability sets in. Figure 2.6 shows simulation results for a moderate control gain G_P and a value for the multiplier of 1.99, which is less than the multiplier $\mu_0 = 2.02$ (i.e., the solutions are asymptotically stable). Figure 2.7 represents the situation when the multiplier is 2.06, which is larger than $\mu_0 = 2.02$ (i.e., we have an unstable case).

Finally, in Batzel and Tran (2000c) the above analysis was extended to include both peripheral and central controllers. This, however, necessitates the introduction of a third equation modeling CO_2 levels in the brain. In addition to analytical studies on

Variable	Unit	Value
G_P	liters/min/mmHg	45.0
I_C	mmHg	35
I_P	mmHg	35
F_p	l/min	6.0
ω_o	—	7.47
nominal τ	min	0.142
μ_O	—	2.02
$\bar{x}$	mmHg	41.48
$\bar{y}$	mmHg	66.9
$\bar{V}$	liters/min	4.59
$\bar{x}\bar{V}_x + \bar{y}\bar{V}_y$	—	44.7
$A_1^2 B_1^2 - (A_2 B_1 + A_1 B_2)^2$	—	−2738.8
$P_{v,CO_2} = 46.0$ $P_{v,O_2} = 40.9$ $P_{i,O_2} = 150.0$		

Table 2.1: Parameters used in stability calculations.

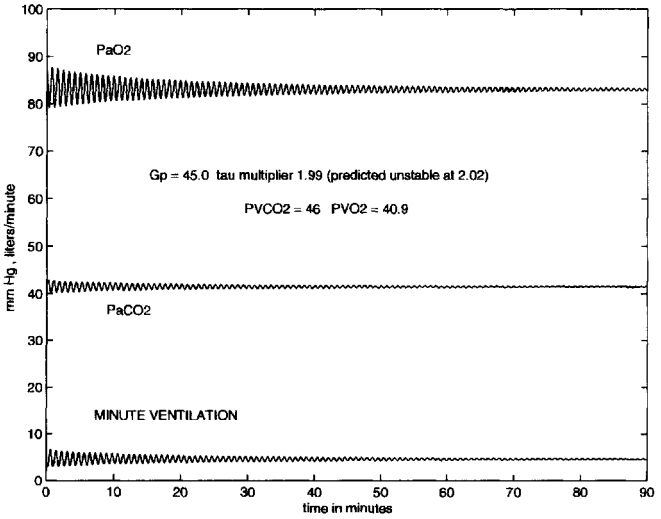

Figure 2.6: Stable 2D basic model with moderate controller gain.

delay-dependent stability, it was shown that the decreased cardiac output (and, hence, increased delay) resulting from the CHF condition can induce instability at certain control gain levels, the central control reduces the instability inherent in the peripheral control mechanism, the tissue compartment dampens oscillations and contributes to stability, and variations in controller gain are critical to the stability of the system. These analytical results were also confirmed numerically through simulations.

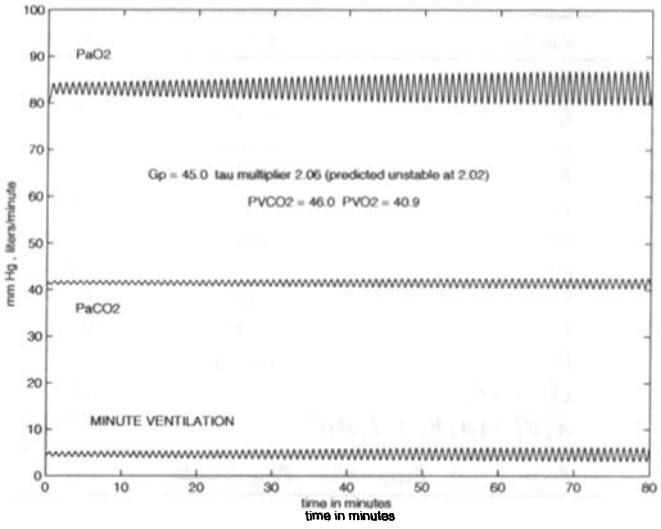

Figure 2.7: Unstable 2D basic model with moderate controller gain.

2.4 Modeling Applications

In this section we discuss some applications of the model described in Section 2.2. General reference parameters are given in Table 2.2 with some supplementary values provided in Table 2.3. Sources for these parameters can be found in Grodins, Buell, and Bart (1967), Khoo et al. (1982), Khoo, Gottschalk, and Pack (1991), and Batzel and Tran (2000a). In the following subsections, changes in parameters, which are needed to model specific cases, are provided or references are given, where parameter values can be found. Control gain parameters and other ventilatory parameters vary depending on whether the model describes ventilation as an average flow of $\dot{V}_E$ or includes a simulation of breath-to-breath changes. See Subsections 2.2.6 and 2.2.7 for further details.

2.4.1 Sleep and PB

It was briefly mentioned in Subsection 2.1.5 that changes during sleep have an impact on respiratory function. Metabolic rates change, muscle tone, and responsiveness to control signals are altered, and upper airway dilational muscle tone is reduced. If Q_{co} is reduced, transport delays are increased. All of these factors influence the respiratory control system, and certain constellations of changes and parameters can create instability in the system. We first discuss some of the physiological features of respiration during sleep.

Respiratory sleep physiology

The sleep state is divided into REM (rapid eye movement) sleep, generally associated with vivid dreaming, and non-REM (NREM) or quiet sleep. The physiological characteristics are quite different (see, e.g., Somers et al., 1993; Becker et al., 1999).

Typically, sleep begins with the transition through preliminary stages of NREM sleep followed by a shifting period of NREM and REM sleep of varying length and depth. Both

Variable	Value	Unit
P_{i,CO_2}	0.0	mmHg
P_{i,O_2}	150	mmHg
$P_{A\text{-}a,O_2}$	4	mmHg
V_{a,CO_2}	3.2	liter
V_{a,O_2}	2.5	liter
V_{T,CO_2}	15.0	liter
V_{T,O_2}	6.0	liter
V_{B,CO_2}	0.9	liter
F_s	6	liter/min
F_p	6	liter/min
Q_{co}	6	liter/min
F_B	0.8	liter/min
MR_{CO_2}	0.220	liter/min
MR_{O_2}	0.270	liter/min
MR_{B,CO_2}	0.04	liter/min
G_C	1.5	liter/(min mmHg)
G_P	30.0	liter/(min mmHg)
I_C	35.5 to 37.0	mmHg
I_P	35.5 to 37.0	mmHg
τ_B	0.14	min
τ_p	0.13	min
τ_T	0.33	min
τ_v	0.56	min
K_{CO_2}	0.0057	1/mmHg
k_{CO_2}	0.224	1
E_F	0.7 to 1.0	—
V_D	0.150	liter
$\dot{V}_D$	2.2	liter/min
$\dot{V}_E$	6.0	liter/min
f_v	15	1/min

Table 2.2: The normal parameters values for respiration simulations.

NREM and REM sleep are important to overall brain function, and the time of transition can be very short as a consequence of sleep deprivation or disruption. NREM sleep is subdivided into four stages (stages S1 to S4) of sleep characterized traditionally by different electroencephalographic waves. During the transition from awake to S4 or quiet sleep, metabolic rates and respiration decrease and (to some extent) Q_{co} decreases as well although the degree seems to depend on individual cases and situations (Mancia, 1993; Krieger et al., 1990). The overall respiratory responsiveness to chemical drive is also reduced, resulting in a fall in ventilation as one transits from the "awake" state through S1 to S4 quiet or NREM sleep. The net effect is a decrease in P_{a,O_2} and an increase in P_{a,CO_2} (Shepard, 1985). This attenuation of responsiveness can influence the stability of

Variable	Value	Unit
a_o	0.2	—
b_o	0.05	mmHg^{-1}
c_o	2.0	—
$P_{A\text{-}a,O_2}$	4.0	mmHg
$V_{\text{car-delay}}$	0.007	liter
$V_{\text{b-delay}}$	0.015	liter
$V_{\text{art-delay}}$	0.9	liter
T_I	0.023	min
T_E	0.043	min
f_v	15	1/min
V_T	0.5	liter

Table 2.3: Miscellaneous standard adult respiratory parameters values for simulations (infant vascular volumes can be derived from infant flow and delay parameters given in tables).

the system and contribute to the appearance of central and obstructive sleep apnea. One aspect of this reduced responsiveness that can influence ventilatory function is a reduction in muscle tone during sleep, which can affect both the ventilatory muscles and the muscles supporting the upper airway patency (dilation). Such changes in muscle tone (and efficient operation), based on neurological activity, have been referred to as the withdrawal of a "wakefulness" stimulus, which is present during the awake state.

The reduction in respiratory responsiveness in the transition from the awake state to S4 can be encapsulated (see, e.g., Khoo, Gottschalk, and Pack, 1991) in the relation

$$\dot{V}_S = G_S(\dot{V}_E - S_K), \tag{2.31}$$

where $\dot{V}_S$ denotes the effective net ventilation during sleep, while $\dot{V}_E$ (minute ventilation) represents the neural control drive generated by the sensory information on blood gas levels transmitted to the respiratory control center. We will refer to $\dot{V}_E$ in this context as the chemical control to distinguish it from $\dot{V}_S$. The quantities G_S and S_K are variables which can be altered to reflect the reduction in responsiveness of the system. The reduction in G_S represents a reduction in the gain factor and decreases smoothly in the transition through the sleep states to a fixed minimum $G_{S,\text{min}}$ at S4. Increasing the quantity S_K (to a maximum S_{K_M}) produces a shift in the operating point of the system. This transition occurs smoothly from awake stage to S1 or S2. Taken together, changes in these quantities represent the reduction in the wakefulness stimulus. The transition from awake state to S4 (defined as the sleep transition time) varies depending on individual physical and physiological conditions and can be quite short depending on the degree of sleep deprivation or extent of sleep disruption. There are a number of scoring procedures for depth of sleep, sleep stages, and sleep transition cycles, including methods utilizing neural net procedures for evaluation (see Bennett et al., 1998; Robert, Guilpin, and Limoge, 1998).

The ventilatory control process maintains upper airway patency by means of upper airway muscles that act against forces tending to collapse these airways. These collapsing forces are generated by pressures produced by the action of inspiration. During the awake

state, the proper balance of opposing forces is maintained, but during sleep this balance can be disrupted as a result of the increase in upper airway resistance, reduction in muscle tone, and ventilatory drive reduction (Becker et al., 1999; Fogel et al., 2003; Ayappa and Rapoport, 2003) leading to OA.

PB and apnea

Periodic breathing (PB) refers to a form of involuntary breathing consisting of a regular pattern of waxing and waning of V_T and sometimes f_v, and interspersed with apneic or near-apneic episodes (see Figure 2.20). A particular type of PB is associated with chronic heart failure (often referred to as congestive heart failure or CHF). This pattern is referred to as Cheyne–Stokes respiration (CSR), and includes the waxing and waning in ventilation with the waning in ventilation clearly ending in apnea. In this case (and, in general, in PB), the apnea is a central apnea (CA) produced by oscillatory swings in the control signal, which periodically reach points of zero drive, because the system response is out of phase with the state of the system (Cherniack, 1999). This can be induced or enhanced by high control gain, large delay, or other factors which disrupt the feedback loop such as those occurring during sleep.

In contrast, obstructive sleep apnea (OSA) occurs when the pharyngeal section of the upper airway collapses, blocking the flow of air even though there is ventilatory drive transmitted to the inspiratory muscles. This occurs only during sleep and is most likely the consequence of a combination of anatomically reduced airway structure and the sleep-induced effects of reduced upper airway muscle tone and increased resistance (Fogel et al., 2003; Ayappa and Rapoport, 2003) as mentioned previously. When CA precedes OA, this is referred to as a mixed apnea episode. Such apneas are often terminated only by arousal or near arousal from sleep, when the effectiveness of the ventilatory control is returned and the wakefulness stimulus is restored. Apnea is related to a number of clinical problems. Nearly 15 million Americans are subject to chronic OSA, which has been associated with a number of serious cardiovascular conditions including HF and hypertension independent of body mass index (Hoffmann et al., 2004). CSR is often found in patients with CHF (see Subsection 2.4.3) and may contribute to the negative spiral of deterioration in heart function (Lorenzi-Filho et al., 1999) and affect clinical outcome (Lanfranchi and Somers, 2003).

Modeling PB, sleep, and apnea

A number of models have been proposed to study respiration, PB, and sleep effects including (Khoo et al., 1982; Khoo, Gottschalk, and Pack, 1991; Longobardo, Cherniack, and Fishman, 1966; Longobardo et al., 1982; Longobardo, Cherniack, and Gothe, 1989; Fincham and Tehrani, 1983a). Stability issues were discussed in Section 2.3. We will now consider the simulation of several respiratory situations.

In the following simulations, we model only the transition from awake stage to S4 NREM sleep. We model the transition to S4 using (2.31) utilizing the following parameter changes:

(i) A sleep transition time is chosen to represent the rate of the transition from the quiet awake state to S4.

(ii) We assume a linear increase in the operating point parameter S_K from 0 to a maximum shift S_{K_M}, which is completed during the first quarter of the sleep transition time (i.e., loosely by stage S1).

(iii) The sleep gain factor G_S is linearly reduced from 1 at the beginning of the sleep transition cycle (no sleep effect) to $G_{S,min}$ (maximum sleep effect) at the end of the sleep transition at S4.

(iv) Tissue metabolic rates are assumed to be reduced by 15% and brain tissue metabolic rate is assumed to drop by about 7.5% in the transition to S4 (Nofzinger et al., 2002). We also assume a small drop in Q_{co} (Bradley and Floras, 2003; Khoo et al., 1982; Mancia, 1993) by 10% in S4. These reductions are represented in the model as linear reductions over the total sleep transition time.

(v) The sleep transition cycle can be interrupted at any point during the sleep transition time if blood gas deviations become so extreme that the chemical control drive $\dot{V}_E$ rises to an arousal threshold $\dot{V}_{ar}$. Once this threshold is reached (arousal occurs), the awake respiratory control is restored and a new sleep transition is initiated

The choice of these parameters determines the rate of sleep transition and the degree of influence of sleep on the net sleep ventilatory control $\dot{V}_S$. The consequent deviations in blood gases and changes in ventilatory control can induce apnea as follows:

(a) If $\dot{V}_S$ reaches a minimum ventilation $\dot{V}_{min}$, then it is assumed that upper airway collapse and OA occurs. Ventilation is then set to zero.

(b) The apnea-induced accumulation in CO_2 and reduction in O_2 cause $\dot{V}_E$ to increase. When $\dot{V}_E$ reaches the arousal threshold $\dot{V}_{ar}$, arousal is assumed to terminate the apnea, and we reset the parameters of (2.31) (including metabolic rates and blood flows) to those of the awake state.

(c) A new cycle of sleep transition is initiated as described in steps (i)–(iv) above.

The following points should be kept in mind when considering these simulations:

- After apnea-terminated arousal, ventilation level and blood gases are not in their original relationship and this can further distort or exacerbate the problem of stable sleep transition, leading to a variety of patterns involving apnea and arousal.
- Upper airway patency is not restored in the model when ventilatory drive $\dot{V}_S$ rises again above the minimum drive $\dot{V}_{min}$. The apnea is assumed to be maintained because of other structural pressures and physiological influences until the arousal threshold is reached (see, for example, the discussion in Khoo, Gottschalk, and Pack, 1991).
- To indicate the sleep transition process, we superimpose the reduction in G_S on the tidal volume simulations. The graph of G_S is scaled in order to be easily distinguished from the graph of the tidal volume. The actual values for G_S can be computed from the information given in the tables.[9] As G_S is considered in the model to

[9]The horizontal parts of the graph correspond to $G_S = 1$. The slope of the descending parts is $(G_{S,min} - 1)$/"sleep transition time". However, the time intervals, where G_S is descending, are accurately represented in the figures.

be reduced linearly, G_S will appear as a continuous piecewise linear curve including horizontal segments (awake state) and segments decreasing to the right indicating reduction in G_S. Note that arousals can reset G_S (and S_K) at any point in the sleep transition cycle, and indeed in the figures, the transitions are not always complete when arousal occurs. As can be seen from the tidal volume figures, cases arise in which there are multiple arousals and arousals without apnea.

- To incorporate the tidal volume effect (as discussed in Subsection 2.2.7), flow ventilatory control gains G_P and G_C, ventilation thresholds $\dot{V}_{ar}$, $\dot{V}_{min}$, and S_{K_M} in the tables have been scaled up by a factor of 2.5 from standard physiological values to correct for the fact that effective inspiration is less than half the time of a breath (and thus ventilatory inflow rate is larger than $\dot{V}_E$). In the tables the scaled-up parameters are marked by an asterisk. Furthermore, we also provide in the tables the physiological minute ventilation $\dot{V}_E$ for the system calculated from (2.1), utilizing the simulated values for tidal volume V_T and the chosen ventilation rate. We denote these values in the tables by *effective* $\dot{V}_E$ and *effective* V_T.

Figures 2.8, 2.9, and 2.10 describe transition to sleep that results in arousal. The initial transition to sleep is chosen, but each subsequent transition occurs because an arousal has reset the control parameters to the awake state. As can be seen from Figure 2.8, these subsequent arousals are due to the significant deviations in P_{a,CO_2} and P_{a,O_2} driving the rise in chemical drive $\dot{V}_E$, and in fact the arousals terminate the sleep transition process before the transition to S4 is achieved. Notice also from Figure 2.9 that no apneas occur in this case but rather a pattern of fragmented sleep emerges. This is indicated by the text "sleep transitions" in the figures, which points to the multiple arousals and restarting of the sleep transition process. In the tidal volume, Figure 2.9, the sawtooth variations represent the rate of reductions in G_S. Flat segments represent no reduction in G_S, and hence the awake state. The left panel of Figure 2.10 represents changes in O_2 saturation, while the right panel illustrates how Q_{co} is reduced. The initial flat segment represents the awake state and the sawtooth segment indicates the rate of reduction and the points at which resettings occur. Again, as the transition to sleep is interrupted by arousals, S4 is not reached, and hence the full reduction in Q_{co} is not achieved nor is the same depth of sleep achieved in each cycle.

Parameter changes for these simulations are provided in Table 2.4. The rise in P_{a,CO_2} and P_{a,O_2} is consistent with data (P_{a,O_2} takes a while to reach steady state) as is the drop in tidal volume. The times at which the first sleep transition begins are given in the tables as are the chosen sleep transition times.

Figures 2.11, 2.12, and 2.13 represent the simulation of a transition to S4 which is faster (1.25 minutes vs. 3 minutes). We also assume a higher $\dot{V}_{min}$ (simulating a greater ease of airway collapse), higher central gain, and lower peripheral gain. Parameter changes are given in Table 2.5. With the parameters given, a sequence of apneic episodes is generated, as can be seen from Figure 2.12.

2.4.2 PB and high altitude

At high altitude a number of features come into play in respiratory response and adaptation. The key feature is the reduction in ambient O_2 levels. As can be seen from the control equation, when P_{a,O_2} falls significantly, the peripheral control response becomes a major

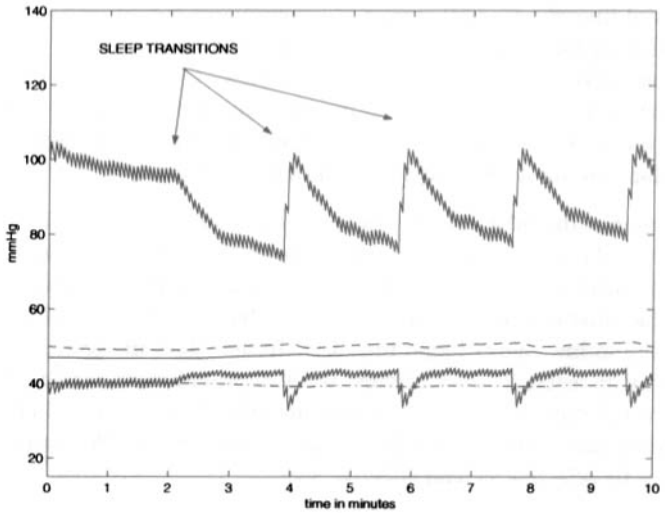

Figure 2.8: Adult sleep transition: blood gases. Upper ragged line—P_{a,O_2}, lower ragged line—P_{a,CO_2}, solid line—P_{v,CO_2}, dashed line—P_{v,B,CO_2}, dotted-dashed line—P_{v,O_2}.

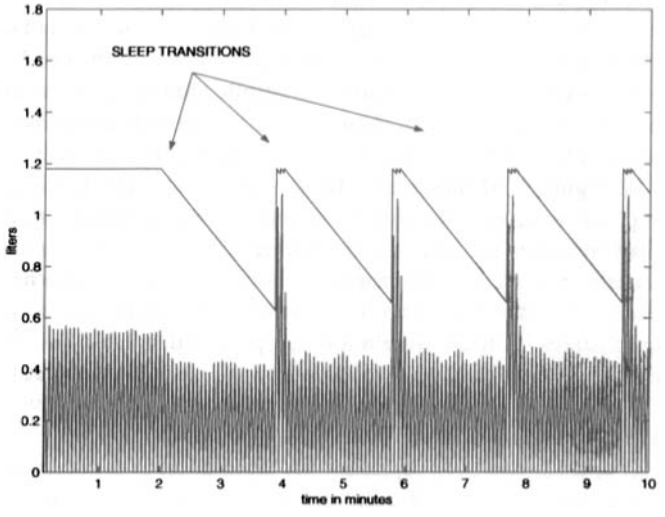

Figure 2.9: Adult sleep transition: tidal volume. The ragged line represents the tidal volume, whereas the sawtooth-shaped line indicates the changes in G_S (but not the actual values).

contributor to ventilation, and this increased responsiveness (control gain) implies a greater potential for the emergence of PB (Cherniack, 1999), especially as the peripheral response acts more quickly. While much early work was motivated by the potential negative aspects of PB, research in high altitude PB has suggested possible benefits of this process. Ghazanshahi and Khoo (1993) suggested that PB could minimize ventilatory work while at the

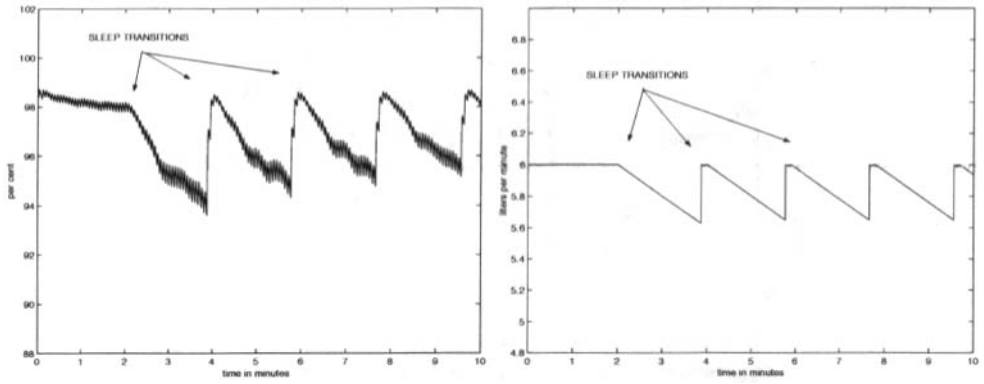

Figure 2.10: Adult sleep transition: O_2 saturation (left panel) and cardiac output (right panel).

Variable	Value	Unit
P_{a,CO_2}	40	mmHg
P_{a,O_2}	95	mmHg
E_I	1	—
MR_{CO_2}	0.230	liter/min
MR_{O_2}	0.290	liter/min
MR_{B,CO_2}	0.040	liter/min
τ_B	0.14	min
τ_p	0.13	min
effective $\dot{V}_E$	7.5	liter/min
effective $\dot{V}_D$	2.4	liter/min
G_P*	0.410	liter/(min mmHg)
G_C*	4.95	liter/(min mmHg)
I_P	36.5	mmHg
I_C	36.5	mmHg
$G_{S,min}$*	0.25	1
S_{K_M}*	14	liter/min
$\dot{V}_{ar}$*	47	liter/min
$\dot{V}_{min}$*	3	liter/min
drop in Q_{co}	10 %	liter/min
sleep transition	3	min
first sleep at	2	min
control formula	(2.19)	—

Table 2.4: The parameter values and key state variable values for simulation of sleep transition: tidal volume model. Quantities marked by an asterisk (*) are scaled by a factor of 2.5 to generate inspiratory drive.

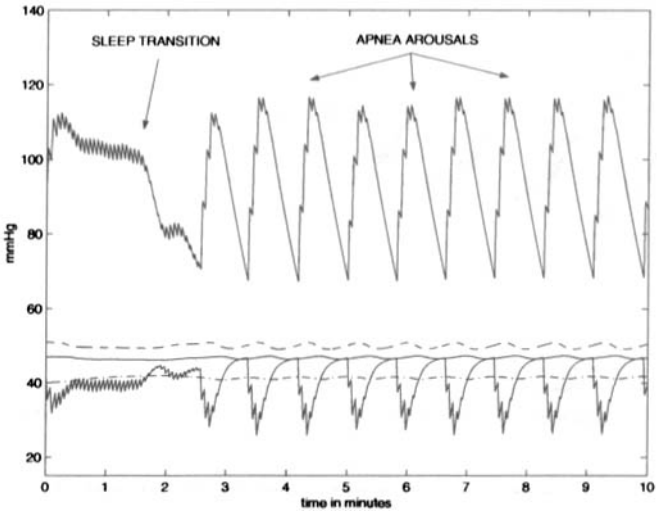

Figure 2.11: Adult sleep transition with apnea: blood gases. Upper ragged line—P_{a,O_2}, lower ragged line—P_{a,CO_2}, solid line—P_{v,CO_2}, dashed line—P_{v,B,CO_2}, dotted-dashed line—P_{v,O_2}.

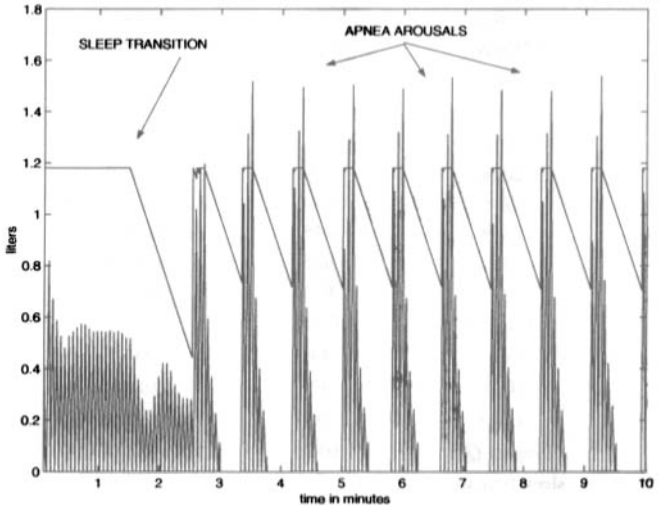

Figure 2.12: Adult sleep transition with apnea: tidal volume. The ragged line represents tidal volume, whereas the sawtooth-shaped line indicates the changes in G_S (but not the actual values).

same time raising average P_{a,O_2} levels as a result of reduced net $\dot{V}_D$, which is the consequence of the PB respiratory pattern of large breaths and apnea. The analysis of Levine, Cleave, and Dodds (1995) argued that even at sealevel, PB may have a positive impact on O_2 saturation, because the oscillatory ventilatory behavior can cause P_{a,O_2} to oscillate

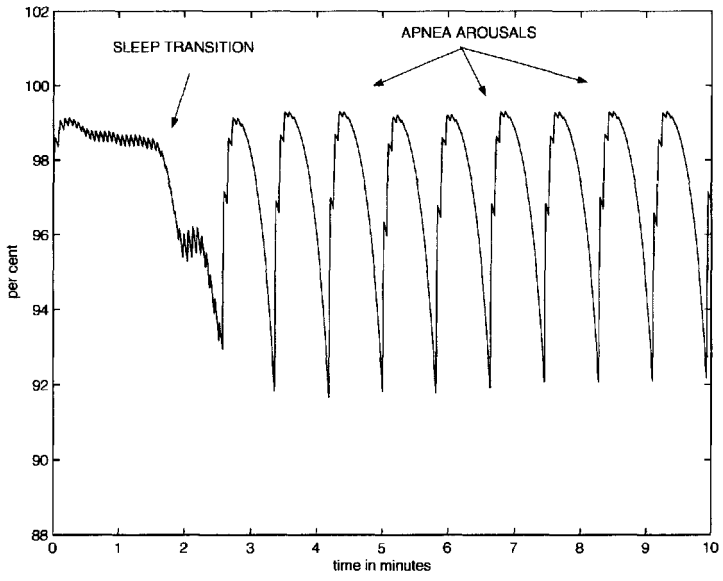

Figure 2.13: Adult sleep transition with apnea: O_2 saturation.

asymmetrically, raising its average level, and thus elevating the mean S_{a,O_2} operating point. Hence, the role of PB in respiratory function may need to be reevaluated and may not always be a sign of negative consequences for the system. However, Salvaggio et al. (1998) reported only a slight influence of PB on the average S_{a,O_2} level at high altitude (during NREM sleep) and Khoo et al. (1996) detailed the numerous sudden arousals and the return of the wakefulness drive that occur during PB at high altitude, with the consequence of significant variation in ventilation and poor sleep quality associated with fragmented sleep. Thus, the issue of the possible advantages of PB is yet to be resolved.

Apneas and arousals increase with increasing altitude and apneas often lead to arousals. However, the results presented in Khoo et al. (1996) indicate that the relation between PB, apnea, and arousals in high-altitude respiration is complex. Arousals can occur after apneic episodes end due to the effects of large perturbations in ventilation and blood gases during PB, and apneic episodes may terminate without arousals. However, arousals, when they do occur, likely contribute to sustaining PB episodes.

The simulations given for high-altitude breathing reflect the early period of exposure to hypoxic-like conditions at an altitude of 14,000 feet, prior to adaptation to the new environment (acclimatization) that begins to take hold after several days. For example, data collected by Moller et al. (2002) indicates that F_B increases during the early exposure period but returns to normal levels after acclimatization. The same is true for Q_{co}. The initial respiratory response to the low ambient O_2 partial pressure and consequent drop in P_{a,O_2} (which can drop to 30 [mmHg] at rest on Mt. Everest at approximately 29,035 feet) is a significant increase in ventilation (Weil, 1986). This ventilatory increase tends to reduce blood CO_2, raising pH, and counteracts the ventilatory drive response to hypoxia, limiting the effectiveness of this response. Fortunately, other changes occur which aid in the transport and utilization of O_2 (Samaja, 1997). See Harris et al. (1998) for comparisons

Variable	Value	Unit
P_{a,CO_2}	40	mmHg
P_{a,O_2}	90	mmHg
F_B	0.75	liter/min
E_F	1	—
MR_{CO_2}	0.220	liter/min
MR_{O_2}	0.270	liter/min
MR_{B,CO_2}	0.042	liter/min
τ_B	0.165	min
τ_p	0.155	min
effective $\dot{V}_E$	7.5	liter/min
effective $\dot{V}_D$	2.4	liter/min
G_P*	0.42	liter/(min mmHg)
G_C*	5.5	liter/(min mmHg)
I_P	36.0	mmHg
I_C	36.0	mmHg
$G_{S,min}$*	0.25	l
S_{K_M}*	14.0	liter/min
$\dot{V}_{ar}$*	46	liter/min
$\dot{V}_{min}$*	4	liter/min
drop in Q_{co}	10%	liter/min
sleep transition	1.25	min
first sleep at	1.5	min
control formula	(2.19)	—

Table 2.5: The parameter changes and key state variable values for simulation of sleep apnea: tidal volume model. Quantities marked by an asterisk (*) are scaled by a factor of 2.5 to generate inspiratory drive.

of P_{a,O_2} at different altitudes and West (2000) for values of alveolar, blood gases, and pH on the summit of Mt. Everest (29,035 Feet).

A general historical review of research in the area of ventilation at high altitude can be found in Weil (1986), while an analytical treatment of stability issues regarding PB at high altitude using a Grodins-type model can be found in Fowler and Kalamangalam (2002).

The essential change in parameters for modeling respiratory function at 14,000 ft. is the reduction in ambient O_2 to 93 [mmHg]. During the early phase of adaptation, cardiovascular quantities Q_{co} and F_B are greatly increased (Khoo et al., 1982; Magosso and Ursino, 2004) because P_{a,O_2} and S_{a,O_2} fall while O_2 demand does not. Metabolic changes occur only after some time and are not included here. As the increase in $\dot{V}_E$ (primarily due to increased peripheral response) is produced by an increase in V_T (Weil, 1986), we use (2.17) for incorporating ventilatory dead space. In the first case depicted in Figures 2.14 and 2.15, with parameter changes given in Table 2.6, we use the control function (2.15), thus using the average flow model to illustrate how PB can be induced. Figure 2.15 shows the central control $\dot{V}_C$ (decreasing thin solid line) and peripheral control $\dot{V}_P$ (dashed oscillating

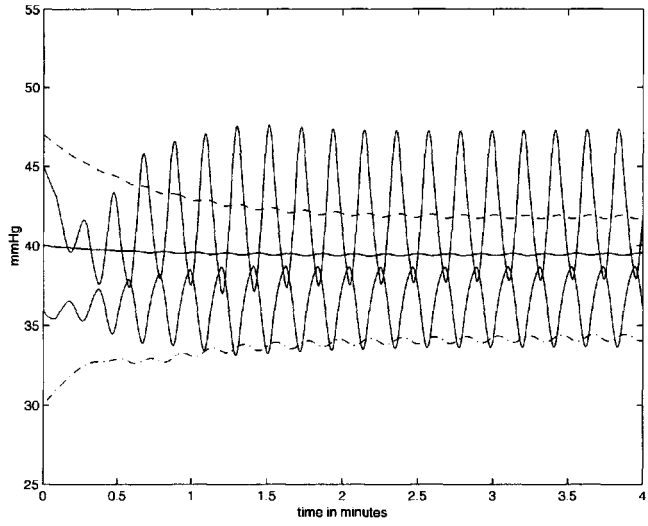

Figure 2.14: Adult PB at high altitude: blood gases. Upper oscillating line—P_{a,O_2}, lower oscillating line—P_{a,CO_2}, solid line—P_{v,CO_2}, dashed line—P_{v,B,CO_2}, dotted-dashed line—P_{v,O_2}.

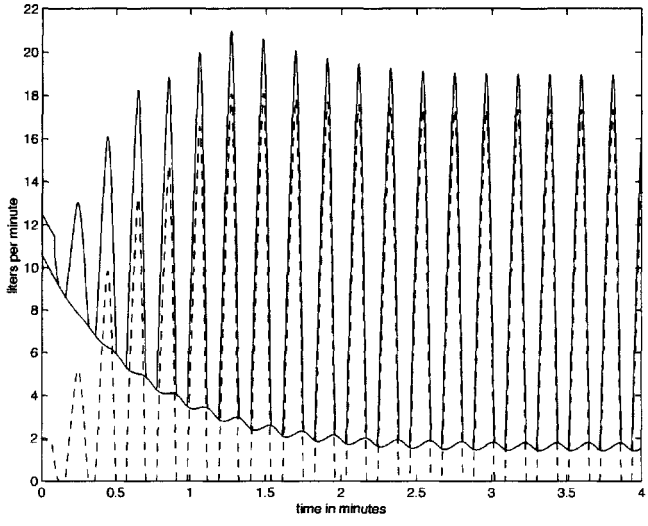

Figure 2.15: Adult PB at high altitude: dashed line—$\dot{V}_P$, lower solid line—$\dot{V}_C$, upper oscillating solid line $\dot{V}_E$.

line) along with minute ventilation (strongly oscillating heavy solid line). The simulation clearly shows how the $\dot{V}_P$ response plays the main role in ventilatory stimulation. This introduces the potential for unstable behavior, because the carotid bodies are highly perfused with arterial blood, producing a quick response time with high gain. This is consistent with analytical results found in Batzel and Tran (2000b, 2000c), and Fowler and

Variable	Value	Unit
P_{a,CO_2}	37	mmHg
P_{a,O_2}	43	mmHg
P_{i,O_2}	93	mmHg
$P_{A\text{-}a,O_2}$	5	mmHg
E_F	1	—
MR_{CO_2}	0.240	liter/min
MR_{O_2}	0.290	liter/min
MR_{B,CO_2}	0.042	liter/min
Q_{co}	12	liter/min
F_B	1.2	liter/min
τ_B	0.078	min
τ_p	0.071	min
τ_T	0.2	min
τ_v	0.4	min
$\dot{V}_E$	8.6	liter/min
$\dot{V}_D$	3	liter/min
G_P	36.3	liter/(min mmHg)
G_C	1.73	liter/(min mmHg)
K_{CO_2}	0.0065	1/mmHg
I_P	35.5	mmHg
I_C	35.5	mmHg
$G_{S,min}$	1	1
S_{K_M}	0	liter/min
no sleep transition	—	min
control formula	(2.15)	—

Table 2.6: The parameter changes and key state variable values for simulation of high altitude: average flow model.

Kalamangalam (2002) as well as in the experimental results of (Cherniack, 1999). Average minute ventilation increases only modestly (though the oscillations increase substantially). As control gains are increased (see the second simulation set with parameters as described in Table 2.7) the ventilatory response is increased, raising P_{a,O_2} levels. Note that PB is introduced even though transport delays have been greatly reduced due to the increase in Q_{co}. As can be seen in Table 2.6, as a consequence of these changes P_{a,CO_2} falls as well as P_{a,O_2}. The fall in P_{a,CO_2}, due to increased ventilation, limits the ventilatory increase induced by hypoxic P_{a,O_2} levels. Ventilation increases during the first few days after arrival at high altitude (White et al., 1987). These adaptations are highly individual (see, e.g., Muza et al., 2001). In this example, the calculated (unstable) steady state indicates that $\dot{V}_E$ rises by 20% which would compare to data as reported in White et al. (1987). A number of factors are involved in the process of acclimatization, and this simulation is designed to show how PB can arise.

In the second case, depicted in Figures 2.16, 2.17, and 2.18, and Table 2.7, we include tidal volume effects. The different control gains imply a different minute ventilation, which

Variable	Value	Unit
P_{a,CO_2}	39	mmHg
P_{a,O_2}	55	mmHg
S_{a,O_2}	82	mmHg
$P_{A\text{-}a,O_2}$	2	mmHg
P_{i,O_2}	95	mmHg
E_F	1	—
MR_{CO_2}	0.240	liter/min
MR_{O_2}	0.290	liter/min
MR_{B,CO_2}	0.042	liter/min
Q_{co}	12.0	liter/min
F_B	1.25	liter/min
τ_B	0.095	min
τ_P	0.089	min
τ_T	0.2	min
τ_v	0.4	min
effective $\dot{V}_E$	10.0	liter/min
effective $\dot{V}_D$	2.8	liter/min
G_P*	0.375	liter/(min mmHg)
G_C*	4.5	liter/(min mmHg)
I_P	36.5	mmHg
I_C	36.5	mmHg
$G_{S,min}$*	0.6	1
S_{K_M}*	14	liter/min
$\dot{V}_{ar}$*	47	liter/min
$\dot{V}_{min}$*	3	liter/min
drop in Q_{co}	0%	liter/min
sleep transition	2.5	min
first sleep at	1.5	min
control formula	(2.19)	—

Table 2.7: The parameter changes and key state variable values for high altitude simulation: tidal volume model. Quantities marked by an asterisk (*) are scaled by a factor of 2.5 to generate inspiratory drive.

is calculated from the tidal volume and the fixed f_v of 15 breaths per second. We include the transition to sleep. In this case, Cheyne–Stokes breathing is introduced intermixed with arousals and a tendency to maintain light sleep states, as discussed in Wickramasinghe and Anholm (1999).

2.4.3 Respiratory complications of HF

As mentioned in Section 2.3, a delay in the feedback control loop can create instability due to inefficient and out-of-phase control response to the state of the system. HF refers

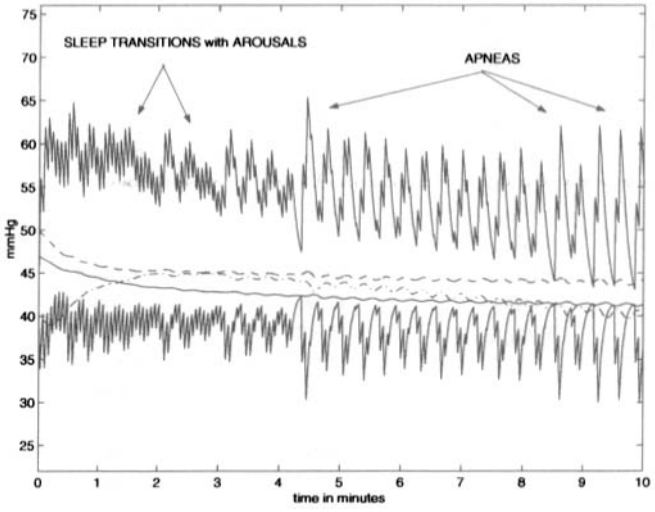

Figure 2.16: Adult PB during sleep at high altitude: blood gases. Upper ragged line—P_{a,O_2}, lower ragged line—P_{a,CO_2}, solid line—P_{v,CO_2}, dashed line—P_{v,B,CO_2}, dotted-dashed line—P_{v,O_2}.

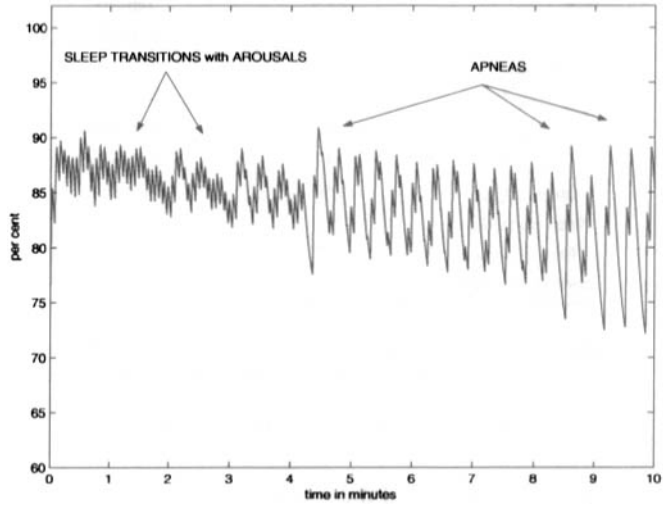

Figure 2.17: Adult PB during sleep at high altitude: O_2 saturation.

to a reduction in the pumping capability of the heart. Chronic HF refers to a continuing degradation of heart function as the loss in heart efficiency leads to conditions, responses, and stresses which reinforce and exacerbate alterations and damage to heart tissue. This degradation of heart function results in a self-reinforcing spiral in heart function. This continuing degradation includes heart remodeling (see Subsection 3.3.1).

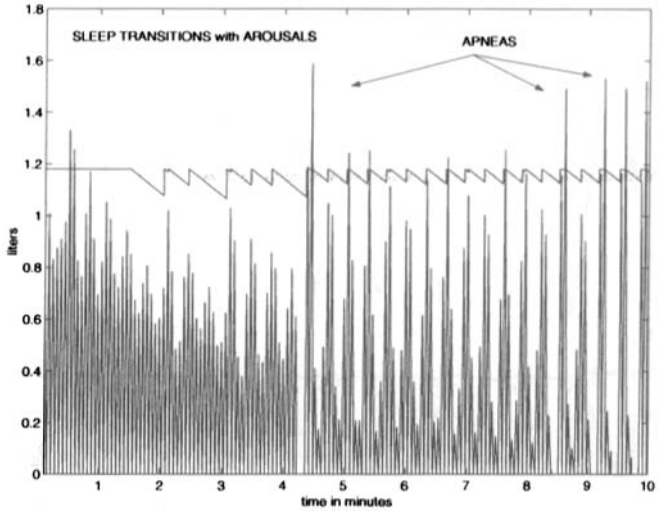

Figure 2.18: Adult PB during sleep at high altitude: tidal volume. The ragged line represents tidal volume, whereas the sawtooth-shaped line indicates the changes in G_S (but not the actual values).

CHF refers to that form of HF which results in a backing up of pulmonary venous flow, creating congestion in the lungs. Since congestion is often seen in HF, the two terms HF and CHF are often used interchangeably. We shall use the term CHF. Further discussion will be found in Section 3.3. We focus here on the impact of CHF on respiratory function. Clearly, due to the reduction in cardiac output, CHF causes an increase in the transport delays discussed in Section 2.3. Transport delays can be increased by up to a factor of 2 in severe cases. Animal research suggests that, if all other factors are held constant, delay in the respiratory control loop needs to be much longer than this to destabilize the system. Nevertheless, CSR is most often associated with CHF patients (Solin et al., 2000), may negatively influence patient prognosis (Lanfranchi and Somers, 2003), and may even be a contributor to the deterioration spiral in heart function. A number of analytical studies have been done to consider the causes of CSR in CHF patients, including the work of Khoo et al. (1982) and Batzel and Tran (2000b). These results show that instability (such as CSR) can be induced by physiologically reasonable increases in delay when this happens in combination with other factors, primarily increased CO_2 gain. In particular, the analytic results show that increased controller gain reduces the delay needed to destabilize the system. Some clinical research supports this prediction. It was shown by Javaheri (1999) that HF patients who are prone to CA are likely to have heightened control response to CO_2. The results in Solin et al. (2000) suggested similar results for CSR in CHF patients (see also Francis et al., 2000; Pinna et al., 2000). Furthermore, results in Batzel and Tran (2000c) suggested that the algorithm for generating changes in $\dot{V}_E$ (i.e., how $\dot{V}_E$ is partitioned into combinations of V_T and f_v) could also reduce the size of the delay needed to destabilize the system.

Notice that in Figure 2.19, there is no influence of sleep on respiratory function in contrast to the results in Subsection 2.4.1 on sleep apnea. In the simulations provided in

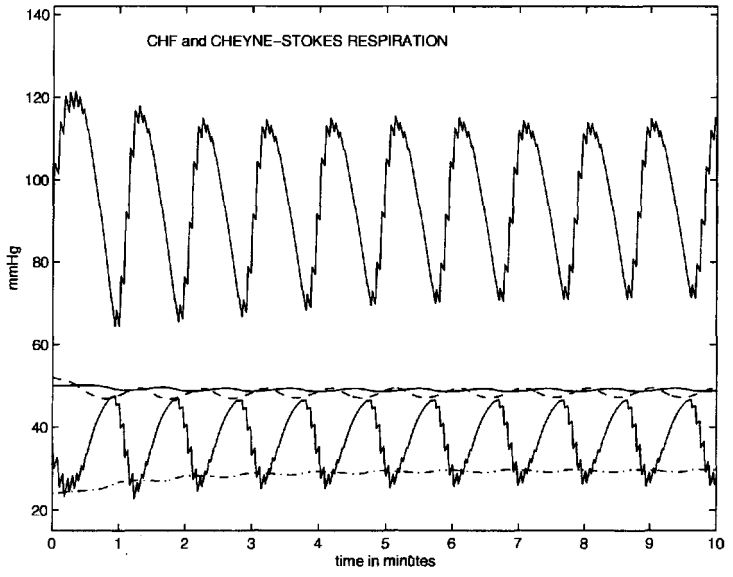

Figure 2.19: CHF respiratory instability: blood gases. Upper ragged line—P_{a,O_2}, lower ragged line—P_{a,CO_2}, solid line—P_{v,CO_2}, dashed line—P_{v,B,CO_2}, and dotted-dashed line—P_{v,O_2}.

that subsection, withdrawal of the wakefulness stimulus perturbed the system sufficiently (in combination with the inherent delay in the system and assumed higher control) to generate apnea. In the case here, we have only an increased delay and controller gain. Parameter values for the CHF simulations are provided in Table 2.8. Figure 2.19 provides the state variables, which exhibit the increase in P_{a,CO_2} and decrease in $\dot{V}_E$ reported in Javaheri (1999). Figure 2.20 illustrates CSR. The time for a single ventilation-apnea cycle is approximately 60 seconds, close to the values reported in Solin et al. (2000) (70 seconds). In this case, variable cardiac output and CBF are modeled as discussed in Section 2.2.8, where the variation in Q_{co} depends on P_{a,O_2} and P_{a,CO_2}, and F_B depends on P_{v,B,CO_2} based on empirical relations provided from several sources including Richardson, Wasserman, and Patterson, Jr. (1961) and Lambertsen (1980). The simulated values for Q and associated delays are given in Figure 2.21.

2.4.4 Other modeling issues

Obstructive Apnea

As was mentioned in Subsection 2.4.1, obstructive apnea (OA) occurs when the ventilatory air passages are blocked at some point resulting in a reduction or loss of air flow to the lungs. This is a common occurrence during sleep when the withdrawal of the wakefulness stimulus can reduce muscle tone, disrupting the usual balance of forces which keep the upper airways (pharynx and larynx) open. OA has become more and more prevalent, and since it may be a new risk factor (independent of body mass index) for hypertension,

Variable	Value	Unit
P_{a,CO_2}	39	mmHg
P_{a,O_2}	90	mmHg
$P_{A\text{-}a,O_2}$	4	mmHg
P_{i,O_2}	150	mmHg
E_F	1	—
MR_{CO_2}	0.220	liter/min
MR_{O_2}	0.270	liter/min
MR_{B,CO_2}	0.042	liter/min
Q_{co} baseline	3.0	liter/min
F_B	0.75	liter/min
τ_B	0.24	min
τ_P	0.22	min
τ_T	0.6	min
τ_V	0.8	min
effective $\dot{V}_E$	7.5	liter/min
effective $\dot{V}_D$	2.6	liter/min
G_P*	0.41	liter/(min mmHg)
G_C*	8.0	liter/(min mmHg)
I_P	36.5	mmHg
I_C	36.5	mmHg
control formula	(2.19)	—

Table 2.8: The parameter changes and the values of the key state variable for CHF: tidal volume model. Quantities marked by an asterisk (*) are scaled by a factor of 2.5 to generate inspiratory drive.

HF, and several other cardiovascular diseases, it has become a serious clinical concern (Hoffmann et al., 2004; Roux, D'Ambrosio, and Mohsenin, 2000).

The dilating forces that act on the upper airway include the effect of dilating muscles whose natural force (depending on inherent tone and mechanical properties) can be enhanced by neural signals from the respiratory control system, incorporating information provided by the chemosensor loop, while local reflex response to inspiration is also observed (Fogel et al., 2003; Ayappa and Rapoport, 2003).

As an example of how one could approach modeling the various forces and effects which produce OA, Longobardo et al. (1982) suggested a basic model to account for the occurrence of OA. Included are control effects of P_{a,CO_2} and P_{a,O_2} on the upper airway muscles through the influence of the ventilatory control loop and the interaction of the upper airway muscles with the thoracic muscles, which oppose the dilating effects of the upper airway muscles themselves. Thus, with the changes in P_{a,CO_2}, P_{a,O_2}, and $\dot{V}_E$ occurring during sleep, and including the withdrawal of the wakefulness stimulus, the ventilatory drive response of the thoracic muscles may produce negative airway pressure sufficient to overcome the altered dilational force of the airway muscles, resulting in a collapse of the upper airway. The equations for this model are

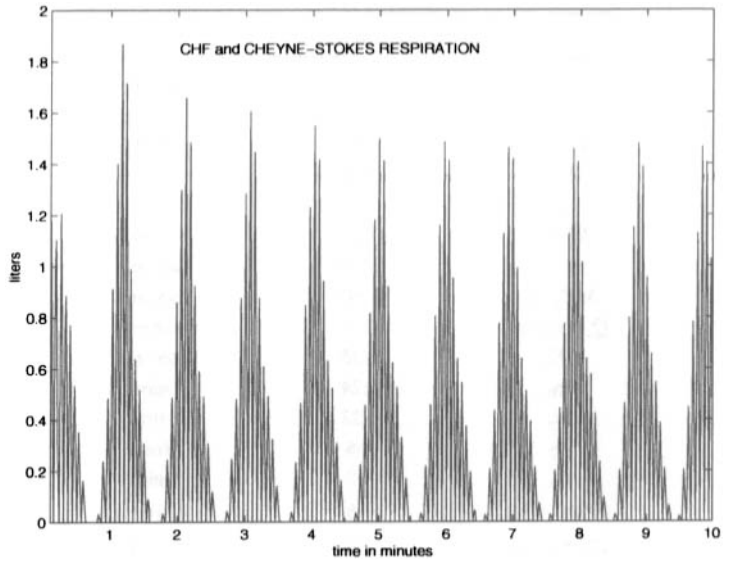

Figure 2.20: CHF respiratory instability: tidal volume.

$$\dot{V}_{\max} = K_1 C^N + K_B,$$

where $\dot{V}_{\max}$ denotes the dilating upper airway force that ventilatory drive must cancel to cause collapse, C, respectively, N, denotes the effect of CO_2, respectively, O_2, on the upper airway force. K_B represents the underlying upper airway muscle tone, which could be affected by sleep, and C^N defines the chemical control effect of CO_2 and O_2 on the upper airway muscles through the ventilatory control loop. K_1 is a constant, whereas C and N are defined as

$$C(t) = 0.8 P_{a,CO_2}(t - \tau_a) + 0.2 P_{B,CO_2}(t),$$
$$N(t) = K_2 \left(\frac{90}{\left(P_{a,O_2}(t - \tau_a) - K_4\right)} \right)^{K_3}.$$

In Table 2.9 we list the values of the parameters $K_1, \ldots, K_4$ and K_B used in the simulations. When ventilatory drive $\dot{V}_E$ (thoracic muscle force) is greater than $\dot{V}_{\max}$, the upper airway collapses. Figure 2.22 illustrates the process. Variations in $\dot{V}_E$ (upper solid line) and $\dot{V}_{\max}$ (dashed line) are depicted over time. When $\dot{V}_E < \dot{V}_{\max}$, ventilation occurs as depicted by the appearance of tidal volume spikes (lower solid line spikes—not shown to scale). Tidal volume disappears when $\dot{V}_E \geq \dot{V}_{\max}$. This representation was generated by incorporating the OA model into the general respiratory model including transitions to sleep, which is indicated in the usual way by including the change in G_S (dashed-dotted line—not shown to scale). As sleep transition occurs and control response diminishes, disproportionate responses by $\dot{V}_E$ and $\dot{V}_{\max}$ cause $\dot{V}_{\max}$ to fall below $\dot{V}_E$, inducing OA which is not terminated immediately at arousal but only when $\dot{V}_E$ falls below $\dot{V}_{\max}$. This may

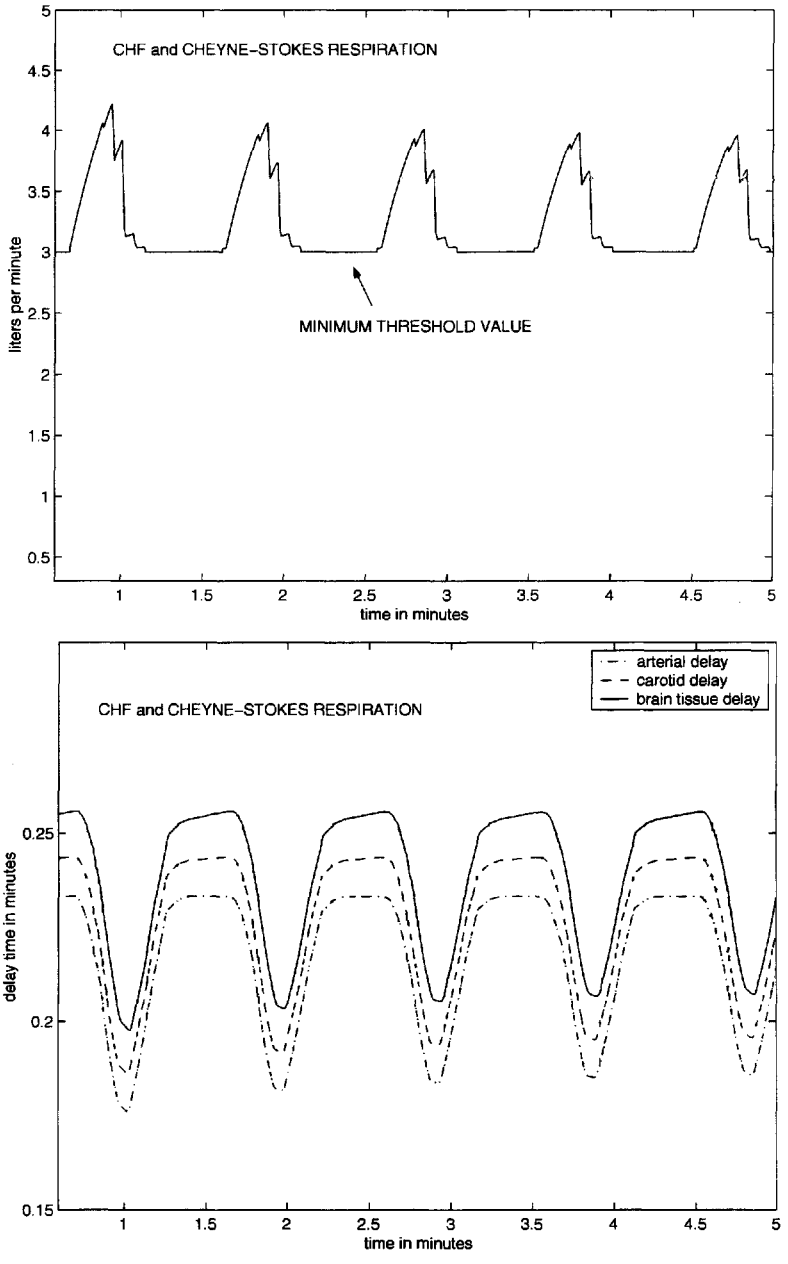

Figure 2.21: CHF respiratory instability: cardiac output (upper panel), transport delays (lower panel).

be the case when arousal is only partial, resetting the awake stimulus, but with negative ventilatory pressure still overcoming the dilating forces. A more complete model would include a richer interaction of control elements.

Variable	Value	Unit
K_B	6.0	liter/min
K_1	0.00005	liter/(min mmHg^N)
K_2	1.50	mmHg^{K_3}
K_3	3.0	—
K_4	32.4	mmHg

Table 2.9: Parameters for OA simulations.

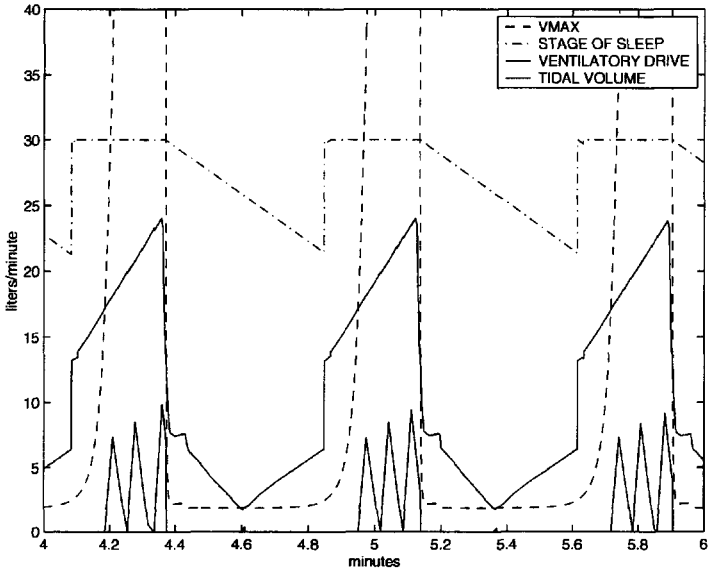

Figure 2.22: OA: model of interaction of physiological forces represented as follows: $\dot{V}_E$—upper solid line, $\dot{V}_{max}$—dashed line, tidal volume—lower solid line spikes (not shown to scale), sleep transition indicated byG_S—solid piecewise linear line.

Infant respiration

Many changes occur in respiratory and cardiovascular physiology during the transition from the fetal period through the neonatal period to childhood (see, e.g., Polin, Fox, and Abman, 2004), which need to be taken into account in modeling infant respiration. The fetus is adapted to efficiently extract O_2 from the system of the mother. Immediately, at postbirth it must respond to a new environment and source of O_2. Hence, the greatest challenges to infant respiration occur during gestation and the immediate postbirth period. Fetal Hb (Hb-F) is part of the adaptation mechanism for the gestational period of life as it has a higher O_2 affinity (ease in binding) than adult Hb (Hb-A). Hb affinity for O_2 and Hb concentration (also higher in the fetus) influence the O_2 carrying capacity of fetal blood.

After birth, the process of adapting to the new environment begins and includes replacing Hb-F with Hb-A. Hb affinity is influenced by a number of factors including the levels of CO_2 and pH (Bohr effect) and temperature. Another key factor is the concentration of 2,3-diphosphoglycerate (2,3-DPG) which binds much more easily to Hb-A than to Hb-F and in this binding reduces Hb oxygen affinity. It is the interplay of the replacement of Hb-F with Hb-A, change in Hb concentration, and change in 2,3-DPG concentration, that accounts primarily for the variations that are seen in the O_2 (dissociation) carrying capacity of fetal and neonatal blood. These variations are shown in Figure 2.3.

Beyond these factors, there are a number of other physiological features that need to be taken into account to reflect the fetal, premature, early, and late neonatal stages.

There can exist a considerable alveolar-arterial gradient, $P_{A\text{-}a,O_2}$ for P_{O_2} (Revow et al., 1989) which is caused mainly by a form of ventilation-perfusion mismatch (Nelson, 1976; Scarpelli, 1990). Because of the mechanical properties (reduced elasticity) of the infant lung, the closing volume (the volume where dynamic compression of the airway begins) is greater than the functional reserve capacity (normal volume after expiration) up to perhaps 6 years of age or older. In fact, airway closure occurs in certain regions of the lung during segments of the normal tidal ventilation cycle in infants. This acts as a true shunt, because blood flowing past alveoli in these areas cannot exchange gases, resulting in a mixing of a portion of systemic venous blood with normal gas-exchanged capillary (arterial) blood. This is referred to as venous admixture. Other factors also tend to increase the ventilation-perfusion mismatch. Further discussion of this can be found in Koch (1968).

Furthermore, not all venous return from the tissue compartment passes through the pulmonary circuit. Some tissue venous return is shunted around the pulmonary circuit. In the very early (sometimes extended) neonate period, some blood passes through heart openings that were necessary during the fetal period, but which should close after birth. Two such pathways are the foramen ovale and the ductus arteriosus. When the foramen ovale is not completely closed and certain other anatomical and physiological conditions exist, some tissue venous blood may bypass the pulmonary circuit. This is referred to as the right-left shunt (R-L shunt) and it causes the blood, with high CO_2 concentration and low O_2 concentration, to mix with the oxygenated pulmonary return blood, which results in changing the relative concentrations of CO_2 and O_2 in systemic arterial blood. While such a condition (patent foramen ovale) is found in up to 25% of adults, the shunt is usually sufficiently small so as to be asymptomatic and undiagnosed.

Left-right shunt is also possible. When the ductus arteriosus does not close completely after birth, under some conditions, blood can flow from the aorta back into the pulmonary circuit (L-R shunt). This can cause a reduction in the blood reaching the tissues and extra stress to the pulmonary circuit. In the simulations that follow, significant functional closure of the foramen ovale and the ductus arteriosus are assumed with a remaining 5% shunt of blood from the systemic venous return to systemic arterial blood flow included (R-L shunt). Consequently, blood entering the tissue compartment has a reduced O_2 partial pressure compared to the P_{a,O_2} level leaving the lung capillaries. Part of this drop is due to the R-L shunt and part is due to the alveolar-capillary difference $P_{A\text{-}a,O_2}$.

Because the foramen ovale and the R-L shunt begin to close after birth, and given the possibility of an increased $P_{A\text{-}a,O_2}$ difference, in modeling the neonate and infant case, it is not appropriate to assume that P_{A,O_2} is nearly equal to P_{a,O_2} as was assumed in the adult model. In the remaining discussion on infant respiration, P_{a,O_2} will represent the partial

pressure of O_2 leaving the lung capillary system. The equations relating the state variable P_{a,O_2} and the partial pressure of O_2 entering the tissue compartment and carotid sensors will now be discussed.

The blood coming from the lungs (rich in O_2) and the blood shunted around the lungs (low in O_2) are remixed resulting in a lower concentration of O_2 than is found in the blood leaving the lungs. The equation reflecting this is as follows:

$$C_{am,O_2} = \alpha C_{v,O_2} + (1-\alpha)C_{a,O_2}, \tag{2.32}$$

where C_{am,O_2} is the mixed concentration of O_2 from shunted blood and lungs, C_{a,O_2} is the concentration of O_2 from the pulmonary capillary system, C_{v,O_2} is the concentration of O_2 from the shunted venous return, and α is the fraction of shunted blood. Note from (2.2) or Figure 2.3 that small changes in concentrations can result in significant changes in partial pressure. P_{am,O_2} represents mixed O_2 arterial pressure calculated from the dissociation laws and will be used as input to the peripheral control equation. The equation for C_{v,O_2} then takes the form

$$V_{T,O_2}\dot{C}_{v,O_2} = -MR_{O_2} + F_s\left(C_{am,O_2} - C_{v,O_2}\right).$$

The blood flow F_p to the lungs is reduced by the shunt factor $1-\alpha$, so that the equation for lung P_{a,O_2} becomes

$$\begin{aligned} V_{A,O_2}\dot{P}_{a,O_2}(t) = {} & 863(1-\alpha)F_p\left(C_{v,O_2}(t-\tau_v) - C_{a,O_2}(t)\right) \\ & + \dot{V}_A\left(P_{i,O_2}(t) - P_{a,O_2}(t)\right). \end{aligned}$$

Two additional transport delays need to be included. First, the transport delay $\tau_{T,a}$ representing the time of shunted venous return C_{v,O_2} in (2.32) to travel to the arterial side for mixing before entering the tissue compartment. This delay depends on the type of shunting that occurs. Computationally, the transport delay for shunted C_{v,O_2} reflects the delay in transport from the output of the tissue compartment through the right and left hearts and to the entrance of the tissue compartment where it is mixed with the oxygenated C_{a,O_2} blood coming from the lung compartment. Similarly, the transport delay $\tau_{T,am}$ is calculated for the delay to the peripheral control for shunted C_{v,O_2} which is then mixed with C_{a,O_2} as input to the peripheral control. Due to lack of data on infant Q_{co}, we proceed in these simulations as follows: For the awake state we choose Q_{co} constant, for the transition from the awake state to the sleeping state we decrease Q_{co} moderately as a linear function of time and, finally, we keep Q_{co} again constant during the sleep state.

A similar set of model adaptations can be derived for the CO_2 equations. However, the impact of shunting on CO_2 partial pressure (which is significant for O_2) is not large and there appears to be little alveolar-arterial CO_2 difference (Nelson, 1976), so that we still continue to assume the relationship $P_{A,CO_2} = P_{a,CO_2}$.

The ventilatory control system of the newborn takes some time to develop the functional properties exhibited by the adult ventilatory control system. It appears that the interacting influences of CO_2 and O_2 develop during the first two months of life (Søvik and Lossius, 2004). Furthermore, the early hypoxic response has a paradoxical biphasic character, which produces a significant increase in $\dot{V}_E$, during the first few minutes of exposure to the hypoxic stimulus, followed by a drop in $\dot{V}_E$ to baseline or below even though the

stimulus persists. Adults also exhibit this second-phase paradoxical response but only after a long period (10 to 20 minutes) of normal hyperpneic response to hypoxia.

The standard view is that this short-term paradoxical biphasic response to hypoxia disappears after the first two weeks of life, but there is an evidence indicating that this phenomenon may persist into the second month (Cohen, Malcolm, and Henderson-Smart, 1997).

Stability in the infant respiratory control is impacted by time delay and controller gain, shunted blood volume, the $P_{\Lambda\text{-}a,O_2}$ difference, and changes in physiological function such as that induced by sleep transition. The consequences of certain combinations of these influences can be the generation of CA and OA.

Typical values for simulation can be found in Nelson (1976), Revow et al. (1989), Tehrani (1993), Nugent and Finley (1987), and Levine, Hathorn, and Cleave (2000). As mentioned above, the changes in the O_2 dissociation curve during the neonatal period, shown in Figure 2.3, need to be taken into account. The values for the parameters a_o, b_o, and c_o in (2.2) are chosen as reported in Revow et al. (1989) based on the data found in Delivoria-Papadopoulos and DiGiacomo (1992). Anatomical dead space is proportionally larger than for adults and calculated as in Numa and Newth (1996). The value for $P_{\Lambda\text{-}a,O_2}$ in infants is also larger than for adults and is the consequence of a lower ventilation-perfusion ratio (implemented by reducing the parameter P_{i,O_2}) and of the assumed R-L shunt. Data on blood gases during sleep as estimated by transcutaneous blood gas measurements can be found in Horemuzova, Katz-Salamon, and Milerad (2000), while in a companion comment by Greenough (2000) the typical error in transcutaneous measurements of P_{a,O_2} is given. References to other sources of data are found in both papers and the problems associated with ascertaining accurate blood gas values (even up to the current time) are discussed.

We simulate in Figures 2.23 and 2.24a 3- to 4- month-old infant whose weight is found by scaling using typical infant growth curves from an assumed typical birth weight of 3.2 kg (see Table 2.10). Where necessary the parameters for the simulations are scaled based on values reported either as "per gram" or reported as typical for a 3.2 kg infant at birth. The simulation of the transition to NREM sleep will be done as in the adult case. After birth, the classic sleep states of REM and NREM sleep cannot be easily identified and it takes some time for the infant to develop the organized sleep architecture of the adult. However, after approximately 3 months, sleep begins most often with NREM sleep, allowing for the simulation of transition to NREM or quiet sleep at sleep onset (Peirano, Algarin, and Uauy, 2003).

Values of state variables in the transition to NREM sleep are shown in Figure 2.23, while episodes of apnea are exhibited in Figure 2.24. Apnea is a common occurrence during infancy and, as can be seen from the discussion on changes in respiratory control in infancy, many factors can influence respiratory control. Furthermore, the continuous change in these factors complicates the analysis process. Hence, modeling efforts in this area are essential to collating current knowledge and testing current hypotheses. In the simulations, apneic episodes are produced with an assumed higher overall control gain and with a proportionally elevated peripheral control gain relative to the increase in central control gain.

Significant withdrawal of the wakefulness stimulus is also assumed as an increased minimum drive to produce obstruction. Obstructive apneic episodes have been associated with higher peripheral gain in some studies. Sudden infant death syndrome (SIDS) has

Variable	Value	Unit
P_{a,CO_2}	37	mmHg
P_{a,O_2}	99	mmHg
P_{am,O_2}	84	mmHg
a_o	0.141	—
b_o	0.063	$mmHg^{-1}$
c_o	3.4	—
K_{CO_2}	0.0050	1/mmHg
V_{a,CO_2}	0.21	liter
V_{a,O_2}	0.175	liter
V_{T,CO_2}	2.0	liter
V_{T,O_2}	0.46	liter
V_{B,CO_2}	0.152	liter
Q_{co}	1.16	liter/min
F_B	0.238	liter/min
E_F	1	—
$P_{A\text{-}a,O_2}$	8	mmHg
MR_{CO_2}	0.034	liter/min
MR_{O_2}	0.038	liter/min
MR_{B,CO_2}	0.011	liter/min
τ_B	0.1	min

Variable	Value	Unit
τ_p	0.084	min
τ_v	0.22	min
τ_T	0.16	min
$\tau_{T,m}$	0.27	min
$\tau_{T,am}$	0.2	min
effective $\dot{V}_E$	1.2	liter/min
effective $\dot{V}_D$	0.5	liter/min
f_v	30	1/min
I_P	33.0	mmHg
I_C	33.0	mmHg
G_P*	9.3	liter/(min mmHg)
G_C*	0.547	liter/(min mmHg)
$G_{S,min}$*	0.4	1
S_{K_M}*	3.3	liter/min
$\dot{V}_{ar}$*	8	liter/min
$\dot{V}_{min}$*	1.1	liter/min
drop in Q_{co}	9 %	liter/min
sleep transition	1.2	min
first sleep at	1.5	min
control formula	(2.15)	—

Table 2.10: The key state and parameters values for infant respiration simulations: tidal volume model. Quantities marked by an asterisk (*) are scaled by a factor of 2.5 to generate inspiratory drive.

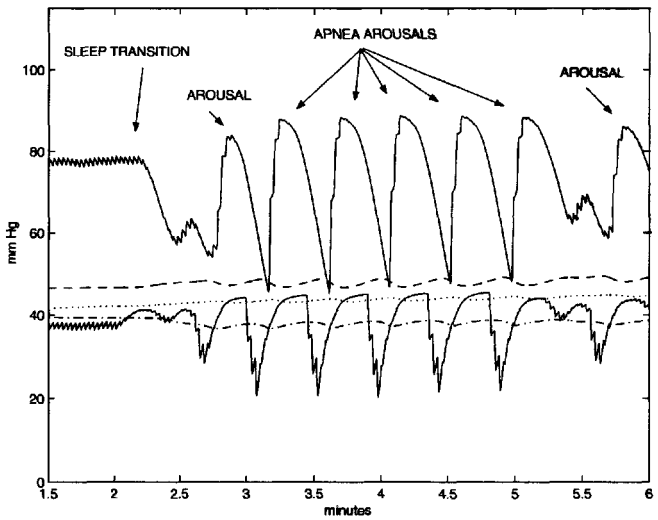

Figure 2.23: Infant sleep transition: blood gases. Upper ragged line—P_{am,O_2}, lower ragged line—P_{a,CO_2}, solid line—P_{v,CO_2}, dashed line—P_{v,B,CO_2}, and dotted-dashed line—P_{v,O_2}.

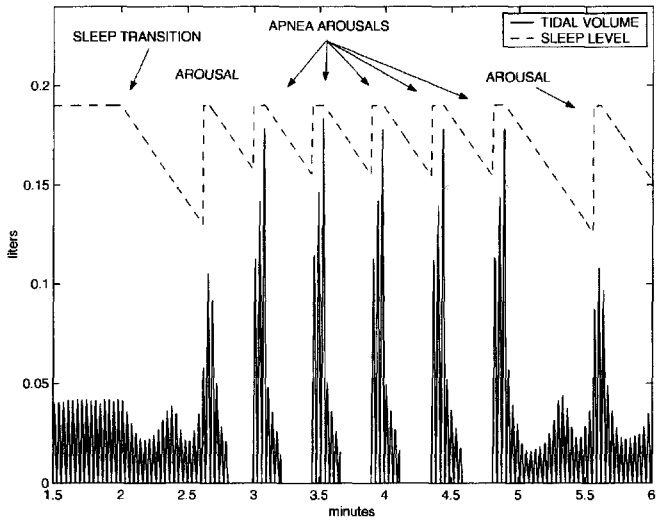

Figure 2.24: Infant sleep transition: tidal volume. The ragged line represents tidal volume, whereas the sawtooth-shaped line indicates the changes in G_S (but not the actual values).

been a key clinical concern for many years, and the incidence of these unexplained sudden deaths has been greatly reduced due to careful assessment of risk factors and to educational programs for parents with the goal of increasing awareness of these risk factors or of eliminating these factors. Of particular importance is to have infants sleeping in the supine position. The actual cause of SIDS has not yet been firmly established. Although severe apnea does not appear to be the direct cause of this syndrome, it has not been ruled out as a contributing factor in the chain of events leading to a SIDS event. For example, sleep deprivation is a risk factor for SIDS and a study by Franco et al. (2004) indicates that sleep deprivation can contribute to heightened arousal thresholds and an increase in the incidence of OA. Conversely, OA can contribute to sleep fragmentation and deprivation. Furthermore, it has also been observed that difficulty in arousal is apparently exacerbated by several risk factors including prone sleeping, and difficulty in arousal is reduced by certain factors which in turn reduce the risk for SIDS. Consequently, difficulty in arousal from sleep is also seen as a risk factor for SIDS (Kahn et al., 2002).

This page intentionally left blank

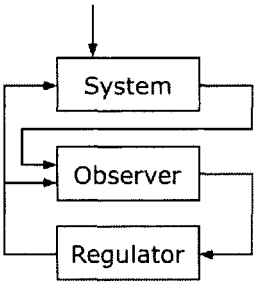

Chapter 3

Cardiorespiratory Modeling

In this chapter we shall introduce a combined model for the cardiovascular and respiratory systems (CVRS) and discuss some important new applications as well as extend applications considered in the previous chapters. We begin with a further discussion of CVRS physiology, which will be needed to motivate and implement the applications.

3.1 Physiology Introduction

The basic elements of the cardiovascular system were discussed in Chapter 1. These included the flow relations in the two cardiovascular circuits and the underlying physical principles upon which they were derived. The key features of heart function, including aspects of ventricular filling, contractility, and heart rate, were discussed as well. Control features in Chapter 1 focused on P_{as} control in exercise, and the control response was implemented via an optimal control approach, which provided a stabilizing control in the transition from rest to aerobic exercise in the bicycle ergometer test. We will now consider in greater detail the control of the CVRS system.

Pressure, volume, flow, and resistance are the primary factors that govern the operation of the cardiovascular system (CVS) and there are a number of interacting control loops which influence these quantities. These include neurological, hormonal, and organ (kidney) action. The control process can be usefully subdivided into global and local control. Global control results from central feedback control mechanisms and tends to act on either the whole system or large parts of the system. There are regional differences in the response to global control signals in different situations. Local control refers primarily to localized self-regulatory mechanisms that respond to local needs and conditions. The CVS control system action can also be classified temporally into short-term, mid-term, and long-term responses.

The respiratory (RS) control process has been described in detail in Chapter 2, and we will focus later in this chapter (see Subsection 3.1.4) on the connections between the CVS and RS control systems.

As mentioned in the introduction, when attempting to understand the action of these control systems, it is useful to consider the fundamental quantities that need to be stabilized. Clearly, metabolism is the main physiological activity, and P_{as} and P_{a,CO_2} are the key

CVRS quantities in maintaining the proper environment for metabolic activity. P_{as} must remain high enough so that, even after the pressure drop that occurs during the transport of blood to the capillaries, there is sufficient residual pressure to ensure a blood flow that will effectively perfuse the intercellular capillary space and deliver nutrients and O_2. In particular, stable P_{as} is needed to ensure that stable cerebral blood flow (CBF) will meet the rather constant, large, and strict metabolic requirements of the brain. Autoregulatory mechanisms in the brain also buffer it from large swings in systemic CVS variables or when P_{as} cannot be maintained. Stable and appropriate pH is necessary for key chemical reactions and, given the relation between pH and P_{a,CO_2} discussed in Chapter 2, it is clear that P_{a,CO_2} should be tightly controlled as well.

3.1.1 Global control of the CVS

Global control of the CVS comprises many pathways that influence its function, including negative feedback mechanisms based on neural control (via parasympathetic and sympathetic autonomic response), hormonal control that supplements neural control, hormonal control arising from other conditions such as when a fight-or-flight situation occurs, renal control, and influences from respiration. We focus in this chapter primarily on those control mechanisms that behave as negative feedback controls. Global control mechanisms are able to act on heart rate, heart contractility, arterial resistance, venous capacitance and compliance, and blood volume to maintain blood pressures and blood flows sufficient to maintain the adequate exchange of elements necessary for metabolic activity.

Sympathetic and parasympathetic control pathways

The autonomic nervous system refers to the general class of involuntary neural activities that are generated in response to a variety of stimuli and that activate responses in various tissues such as smooth muscles, glands, and other organs. Nerve pathways carrying information from sensory sites to the central control centers are referred to as afferent pathways, while efferent pathways carry information to peripheral target organs and tissues, generating a control response.

Key to autonomic CVS control are the sympathetic and parasympathetic pathways that transmit responses from the central control processing center located in the medulla, which integrates actions from several regions including the hypothalamus and vasomotor centers. These responses are based on information provided to the central control by various sensory sites. The sympathetic efferent nerve system is widely distributed throughout the body tissues, and hence tends to generate broad coordinated responses (although not with equal effect in every region). The parasympathetic system is not so widely distributed throughout tissues and primarily targets specific organs and responses.

Generally speaking, an increase in sympathetic nerve stimulation increases cardiovascular variables such as heart rate, contractility, arterial resistance, and venous tone, while the parasympathetic system tends to generate the opposite responses and to act somewhat more quickly. We will be primarily concerned with parasympathetic influence on the heart (transmitted via the vagus nerve), although this system also influences vasodilation and other organ activities under special circumstances.

Another way to view the two systems is that sympathetic action is involved in system activation and the parasympathetic is involved in recuperation. To a great degree, the response characteristics of the two systems depend on the neurotransmitters released during excitation of the terminal neuronal synapses (primarily noradrenaline for sympathetic and acetylcholine for parasympathetic terminal synapses). For example, due to the biochemical nature of the neurotransmitters of the parasympathetic system, its effects on H occur faster than the sympathetic effects. The chemical basis for the transmission of these nerve impulses was established by Otto Loewi (see, for example, Loewi, 1921; Loewi and Navatril, 1926).

An underlying sympathetic activity sets the baseline tone for the vascular structure of the CVS. Physiological responses to sympathetic stimulation differ in various tissue regions depending on the nature of the stimulus. In hemorrhage, vasoconstriction occurs over a wide spectrum of tissues, while in localized exercise, such as weight lifting using one arm, the general response can include vasoconstriction in nonactive muscle and splanchnic regions to support pressure, while sympathetic vasoconstriction is attenuated or deactivated in the active muscle. The generalized vasoconstriction helps to compensate for reduced arm resistance caused by local metabolically induced vasodilation in the active muscle that promotes increased blood flow to that active muscle. A variety of explanations have been proposed to account for the complex interaction of global sympathetic and local mechanisms that result in the net vasodilation needed for increased blood flow to an active muscle (see, e.g., Ichinose and Nishiyasu, 2005; Buckwalter et al., 2004; Joyner and Proctor, 1999; Rowell, 2004). Note that, to a large extent, special circulations such as the cerebral circulation are, to a degree, detached from global control of vasoconstriction given that the blood flow needs of key organs such as the brain cannot be compromised. Some degree of interaction of sympathetic activity and cerebral circulation may well exist, however, as indicated in Jordan et al. (2000). Similar considerations apply to coronary flow.

The baroreflex and neural short-term control

Short-term control of blood pressure refers to control mechanisms that respond in seconds or minutes to stabilize blood pressure and it is critical for the immediate control of orthostatic stress. Short-term control depends primarily on the baroreflex response, which stabilizes pressure by means of neural negative feedback. The main sensory sites for baroreflex control are shown in Figure 3.1. They consist of sensory cell groupings calibrated for the high-pressure systemic arterial subcircuit, and cell structures calibrated for the low-pressure systemic venous subcircuit and pulmonary circuits. Both are types of mechanoreceptors or stretch receptors responding to pressure induced stretching of these sensory structures. One short-term neural baroreflex feedback loop response is shown in Figure 3.2.

Sometimes the terms *baroreceptor* and *baroreflex* are used to refer only to the high pressure sensor-response loop, but we will use the broader meaning of baroreflex (baro means "pressure" or "heavy" in Greek) to refer to either the high or low pressure reflex loops.

Sensory firing in response to pressure induced stretch (baroreflex sensitivity) in the arterial baroreceptors depends on both the amount and rate of change in the induced stretching (Kenner, Baertschi, Allison, and Ono, 1974). Arterial baroreceptors react differently to systole and diastole, and also respond to information provided by the pulsatility of heart

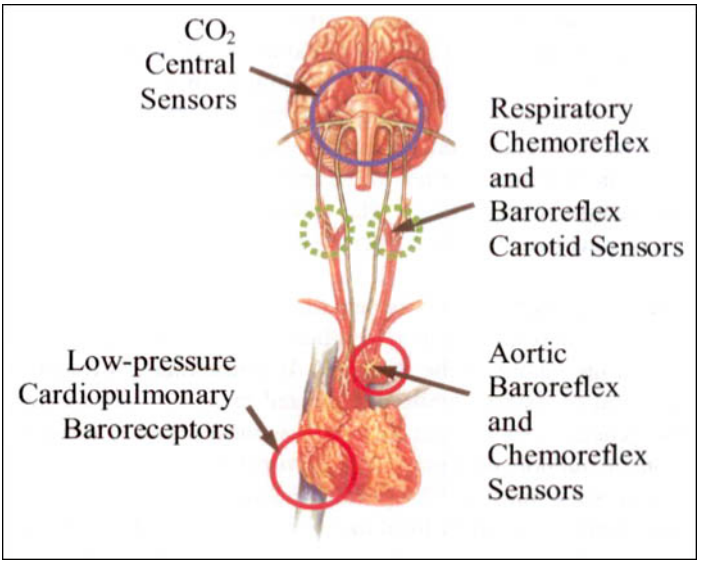

Figure 3.1: CVS sensory sites.

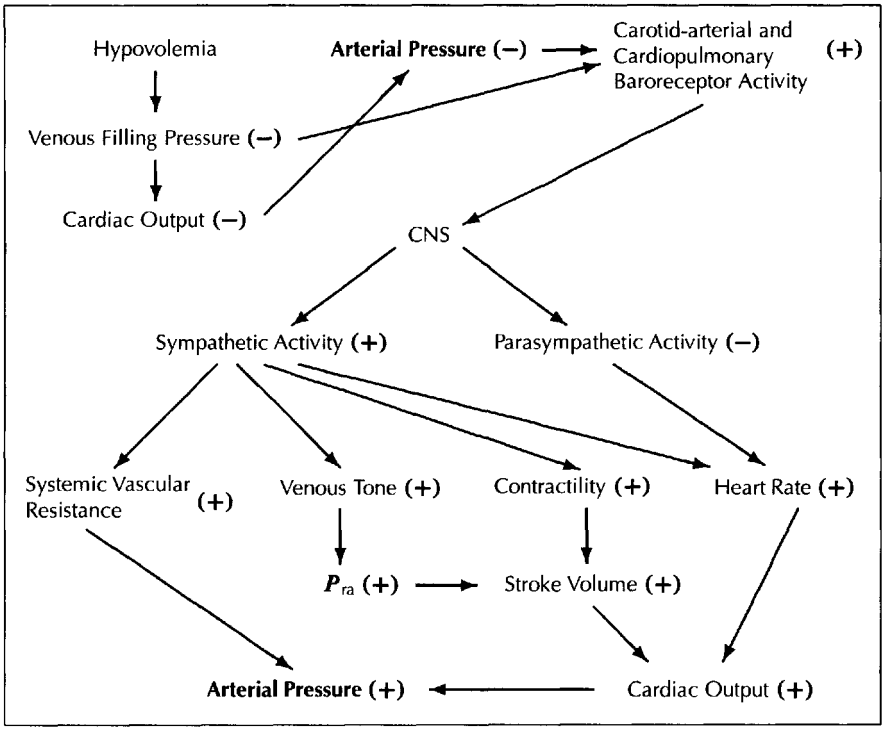

Figure 3.2: Baroreceptor control loops, adapted from Klabunde (2005).

output. This is important in moderate hemorrhage, for example, when there is a decrease in pulse pressure as stroke volume diminishes with reduced blood volume, but, due to other control responses, no change in mean arterial pressure (MAP) occurs (Levick, 2003). Hence, in some applications, a pulsatile model is a necessary constituent. For examples of modeling pulsatility see, e.g., deBoer, Karemaker, and Strackee (1987); Ursino, Fiorenzi, and Belardinelli (1996); Ursino (1998); and Danielsen and Ottesen (2001).

Systemic arterial and cardiopulmonary sensors

The primary systemic arterial (high-pressure calibrated) baroreflex sensors are the carotid baroreceptors and the aortic baroreceptors (located at the carotid sinus and aortic arch, respectively). We will refer to these receptors jointly as the systemic arterial baroreflex. These sensors send afferent nerve information about systemic arterial pressure to the central nervous system (CNS) control located in the medulla. This information is translated into sympathetic and parasympathetic efferent control responses, which adjust MAP through various combinations of changes in heart rate, contractility, systemic resistance, venous tone, and unstressed blood volume. An interesting question in regards to these high-pressure sensory sites is, why there are two such sites and what role the physical distance separating these sites may play. Note that there are also pulmonary arterial (low-pressure) sensors that respond to pulmonary arterial pressure (see below). It has been clearly established that the carotid and aortic arterial baroreceptors are important in short-term control of MAP but, until recently, no role was seen for this arterial baroreflex loop in long-term control. Current research suggests that this view may need to be reconsidered (Thrasher, 2004). There are in fact two types of arterial baroreceptor cells A-efferent and C-efferent, which exhibit different characteristics, for example, it appears the former type resets its operating point quickly, while the later type does not, suggesting that the later type may maintain some responsiveness to original MAP (a form of long-term control) even when the former type adapts to new steady-state conditions.

Low-pressure (cardiopulmonary) sensors are located in regions near venoatrial junctions, in areas of the pulmonary artery and pulmonary return veins, and in the atria and ventricles of the heart. The key sensors are at the right atrial junction with the superior and inferior vena cava (similar sensors also found at the pulmonary venoatrial junction). In relation to the heart, these low pressure sensors can be thought of as providing information about input conditions to the heart, while the key carotid-aortic sensors, discussed above, provide data on the output of the heart. These low pressure sensors play a role in both short-term baroreflex and longer-term (renal) control, responding to changes in venous filling and atrial pressure (and hence changes in blood volume). We will refer to this feedback loop as the cardiopulmonary baroreflex. When there is an increased cardiac volume, the feedback response (in addition to the effects of the Frank–Starling mechanism) maintains proper ventricular filling, stroke volume, and normal heart pumping activity in the short-term primarily by increasing H. It is likely that vascular resistance and tone are decreased as well (Hughson et al., 2004). Central venous pressure is the venous pressure at the entrance to the right atrium. When central venous pressure falls, sympathetically induced effects influence vascular constriction and perhaps venous tone (Brown et al., 2003; Hughson et al., 2004), raising central venous pressure sufficiently to dampen any disturbance of MAP. Information from these sensors is also translated into sympathetic signals to the renal

blood volume control system which acts on a longer-time scale to stabilize blood volume and hence pressures.

Since both pulmonary and systemic circuits are linked, so are flow and pressure changes. The degree, nature, and target of the response induced by each sensory system may vary based on the degree and type of sensor stimulation. For example, when a lower body negative pressure (LBNP) is applied to the outside of a lower segment of the body of a human subject, blood is drawn into this lower vasculature, and the result is a reduction in venous return and an initial unloading of the venoatrial cardiopulmonary sensors. It is widely (but not universally) accepted (Ichinose et al., 2004; Brown et al., 2003) that low-level LBNP (−20 [mmHg]) unloads the right venoatrial sensors, but does not greatly impact the systemic arterial sensors. However, when high levels of LBNP (−40 [mmHg]) are applied, it appears that both sites are activated.

It must be kept in mind that certain feedback responses (based on the type of stress induced) may include possible changes in vascular tone, with or without influencing H (as in low LBNP; see Furlan et al., 2001), and certain elements of the individual cardiopulmonary and arterial reflexes may involve counteracting or inhibiting influences with regard to other elements. See, for example, the discussion in Brown et al. (2003) or Ichinose et al. (2004).

A number of experimental approaches are possible to study these interactions such as applying low-level LBNP as mentioned above, which "unloads" the cardiopulmonary sensors. Another experimental approach involves carotid stimulation by applying suction or occlusion (pressure) in the neck. Suction stretches the carotid arterial baroreceptors, mimicking a rise in pressure and triggering higher parasympathetic and lower sympathetic activity, while neck pressure compresses these sensors, mimicking a fall in pressure and the opposite effects. The impact of cardiopulmonary unloading on carotid baroreceptor function (such as sensitivity) can be studied by application of various neck pressure disturbances. Under the assumption that low-level LBNP does not directly influence carotid activity, measured change in carotid responses to calibrated neck pressure or suction can be studied in relation to cardiopulmonary interaction as in Ichinose et al. (2004).

Clearly, such interactions are hard to examine experimentally, and the nature and degree of interaction and prioritization of responses between the (systemic) arterial and the cardiopulmonary baroreflex loops remain to be completely mapped out (Barbieri, Triedman, and Saul, 2002). In passing, it should be noted that the distribution of the baroreflex and cardiopulmonary sensor sites appears to add a degree of redundancy to the control sensory system.

In regards to possible cardiopulmonary modulation of arterial baroreflex gain during varying levels of LBNP, some studies reported such an effect, which enhances the baroreflex response (Pawelczyk and Raven, 1989; Barbieri et al., 2002; Ichinose et al., 2004), while other recent work does not (Brown et al., 2003).

The cardiopulmonary response may have an element of feedforward control acting as an early response, which presets the arterial side response during certain hemodynamic stresses (Hughson et al., 2004).

Chemoreceptors

The control mechanism for systemic arterial pressure can also access and respond to blood gas levels via chemosensors located in the carotid bodies, which are interconnected with (if not the same as) the respiratory stimulating chemosensors. Chemosensors are also found in the aortic bodies (see Figure 3.1). When these peripheral chemosensors are activated, they stimulate responses by the blood pressure control loop. A change in blood pressure, given the high perfusion in these chemosensitive areas, can be translated into alterations in blood gas concentrations that activate these chemosensors. This response usually becomes significant only when blood pressure changes induce significant blood gases alterations. This occurs at low blood pressure levels, where the baroreflex stretch receptors begin to lose their responsiveness to pressure change. The CVS reflex response (in the absence of ventilatory effects as discussed below) to chemoreflex stimulation, by hypoxia or hypercapnia (from whatever source), is sympathetically induced vasoconstriction, splanchnic venoconstriction (Levick, 2003), and also mild bradycardia (De Burg Daly, 1986; Kara, Narkiewicz, and Somers, 2003; Leuenberger et al., 2001). Chemoreceptors also found in the medulla respond to hypercapnia (C. Jiang, A. Rojas, A. Wang, and X. Wang, 2005). Further discussion on chemoreceptor activity and its relation to respiration and blood gas levels is given in Subsection 3.1.4.

Neural action of the baroreflex

As mentioned above, since all pressures and flows are linked throughout the CVS, it is difficult to separate individual responses and influences, although animal experiments can be done in this direction such as artificially holding one pressure constant while varying another. One area where much remains to be learned is the role and degree of influence of the pulmonary and atrial sensors in general control. Clearly, they appear to add some redundancy to the system as do the hormonal loops of blood pressure vasoconstrictor control (compare Figures 3.2 and 3.4). In considering CVS global control interactions, it is useful to recall the relation between cardiac output Q_{co}, systemic resistance R_s, systemic arterial pressure P_{as}, and systemic venous pressure P_{vs}, given by

$$P_{as} - P_{vs} \approx P_{as} = Q_{co} R_s. \tag{3.1}$$

Mathematically, all quantities are independent but, physiologically, P_{as} is the dependent variable (P_{vs} is very low and often dropped in approximations), while Q_{co} and R_s are independent variables altered by global and local reflexes. Raising R_s, for example, while holding Q_{co} constant, will result in an increase in P_{as}. In practice, the cause of a change in R_s may impact mechanisms that influence Q_{co}, so that the actual steady-state disposition of these variables is dictated by the target value for P_{as} incorporated into the baroreflex control.

Several distinct feedback loops have been identified as follows:

- *The systemic arterial baroreflex loop*: When there is an increase in P_{as}, sympathetic activity is reduced and parasympathetic activity increased. Increased parasympathetic activity quickly slows down H and lowers P_{as}. Reduced sympathetic activity also reduces H, contractility S, and systemic resistance R_s, all of which act to lower P_{as}. There may also be a reduction in venous tone, which raises the unstressed

volume V_u. When there is a reduction in P_{as}, there is a reduction in baroreceptor activity and an opposite set of responses is generated. The partition of the response into changes in H, S, R_s, and V_u can be highly individual. The evoked control response depends on the cause for that perturbation of P_{as}. For example, during an acute drop in blood volume, the venous return and the right atrial pressure $P_{r,a}$ are reduced, followed by a drop in cardiac output Q_{co} and hence P_{as}. Baroreflex stimulation will increase H, S, and R_s to various degrees, with any increase in cardiac output bounded by the baroreflex target pressure and the relation (3.1). See Figure 3.2 for a schematic of the possible control responses. During generalized exercise, on the other hand, there is an initial net drop in R_s due to reduction of local resistance to increase local blood flow (see Section 3.2). Pressure will be stabilized primarily by changes in H and S, with contributions also from increases in R_s in the cutaneous and splanchnic circulations.

- *The left venoatrial loop*: The left venoatrial sensors respond to venous filling pressure and atrial volume. When these quantities are increased, the sympathetic activation response based on this sensory information is to increase H in the short term (Levick, 2003), allowing for heart rate to keep up with increased blood input to the heart. This cardiopulmonary response does not, at the same time, trigger parasympathetic activity as would arterial baroreflex stimulation (Levick, 2003), illustrating that not all sensory systems activate every response path. Note that, insofar as any increase in volume is translated into increased P_{as}, the systemic arterial baroreflex would tend to respond with some degree of counteracting effect unless there are factors which cause one response factor to dominate another. Simultaneously, sympathetic activation is reduced to the kidney by the venoatrial activation and, acting in concert with hormonal influence, stimulates a decrease in blood volume. The net response to an increase in atrial pressure is to smooth out cardiac volume increases by utilizing increased heart rate to match outflow to inflow (Levick, 2003), while the kidney reduces overall volume. Hence this loop is responsive to blood volume increase. During volume reduction, the renal part of the loop aids in raising the overall blood volume, while a reduction in H allows more complete ventricular filling. See Figure 3.3 for a schematic of kidney response pathways for volume control. Further details are also provided in Chapter 4. Note that the Frank–Starling mechanism also matches the contractility to atrial filling. During significant hypovolemia, such as hemorrhage, both baroreflex loops support changes that restore arterial pressure (Levick, 2003).

- *Atrial-ventricular sensors*: These sensors tend to respond during maximal loading, and the autonomic response reduces H and peripheral vasoconstriction (Levick, 2003) and may act to buffer against too high stresses.

Much remains to be learned about the interaction between these various baroreflex loops. Modeling such systems, in conjunction with data from patients with various types and degrees of autonomic failure, patients with orthostatic intolerance disorders (OID) (see Section 3.3), or patients with neural impairment or medicinally altered function, can provide possible avenues to explore these loops in humans, where direct measurement is less accessible and data such as that acquired in animal experiments are not possible to collect.

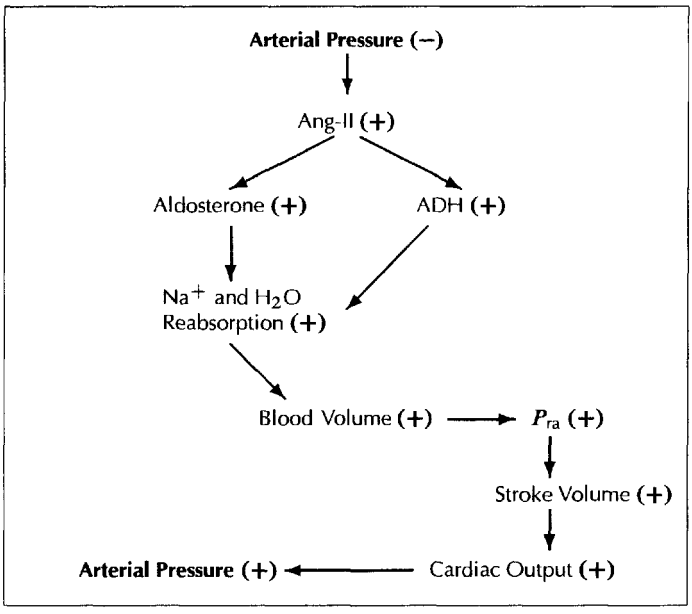

Figure 3.3: Key kidney reflex control loops, adapted from Klabunde (2005).

Hormonal short-term control

There are a number of hormonal control loops that are invoked by sympathetic activation generated by the baroreflex control. Of major importance is the renin-angiotensin-aldosterone system (RAAS), which influences vasoconstriction and also is involved in the longer-term control of blood volume by the kidneys (see below). The RAAS short-term blood pressure control loop response to changes in P_{as} is parallel to the direct neural sympathetic vascular changes. A decrease in P_{as} stimulates the baroreflex and sympathetic sites in the kidneys, leading to an increase (via a chemical production chain involving renin and angiotensin I) in baseline angiotensin II (Ang-II), which is a potent vasoconstrictor. This increases the systemic resistance and supports the stabilization of P_{as}. The baroreflex-hormonal vasoconstrictor response loop to a decrease in blood volume or MAP is illustrated in Figure 3.4, including several hormonal feedback loops. These feedback loops add important redundancy to the overall control system. The change in renal artery pressure also stimulates sympathetic activation of the RAAS chain.

Renal control and long-term control

Longer term responses are also activated when a perturbation in blood pressure or blood volume persists. These responses can take several hours to influence the system. Stabilization of blood volume (influencing blood pressure stability) is a key element in long-term control. Stable blood volume depends partly on the balance between plasma and interstitial fluid exchange via the equilibration of hydrostatic and oncotic (or colloid osmotic) pressures, supplemented by lymph flow circulation. It also depends on the ability to retain or

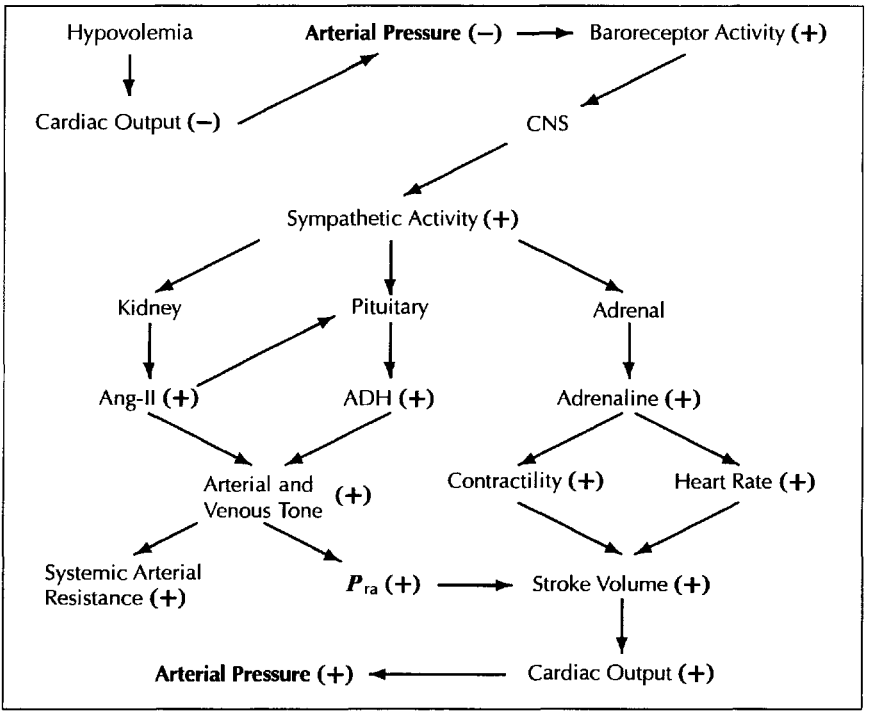

Figure 3.4: Hormonal vasoconstrictor control loops, adapted from Klabunde (2005).

excrete fluid from the fluid system at large, and the kidney is the primary component in carrying out these latter tasks.

Sodium is the major component of extracellular fluid and is a key determiner of fluid balance. Hence, an important factor in the fluid retention and excretion functions of the kidneys is the ability to retain or excrete sodium, a function which is independently controlled.

Renal control of fluid volume includes the process referred to as pressure natriuresis, which automatically influences fluid absorption or excretion via pressure gradients developed within the kidney filtration structure. The kidney is also a component of the overall negative feedback control system which stabilizes pressure. One such pathway is shown in Figure 3.3. The activation of the RAAS as a result of reduced pressure or volume will not only induce vascular constriction, but will also lead to the release of the hormone aldosterone. Aldosterone induces kidney action, which results in the retention of Na^+ and water. This system also stimulates the release of ADH (anti-diuretic hormone), which further encourages water retention. The aldosterone and ADH responses take place over several hours and hence represent a long-term feedback loop as compared to the baroreflex and vascular constriction responses, which are almost immediate.

3.1.2 Local control of the CVS and autoregulation

In cardiovascular control, autoregulation refers primarily to the process of maintaining stable tissue perfusion against pressure disturbances. The term "metabolic theory" in this

context refers to a proposed metabolic basis to explain the means by which stable flow is maintained. Autoregulation is not the only local (or intrinsic) process that provides automatic local response to changing local conditions. Local flow is also regulated based on changes in metabolic needs such as occur during exercise and in response to temperature.

We will use the term self-regulating (local) control to refer to local physiological reflex responses to local conditions that do not flow from a central feedback loop. We will look at two self-regulating vascular controls: metabolic demand control and autoregulatory flow stabilization. In either form of self-regulating local control, there can be a number of intermediate chemical agents that mediate between levels of key state variables such as pressure, blood gas levels, and flow. Furthermore, the local control response and characteristics of the self-regulating local control vary in different tissues and organs.

We also mention again, though we do not go into detail (see Chapter 4), the important interstitial-capillary fluid exchange control (autotransfusion), which aids in the stabilization of blood volume.

Control of metabolic demand

Metabolic demand control refers to the process of altering local tissue flow based on metabolic demand. This is carried out by varying the degree of vasoconstriction, which influences vascular resistance. For example, skeletal muscle blood flow closely tracks metabolic rate. As metabolic activity increases, vasodilation increases local flow (metabolic hyperemia) (Levick, 2003). The vasodilators, responsible for this vascular response, and the overall mechanisms, responsible for this hyperemia in various states, are still actively investigated (Rowell, 2004). It is important to emphasize that as physical action becomes more intense compared to the rest state, further control actions are recruited and new interactions develop. In moderate exercise, for example, it seems that a muscle pump phenomenon must supplement metabolic vasodilation to induce hyperemia by forcing blood through moving muscles (Rowell, 2004). On the other hand, as will be mentioned later, cardiac muscle also responds to metabolic need, but a muscle pump effect is not likely a factor in this case (Rowell, 2004), and the response of coronary flow to increased activity must therefore be metabolic or involve some form of sympathetic activity.

In the model presented in Section 3.2, metabolic control is quantified by a relation between systemic resistance and venous O_2 concentration based on the model provided by Peskin (1981). This reflects the coupling between metabolic activity and vasodilation, but does not specify that O_2 is a direct vasodilation agent.

Autoregulation

Myogenic control refers to an autoregulatory mechanism that responds to local perturbations in blood pressure, acting to maintain constant flow when input pressures increase or decrease. This mechanism responds to pressure induced stretching of smaller vascular elements on the arterial side by inducing constriction and resistance, and thus limiting pressure induced change in flow (in a quantitative interaction reflected in the relation described by (3.1)). If local blood flow F is substituted for Q_{co} in this equation, we see that constant flow requires resistance to increase if pressure increases. Myogenic autoregulation likely plays the major role in CBF stabilization (Levick, 2003; Schubert and Mulvany, 1999). While

this autoregulatory mechanism is conceptually straightforward, the physiological details have not been completely elucidated. Other autoregulatory mechanisms are likely involved in flow stabilization. For example, changes in concentration of metabolic elements due to a pressure induced increase in flow may stimulate vasoconstriction (Schubert and Mulvany, 1999). Models have been developed to study the underlying mechanisms responsible for autoregulation (see, e.g., Starc, 2004).

Autoregulation and local control of special organs

Cerebral blood flow

For an adult human, O_2 consumption in the brain is about 20% of the total metabolic demand and CBF is about 15% of the cardiac output, even though the adult human brain is only approximately 2% of the body weight (Magistretti, Pellerin, and Martin, 1995). Clearly then, cerebral metabolic demands are of paramount importance and these demands require that CBF be tightly controlled and responsive to metabolic needs. In addition, the brain is contained in an inflexible volume (the skull), which places added conditions on the control of CBF and cerebral fluid volume. Cerebral regional and total circulation are altered by metabolic autoregulatory activity and buffered from blood pressure changes by myogenic autoregulation.

Autoregulation of CBF (primarily myogenic control) is usually quantified in terms of variations in P_{as}, and over a range of pressure values from about 80 to 160 [mmHg], CBF is maintained at a nearly constant level (V. Novak et al., 1998). Note that this range of flat CBF response to pressure will be shifted due to conditions such as hypercapnia, hypocapnia, hypotension, and hypertension (see Figure 3.5).

To ensure proper CBF, the global baroreflex control seeks to stabilize P_{as} providing a stable pressure gradient for CBF, while autoregulation smoothes out any systemic or regional pressure variations influencing CBF and regional flow.

In regards to metabolic influences, it is known that CO_2 in brain tissue has a strong effect on the degree of cerebral vasoconstriction, inducing vasodilation as CO_2 rises. This impact can be quantified in terms of levels of P_{a,CO_2}. For values of P_{a,CO_2} between 20 and 80 [mmHg], CBF responds linearly with an increase of 1–2 [ml] per minute per 100 [g] for each increase of 1 [mmHg] in P_{a,CO_2} (Brian, 1998).

In regards to O_2 and metabolic demand control, the nature and degree of coupling of O_2 to CBF are still topics of research (Mintun et al., 2001; Davis et al., 1998). It is clear that aggregate CBF is determined by overall metabolic rate. Thus delivery of sufficient O_2 and glucose to brain tissue is ensured and, during a significant hypoxic challenge vasodilation, certainly occurs to aid in alleviating this challenge (Pearce, 1995). This reflects the general view (see, for example, Van Mil et al., 2002) that CBF varies (via metabolic control mechanisms) in coordination with O_2 demand and transient O_2 deficit. However, questions regarding the degree of direct coupling of regional O_2 to regional CBF have not been resolved (Mintun et al., 2001). For example, on the one hand, CBF is certainly directly linked to regional neural activity (and thus by implication to O_2 usage), as can be seen in studies such as Davis et al. (1998). However, when regional neural activity increases, CBF appears to increase much more than the O_2 demand associated with that increase in neural activity. One explanation (among several hypotheses) put forward is that the diffusion of O_2 is not

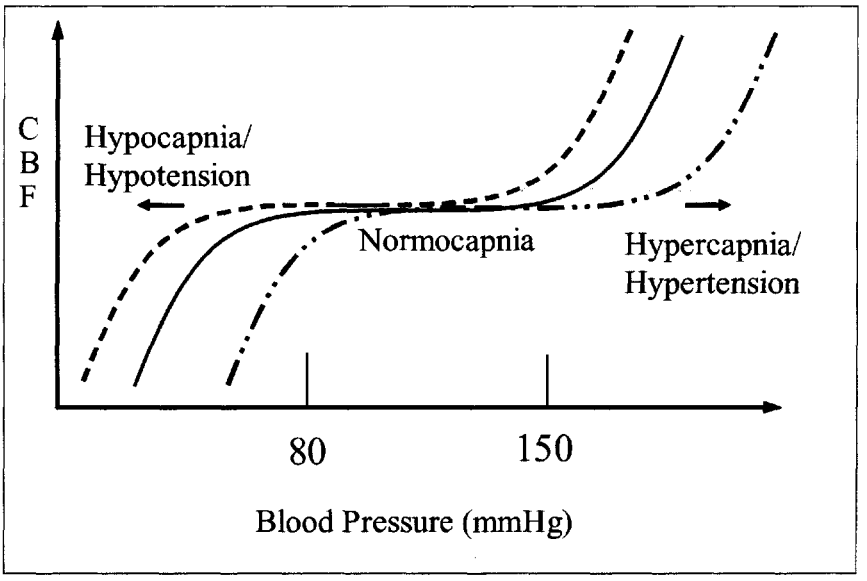

Figure 3.5: CBF flow and CO_2 levels.

as efficient as CO_2 diffusion thus requiring concentration levels of tissue O_2 higher than metabolically necessary to ensure adequate O_2 delivery (Buxton and Frank, 1997). Other studies suggest that O_2 baseline tissue concentration is so high that factors other than O_2 metabolic usage must be responsible for the observed link between increased neural activity and increased CBF (Mintun et al., 2001). Hence, the distribution of regional CBF in response to neural activity may be only partly associated with the influence of an O_2 short-term deficit as observed in Davis et al. (1998).

In the case where hypoxia develops at the systemic level, such as during apnea, influences on CBF via vasodilation occurs, but the respiratory response of higher $\dot{V}_E$ reduces CO_2 and this promotes vasoconstriction. This tends to counteract any direct systemic hypoxia-induced cerebral vasodilation (Levick, 2003), and can be a complicating factor for stable function.

In regards to global and local control interaction, as mentioned in Subsection 3.1.1, global constriction by sympathetic activity in response to baroreflex stimulation does not in the main influence brain vasculature. However, attenuation by sympathetic action of CO_2 induced changes in CBF has been observed and may indicate some interaction of autoregulatory and global effects, as noted in Jordan et al. (2000). Thus, it can be seen that many aspects of CBF control are under current investigation. For an excellent review of issues in CBF control and measurement methods, see Panerai (1998).

Coronary blood flow

Coronary blood flow must also be maintained at levels sufficient to meet the high metabolic demand of cardiac tissue, which even at baseline activity results in a high extraction of O_2. Hence, coronary flow is tightly coupled to metabolic demand (Rowell, 2004). As with the cerebral circulation, global vasoconstriction or vasodilation stimulated by baroreflex

activation of sympathetic activity does not impact coronary blood flow. This is due to the complex interaction of several effects (Levick, 2003). Changes in coronary flow to meet increased demand is accomplished primarily through local metabolic vasodilation, but the precise agent(s) of vasodilation, the details of activation pathways, and the correspondence to local vasocontrol pathways in skeletal muscle are still under investigation (Rowell, 2004). Coronary flow is held steady during variations in blood pressure by autoregulation (with probably a significant contribution from myogenic control) over a wide range of values of P_{as}, insuring adequate and steady flow to meet metabolic demands (Schubert and Mulvany, 1999). As an interesting aside, showing the complexity of interacting effects influencing coronary flow, the so-called Gregg's phenomenon states that coronary metabolic activity (via contractility) increases with increased coronary flow. This complicates the regulation of coronary flow as modeled in Dankelman, Stassen, and Spaan (1999). Another complicating factor is that coronary flow occurs primarily during diastole.

Renal blood flow

Renal blood flow accounts for about 20% of total blood flow and of that amount about 20% of the plasma along with small proteins and chemicals are filtered every minute. As red blood cells represent about 40% of total blood volume that means that about 125 [ml/min] or 180 [liters/day] are filtered, which makes the kidneys an amazing filtering device. Sufficient and constant blood pressure at the entrance to a nephron (the fundamental filtration element of the kidney) is needed to force the filtration process, and efficient autoregulatory and feedback loop mechanisms exist to ensure that the appropriate blood pressure environment is maintained.

3.1.3 Blood volume shift

Blood volume is an important determiner of CVS function. It influences vascular pressures, filling pressure of the heart, and overall pressure distribution as well as influencing the efficiency of nutrient transport. Both blood volume loss, due to hemorrhage, and blood volume shift to the lower body (as in the transition from the supine position to standing) result in a number of related CVS compensatory actions. The short-term response to a hypovolemic challenge is illustrated in Figure 3.2.

Unstressed volume V_u refers to the blood volume which is held in a vascular vessel at zero transmural (across the vessel wall) pressure (as briefly discussed in Subsection 1.2). It is that volume which fills out the natural shape of the vessel without placing stress on the vessel walls. Stressed volume V_s is the difference between the total volume and the unstressed volume of the vascular vessel, and is thus the additional volume added due to the transmural pressure extending the vascular walls.

Capacitance is the function that describes the total blood volume that a vascular vessel contains at a certain transmural pressure. This total volume is the sum of the stressed and unstressed volumes. Compliance is the derivative of the capacitance function with respect to pressure (at a given pressure), and thus describes the rate of change in total volume as the pressure is changed. In physical terms, compliance measures the distensibility of the vessel walls under pressure stress.

Clearly, a change in pressure will alter the stressed volume. In a given vascular vessel, the relation between pressure and total volume is nonlinear, because the compliance

and unstressed volume of the vessel depend on structural characteristics of the vessel walls, which vary as the walls are expanded or contracted. A simplified equation for the capacitance function which separates the stressed and unstressed volume components is given as

$$V(P) = c(P)P + V_u, \tag{3.2}$$

where V is the vascular volume, c is compliance, P is pressure, and V_u is the unstressed volume. The dependency of c on pressure, $c = c(P)$, arises through structural properties of the vasculature. Unstressed volume V_u may depend indirectly on pressure, for instance, via baroreflex control. Stressed volume appears as $V_s = c(P)P$ in this equation.

A more extensive discussion of these key blood volume elements is given in Subsections 4.4.1 and 4.4.2. Figure 4.2 illustrates the relation between these elements for a typical vascular element. In this figure, the dashed line represents the tangent of the pressure-volume curve at the given pressure with slope equal to the compliance.

We note that the intercompartmental flows depend on the relative pressures between compartments, measured in relation to a reference pressure such as atmospheric pressure. This dynamic (or stressed) pressure is not influenced by any change in transmural pressure such that is induced by LBNP. Hence, the volume shift induced by LBNP is taken as a change in unstressed volume, which will not directly influence the intercompartmental flows. Indirectly, LBNP influences these flows because an increase in unstressed blood volume implies a reduction in stressed volume, which impacts the overall state of the system and hence the dynamic pressures. Unstressed volume is a significant component of total blood volume, and hence a significant determiner of blood volume distribution (compare, for example, the discussion in Subsection 1.6.1).

It appears that the control of unstressed volume plays a major role and this quantity can be influenced by sympathetic activity (Magder and De Varennes, 1998). Changes in compliance can also occur, for example, as a consequence of the nonlinearity of the pressure-volume curve in certain tissue regions and part of the pressure spectrum. For example, the compliance in the limbs decreases as pressure increases (Risk et al., 2003). The sympathetic influence on compliance may also exist and probably depends on regional tissue characteristics. Arterial side vascular resistances can influence volume shift by changing the output pressures which, in conjunction with autoregulatory local effects, can shift blood volume. One goal of CVS control modeling is to quantify in detail how these diverse factors interact. Further aspects of volume control and capacitance will be discussed in the applications in this chapter and in Chapter 4.

3.1.4 Interaction of CVS and RS control

Clearly the cardiovascular and respiratory systems are interconnected, both acting to satisfy the requirements of stable metabolism. The traditional approach was to study these two systems as though they were essentially independent (see, for example, the discussion in De Burg Daly, 1986). According to this view, in normal rest conditions, ventilation and pulmonary blood flow coordination requires only indirect coordination through the interplay of the individual negative feedback controls of the CVS and RS, responding to metabolic demand and particular control constraints such as stable blood pressure. Important to this interplay is the fact that, blood so quickly, efficiently, and completely loads and

unloads blood gases in the alveoli, that blood gas transport is essentially limited only by the pulmonary perfusion rate.

However, beyond this interplay and loose coordination of independent system elements, it is clear that there are a number of key links between the two systems that require an integrative view of what can be referred to as the cardiovascular-respiratory system (CVRS). Even in the normal rest state, a degree of active coupling between ventilation and blood flow likely exists, as for example, in respiratory sinus arrhythmia (RSA), which may aid pulmonary gas exchange by influencing ventilation-perfusion coupling and via cardiopulmonary and pulmonary sensors signaling changes in Q_{co}, which may influence $\dot{V}_E$ (De Burg Daly, 1986). The lung inflation reflex attenuates vagal influence of H when ventilation increases as during hypoxia.

During the normal, but more extreme, situation of exercise (which can be viewed as a form of stress), the need to match the activity of the two systems is more critical, and the systems respond in a more coordinated fashion, requiring additional modes of control. CVS and RS coordination and interaction are also complicated by stresses imposed by extreme but abnormal conditions such as asphyxia, hemorrhage, apnea-induced hypoxia, and many other clinical conditions, which distort the usual functional relations.

Some of the key links between the CVS and RS have been mentioned in both Section 2.1 and Subsection 3.1.2, and include blood gas influence on local vascular constriction and blood flow influence on respiratory feedback delay.

The nature and degree of interaction of related CVS and RS controls often depend on the type and degree of the stimulus. For example, hypoxia induced during apnea results in systemic vasoconstriction, while hypoxia occurring during spontaneous breathing results in systemic vasodilation (Leuenberger et al., 2001).

Interaction of chemosensors

The close connection between CVS and RS control is nicely exemplified by the physical proximity of the carotid and aortic baroreceptors and peripheral chemoreceptors. Indeed, the chemoreceptors that influence blood pressure and the respiratory reflexes, found at the carotid sinus and aortic arch essentially the same set of chemical sensory cells influencing both the CVS and RS under normal conditions primarily act as respiratory sensors (Levick, 2003). In considering the chemoreflex impact on the CVS and RS, it is important to keep in mind that changes in blood gases at chemosensor sites can be due to changes in the respiratory environment (ventilatory effect) or due to reduced blood flow to the sensors (cardiovascular effect). We consider the function of the peripheral chemosensors here, which respond to hypoxia and which appear to be more influenced by other feedback loops (Kara, Narkiewicz, and Somers, 2003), but the central chemosensor function should also be taken into account when considering responses to significant hypercapnia.

We mentioned previously that the CVS response to pure hypoxic peripheral chemosensor stimulation is increased by sympathetic-induced vasoconstriction and induced mild bradycardia (De Burg Daly, 1986; Kara, Narkiewicz, and Somers, 2003; Leuenberger et al., 2001). In addition, the lung inflation reflex (see also Subsection 2.1.5) represents another feedback element relevant to this situation. This reflex involves lung stretch receptors whose signal (resulting from ventilatory activity) also influences the central cardiovascular control centers, inhibiting parasympathetic and sympathetic responses (De Burg

Daly, 1986; Levick, 2003; Ursino and Magosso, 2003). These feedback pathways, along with baroreflex influences, lead to complex patterns of control interaction.

In response to a mild reduction in intake of O_2, either due to insufficient ventilation rate or reduced ambient O_2, the RS increases ventilation. CVS response to chemoreflex stimulation is vasoconstriction due to enhanced sympathetic activation, but this would be mainly counteracted (since the chemoresponse is moderate in this case) by the local metabolic vasodilation and the inhibiting effects of the lung inflation reflex. Hence, the primary response to moderate changes in intake of O_2 is a respiratory response, and the CVS and RS chemoresponses can be seen decoupled to a certain degree. Similar considerations apply to heightened CO_2. The need for coordination and the significance of interaction of the CVS and RS reflexes occur during more extreme cases of hypoxia, especially when combined with hypercapnia, hemorrhage (hypotension), and in certain diseases (Levick, 2003; Kara, Narkiewicz, and Somers, 2003; Prabhakar and Peng, 2004).

In hypoxia, ventilation is significantly increased due to the respiratory chemoreflex (except during apnea). The CVS response to hypoxic chemosensor stimulation is the above-mentioned increase in sympathetic-induced vasoconstriction and induced bradycardia. When spontaneous breathing occurs during hypoxia, the lung inflation reflex and local vasodilation will limit the sympathetic vasoconstriction effect, but tachycardia is also observed. This tachycardia, observed in hypoxia when breathing occurs (no apnea), is not due to any direct pathway of chemoreflex influence on H (De Burg Daly, 1986), but is likely due to the increased lung activity. This activity triggers reduction in parasympathetic vagal activity (see also sinus arrhythmia below), creating an increase in H that more than compensates for any typical chemoreflex-induced bradycardia (Levick, 2003). Any improvement in blood pressure and flow will aid in O_2 delivery. Hence, the two responses would be generally supportive.

Hypoxia induced by apnea complicates this scenario as the lung action stimulation of heart rate is absent and bradycardia occurs, together with vasoconstriction (a condition sometimes referred to as the diving reflex) (Kara, Narkiewicz, and Somers, 2003).

When P_{as} drops for whatever reason, chemoreceptors respond (primarily during larger pressure drops), because the drop in pressure induces a drop in perfusion and consequently a drop in O_2 stimulation and an increase in CO_2 stimulation. The response in this case is again vasoconstriction, which helps to support blood pressure. This chemoreflex response can be very important when P_{as} drops below the baroreflex response threshold such as in clinical shock. Such a fall in P_{as} in circulatory shock is also accompanied by rapid breathing that contributes to the increase in H (as described above). This is a common response to hypotension induced by hemorrhage (Levick, 2003), and the combined emergency response supports pressure and aids in O_2 delivery.

Complicating this picture is the fact that the baroreflex appears to have an inhibitory influence, which blunts the chemoreflex CVS control (Kara, Narkiewicz, and Somers, 2003) due to interference of afferent signals. This may explain the fact that small changes in P_{as}, which activate the chemoreflex, do not seem to impact ventilation.

It is clear that the chemoreceptors are responding to two different conditions: low blood pressure and low O_2 levels. Not all feedback pathways are in every case coordinated, with different responses dominating in different circumstances. Quantitative models reflecting these interactions are of great value for basic research and clinical application. For

example, essential hypertension has been associated with heightened carotid body sensory response and ventilatory response to hypoxia (Prabhakar and Peng, 2004).

CVS *and* RS *interaction in* CBF

As mentioned earlier, in Subsection 3.1.2, CBF is held relatively constant over a wide range of blood pressure values. As can be seen in Figure 3.5, this range shifts due to conditions of hypercapnia or hypocapnia. Thus, respiratory function is an important factor to take into account when considering issues involved in CBF.

Cardiorespiratory rhythms

As cardiac and respiratory function are cyclic in nature, arising from patterns in H and $\dot{V}_A$, there arises the possibility of rhythmic interaction between these cycles. Because of interconnections of nerve pathways in the medula, we expect some interaction of CVS and RS control. One form of interaction is termed modulation, which occurs when one cycle influences the characteristics of another cycle.

The classic example of modulation is RSA, in which the respiratory rhythm creates cyclic variations in H. This appears to be mediated primarily through signals from the lung stretch receptors and/or inspiratory rhythm neurons or related central respiratory pattern factors, while other factors play a role in the degree of modulation (Giardino et al., 2003). Periodically (during the inspiratory phase), the above-mentioned neural signals interfere with parasympathetic efferent fibers (vagus nerve), attenuating parasympathetic drive and in consequence raising H. Parasympathetic stimulation occurs during expiration and the combined effect imposes a rhythmic variation on H that corresponds to the pattern of $\dot{V}_A$. In this case, there is no causal linkage determining the fundamental value of H by $\dot{V}_A$, but a rhythmic variation is superimposed on whatever inherent H and is independently generated by the CVS demands. This effect is likely more than merely a physiological artifact, as it has been suggested by several researchers that RSA has a role in matching ventilation to perfusion within each respiratory cycle, and thus improving ventilation-perfusion coordination (Giardino et al., 2003; Yasuma and Hayano, 2004). RSA is just one source of heart rate variability (HRV), where HRV is defined as variations in the sequence of intervals between beats of the heart.

Synchronization refers to a second stronger form of interaction in which two cycles become linked either in frequency or phase: when one frequency changes, for example, so does the other in an equivalent way. When noise and stochastic influences are included, the precise definition of these ideas becomes more complicated. A clear description of these concepts can be found in Schäfer et al. (1999).

There is a large literature addressing methods by which coupling of various CVS and RS oscillations can be defined, detected, and interpreted and an excellent introduction can be found in Glass (2001). Linkage can be through a number of channels, including interaction of nerve pathways as well as other forms of reflex interaction. These oscillatory linkages can aid in diagnosis or parameter grouping of patients. Note that while HRV is reduced in the elderly and diabetics, the effects of long-term reduced HRV is under active investigation. See, for example, Taylor et al. (2001) and Glass (2001). Respiratory influence on cardiovascular rhythms has been demonstrated in many settings, but the nature

and degree of corresponding cardiovascular influences on respiratory rhythm are still being investigated (Stefanovska, 2002).

CVS and RS during exercise

There are two fundamental points about cardiovascular and respiratory function during aerobic exercise: (a) cardiac output and ventilation keep up with metabolic demand and (b) blood pressure increases to some degree, while blood gas deviations are minimal, and neither of these conditions is appropriate for generating baroreflex or chemoreflex feedback responses that account for the metabolically necessary increases in Q_{co} and $\dot{V}_A$. Hence, other mechanisms must be involved in determining CVS and RS action during exercise. These mechanisms, that account for the substantial responses during exercise, remain an issue of controversy (Ursino and Magosso, 2003; Levick, 2003).

Furthermore, distinction must be made between moderate and strenuous, aerobic and anaerobic, upright and supine, as well as isometric and isotonic forms of exercise, when considering CVS and RS response. We will consider only moderate aerobic exercise (up to the aerobic threshold).

Heart rate and ventilation increase almost instantly with the onset of exercise, while local vasodilation of active muscle begins to increase blood flow locally and reduce total resistance (Rowland, 2005). Even with this effect on net resistance, arterial pressure rises modestly, since Q_{co} increases substantially and global vasoconstriction is invoked. During exercise, steady-state values of Q_{co} and H have been found to increase proportionally with net body metabolic demand and work rate (Levick, 2003), and Q_{co} may be 4 or more times higher during strenuous exercise. Stroke volume remains little changed as supine exercise increases and, during increasing upright exercise, plateaus after a 30–40% initial gain (Rowland, 2005). Hence it is clear that control of stroke volume does not play the major role in increasing blood flow during exercise. Stroke volume does increase with training, so that well-conditioned athletes require a lower resting heart rate due to increased resting stroke volume. As a consequence, athletes have the ability to generate a greater increase in cardiac output during exercise. Ventilation also increases linearly with steady-state O_2 demand (work rate) (Wasserman, Whipp, and Casaburi, 1986) and can increase 10-fold or more during strenuous exercise. Tidal volume and frequency increase similarly during increases through lower workloads with tidal volume change tending to plateau at high workloads at about 0.7 of inspiratory capacity (Neder et al., 2003).

One mechanism that is proposed to account for the rapid and significant physiological changes at the onset of exercise assumes that the initial brain center activation that induces exercise activity also triggers the initial CVS and RS responses. This is referred to as a central command mechanism (Ursino and Magosso, 2003) and is considered a feedforward mechanism that prepares the system for activity (an open loop response in the sense that there is no response to current conditions). There is evidence of sympathetic activity generated by cortical regions which would support this hypothesis (Dampney et al., 2002).

There are also distributed receptor sites, which trigger adjustments that shift the system to new operating levels such as that seen in the transition from rest to exercise. Muscle mechanoreceptors are an excellent example of such a mechanism. These receptors respond to muscle activity and may partly trigger the early stimulation of the heart by depressing parasympathetic vagal activity (Levick, 2003). The initial response may be considered

feedforward while it is also feedback, as the level of stimulation depends on the level of exercise.

In addition, metabolic receptors (metaboreceptors) exist in muscle tissue, which promote enhanced cardiovascular function by responding to metabolic byproduct concentrations. Raised metabolite concentrations, due to increased activity or reduced blood flow in contracted muscle, contribute to sympathetic activation at least in static exercise (Rowell, 2004). In static exercise, the contracted muscles inhibit blood flow and render ineffective local vasodilation. However, the sympathetic response in this case increases blood pressure, counteracting the restriction to flow and improving the delivery of blood to the metabolically active muscles. The mechanoreflex, metaboreflex, baroreflexes, and central command interact in complex ways depending on the degree and type of exercise. While a detailed quantitative model for exercise response does not exist, it is clear that a combination of central command, learned response, and reflex activity, such as the mechanoreceptor reflex, must initiate the coordinated response to exercise (see discussions in Levick, 2003; Dampney et al., 2002).

The centralized sensory sites (such as the arterial baroreflex sensors) also are involved in setting and controlling the physiological operating point associated with exercise. Blood pressure varies little at the onset of exercise, but rises smoothly with workload until the new exercise steady state is reached. The baroreflex continues to function as a control loop, but its operating point is reset to be consistent with the higher blood pressures needed for heightened CVS function. Such a resetting may thereby involve the baroreflex in raising the CVS to the exercise state (DiCarlo and Bishop, 2001), but in any case, without such a resetting (or disengagement), the baroreflex would tend to act against the heightened pressure and any attempt to vasodilate blood vessel to combat perceived heightened pressure will compromise blood distribution to active muscles. This resetting may reflect a mode of operation of central command (DiCarlo and Bishop, 2001), while other mechanisms such as the muscle mechanoreceptor exercise pressor reflex may also be involved (Gallagher et al., 2001).

The increases in Q_{co} and generalized vasoconstriction may have in part a central command origin, but are supplemented by the metaboreceptors (at least during static exercise, Levick, 2003) and mechanoreceptors and depend also on the muscle pump, respiratory pump, and lung stretch receptors, all of which contribute to stimulating and matching CVS function to metabolic needs. Increased global vasoconstriction helps to channel blood to local active muscle regions, where metabolic vasodilation is occurring and simultaneously supports MAP by counteracting the reduction in resistance caused by that vasodilation. How vasodilation overcomes vasoconstriction in active muscle, where it is metabolically necessary, is still an area of active research (see, e.g., Rowell, 2004). Indeed, all of these mechanisms involved in adaptation to exercise demand are still under active investigation (Rowell, 2004).

The initial increase in ventilation may also be due to a central command reaction (see, e.g., the discussion in Ursino and Magosso, 2003; Dampney et al., 2002). Such a coupled central response is suggested by the above-mentioned fact that blood gases do not change appreciably, which argues that exercise induced changes in pulmonary blood flow F_p (and Q_{co}) and $\dot{V}_A$ must be tightly linked, for otherwise there should be some deviation from the standard stable values (Wasserman et al., 1986).

After the initial jump in ventilation, any further sustained increase in ventilation may be due, at least in part, to stimulation of the peripheral chemoreceptors. The mechanism for this stimulation (which cannot be blood gas deviations) may be due to blood-borne, exercise generated, metabolic byproducts such as circulating cathecholamines, lactic acid, or K^+ (Prabhakar and Peng, 2004). Indeed, circulating metabolic agents may represent another dimension of feedback control similar to hormone control.

Many other elements, such as temperature control, are involved in the intricate coordination of the combined CVS-RS response to exercise, and this remains an area of current research.

3.2 The Combined Model

In this section we consider a combined model of the RS and CVS based on models developed in Chapters 1 and 2. In linking the two models together, we need to consider the roles of the various compartments (see Figure 3.6). The lung and tissue compartments in the respiratory submodel are at the same time the peripheral regions in the CVS submodel, which we assumed to be resistance vessels with resistances R_p and R_s. Whereas Q_{co}, F_s, and F_p were equated in the RS model, they are now to be distinguished. In particular, instead of Q_{co}, we now have Q_ℓ and Q_r, the cardiac output of the left, respectively, the right, heart. All compartments represent volumes: blood gas volumes in the RS and vascular volumes in the CVS. In the simplest formulation of the model, the links between the two subsystems consist of the following: blood flows in the CVS component influence respiratory gas partial pressures; venous O_2 concentration C_{v,O_2} influences systemic resistance; the physiological controls $\dot{H}$ and $\ddot{V}_A$; and the cost functional which tracks physiologically measured values such as P_{as}, P_{a,CO_2}, and P_{a,O_2}. As we will see, this model is adaptable to a number of conditions and one can easily expand its control features.

3.2.1 Model equations

The equations for the cardiovascular component are essentially the same equations as in Chapter 1 and are given as

$$\begin{aligned}
c_{as}\dot{P}_{as} &= Q_\ell - F_s,\\
c_{vs}\dot{P}_{vs} &= F_s - Q_r,\\
c_{ap}\dot{P}_{ap} &= Q_r - F_p,\\
c_{vp}\dot{P}_{vp} &= F_p - Q_\ell,\\
\dot{S}_\ell &= \sigma_\ell,\\
\dot{S}_r &= \sigma_r,\\
\dot{\sigma}_\ell &= -\gamma_\ell\sigma_\ell - \alpha_\ell S_\ell + \beta_\ell H,\\
\dot{\sigma}_r &= -\gamma_r\sigma_r - \alpha_r S_r + \beta_r H.
\end{aligned} \tag{3.3}$$

As long as we are not considering central ventilatory control, the model for the RS consists only of the first four equations in system (2.14), as given in Subsection 2.2.5, (however, see the remark concerning (3.10) below):

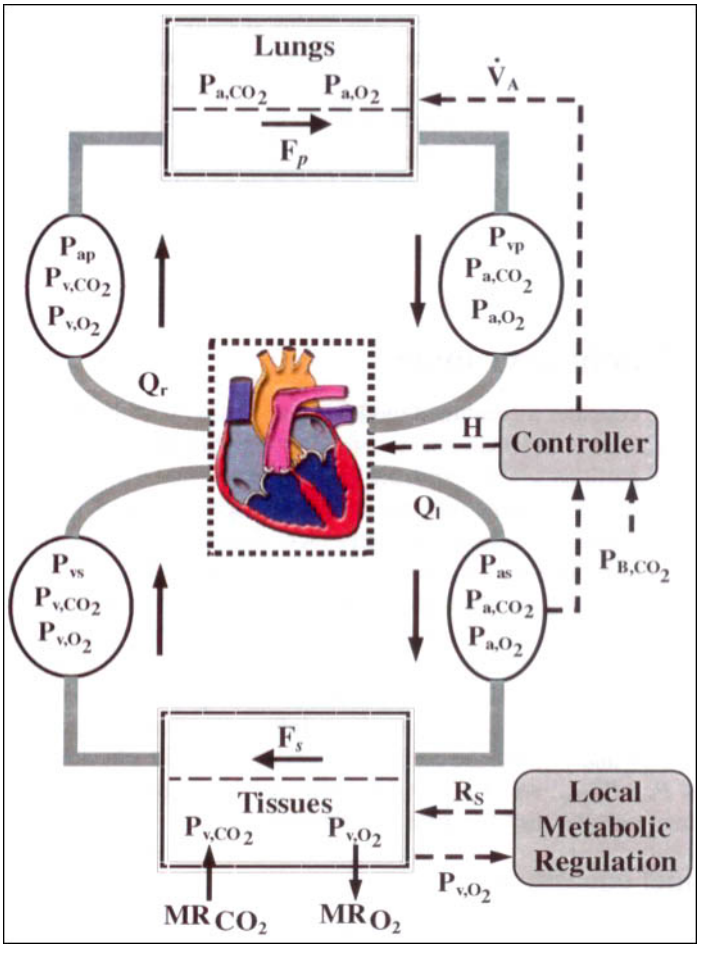

Figure 3.6: Combined CVS and RS model block diagram.

$$
\begin{aligned}
V_{A,CO_2}\dot{P}_{a,CO_2}(t) &= 863F_p\left(C_{v,CO_2}(t-\tau_v) - C_{a,CO_2}(t)\right) \\
&\quad + \dot{V}_A\left(P_{i,CO_2} - P_{a,CO_2}(t)\right), \\
V_{A,O_2}\dot{P}_{a,O_2}(t) &= 863F_p\left(C_{v,O_2}(t-\tau_v) - C_{a,O_2}(t)\right) \\
&\quad + \dot{V}_A\left(P_{i,O_2} - P_{a,O_2}(t)\right), \\
V_{T,CO_2}\dot{C}_{v,CO_2}(t) &= MR_{CO_2} + F_s\left(C_{a,CO_2}(t-\tau_T) - C_{v,CO_2}(t)\right), \\
V_{T,O_2}\dot{C}_{v,O_2}(t) &= -MR_{O_2} + F_s\left(C_{a,O_2}(t-\tau_T) - C_{v,O_2}(t)\right),
\end{aligned}
\tag{3.4}
$$

The delays that appear in these equations are the ones described in Subsection 2.2.5 (see also Figure 2.2). As in Chapter 2, these delays are implicitly determined by the development

of the system in the past. In order not to interrupt the considerations of this subsection, we defer a detailed discussion of this aspect to Subsection 3.2.2.

The controls are given by $\dot{H}$ and $\ddot{V}_\Lambda$; i.e., we have the following control equations:

$$\begin{aligned} \ddot{V}_\Lambda &= u_1, \\ \dot{H} &= u_2. \end{aligned} \tag{3.5}$$

The auxiliary cardiac and respiratory equations are the same as those described previously. Dissociation relations are as in (2.2) and (2.4). Furthermore, we still have the constraint (1.5),

$$c_{as} P_{as} + c_{vs} P_{vs} + c_{ap} P_{ap} + c_{vp} P_{vp} \equiv V_{tot}, \tag{3.6}$$

which can be used to reduce the cardiovascular model by one equation (expressing P_{ap} by the other pressures in the CVS, for instance).

For comparison to the extension to orthostatic stress in Section 3.3, we repeat here the relations for the peripheral flows F_s, and F_p,

$$\begin{aligned} F_s &= \frac{1}{R_s}(P_{as} - P_{vs}), \\ F_p &= \frac{1}{R_p}(P_{ap} - P_{vp}). \end{aligned} \tag{3.7}$$

Particular note should be made of the relation given by (1.24),

$$R_s = A_{pcsk} C_{v,O_2}, \tag{3.8}$$

which was the basic relation for the submodel (1.27) concerning the autoregulation process in Section 1.2. In the combined model C_{v,O_2}, respectively, P_{v,O_2}, is a state variable, so that (3.8) can be considered as the submodel for the autoregulation process in the combined model. We remind the reader that (3.8) exhibits only the metabolic aspect for the control of the local demand. Myogenic and other autoregulatory influences will be further discussed in Subsection 3.3.4. The following considerations show that also in the combined model, we can derive a differential equation for R_s, which is analogous to (1.27) in the basic model for the CVS as considered in Chapter 1.

Using the dissociative relation (2.2) for O_2, with $c_o = 2$ in (3.8), we obtain

$$R_s(t) = A_{pcsk} a_o \left(1 - e^{-b_o P_{v,O_2}(t)}\right)^2.$$

Taking derivatives with respect to t and using the differential equation for P_{v,O_2} in (3.4), together with (3.7), we obtain after some computations

$$\begin{aligned} \dot{R}_s(t) = {} & \frac{2a_o b_o}{V_{T,O_2}} \left(1 - e^{-b_o P_{v,O_2}(t)}\right) e^{-b_o P_{v,O_2}(t)} \\ & \times \left(A_{pcsk} \left(\frac{P_{as}(t) - P_{vs}(t)}{R_s(t)} C_{a,O_2}(t - \tau_T) - MR_{O_2} \right) + P_{vs}(t) - P_{as}(t) \right). \end{aligned}$$

It should be observed that

$$2a_0b_0\Big(1-e^{-b_0P_{v,O_2}}\Big)e^{-b_0P_{v,O_2}}=\frac{dC_{v,O_2}}{dP_{v,O_2}},$$

where C_{v,O_2}, as a function of P_{v,O_2}, is given by (2.2). With this, we obtain

$$\dot{R}_s(t)=\frac{1}{V_{T,O_2}}\cdot\frac{dC_{v,O_2}}{dP_{v,O_2}}(t)\\ \times\left(A_{pcsk}\Big(\frac{P_{as}(t)-P_{vs}(t)}{R_s(t)}C_{a,O_2}(t-\tau_T)-MR_{O_2}\Big)+P_{vs}(t)-P_{as}(t)\right).$$

This equation reduces to (1.27) if we take a linear approximation

$$C_{v,O_2}=K_{v,O_2}P_{v,O_2}+k_{v,O_2}$$

for the dissociative relation and if we assume, in addition, that C_{v,O_2} is constant (as was done in Section 1.2). Indeed, we get

$$\dot{R}_s(t)=\frac{K_{v,O_2}}{V_{T,O_2}}\left(A_{pcsk}\Big(\frac{P_{as}(t)-P_{vs}(t)}{R_s(t)}C_{a,O_2}-MR_{O_2}\Big)+P_{vs}(t)-P_{as}(t)\right),$$

which is (1.27) if we identify the parameter K, respectively, M_T, of the basic model with $V_{T,O_2}/K_{v,O_2}$, respectively, MR_{O_2}.

Sources for state and parameter values can be found, e.g., in Timischl (1998) and Batzel, Kappel, and Timischl-Teschl (2005).

3.2.2 State dependency of the delays

As long as the model is given by (3.3), (3.4), and (3.5), the only delays in the model are τ_v and τ_T. Considerations analogous to those leading to conditions (2.20), (2.21) give the following implicit equations for τ_v and τ_T:

$$\int_{-\tau_T}^{0}(Q_\ell)_t(s)\,ds=V_3\quad\text{and}\quad\int_{-\tau_v}^{0}(Q_r)_t(s)\,ds=V_4,$$

where V_3, respectively, V_4, is the volume of the vasculature connecting the lung region with the tissue region, respectively, the tissue region with the lung region. V_3 is essentially the volume of the venous pulmonary compartment plus a fraction of the volume of the arterial systemic compartment. Similarly, V_4 is a fraction of the volume of the venous systemic compartment plus the volume of the arterial pulmonary compartment.

Since Q_ℓ and Q_r are functions of the state variables of the system (compare the formulas (1.35)), we see that τ_v and τ_T are functions of the past history of the system state x,

$$\tau_v=\tau_v(x_t),\quad\tau_T=\tau_T(x_t).$$

Thus we have shown that the delays τ_v and τ_T are state-dependent point delays.

If, instead of the first equation in (3.5), we take the empirical control (3.10), together with the additional model equation (3.11), then we have the additional delays τ_p and τ_B. The conditions which determine τ_B are (compare (2.20) and (2.21))

$$\int_{-\tau}^{0} (F_B)_t(s)\,ds = V_1, \quad \int_{-\tau_B}^{-\tau} (Q_\ell)_t(s)\,ds = V_2.$$

Analogously, we get for τ_p the conditions

$$\int_{-\tau_1}^{0} (F_B)_t(s)\,ds = \tilde{V}_1, \quad \int_{-\tau_p}^{-\tau_1} (Q_\ell)_t(s)\,ds = V_2,$$

where $\tilde{V}_1$ is the volume of the vasculature connecting the origin of the carotid artery with the carotid sinus. If, in our model with empirical control, the flow F_B is a given nonconstant function of t, we see that we have

$$\tau_B = \tau_B(t, x_t), \quad \tau_p = \tau_p(t, x_t);$$

i.e., these delays can be state and time dependent.

3.2.3 Control formulation

The state of the system is described by the vector

$$x = \big(P_{as}, P_{vs}, P_{ap}, P_{vp}, S_\ell, \sigma_\ell, S_r, \sigma_r, P_{a,CO_2}, P_{a,O_2}, P_{v,CO_2}, P_{v,O_2}, \dot{V}_A, H\big)^T \in \mathbb{R}^{14}.$$

The controls are described by (3.5). In this formulation we include ventilation in the control via the relation $\ddot{V}_A = u_2$. Hence, dead space is implicitly built into the alveolar ventilation. In order to obtain a stabilizing feedback control, we proceed as in Section 1.4. Under the assumption that the sensory system measures levels of P_{as}, P_{a,CO_2}, and P_{a,O_2} via the carotid and aortic bodies, we introduce the following quadratic cost functional:

$$\begin{aligned} J(u(\cdot), x^{\text{final}}) = \int_0^\infty \big(&q_{as}^2 (P_{as}(t) - P_{as}^{\text{final}})^2 + q_o^2 (P_{a,O_2}(t) - P_{a,O_2}^{\text{final}})^2 \\ &+ q_c^2 (P_{a,CO_2}(t) - P_{a,CO_2}^{\text{final}})^2 + q_1 u_1(t)^2 + q_2 u_2(t)^2\big)\,dt. \end{aligned} \tag{3.9}$$

Further sensory loops can be included involving implementation of the low-pressure sensors on the venous side. Under the *assumption that the delays are constant* we can use the same process for calculating the optimal control as described in Section 1.4.

Step 1: Compute the "final" steady state x^{final}, which corresponds to choice of parameters characterizing this final state. Compute the "initial" steady state x^{initial} defined by parameter choices which simulate the initial steady state from which the system starts. This initial state will be the initial condition for the simulation and the control will be designed to transfer the system from the initial to the final state. The steady-state relations show that there are two free variables whose values must be chosen. We use H and P_{a,CO_2} as these values are well known for many states.

Step 2: Linearize the system around the final steady state.

Step 3: Calculate the feedback gain matrix for the linear quadratic regulator problem that will move the linearized system to the final state (which is the zero state), minimizing the cost (3.9).

Step 4: The feedback gain matrix will provide a control for the nonlinear system that is suboptimal but stabilizing.

In regards to implementing the ventilation control we may, alternatively, include an empirical relation for $\dot{V}_E$ such as that given in (2.15),

$$\begin{aligned}\dot{V}_E = {} & G_P e^{-0.05 P_{a,O_2}(t-\tau_P)} \max\bigl(0,\, P_{a,CO_2}(t-\tau_p) - I_P\bigr) \\ & + G_C \max\left(0,\, P_{v,B,CO_2}(t) - \frac{MR_{B,CO_2}}{K_{CO_2} F_B} - I_C\right),\end{aligned} \tag{3.10}$$

which also necessitates one further state equation for the brain compartment,

$$V_{B,CO_2} \dot{C}_{v,B,CO_2}(t) = MR_{B,CO_2} + F_B \left(C_{a,CO_2}(t-\tau_B) - C_{v,B,CO_2}(t)\right). \tag{3.11}$$

Any transition from an initial steady state to a final state can be cast in this formulation. We will discuss in the following section the transition from awake to sleep in the CHF case, and transition from supine to upright in tilt table and LBNP tests, using adaptations of the above model.

Baseline parameters and units used for the simulations in this chapter are given in Tables 3.1 and 3.2.

3.2.4 Steady-state relations

The equations of the combined model as given by (3.3), (3.4), and (3.5), together with constraint (3.6) and auxiliary equations (3.7), (3.8), show that there exists a two-parameter set of equilibria. In order to fix a specific equilibrium, we have to fix the equilibrium values for two state variables. We choose to fix the equilibrium value H^{equ} for H and the equilibrium value P^{equ}_{a,CO_2}. The value for H^{equ} can be easily determined from measurements, whereas the value for P^{equ}_{a,CO_2} can be taken as 40 [mmHg]. In the following computations we usually delete the superscript "equ".

In order to compute the equilibrium values for the state variables of the combined model we proceed in two steps. We first consider the respiratory part of the system and express all respiratory state variables and the blood flow F in the cardiovascular part as functions of $\dot{V}_A$. Then we use the calculations presented in Subsection 1.3.1 to reduce the problem to one nonlinear equation for $\dot{V}_A$.

As in Subsection 1.3.1, we start with the observation that in an equilibrium situation we have $F_p = F_s = Q_\ell = Q_r =: F$. From the model equations (3.4) for the respiratory part, together with the dissociation relations given by (2.2) (with $c_o = 2$) and (2.4), we obtain

Parameter	Value	Unit
V	5.0	liter
c_{as}	0.0120	liter/mmHg
c_{vs}	0.6630	liter/mmHg
c_{ap}	0.0271	liter/mmHg
c_{vp}	0.1204	liter/mmHg
c_ℓ	0.0129	liter/mmHg
c_r	0.0607	liter/mmHg
α_ℓ	89.47	min^{-2}
α_r	28.46	min^{-2}
β_ℓ	85.89	mmHg/min
β_r	2.08	mmHg/min
γ_ℓ	37.33	min^{-1}
γ_r	11.88	min^{-1}
R_ℓ	11.350	mmHg min/liter
R_r	4.158	mmHg min/liter
A_{pesk}	141.84	mmHg min/liter
R_p	1.965	mmHg min/liter
τ_p	0.13	min
τ_T	0.6	min

Parameter	Value	Unit
MR_{O_2}	0.310	liter/min
MR_{CO_2}	0.266	liter/min
MRB_{CO_2}	0.042	liter/min
F_B	0.800	liter/min
P_{i,CO_2}	0.0	mmHg
P_{i,O_2}	150.0	mmHg
V_{B,CO_2}	0.900	liter
V_{A,CO_2}	3.20	liter
V_{A,O_2}	2.50	liter
V_{T,CO_2}	15.00	liter
V_{T,O_2}	6.00	liter
G_C	1.44	liter/(min mmHg)
G_P	30.24	liter/(min mmHg)
I_C	35.5	mmHg
I_P	35.5	mmHg
a_0	0.20	1
b_0	0.05.0	mmHg^{-1}
c_0	2.00	—
k_{CO_2}	0.244	1
K_{CO_2}	0.0065	1/mmHg

Table 3.1: Basic parameter values for CVRS congestive case. Parameters were taken from (Timischl, 1998) and (Batzel, Kappel, and Timischl-Teschl, 2005).

Parameter	Value
c_{ap}	0.0073
c_{vp}	0.0160
α_ℓ	89.47
α_r	28.46
β_ℓ	68.712
β_r	1.664
γ_ℓ	37.33
γ_r	11.88
R_ℓ	11.350
R_r	4.158
R_p	1.375
R_a	0.1
R_v	0.1

Parameter	Value
MR_{O_2}	0.290
MR_{CO_2}	0.244
P_{i,CO_2}	0.0
P_{i,O_2}	150.0
V_{A,CO_2}	3.20
V_{A,O_2}	2.50
V_{T,CO_2}	15.00
V_{T,O_2}	6.00
a_0	0.20
b_0	0.05
c_0	2.00
k_{CO_2}	0.244
K_{CO_2}	0.0065

Parameter	Value	
	hips case	ribs case
δ	0.500	0.300
$c_{as,up}$	0.0012	0.0007
$c_{as,lo}$	0.0012	0.0017
$c_{vs,up}$	0.1560	0.0420
$c_{vs,lo}$ (rest)	0.0228	0.1368

Table 3.2: Basic parameter values for orthostatic stress case. Parameters were taken from (Heldt et al., 2002) and (Timischl, 1998). R_a and R_v were chosen reasonably small.

$$-\dot{V}_A(P_{a,CO_2} - P_{i,CO_2}) + 863FK_{CO_2}(P_{v,CO_2} - P_{a,CO_2}) = 0, \tag{3.12}$$

$$\dot{V}_A(P_{i,O_2} - P_{a,O_2}) + 863Fa_o\Big(\big(1 - e^{-b_o P_{v,O_2}}\big)^2 - \big(1 - e^{-b_o P_{a,O_2}}\big)^2\Big) = 0, \tag{3.13}$$

$$MR_{B,CO_2} + K_{CO_2}F_B(P_{a,CO_2} - P_{v,B,CO_2}) = 0, \tag{3.14}$$

$$MR_{CO_2} + K_{CO_2}(F - F_B)(P_{a,CO_2} - P_{v,CO_2}) = 0, \tag{3.15}$$

$$-MR_{O_2} + (F - F_B)a_o\Big(\big(1 - e^{-b_o P_{a,O_2}}\big)^2 - \big(1 - e^{-b_o P_{v,O_2}}\big)^2\Big) = 0. \tag{3.16}$$

Equations (3.12)–(3.16) are considered as equations for P_{v,B,CO_2}, P_{a,O_2}, P_{v,O_2}, P_{v,CO_2}, and F in terms of P_{a,CO_2} and $\dot{V}_A$. The CBF F_B is assumed to be a given constant. Then we get from (3.14)

$$P_{v,B,CO_2} = P_{a,CO_2} + \frac{MR_{B,CO_2}}{K_{CO_2}F_B}. \tag{3.17}$$

We write (3.12), (3.13), (3.15), and (3.16) as

$$F = \frac{\dot{V}_A}{863K_{CO_2}} \cdot \frac{P_{a,CO_2} - P_{i,CO_2}}{P_{v,CO_2} - P_{a,CO_2}}, \tag{3.18}$$

$$F = \frac{\dot{V}_A}{863a_o} \cdot \frac{P_{a,O_2} - P_{i,O_2}}{\big(1 - e^{-b_o P_{v,O_2}}\big)^2 - \big(1 - e^{-b_o P_{a,O_2}}\big)^2}, \tag{3.19}$$

$$F - F_B = -\frac{MR_{CO_2}}{K_{CO_2}(P_{a,CO_2} - P_{v,CO_2})}, \tag{3.20}$$

$$F - F_B = \frac{MR_{O_2}}{a_o\big((1 - e^{-b_o P_{a,O_2}})^2 - (1 - e^{-b_o P_{v,O_2}})^2\big)}. \tag{3.21}$$

From (3.18) and (3.20), respectively, (3.19) and (3.21), we obtain

$$\frac{F}{F - F_B} = \frac{\dot{V}_A}{863MR_{CO_2}}(P_{a,CO_2} - P_{i,CO_2}), \tag{3.22}$$

$$\frac{F}{F - F_B} = -\frac{\dot{V}_A}{863MR_{O_2}}(P_{a,O_2} - P_{i,O_2}). \tag{3.23}$$

These two equations imply

$$P_{a,O_2} = P_{i,O_2} - \frac{MR_{O_2}}{MR_{CO_2}}(P_{a,CO_2} - P_{i,CO_2}). \tag{3.24}$$

Using this in (3.23), we get

$$F\Big(1 - \frac{\dot{V}_A}{863MR_{CO_2}}(P_{a,CO_2} - P_{i,CO_2})\Big) = -F_B\frac{\dot{V}_A}{863MR_{CO_2}}(P_{a,CO_2} - P_{i,CO_2})$$

and, consequently,

$$F = F_B\frac{\dot{V}_A(P_{a,CO_2} - P_{i,CO_2})}{\dot{V}_A(P_{a,CO_2} - P_{i,CO_2}) - 863MR_{CO_2}}. \tag{3.25}$$

Using this in (3.20), we get after some simple calculations

$$P_{v,CO_2} = P_{a,CO_2} - \frac{MR_{CO_2}}{K_{CO_2} F_B} + \dot{V}_A \frac{P_{a,CO_2} - P_{i,CO_2}}{863 K_{CO_2} F_B}. \tag{3.26}$$

From (3.20), (3.21), and (3.26), we obtain

$$a_o\Big(\big(1 - e^{-b_o P_{a,O_2}}\big)^2 - \big(1 - e^{-b_o P_{v,O_2}}\big)^2\Big) = \frac{MR_{O_2}}{F_B} - \frac{MR_{O_2}}{863 MR_{CO_2} F_B} \dot{V}_A (P_{a,CO_2} - P_{i,CO_2})$$

and

$$P_{v,O_2} = -\frac{1}{b_o} \ln\left(1 - \left(\frac{MR_{O_2}}{F_B a_o} + \big(1 - e^{-b_o P_{a,O_2}}\big)^2 - \dot{V}_A \frac{P_{i,O_2} - P_{a,O_2}}{863 F_B a_o}\right)^{1/2}\right). \tag{3.27}$$

Note that P_{v,B,CO_2}, given by (3.17), is a function of P_{a,CO_2}. From (3.24), we see that also P_{a,O_2} depends on P_{a,CO_2} only. The other variables F, P_{v,CO_2} and P_{v,O_2} as given by (3.25), (3.26) and (3.27) are functions of P_{a,CO_2} and $\dot{V}_A$.

We next turn to the "cardiovascular" equations (3.3). We can proceed as in Subsection 1.3.1. The only difference is that R_s is now given by

$$R_s = A_{pcsk} C_{v,O_2} = A_{pcsk} a_o \Big(1 - e^{-b_o P_{v,O_2}}\Big)^2 \tag{3.28}$$

instead of (1.43). Equation (3.28), together with (3.27), shows that R_s is a function of P_{a,CO_2} and $\dot{V}_A$. Since this is also true for F (see (3.25)), the equilibrium values for the "cardiovascular" state variables P_{as}, P_{vs}, P_{ap}, and P_{vp} are also functions of P_{a,CO_2}, which is given, and $\dot{V}_A$, which still has to be determined. Since H^{equ} is assumed to be given, (1.46) is a nonlinear equation for the equilibrium value of $\dot{V}_A$. Once this value has been determined, we get the equilibrium values for the other state variables from (1.44), (3.17), (3.24), (3.26), and (3.27).

These equilibrium computations also show that the empirical control law for the alveolar ventilation $\dot{V}_A$, discussed in Subsection 2.2.6, can only be valid for a rather restricted range of metabolic rates for CO_2 and O_2 in tissues. From (2.15) and (2.16), we obtain

$$\begin{aligned}\dot{V}_A = {} & E_F G_P e^{-0.05 P_{a,O_2}(t-\tau_p)} \max\big(0, P_{a,CO_2}(t - \tau_p) - I_P\big) \\ & + E_F G_C \max\Big(0, P_{v,B,CO_2}(t) - \frac{MR_{B,CO_2}}{K_{CO_2} F_B} - I_C\Big).\end{aligned}$$

In an equilibrium situation with $P_{a,CO_2} = 40$ [mmHg], we obtain, also using (3.17),

$$\begin{aligned}\dot{V}_A &= E_F G_P e^{-0.05 P^{equ}_{a,O_2}} \max\big(0, P^{equ}_{a,CO_2} - I_P\big) + E_F G_C \max\big(0, P^{equ}_{a,CO_2} - I_C\big) \\ &= E_F G_P e^{-0.05 P^{equ}_{a,O_2}} \max\big(0, 40 - I_P\big) + E_F G_C \max\big(0, 40 - I_C\big).\end{aligned} \tag{3.29}$$

Under normal circumstances we have $P_{i,CO_2} = 0$, which we assume from now on. Since the blood flow F in an equilibrium situation has to be nonnegative, we get from (3.25) the inequality

$$\dot{V}_A \geq \frac{863 MR_{CO_2}}{P^{equ}_{a,CO_2}} = \frac{863}{40} MR_{CO_2}. \tag{3.30}$$

Equation (3.24) in the situation we are considering here gives

$$P_{\mathrm{a,O_2}}^{\mathrm{equ}} = P_{\mathrm{i,O_2}} - 40\,\frac{MR_{\mathrm{O_2}}}{MR_{\mathrm{CO_2}}}.$$

Using this in (3.29) and observing inequality (3.30), we get

$$E_{\mathrm{F}}\,G_{\mathrm{P}}^{-0.05P_{\mathrm{i,O_2}}}\,e^{0.05\cdot 40 MR_{\mathrm{O_2}}/MR_{\mathrm{CO_2}}}\max(0,40-I_{\mathrm{P}}) + E_{\mathrm{F}}\,G_{\mathrm{C}}\max(0,40-I_{\mathrm{C}}) \geq \frac{863}{40}MR_{\mathrm{CO_2}}.$$

This shows that we cannot have $I_{\mathrm{P}} \geq 40$ and $I_{\mathrm{C}} \geq 40$ at the same time; i.e., we must have $\min(I_{\mathrm{P}}, I_{\mathrm{C}}) < 40$. Furthermore, we get, after some computations,

$$MR_{\mathrm{O_2}} \geq \frac{1}{2}MR_{\mathrm{CO_2}}\Big(0.05P_{\mathrm{i,O_2}} + \ln\big(21.575MR_{\mathrm{CO_2}} - E_{\mathrm{F}}\,G_{\mathrm{C}}(40-I_{\mathrm{C}})\big) - \ln\big(E_{\mathrm{F}}\,G_{\mathrm{P}}(40-I_{\mathrm{P}})\big)\Big) \tag{3.31}$$

in case $I_{\mathrm{C}} < 40$ and $I_{\mathrm{P}} < 40$,

$$MR_{\mathrm{O_2}} \geq \frac{1}{2}MR_{\mathrm{CO_2}}\big(0.05P_{\mathrm{i,O_2}} + \ln(21.575MR_{\mathrm{CO_2}}) - \ln\big(E_{\mathrm{F}}\,G_{\mathrm{P}}(40-I_{\mathrm{P}})\big)\big) \tag{3.32}$$

in case $I_{\mathrm{P}} < 40$ and $I_{\mathrm{C}} \geq 40$, respectively,

$$MR_{\mathrm{CO_2}} \leq 21.575^{-1}E_{\mathrm{F}}\,G_{\mathrm{C}}(40-I_{\mathrm{C}}) \tag{3.33}$$

in case $I_{\mathrm{P}} \geq 40$ and $I_{\mathrm{C}} < 40$.

Introducing the constants

$$a = \frac{1}{40}P_{\mathrm{i,O_2}} - \frac{1}{2}\ln\big(E_{\mathrm{F}}\,G_{\mathrm{P}}(40-I_{\mathrm{P}})\big),$$
$$b = 21.575 \quad \text{and} \quad c = E_{\mathrm{F}}\,G_{\mathrm{C}}\max(0,40-I_{\mathrm{C}}),$$

inequalities (3.31) and (3.32) can be written as

$$MR_{\mathrm{O_2}} \geq f(MR_{\mathrm{CO_2}}),$$

where

$$f(x) = x\big(a + 0.5\ln(bx-c)\big) \quad \text{for } x > c/b, \tag{3.34}$$

whereas inequality (3.33) reduces to

$$MR_{\mathrm{CO_2}} \leq \frac{c}{b}.$$

Since we have $f(x) \leq 0$ for $c/b < x \leq c/b + e^{-2a}/b$, we see that inequality (3.31) does not pose any restriction onto $MR_{\mathrm{O_2}}$ for $MR_{\mathrm{CO_2}} \leq c/b + e^{-2a}/b$. It is also easy to see that $f(x)/x$ is monotonically increasing with $\lim_{x\to\infty} f(x)/x = \infty$. This shows that inequalities (3.31) and (3.32) cannot be true for large values of $MR_{\mathrm{CO_2}}$. Obviously, the same is true for inequality (3.33). For a respiratory quotient $MR_{\mathrm{CO_2}}/MR_{\mathrm{O_2}}$ in the range 0.7–1.0, the admissible range for $MR_{\mathrm{CO_2}}$ according to (3.34) changes from the interval $[0, 0.2805]$ to the interval $[0, 0.2535]$. This shows that the empirical control law (2.15) cannot be valid for large $MR_{\mathrm{CO_2}}$. In Figure 3.7 we depict the graph of f in case $I_{\mathrm{P}} < 40$ and $I_{\mathrm{C}} < 40$ for a realistic choice of parameters.

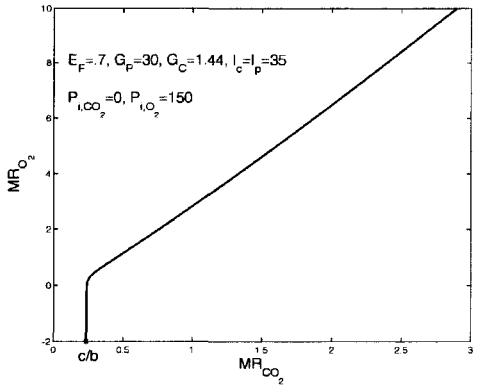

Figure 3.7: Graph of f as given by (3.34).

3.3 Modeling Applications

In this section, we consider various applications and extensions of the CVRS model and we employ the optimal control approach developed above, with the exception of the CBF model in Subsection 3.3.4. Since this approach involves computing a control for the system linearized around a steady state, we will assume constant transport delays, choosing these delays in relation to the baseline Q_{CO} and F_B flow values assumed for particular situations. Even though these flows will, in some cases, be time dependent, since these quantities do not change substantially, the assumption of constant delays is an acceptable simplification.

3.3.1 CHF

We briefly discussed heart failure (HF) in Subsection 2.4.3, noting that chronic heart failure refers to the continuing degradation of the heart function as the CVS response to this reduced heart effectiveness induces stresses, which reinforce and exacerbate the reduction in the heart function. This is in contrast to acute failure which is the result of tissue damage such as that occurs in a heart attack. An example of the changes that occur in the progression of HF can be seen in the damaging remodeling of the heart structure (Jessup and Brozena, 2003) that emerges as the heart and CVS control alter their actions to counteract a loss in heart pumping efficiency and reduction in blood delivery to the tissues.

HF is primarily a ventricular dysfunction problem and can involve the left or right heart or both. HF can be subdivided into types of functional failure: systolic failure, where the ventricle exhibits reduced ability to pump out blood, and diastolic failure, where the filling process of the heart is impaired. Another subdivision compares backward failure, which focuses on the pumping heart that cannot keep up with the blood coming to it, and forward failure focusing on the pumping heart that cannot deliver sufficient blood to meet metabolic needs in the organs. Because the heart is part of a circuit, these distinctions are not completely obvious. That is, the failure to pump the blood delivered can also represent a failure to deliver sufficient blood to the tissues.

As mentioned in Subsection 2.4.3, fluid congestion in the lungs is a symptom of HF, which occurs when the inefficiency of the left heart pump results in a buildup in pulmonary

venous blood volume with P_{vp} forcing fluid into the lungs. The term congestive heart failure (CHF) is used to reflect this situation. Edema in the lower body can develop for similar reasons when the right heart fails.

We will restrict our focus to the chronic heart failure case and continue as previously to reference this condition by CHF, which is commonly used synonymously for HF. The case we simulate below is left ventricular (systolic) heart failure, which is the most common form seen, although clear epidemiological definitions of the various manifestations of HF is still lacking and represents a difficulty for consistent diagnosis and evaluation of experimental data (Adams, 2001).

Obstructive apnea (OA) is becoming recognized as a significant risk factor for a cluster of cardiovascular diseases including heart failure, stroke, and hypertension (Lanfranchi and Somers, 2003; Hoffmann et al., 2004). Furthermore, central apnea (CA), when it occurs with CHF (Javaheri, 1999), is associated with increased mortality from that disease (Lanfranchi and Somers, 2003).

The development of chronic (progressive) HF and essential hypertension has been associated with increased sympathetic activity, and in turn excess sympathetic activity has been associated with OA (Hoffmann et al., 2004). CSR is seen in CHF (Brack, 2003) as are other manifestations of sleep disordered breathing, including CA and OA (Lanfranchi and Somers, 2003). Sensitivity to CO_2 and increased delay (Javaheri, 1999; Cherniack, 1999) seen in CHF patients with CSR may contribute to the predisposition to CSR. Hence, there is an interlocking set of factors which may be involved in precipitating CHF, or contributing to the progression of the disease.

The model developed by Timischl (1998) was extended in Batzel (2005) to study CHF and the relation to CSR by incorporating delays in the model and considering the impact of control gain levels to unstable behavior. As CSR occurs during sleep (see Section 2.1), simulations of CHF-CSR in this section will include the transition from the quiet rest state to S4 stage as discussed in Section 2.4.

Mathematical setting

The model described in the previous section given by (3.3), (3.4), and (3.5) can be represented in general terms in the form

$$\dot{x}(t) = f(x(t), x(t-\tau_v), x(t-\tau_T); w) + B\,u(t), \quad x_0 = \phi. \tag{3.35}$$

Here $\tau_p < \tau_T$, $\phi \in C$, where $C = C([-\tau_T, 0]; \mathbb{R}^{14})$ and

$$B = \begin{pmatrix} 0 & 0 \\ \vdots & \vdots \\ 0 & 0 \\ 1 & 0 \\ 0 & 1 \end{pmatrix} \in \mathbb{R}^{14\times 2}.$$

The symbol w denotes the vector of weights in the cost functional (3.9). Corresponding to this cost functional, we define the output

$$\begin{aligned} y(t) &= \mathrm{col}\big(q_{as}(P_{as}(t) - P_{as}^{\text{final}}), q_o(P_{a,CO_2}(t) - P_{a,CO_2}^{\text{final}}), q_c(P_{a,O_2}(t) - P_{a,O_2}^{\text{final}})\big) \\ &= D(x(t) - x^{\text{final}}), \end{aligned}$$

where

$$D = \begin{pmatrix} q_{as} & 0 & 0 & 0 & \cdots & 0 \\ 0 & q_O & 0 & 0 & \cdots & 0 \\ 0 & 0 & q_c & 0 & \cdots & 0 \end{pmatrix} \in \mathbb{R}^{3\times 14}.$$

In simulating a CHF scenario, we incorporate into the model the physiological ventilation control (3.10), which now becomes an auxiliary equation expressing $\dot{V}_A$ in terms of the state variables P_{a,CO_2}, P_{a,O_2}, and P_{v,B,CO_2}. The dimension of the system remains the same, because we can delete the first equation in (3.5), but have to include in addition (3.11). This introduces the two additional delays τ_p and τ_B. The control $u(t) := u_2(t) = \dot{H}(t)$ is still derived as an optimal control for the cost functional (3.9), where the terms involving P_{a,CO_2}, P_{a,O_2}, and u_1 are omitted; i.e., we have

$$J(u(\cdot), x^{\text{final}}) = \int_0^\infty \left(q_{as}^2 (P_{as}(t) - P_{as}^{\text{final}})^2 + u(t)^2\right) dt.$$

Thus we have only one observation, $y(t) = q_{as}(P_{as}(t) - P_{as}^{\text{final}})$. Since the optimal control is invariant with respect to constant factors in the cost functional, we normalize the weight for the control $u(\cdot)$ to one. Therefore, w reduces to q_{as}. Thus, the matrices B and D simplify to

$$B = \text{col}(0, \ldots, 0, 1) \in \mathbb{R}^{14\times 1} \quad \text{and} \quad D = (q_{as}, 0, \ldots, 0) \in \mathbb{R}^{1\times 14}.$$

See Batzel (2005) for further details about this model. In particular, to simplify computations, we assume that the delays are constant and that in addition $\tau_v = \tau_T$ and $\tau_B = \tau_p$.

A number of results on approximation of feedback control for delay systems, using various approximating schemes, have been developed. We employ the method given in Kappel and Propst (1984) which employs Legendre polynomials. Other examples can be found in (Kappel and Salamon, 1987) or (Ito and Kappel, 1991) which utilize spline approximation schemes. In these approaches the control is found for approximating systems defined on finite-dimensional subspaces of $\mathbb{R}^n \times L^2([-h, 0]; \mathbb{R}^n)$. In our computations we used the first 5 Legendre polynomials. The derived control will be an approximate control for the original system, because the analysis of this scheme, described in Kappel and Propst (1984), shows that the control for the approximating system converges to the control for the original system, as the approximating system converges to the actual system in an appropriate sense.

To set up the system for this numerical treatment, we have to define the target steady state. The unstable respiratory behavior CSR can occur in patients with CHF, primarily during sleep. Hence, we will seek to stabilize system (3.35) to the equilibrium x^{final}, which in our case is the S4 stage equilibrium. We first shift the equilibrium to the origin by introducing a new variable ξ by

$$\xi(t) = x(t) - x^{\text{final}}$$

and replace $x(t)$ in the right-hand side of (3.35) with $x^{\text{final}} + \xi(t)$. For fixed time t, we expand the resulting function around $\xi = 0$. For this expansion, we are treating $x(t - \tau_p)$ and $x(t - \tau_T)$ as independent variables. This yields $\dot{\xi}(t) = \dot{x}(t)$ and

$$\dot{\xi}(t) = A_1\xi(t) + A_2\xi(t - \tau_p) + A_3\xi(t - \tau_T) + Bu(t) + o(\xi)(t).$$

The matrices $A_i \in \mathbb{R}^{14\times 14}$, $i = 1, 2, 3$, are the Jacobians of $f = f(z_1, z_2, z_3; w)$ with respect to z_1, z_2, and z_3, respectively, evaluated at $z_1 = z_2 = z_3 = x^{\text{final}}$:

$$A_1 = \frac{\partial f}{\partial z_1}(x^{\text{final}}; q_{\text{as}}),$$
$$A_2 = \frac{\partial f}{\partial z_2}(x^{\text{final}}; q_{\text{as}}),$$
$$A_3 = \frac{\partial f}{\partial z_3}(x^{\text{final}}; q_{\text{as}}).$$

The expression $o(\xi)$ collects higher-order terms, i.e., $\lim_{\xi \downarrow 0} o(\xi)/(\|\xi\|) = 0$.

Note that the original state equations were already linear with respect to the control u. By neglecting the terms of order $o(\xi)$, we arrive at the following linear control system:

$$\dot{\xi}(t) = A_1\xi(t) + A_2\xi(t - \tau_p) + A_3\xi(t - \tau_T) + Bu(t),$$
$$y(t) = D\xi(t),$$
$$\xi(t) = x^{\text{initial}} - x^{\text{final}}, \quad -\tau_T \le t \le 0.$$

This is a special case of the general linear hereditary control system

$$\dot{x}(t) = Lx_t + Bu(t), \quad t \ge 0,$$
$$y(t) = Dx(t),$$

as discussed in Appendix C. Given this formulation, we are able to apply the approximation scheme for feedback controls for delay systems, using Legendre polynomials found in Kappel and Propst (1984). As already mentioned above, in this approach, the control is found for approximating systems defined on finite-dimensional subspaces of $\mathbb{R}^n$ x $L^2([-\tau_T, 0]; \mathbb{R}^n)$, utilizing Legendre polynomials.

Modeling sleep

We have previously discussed the effects of sleep on RS function in Subsection 2.4.1. In regards to CVS function, in NREM sleep sympathetic activity is reduced and H, P_{as} fall. Generally, Q_{co} is also reduced, but the degree of the reduction depends on the situation and the individual. Research suggests that peripheral resistance also falls as can stroke volume. This would follow at least partly from the reduced sympathetic activity. Further details and comparative parameter changes from awake to NREM sleep can be found in Somers et al. (1993), Mancia (1993), Podszus (1997), Shepard (1985), Bevier, Bunnell, and Horvath (1987), and Schneider et al. (1997).

To set up the simulation of transition to steady state S4 stage, we carry out the four steps described in Subsection 3.2.3. Table 3.1 gives standard parameter values for this model unless otherwise noted in a given table. Parameter changes for a healthy individual that reflect S4 stage, similar to those described in Subsection 2.4.1, are given in Table 3.3 with steady state values for the awake and sleep states given in Table 3.4. With $u_2 = \ddot{V}_A$ removed from the optimal control, there is now only one free variable, and we choose H whose values are reasonably standard in rest and sleep. We assume a decrease in metabolic

Parameter	Awake	Sleep
A_{pcsk}	141.9	134.8
β_ℓ	85.89	77.3
β_r	2.08	1.874
R_p	1.965	1.965
V_{tot}	5.0	5.0
H	75.02	68.02
MR_{O_2}	0.310	0.260
MR_{CO_2}	0.266	0.226
MR_{B,CO_2}	0.042	0.0399
G_S	1.0	0.6
S_{K_M}	0	4.2

Table 3.3: Parameters changes: wake to sleep transition for a healthy individual.

State	Awake	Sleep
H	75.02	68.02
P_{as}	99.92	85.7
P_{ap}	17.25	16.08
P_{vs}	3.675	3.977
P_{vp}	7.434	7.459
P_{a,CO_2}	39.156	42.7
P_{a,O_2}	104.37	100.47
P_{v,CO_2}	47.35	50.52
P_{v,O_2}	34.74	35.57
P_{v,B,CO_2}	47.23	50.34
Q_ℓ	4.99	4.39
Q_r	4.99	4.39
R_s	19.26	18.61
S_ℓ	72.018	58.8
S_r	5.489	4.48
$\dot{V}_A$	5.86	4.53
$V_{str,\ell}$	0.066	0.0645
$V_{str,r}$	0.066	0.0645

Table 3.4: State changes: wake to sleep transition for a healthy individual.

rates, and reduced sympathetic effect, which influences contractility and systemic resistance. The reduction of wakefulness stimulus is modeled as in (2.31).

As can be seen from the tables, the model exhibits the decrease in P_{as} and $\dot{V}_A$ that is observed in the sleep state (Krieger et al., 1990; Phillipson and Bowes, 1986; Podszus, 1997; Mateika et al., 1992; Somers et al., 1993). The model also exhibits decreases in Q_{co} primarily due to a drop in H, as reported in Shepard (1985) or Schneider et al. (1997). The minor change in stroke volume (compare Schneider et al., 1997) depends on the degree of attenuation of sympathetic influence on contractility and systemic resistance, which varies

from one individual to another. A fall in P_{a,O_2} and a rise in P_{a,CO_2} are seen (Phillipson and Bowes, 1986; Shepard, 1985).

Given that there is no coronary volume compartment, the pulmonary to systemic circuit volumes ratios are more on the order of those given in Section 1.2 (see for comparison Levick, 2003). Furthermore, unstressed volume is not included (see (3.2) and the discussions in Sections 1.2 and Subsection 3.1.3), so that the typical proportions of pulmonary to systemic circuit volumes can be somewhat distorted. The focus is on reasonable pressure-flow relations, given that stressed volume represents dynamic volume, while unstressed volume represents distribution of volume that fills a vascular element at zero transmural pressure. For consideration of unstressed volume, see the following section on orthostatic and LBNP stress.

Modeling chronic heart failure

In the following simulation we consider severe left ventricular (systolic) failure with a certain degree of pumping impairment of the right heart, which has developed as a consequence of the left heart failure. Ventricular failure is modeled by a reduction in contractility via the parameters β_ℓ and β_r. We further consider the influence of the change in state from awake to sleep on respiratory function, modeling a quick sleep transition. A comparison of Tables 3.3 and 3.4 for the normal case with Tables 3.5 and 3.6 for the CHF case will indicate which changes influence the respiratory stability. Notice, in particular, that the global responses of the CVS to reduced Q_{co} include increased systemic resistance and control mechanisms that increase blood volume. As a result of the severe left ventricular failure and reduced left heart pumping ability, blood volume rises in the pulmonary circuit as do P_{ap} and P_{vp} which can lead to lung congestion. According to the discussion in Tsuruta

Parameter	Awake	Sleep
V_{tot}	6.9	6.9
A_{pesk}	241.1	229.07
β_ℓ	12.88	11.60
β_r	1.46	1.31
R_p	2.162	2.162
H	92.02	80.02
I_C	35.5	35.5
I_P	35.5	35.5
G_S	1.65	0.495
S_{K_M}	0	5.2
τ_p	0.19	0.19
τ_T	0.6	0.6
c_{as}	0.01202	0.01202
c_{vs}	0.6730	0.6730
c_{ap}	0.02607	0.02607
c_{vp}	0.1104	0.1104

Table 3.5: Parameters changes wake to sleep transition for left-right CHF.

State	Awake	Sleep
H	92.02	80.02
P_{as}	94.46	75.54
P_{ap}	28.62	26.86
P_{vs}	3.99	4.48
P_{vp}	21.14	20.61
P_{a,CO_2}	37.81	44.00
P_{a,O_2}	105.9	98.92
P_{v,CO_2}	49.63	55.90
P_{v,O_2}	26.66	26.36
P_{v,B,CO_2}	45.89	51.67
Q_ℓ	3.46	2.89
Q_r	3.46	2.89
R_s	26.14	24.57
S_ℓ	13.25	10.37
S_r	4.71	3.69
$\dot{V}_A$	6.07	4.39
$V_{str,\ell}$	0.0376	0.0361
$V_{str,r}$	0.0376	0.0361

Table 3.6: State changes wake to sleep transition for left-right CHF.

et al. (1994), the proportion of pulmonary blood volume can increase by up to 50% as a result of the failure in left ventricular pumping action and the increased blood storage. The increased pulmonary pressures (O'Dell et al., 2005) imply an increase in stored volume for the pulmonary system according to (1.1), reflecting the pressure-volume-compliance relation. A complete model that precisely reflects standard blood volume proportions needs to consider, as mentioned above, a number of subcompartments, including a cardiac compartment, the unstressed volume, and the nonlinearity of the compliance characteristics of the vascular elements, as discussed further in Subsection 3.3.2. We assume a small drop in compliance as the pulmonary pressures rise (see Risk et al., 2003), though more experimental research and modeling studies need to be done in the area of volume distribution and nonlinear compliance. The simulations shown in Figures 3.8 and 3.9 exhibit the prediction that unstable breathing patterns, such as CSR in CHF patients, may be at least partly precipitated by the presence of increased CO_2 sensitivity (Javaheri, 1999; Cherniack, 1999; Prabhakar and Peng, 2004), in conjunction with the extended transport delay in patients with severe CHF (Pinna et al., 2000; Batzel, Kappel, and Timischl-Teschl, 2005). Note that in this case we are exhibiting minute ventilation so that the oscillations shown in Figure 3.9 indicate increases and decreases in minute ventilation rate not tidal volume. For comparison to other modeling attempts of CHF see (Tsuruta et al., 1994; Francis et al., 2000).

3.3.2 Orthostatic and LBNP stress

Orthostatic stress refers to the impact of gravity on cardiovascular function. In the supine position, all fluids are subject to an equivalent influence of gravity. Upon standing, a graded hydrostatic force is induced on what is in effect a column of blood from foot to head. In fact the arterial transmural blood pressure in the feet can change from 100[mmHg]

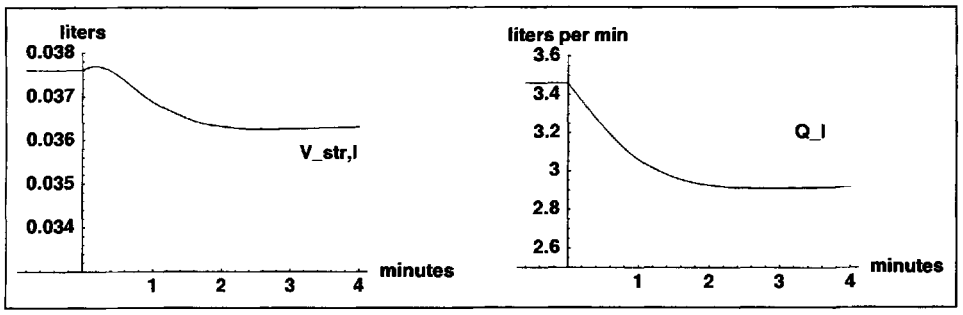

Figure 3.8: $V_{\text{str},\ell}$ and Q_ℓ in severe CHF.

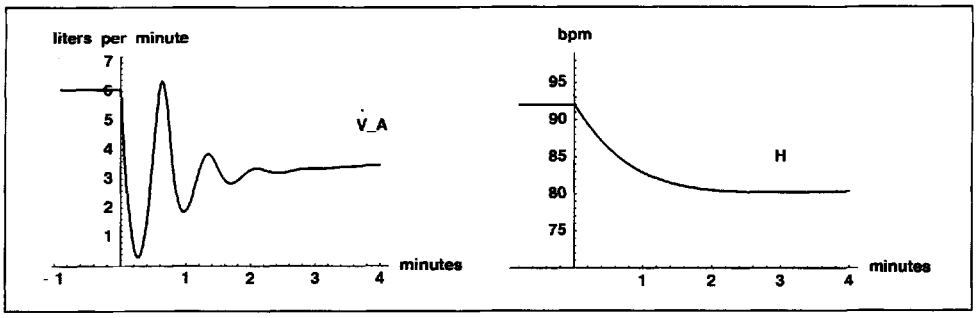

Figure 3.9: Ventilation and H in severe CHF.

to 200 [mmHg] in the transition from lying down to standing up. The net impact of the gravitational force is to induce a pooling of blood in the lower extremities in the order of 500 [ml] or more. This shift in blood volume distribution acts as a challenge to stable arterial pressure. To compensate, the baroreflex reacts by inducing a (highly individualized) combination of responses, including an increase in heart rate, contractility, and systemic resistance, and possibly a decrease in venous compliance and unstressed volume. These changes will, in general, restore blood pressure before CVS function is compromised. The common result of insufficient compensation is a reduction in CBF sufficient to cause dizziness or syncope which is terminated by the compensatory response of sitting or lying down to reduce the perturbation induced by gravity.

A number of clinical problems are connected to insufficient or inappropriate control of orthostatic stress. These include the postural orthostatic tachycardia syndrome (POTS), which is often seen in young people and various manifestations of OI in elderly people that can result in injurious falls (a major cause of emergency room visits in the elderly population). Other clinical problems are related to insufficient autonomic function due to neurological damage such as is seen in diabetics. This damage can impact control response as can altered orthostatic response due to changes in vascular compliance and other autonomic changes, which are the result of aging.

To study orthostatic stress, a number of tests have become standard, including the sit-to-stand test and the more experimentally controllable head-up-tilt test (HUT). In the HUT test a subject is placed in the supine position for some minutes until a restful steady state

is reached. At that point, the table upon which the subject is lying is smoothly tilted over a span of seconds to a degree of tilt up to 70 degrees or more. Noninvasive measurements of H, P_{as}, and perhaps other variables are recorded. Such tests can help discern if autonomic function is impaired or if the subject is prone to OI or POTS. A diagram of the HUT test is given in Figure 3.10.

The lower-body negative pressure (LBNP) test is used as an alternative and highly controllable means of inducing orthostatic stress effects and has been extensively used in research on the effects of weightlessness. In this test, the lower body is placed in a chamber and air is removed to create a partial vacuum. This reduces the outside pressure element in the vascular transmural pressure gradient, inducing a suction on vascular walls and raising the unstressed volume of the vascular elements.

The minimal extensions to the basic CVRS model needed to study orthostatic stress are illustrated in Figure 3.11. In orthostasis, blood is shifted to the lower extremities and hence we must distinguish between upper and lower systemic blood volume compartments. We ignore the much smaller orthostatic effects on the pulmonary circuit in this case. For comparison to other modeling approaches, see Heldt et al. (2002).

In Chapter 1, the baroreflex control loop was represented by (1.29) with cost functional (1.47) and with control H, and in Section 3.2 this control was extended to include a respiratory component represented by (3.5) with cost functional (3.9). We now include feedback control of unstressed volume V_u and R_s. These additions further fill out the control diagram illustrated in Figure 3.2. We have omitted the autonomic control of contractility and venous compliance, but these elements could, in principle, be included in the optimal control as well. Contractility was omitted because much less information is available on sympathetic control of contractility, in part because contractility is also influenced by other factors such as the Bowditch effect and the Frank–Starling mechanism. Changes in venous compliance are certainly induced by autonomic control, but the degree to which these effects contribute to combating volume shift is still an area of research. See, for example, Rowell (2004).

The refinement of the model to include upper and lower compartments of both the arterial and venous vasculatures (see Figure 3.11) requires that we add several new flow equations for the CVS,

$$\begin{aligned} F_v &= \frac{1}{R_v}\max\left(0,\, P_{vs,lo} - P_{vs,up}\right), \\ F_a &= \frac{P_{as,up} - P_{as,lo}}{R_a}, \\ F_{s,up} &= \frac{P_{as,up} - P_{vs,up}}{R_{s,up}}, \\ F_{s,lo} &= \frac{P_{as,lo} - P_{vs,lo}}{R_{s,lo}}, \\ F_p &= \frac{P_{ap} - P_{vp}}{R_p}. \end{aligned} \tag{3.36}$$

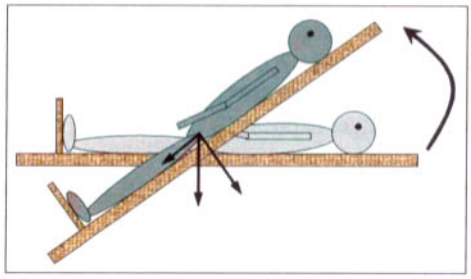

Figure 3.10: HUT test for orthostatic stress.

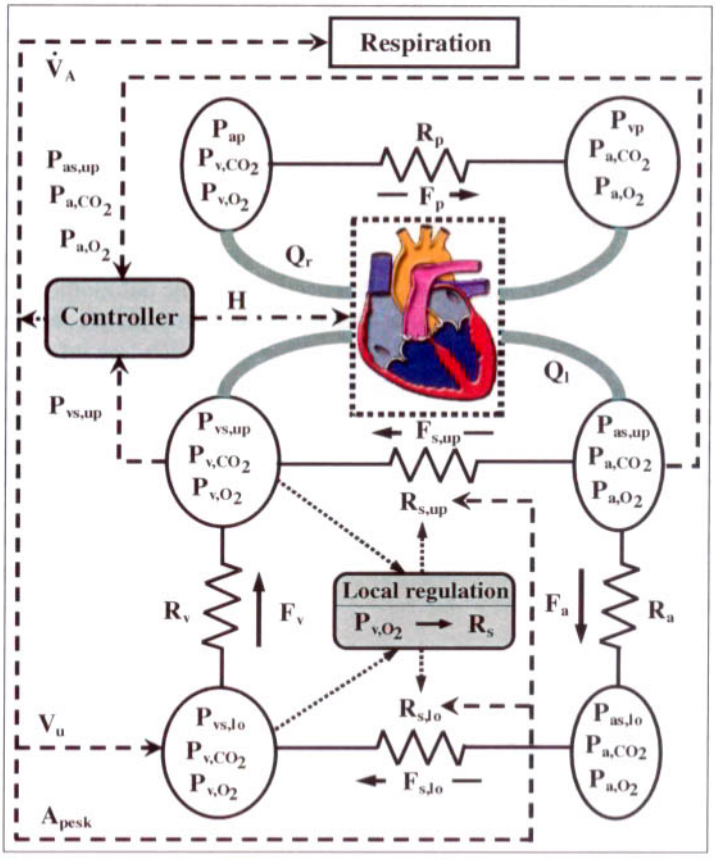

Figure 3.11: Block diagram of the CVRS model for orthostatic stress.

The previous subscript notation is extended to include the additional symbols "up" and "lo" for upper and lower compartments, respectively. These flow equations are derived in the same manner as those for the basic model and follow in a straightforward manner from the information provided in Figure 3.11. Note that the pulmonary circuit remains the same.

A new feature is the max function in the first equation, which implements the action of the venous valves to avoid backflow. The other auxiliary equations are, in general, the same as for the basic system.

The "cardiovascular," respectively, the "respiratory," equations are given as

$$\begin{aligned}
c_{\mathrm{as,up}}\dot{P}_{\mathrm{as,up}} &= Q_\ell - F_{\mathrm{a}} - F_{\mathrm{s,up}},\\
c_{\mathrm{as,lo}}\dot{P}_{\mathrm{as,lo}} &= F_{\mathrm{a}} - F_{\mathrm{s,lo}},\\
c_{\mathrm{vs,lo}}\dot{P}_{\mathrm{vs,lo}} &= F_{\mathrm{s,lo}} - F_{\mathrm{v}} - \dot{c}_{\mathrm{vs,lo}}P_{\mathrm{vs,lo}} - \dot{V}_{\mathrm{u}},\\
c_{\mathrm{vs,up}}\dot{P}_{\mathrm{vs,up}} &= F_{\mathrm{v}} - Q_{\mathrm{r}} + F_{\mathrm{s,up}},\\
c_{\mathrm{ap}}\dot{P}_{\mathrm{ap}} &= Q_{\mathrm{r}} - F_{\mathrm{p}},\\
c_{\mathrm{vp}}\dot{P}_{\mathrm{vp}} &= F_{\mathrm{p}} - Q_\ell,\\
\dot{S}_\ell &= \sigma_\ell,\\
\dot{S}_{\mathrm{r}} &= \sigma_{\mathrm{r}},\\
\dot{\sigma}_\ell &= -\gamma_\ell\sigma_\ell - \alpha_\ell S_\ell + \beta_\ell H,\\
\dot{\sigma}_{\mathrm{r}} &= -\gamma_{\mathrm{r}}\sigma_{\mathrm{r}} - \alpha_{\mathrm{r}}S_{\mathrm{r}} + \beta_{\mathrm{r}}H,
\end{aligned} \tag{3.37}$$

respectively,

$$\begin{aligned}
V_{\mathrm{A,CO_2}}\dot{P}_{\mathrm{a,CO_2}} &= 863F_{\mathrm{p}}\left(C_{\mathrm{v,CO_2}} - C_{\mathrm{a,CO_2}}\right) + \dot{V}_\Lambda\left(P_{\mathrm{i,CO_2}} - P_{\mathrm{a,CO_2}}\right),\\
V_{\mathrm{A,O_2}}\dot{P}_{\mathrm{a,O_2}} &= 863F_{\mathrm{p}}\left(C_{\mathrm{v,O_2}} - C_{\mathrm{a,O_2}}\right) + \dot{V}_\Lambda\left(P_{\mathrm{i,O_2}} - P_{\mathrm{a,O_2}}\right),\\
V_{\mathrm{T,CO_2}}\dot{C}_{\mathrm{v,CO_2}} &= MR_{\mathrm{CO_2}} + F_{\mathrm{s}}\left(C_{\mathrm{a,CO_2}} - C_{\mathrm{v,CO_2}}\right),\\
V_{\mathrm{T,O_2}}\dot{C}_{\mathrm{v,O_2}} &= -MR_{\mathrm{O_2}} + F_{\mathrm{s}}\left(C_{\mathrm{a,O_2}} - C_{\mathrm{v,O_2}}\right),
\end{aligned}$$

whereas the controls are

$$\begin{aligned}
\dot{H} &= u_1,\\
\ddot{V}_\Lambda &= u_2,\\
\dot{V}_{\mathrm{u}} &= u_3,\\
\dot{A}_{\mathrm{pesk}} &= u_4.
\end{aligned}$$

Unstressed volume

In the third equation of (3.37), the term $\dot{V}_{\mathrm{u}}$ indicates how the control of unstressed volume is implemented. While unstressed volume occurs throughout the body, the most significant reservoir of controllable unstressed volume occurs in the splanchnic region. For simplicity, we assume that, only the unstressed volume in the splanchnic region is controllable. By incorporating $\dot{V}_{\mathrm{u}}$ into the third equation of (3.37), we are placing the splanchnic region in the lower systemic compartment. As a further simplification, we implement the vascular pressure-volume relation using

$$V = cP + V_{\mathrm{u}},$$

where symbols are defined as in (3.2). In this simplification there is no explicit functional dependence of compliance on pressure. Given the limited data available, we will change

the compliance c smoothly between the values for each initial and final state, using experimentally measured data such as that given in Risk et al. (2003). We will also assume that the unstressed volume is varied based on the sympathetic baroreflex control loop alone and not attempt to quantify any variation in V_u due to changes in vascular structural characteristics induced by vascular pressure (see Subsection 3.1.3). Total CVS blood volume V_{tot} is given by

$$c_{as,up}P_{as,up}(t) + c_{as,lo}P_{as,lo}(t) + c_{vs,up}P_{vs,up}(t) + c_{vs,lo}(t)P_{vs,lo}(t) + c_{vp}P_{vp}(t) + c_{ap}P_{ap}(t) + V_u(t) \equiv V_{tot}. \quad (3.38)$$

Systemic resistance and compliance

The relation between the total systemic resistance and the upper and lower compartments resistances, $R_{s,up}$, respectively, $R_{s,lo}$, is given by

$$\frac{1}{R_s} = \frac{1}{R_{s,up}} + \frac{1}{R_{s,lo}}.$$

With a constant $\delta \in (0, 1)$, we obtain

$$\frac{1}{R_{s,up}} = \frac{\delta}{R_s} \quad \text{and} \quad \frac{1}{R_{s,lo}} = \frac{1-\delta}{R_s}.$$

The constant δ characterizes the subdivision of the systemic compartments (arterial and venous) into lower and upper compartments. Using (1.24), we get

$$R_{s,up} = \frac{1}{\delta}A_{pesk}C_{v,O_2},$$
$$R_{s,lo} = \frac{1}{1-\delta}A_{pesk}C_{v,O_2}.$$

If we consider the compliance c_{as} of the arterial systemic compartment and the compliances $c_{as,up}$, $c_{as,lo}$ of the upper and lower part, respectively, we get $c_{as} = c_{as,up} + c_{as,lo}$, which leads to $c_{as,up} = \tilde{\delta}c_{as}$ and $c_{as,lo} = (1-\tilde{\delta})c_{as}$ for some constant $\tilde{\delta} \in (0, 1)$. We assume that $\tilde{\delta} = \delta$, i.e.,

$$c_{as,up} = \delta c_{as} \quad \text{and} \quad c_{as,lo} = (1-\delta)c_{as}.$$

We will now consider adaptations of this model to implement HUT and LBNP tests.

The HUT *test*

One way to implement orthostatic stress is to modify the auxiliary flow equations (3.7) by introducing a gravitational effect P_{grav}, as developed in Fink et al. (2004),

$$F_v = \frac{1}{R_v}\max\left(0;\, P_{vs,lo} - P_{vs,up} - P_{grav}\right),$$
$$F_a = \frac{P_{as,up} - P_{as,lo} + P_{grav}}{R_a},$$
$$F_{s,up} = \frac{P_{as,up} - P_{vs,up}}{R_s},$$
$$F_{s,lo} = \frac{P_{as,lo} - P_{vs,lo}}{R_s},$$
$$F_p = \frac{P_{ap} - P_{vp}}{R_p}.$$

As in (3.36) the max function implements the action of the venous valves to avoid backflow. P_{grav} represents the hydrostatic pressure induced on the lower compartments. The HUT test is simulated by a smooth increase in P_{grav} up to the desired degree of tilt (Fink et al., 2004).

The LBNP *test*

We define the lower compartment to be that part of the lower body under LBNP stress, and thereby subject to an outside partial vacuum that pulls blood into this compartment. We implement this case as follows.

We begin with the following generic volume relation for a compliant vascular compartment under LBNP stress:

$$\frac{d}{dt}\left(c(P + P_{LBNP}) + \bar{V}_u\right) = F_{in} - F_{out}, \tag{3.39}$$

where $\bar{V}_u$ denotes the unstressed volume of the compartment, P represents the dynamic pressure, P_{LBNP} the pressure induced by the LBNP stress, and F_{in} and F_{out} denote blood flow into and out of the compartment, respectively. According to this expression, we are assuming that the pressure-volume relation for the induced P_{LBNP} will be determined by the compliance c of the vessel. As discussed in Subsection 3.1.3, this LBNP-induced volume increase is considered an addition to unstressed volume, which can be seen from noting that when the LBNP pressure reaches its target fixed level, it can be eliminated from the differential equation (3.39). Furthermore, assuming $P_{LBNP} = 35$ [mmHg], then $P_{vs,lo} \ll P_{LBNP}$, and the compliance associated with the vessel may drop substantially in the transition to the LBNP stress state for the system(see, for example, Risk et al., 2003).

We assume that the LBNP stress is applied at the ribs so that the lower compartment contains the splanchnic region, where we assume controllable V_u is located. We derive the following equations using (3.39) to replace the second and third equations in (3.37) to include LBNP stress:

$$c_{as,lo}\dot{P}_{as,lo} = F_a - F_{s,lo} - c_{as,lo}\dot{P}_{LBNP}, \tag{3.40}$$
$$c_{vs,lo}\dot{P}_{vs,lo} = F_{s,lo} - F_v - \dot{c}_{vs,lo}(P_{vs,lo} + P_{LBNP}) - c_{vs,lo}\dot{P}_{LBNP} - \dot{V}_u. \tag{3.41}$$

As in the HUT test we increase the LBNP effect smoothly up to the maximum negative pressure. Note that a V_u term occurs in (3.41) but not (3.40), because we assume that the unstressed volume in the lower arterial compartment (as well as in all other compartments

except the lower venous compartment) is constant. Also, in the relation for total blood volume (3.38), we include the LBNP induced volume and the changes to unstressed volume,

$$c_{as,up}P_{as,up}(t) + c_{as,lo}\big(P_{as,lo}(t) + P_{LBNP}(t)\big) + c_{vs,up}P_{vs,up}(t) \\ + c_{vs,lo}(t)\big(P_{vs,lo}(t) + P_{LBNP}(t)\big) + c_{vp}P_{vp}(t) + c_{ap}P_{ap}(t) + V_u(t) \equiv V_{tot}.$$

Given this model adaptation, we simulate the following case: application of an LBNP stress of 35 [mmHg] applied at the ribs for a subject designated as subject C. The results of adapting the model to this case using measurements of H and $P_{as,up}$ (typical arterial mean blood pressure) are given in Tables 3.7, 3.8, and 3.9 and Figures 3.12 and 3.13. Table 3.8 provides the steady states of the state variables and state-dependent variables for both the steady state "rest," before the LBNP test begins, and steady state "LBNP," where a fixed LBNP of 35 [mmHg] applied. Table 3.7 includes control weights and parameters that change with the type and degree of LBNP stress, while parameters that are fixed for all cases are given in Table 3.2 in Section 3.2.

Note, in particular in Table 3.7, that V_{tot} and $c_{vs,lo}$ vary between the "rest" and "LBNP" states. The reduction in V_{tot} comes from an assumed small volume shift of fluid from the blood to the interstitial fluids, which occurs during orthostasis and likely during LBNP as well (compare Lundvall et al., 1993; Heldt et al., 2002; Aratow et al., 1993). The reduction in $c_{vs,lo}$ comes from the above-mentioned nonlinearity of the pressure-volume curve as transmural pressure increases due to the LBNP stress (Risk et al., 2003).

A discussion of changes that occur during orthostatic and LBNP stress can be found in Heldt et al. (2002). Typical changes in CVS state values during 35 [mmHg] LBNP can be found in Convertino, Ludwig, and Cooke (2004), and in our simulation they include: a drop in Q_{co} of 30%, an increase in R_s of about 40%, a small drop in $P_{as,up}$ of 2.5%, an increase in H of about 17%, and a drop in stroke volume V_{str} of 37%.

Table 3.9 reflects the net volume changes that occur in the transition from the *initial* equilibrium state of rest (characterized by superscript "i" as in earlier cases) to the *final* LBNP equilibrium state (characterized by the superscript "f"). These volume changes are $\Delta V_{s,lo}$, $\Delta V_{u,lo}$, ΔV_{LBNP}, and ΔV_{lo} and are defined by

$$\Delta V_{s,lo} = c^i_{vs,lo}P^i_{vs,lo} - c^f_{vs,lo}P^f_{vs,lo} + c^i_{as,lo}P^i_{as,lo} - c^f_{as,lo}P^f_{as,lo},$$

Parameters	Rest	LBNP
V_{tot}	5.304	5.065
$c_{vs,lo}$	0.137	0.055
$\bar{c}_\ell$	0.017	
$\bar{c}_r$	0.079	

State variable	Weights
$P_{as,up}$	1.000
$P_{vs,up}$	0.063
P_{a,CO_2}	1.180
P_{a,O_2}	9.585

Control variable	Weights
u_1	0.307
u_2	3.483
u_3	0.012
u_4	4.5e-004

Table 3.7: Subject C—ribs case: Adjusted parameters (total blood volume, compliance of lower venous compartment, capacitance of the ventricles) and weights used in the optimal control approach.

State	Rest	LBNP	Change
neg. press.	0	35	
$P_{as,up}$	85.000	81.000	−5%
$P_{as,lo}$	84.429	80.561	−5%
$P_{vs,lo}$	6.815	3.352	−51%
$P_{vs,up}$	6.244	2.913	−53%
P_{vp}	9.295	5.735	−38%
P_{a,CO_2}	40.000	40.000	0%
P_{a,O_2}	102.459	102.459	0%
P_{v,CO_2}	44.578	45.958	3%
P_{v,O_2}	46.195	40.898	−11%
S_ℓ	61.439	69.119	13%
S_r	4.677	5.262	13%
H	80.000	90.000	13%
$\dot{V}_A$	5.264	5.264	0%
V_u	3.607	2.395	−34%
A_{pcsk}	58.591	81.120	38%

Variable	Rest	LBNP	Change
P_{ap}	20.574	14.400	−30%
R_s	9.507	12.297	29%
$V_{str,\ell}$	0.102	0.070	−32%
$V_{str,r}$	0.102	0.070	−32%
Q_{co}	8.200	6.300	−23%
$F_{s,up}$	2.485	1.905	−23%
$F_{s,lo}$	5.715	4.395	−23%
V_s	1.697	0.751	−56%

Table 3.8: Subject C—ribs case: Steady states and auxiliary values.

Sum of changes in the lower compartments	
$\Delta V_{s,lo}$	−0.755
$\Delta V_{u,lo}$	−1.212
ΔV_{LBNP}	1.974
ΔV_{lo}	0.006

Table 3.9: Subject C—ribs case—sum of volume changes in the lower compartments.

$$\Delta V_{u,lo} = \begin{cases} 0, & \text{hips case,} \\ \dot{V}_u, & \text{ribs case,} \end{cases}$$

$$\Delta V_{LBNP} = (c^f_{vs,lo} + c^f_{as,lo}) P_{LBNP},$$

$$\Delta V_{lo} = \Delta V_{s,lo} + \Delta V_{u,lo} + \Delta V_{LBNP},$$

where $\Delta V_{s,lo}$ describes the change in stressed volume of the lower compartments (both arterial and venous), $\Delta V_{u,lo}$ describes the change in unstressed volume of the lower compartments, ΔV_{LBNP} is the volume (arterial and venous) induced by the LBNP stress, and ΔV_{lo} gives the net change of the total volume in lower compartment. ΔV_{LBNP} is calculated using compliances $c^f_{vs,lo}$ and $c^f_{as,lo}$, correlated with the chosen LBNP pressure using values from Risk et al. (2003).

Much work remains to be done to develop a clear picture of the global control mechanisms and autoregulatory influences that react to orthostatic and LBNP stress. Control of systemic resistance is an important factor (Cooke, Ryan, and Convertino, 2004; Convertino et al., 2004), but not enough quantitative data exists about how unstressed volume changes

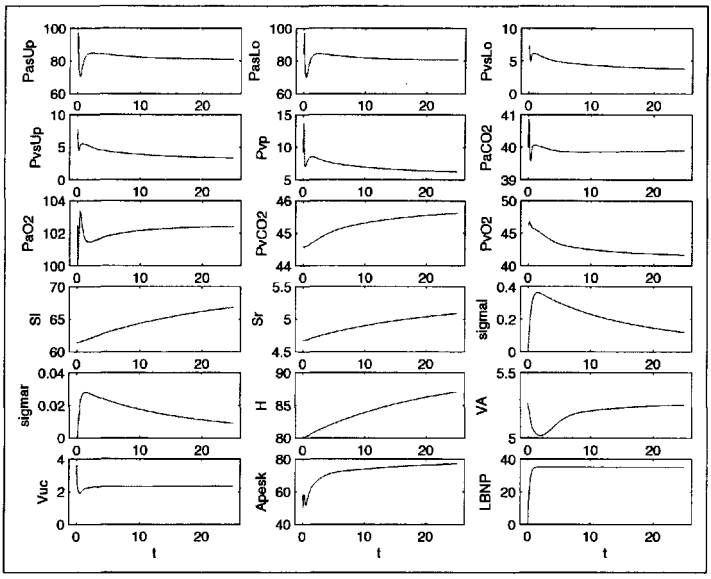

Figure 3.12: Model outputs for some state variables in the rib LBNP case.

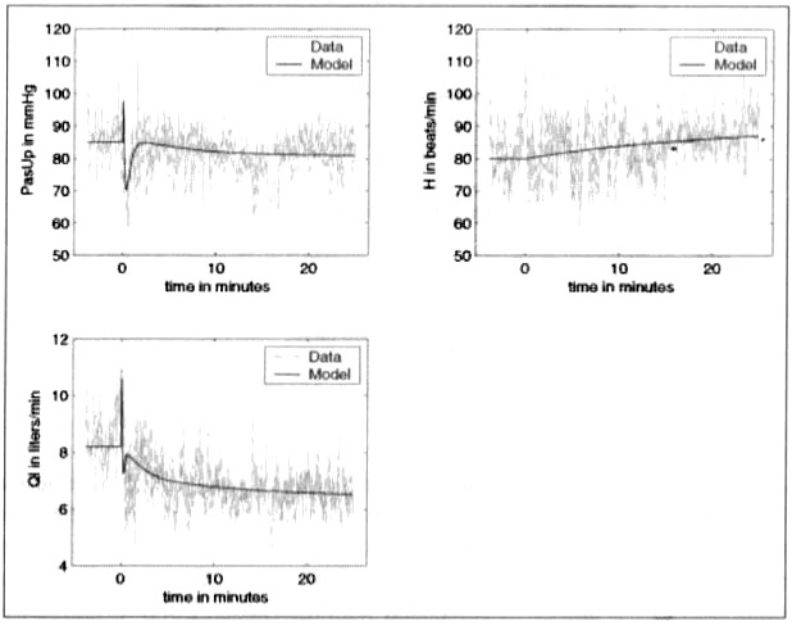

Figure 3.13: Data and model simulations for P_{as}, H, and Q_ℓ in the rib LBNP case.

in the diverse parts of the body, in general, and in particular how this volume is recruited during hypovolemic stress. We made an initial approach by assuming that controllable V_u lies primarily in the splanchnic region (Pang, 2001). Uncontrolled unstressed volume is distributed throughout the body, but does not impact the dynamic equations. In the ribs case of LBNP, the splanchnic region is included in the lower systemic compartments, so that LBNP puts an extreme stress on vascular volume as can be seen in the changes exhibited in Table 3.9. As can be seen from the changes exhibited in Table 3.9, there is a significant drop in $V_{u,lo}$ to replace the significant volume "lost" due to the LBNP stretch of the vasculature from the ribs downward. A significant drop in stressed blood volume $V_{s,lo}$ is predicted as well. We assume that changes in controlled unstressed volume is primarily mediated through sympathetic effects (Pang, 2001). Figure 3.12 gives dynamic representation of the principal state variables, while Figure 3.13 shows the fit to the data of subject C.

3.3.3 Blood volume control and hemorrhage

Hemorrhagic shock refers to the situation where there is insufficient O_2 perfusion of key organs due to a significant loss of blood volume (hemorrhage). When blood volume decreases, the initial reaction is a drop in stroke volume due to reduced ventricular filling and its consequences for the Frank–Starling mechanism. With less cardiac output, arterial pressure falls which activates the baroreflex loops previously discussed. A 10% loss of blood has no significant impact on the system beyond what is sometimes exhibited by blood donors. As blood loss increases, the system response becomes stronger and more comprehensive until a point is reached where the response has attained its maximal intensity and effectiveness and can no longer compensate for further falling pressure. Depending on the acuteness, degree, and duration of blood loss, in conjunction with complicating interacting effects of the CVS itself (see, e.g., Secher et al., 1992), a negative and worsening spiral of deteriorating CVS function can develop.

- Loss of blood pressure and reduced blood flow can damage cardiac and kidney functions, which further compromises the control response dependent on these key organs.
- This reduction in the effectiveness of the control response to a pressure fall further compromises blood pressure and flow and aggravates the damage to CVS function and control.
- This negative spiral can become irreversible, unless it is blocked in time by transfusion. Any inefficiencies or complications in the transfusion protocol becomes crucial as the threshold for the onset of this irreversible negative spiral is approached.

An important observation from an editorial of the *New England Journal of Medicine* (Ely and Bernard, 1999) stated that "The art of fluid administration and hemodynamic support is one of the most challenging aspects of treating critically ill patients." This is true not only in regards to maintaining RBC levels for tissue oxygenation, but also in regards to supporting circulation. In a recent review by the World Health Organization (WHO) Pre-Hospital Trauma Care Steering Committee (Kwan et al., 2003), the conclusion was as follows:

> "There is uncertainty about the effectiveness of fluid resuscitation in patients with bleeding following trauma .... Large, well concealed, randomized controlled trials are urgently needed to establish the optimal fluid resuscitation strategy in hemorrhaging trauma patients, with a focus on special types of injuries likely to benefit from the appropriate resuscitation strategy in terms of timing and volume of fluids given."

(Compare also Moore et al., 2004.) It is clear that a comprehensive mathematical model that quantitatively reflects the control mechanisms involved in the response to hypovolemia induced by hemorrhage will be very useful in the design of hemorrhage related transfusion protocols especially in cases where the patient has complicating medical conditions. Optimal treatment of acute hemorrhage can involve a number of questions:

- How severe is the blood loss after diagnosing a hemorrhage (noting that diagnosing a hemorrhage may not be a trivial task)?
- What fluid is best to treat the acute hemorrhage in a particular situation and is there an optimal procedure of administration? There are a number of replacement fluid options available and treatment decisions include choices such as
  - isotonic versus hypertonic fluids,
  - whole blood versus packed blood,
  - crystalloid versus noncrystalloid fluids.
- Depending on the injury, should fluid replacement begin before or after the hemorrhage has been stopped?
- Are there specific complicating reactions for individuals who have medical conditions? Such situations could include
  - patients with heart disease with anemia, for whom transfusions may raise venous pressure and precipitate acute HF,
  - patients with liver damage, kidney disease, or diabetes, as well as older patients, for whom certain fluid characteristics may initiate complicating reactions to these fluids.

A discussion of fluid replacement strategies can be found in Tremblay, Rizoli, and Brenneman (2001). In certain cases, depending on the type of fluids and state of the patient, the process of fluid replacement may hinder the natural interstitial auto-transfusion effect. Modeling the different types of fluids should take into account the osmotic properties, that influence autotransfusion, and the viscous properties, that effectively change the systemic resistance, as well as other fluid specific characteristics.

An algorithm for optimal control response

As a first step in studying control response to hemorrhage, we present an optimal control formulation which can be used to explore basic system interaction. As the modeling process is expanded and more detail of the control is explicitly modeled, the optimal control

feature can be used to close the loop in those areas, where the physiological mechanisms are not sufficiently understood. To implement an optimal control, we make the following assumptions:

(i) At each time t the control tries to steer the system to an equilibrium, where the arterial systemic pressure $\bar{P}_{\text{as}}$ equilibrium value equals the pressure $P_{\text{as},0}$ before the hemorrhage occurred.

(ii) There is a maximal heart rate $H_{e,\max}$ (~ 130 beats/min) acceptable at an equilibrium.

(iii) If, at the calculated equilibrium with $\bar{P}_{\text{as}} = P_{\text{as},0}$, the heart rate is larger than $H_{e,\max}$, then the control tries to steer the system to the equilibrium with $\bar{H} = H_{e,\max}$.

Let $\bar{p}_t$ be the system parameter vector at time t. Note that the parameter vector will change with time. This is due to some or all of the following effects:

(a) a change in V_{tot} as a consequence of hemorrhage, infusion, and exchange processes with the interstitium (capillary refill, loss of crystalloid, or colloid substitutes from plasma into the interstitium),

(b) changes in R_s and R_p as a consequence of changing viscosity of blood,

(c) changes in heart tissue contractilities due to tissue damage from low O_2 delivery to cardiac tissue.

In view of the assumptions given above, the control $u(t)$ at time $t \geq 0$ is calculated as follows.

Step 1: Determine the parameter vector $\bar{p}_t$ at time t that represents changes in the system. This will be updated by blood loss, infusion, etc. over time.

Step 2: Compute the steady state of the system $\bar{x}_{e,t}$ with $\bar{P}_{\text{as}} = P_{\text{as},0}$, parameter vector $\bar{p}_t$, and $\Delta V_{\text{hem}} = 0$, i.e., as if blood loss had been stopped at time t (for analogous computations see Section A.1 of Appendix A). This represents the goal of the system at time t and it means that we try to restore the original blood pressure with the altered parameter environment.

Step 3: If the steady state value for heart rate $\bar{H} \leq H_{e,\max}$, then accept $\bar{x}_{e,t}$, and compute the feedback control (see Section 1.4) that would transfer the system to the steady state $\bar{x}_{e,t}$ which is the current goal.

Step 4: If $\bar{H} > H_{e,\max}$, then the system cannot respond any further with changes in H, and we then calculate $\bar{x}_{e,t}$ with $\bar{H} = H_{e,\max}$, parameter $\bar{p}_t$, and $\Delta V_{\text{hem}} = 0$ (see Subsection 1.3.1). This will imply a lower blood pressure. We then compute the control that follows from this new steady state (see Section 1.4).

This process is repeated as we simulate blood loss, change in resistance (viscosity), transfusion, interstitial exchange, or tissue damage.

Simulated cardiovascular responses to hemorrhage

We consider the reduced model of Section 1.2 using only $\dot{H}$ as control. We will consider only the simplest case: a systemic arterial hemorrhage with a control response, consisting

only of increasing H as in the algorithm discussed above. We do not include autotransfusion or change in blood viscosity. The state equations are given as

$$\begin{aligned}
c_{as}\dot{P}_{as} &= Q_\ell - F_s - \Delta V_{hem},\\
c_{vs}\dot{P}_{vs} &= F_s - Q_r,\\
c_{ap}\dot{P}_{ap} &= Q_r - F_p,\\
c_{vp}\dot{P}_{vp} &= F_p - Q_\ell,\\
\dot{S}_\ell &= \sigma_\ell,\\
\dot{S}_r &= \sigma_r,\\
\dot{\sigma}_\ell &= -\gamma_\ell\sigma_\ell - \alpha_\ell S_\ell + \beta_\ell H,\\
\dot{\sigma}_r &= -\gamma_r\sigma_r - \alpha_r S_r + \beta_r H,\\
\dot{H} &= u,
\end{aligned} \tag{3.42}$$

where the relation

$$V_{tot} = c_{as}P_{as} + c_{vs}P_{vs} + c_{ap}P_{ap} + c_{vp}P_{vp} + V_u - V_{hem\text{-}sum}$$

can be used to reduce the set of state equations by solving for P_{ap}, for instance. As in the LBNP case, we include unstressed volume but only as a constant. In the first equation of (3.42), the term ΔV_{hem} represents blood loss in liters/min from the systemic arterial compartment and $V_{hem\text{-}sum}$ represents the currently accumulated blood loss since hemorrhage began. For the example given here, blood loss is modeled as a constant reduction over 1 min with accumulated loss of 25% of the original blood volume. Blood loss from the arterial compartment was assumed proportional to blood pressure. We did not include in this basic example, however, would expect that, at this level of loss, autoinfusion of fluid from the interstitial region would supplement the $\dot{H}$ control to restore volume and pressure. Parameter values are given in Table 3.10. As can be seen in Figure 3.14, as V_{tot} drops so does P_{as}, and the control system responds with an increase in H that supports and stabilizes pressure, but in this example the H response is not completely able to control the drop in P_{as}. However, we did not include in this basic model other control factors such as varying unstressed volume or the effects of autotransfusion. We would expect that, at this level of loss, autoinfusion of fluid from the interstitial region would by itself sufficiently supplement the $\dot{H}$ control to restore volume and pressure. This example shows that H, the quickest control response, needs support from other mechanisms to restore the system.

3.3.4 CBF and OID

As discussed earlier in this chapter, orthostatic intolerance disorders (OID), which are manifested by dizziness, falls, or syncope, are observed in healthy and diseased people, but the frequency of occurrences is increased in people, suffering from cardiovascular diseases (Blackmer, 1997; Dobkin, 1989; Eigenbrodt, 2000). OID is the result of inadequate orthostatic regulation that involves complex interactions among various mechanisms of short-term cardiovascular and respiratory blood flow and blood pressure control. For example, syncope, observed in some OID patients, might be due to cerebral hypoperfusion triggered

Parameter	Value	Unit
V_{tot}	5.0	liter
V_u	3.25	liter
ΔV_{hem}	1.25	l/min
P_{as}	96.82	liter/mmHg
c_{as}	0.002	liter/mmHg
c_{vs}	0.149	liter/mmHg
c_{ap}	0.0073	liter/mmHg
c_{vp}	0.016	liter/mmHg
c_ℓ	0.01289	liter/mmHg
c_r	0.06077	liter/mmHg
α_ℓ	89.47	min^{-2}
α_r	28.46	min^{-2}
β_ℓ	68.71	mmHg/min
β_r	1.67	mmHg/min
γ_ℓ	37.33	min^{-1}
γ_r	11.88	min^{-1}
R_ℓ	11.350	mmHg min/liter
R_r	4.158	mmHg min/liter
R_p	1.965	mmHg min/liter
R_s	18.41	mmHg min/liter
H_{max}	130	l/min
κ	0.50	—

Table 3.10: Parameters for simulations of hemorrhage.

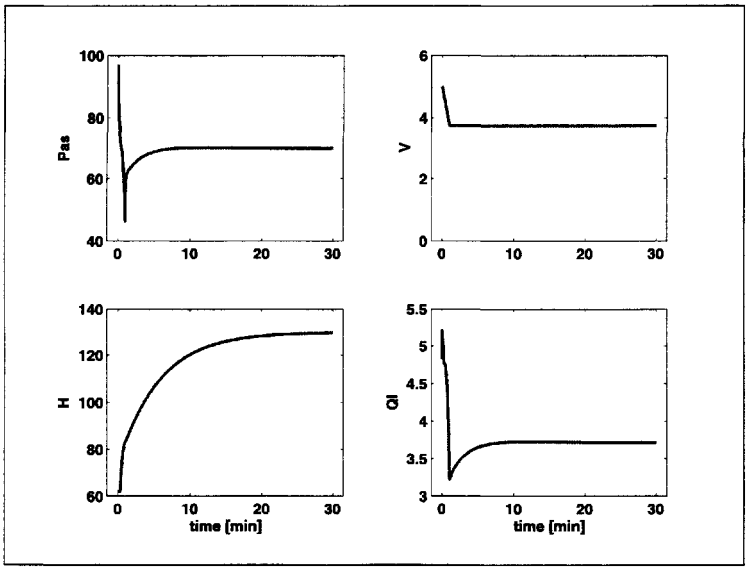

Figure 3.14: Key states during hemorrhage.

by impaired short-term control regulations (P. Novak et al., 1997; V. Novak et al., 2003). It may occur as a response to blood pressure reduction due to low blood volume, impaired afferent or efferent baroreflex responses, or from cerebral hypoperfusion induced by hyperventilation (Evans, 1995; Dowden and Allen, 1997). These biological mechanisms are difficult to separate using only clinical procedures such as HUT or sit-to-stand. To develop better strategies to treat and diagnose OI, it is important to understand the underlying mechanisms leading to these disorders.

Cardiovascular compartmental model

In this section, we will describe a mathematical model (Olufsen et al., 2005; Olufsen et al., 2004), which is based on physiological mechanisms, that can predict dynamic changes in beat-to-beat arterial blood pressure and middle cerebral artery blood flow velocity during postural change from sitting to standing. This cardiovascular model consists of five compartments representing systemic arteries (brain, upper body, lower body, aorta, and finger), four compartments representing systemic veins (brain, upper body, lower body, and vena cava), and two compartments representing the left atrium and the left ventricle (see Figure 3.15). Each compartment includes a capacitor to represent compliant volume of arteries or veins. All compartments are separated by resistors representing resistance of the vessels. The compartment representing the left ventricle has two valves (aortic and mitral valves). Following convention from electrical circuit theory, resistors R are marked with zigzag lines, capacitors c with dashed parallel lines inside the compartments, and aortic and mitral valves with short lines inside the compartment that represents the left ventricle. In addition, "Cer." is used for cerebral. This model can predict pressure in each of

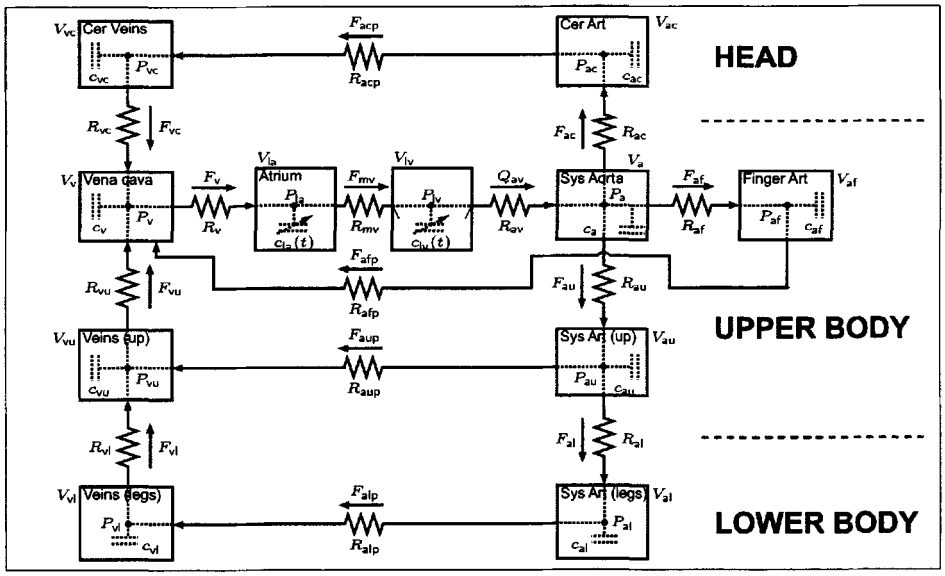

Figure 3.15: Compartment model of the closed-loop cardiovascular system.

these compartments and the flow between all compartments. Each compartment comprises a capacitor that represents a compliant volume (inverse elasticity), and resistance to flow is obtained by separating each compartment by a resistor.

Equations for the cardiovascular model were derived following analogous equations obtained from electrical circuits. Following this analogy, pressure P [mmHg] plays the role of voltage, volumetric flow F [cm^3/sec] plays the role of current, and volume V [cm^3] plays the role of electrical charge. The basic equations that predict blood pressure and flow were obtained by computing the volume of each compartment $V_i = c_i P_i + V_{u,i}$ [cm^3], where c_i [cm^3/mmHg] is the compliance, P_i is the pressure, and $V_{u,i}$ is the unstressed volume of the ith compartment. For each compartment, the rate of change of the volume is given by

$$\frac{dV_i}{dt} = F_{\text{in}} - F_{\text{out}}, \tag{3.43}$$

where F_{in} and F_{out} represent the flows entering and leaving compartment i, respectively. Each of these flows (located between compartments) was determined, using Kirchhoff's current law, as the difference between the pressure in the compartments that precede and follow compartment i, that is,

$$F_{\text{in}} = \frac{P_{i-1} - P_i}{R_{\text{in}}}, \qquad F_{\text{out}} = \frac{P_i - P_{i+1}}{R_{\text{out}}},$$

where R_i [mmHg sec/cm] is the resistance to the flow. More specifically, if the ith compartment represents arteries in the lower body, then $P_i = P_{\text{al}}$, $P_{i-1} = P_{\text{au}}$, $P_{i+1} = P_{\text{vl}}$, $F_{\text{in}} = F_{\text{al}}$, $F_{\text{out}} = F_{\text{alp}}$, $R_{\text{in}} = R_{\text{al}}$, and $R_{\text{out}} = R_{\text{alp}}$. Differentiating the volume equation $V_i = c_i P_i + V_{u,i}$ and inserting (3.43) gives

$$c_i \frac{dP_i}{dt} = F_{\text{in}} - F_{\text{out}} - P_i \frac{dc_i}{dt}, \tag{3.44}$$

where it is assumed that $c_i(t)$ varies as a function of time t and the unstressed volume is constant. Our basic model, shown in Figure 3.15, gives rise to a nonlinear system of eleven differential equations. Of these eleven equations, nine equations are of the form (3.44) and two are of the form (3.43), one for the left ventricle, and one for the left atrium (indicated by subscripts "lv" and "la," respectively). Note that this model does not incorporate a submodel for the pulmonary circuit including the right heart.

Pulsatile flow

To model the left ventricle as a pump, the states of the mitral and aortic valves must be modeled. During diastole, the mitral valve opens, while the aortic valve closes, allowing blood to enter the left ventricle. Then isometric contraction begins, increasing the ventricular pressure. Once the ventricular pressure exceeds the aortic pressure, the aortic valve opens, propelling the pulse wave through the vascular system. It is noted that, for young healthy people, both valves cannot open simultaneously. Following (Rideout, 1991), the state of the valves is modeled in (Olufsen et al., 2005) as

$$R_k = \min\{R_k + e^{-10(P_{\text{in}} - P_{\text{out}})}, 5000\},$$

where the subscript k represents either the mitral valve or the aortic valve. The symbols P_{in} and P_{out} represent the pressures in the compartments that precede and follow the resistors represented by R_k. The rationale for this expression is that a closed valve will result in a large resistance (or no flow), while an open valve will yield a small resistance (or normal flow). The minimum value is introduced to avoid numerical issues with large numbers.

In (Olufsen et al., 2005), the pumping action of the heart was realized by varying the left ventricular blood pressure. To obtain a pulse wave that is propagating along the artery, the left ventricular pressure was described in terms of an activation function $g(t, H)$ (Danielsen and Ottesen, 2001; Ottesen and Danielsen, 2003). The advantage of this model is its ability to account for varying heart rate and to specify the onset of the ventricular contraction and relaxation. Its disadvantage is that several additional parameters are introduced. This model predicts atrial pressure P_{la} and ventricular pressure P_{lv} as functions of volume and cardiac activation of the form

$$P = a\big(V(t) - b\big)^2 + \big(c(t)V(t) - d\big)g(t, H), \qquad P = P_{\text{la}} \text{ or } P_{\text{lv}}. \tag{3.45}$$

The parameter a [mmHg/cm^3] represents ventricular elastance during relaxation, b [cm^3] represents ventricular volume at zero diastolic pressure, $c(t)$ [mmHg/cm^3] represents contractility, and d [mmHg] is related to the volume-dependent and volume-independent components of the developed pressure. The activation function $g(t, H)$, defined over the length of one cardiac cycle, is described by a polynomial of degree $n + m$, $g(t, H) = f(t, H)/f(t_p, H)$, where

$$f(\tilde{t}, H) = \begin{cases} P_p \dfrac{\tilde{t}^n\big(\beta(H) - \tilde{t}\big)^m}{n^n m^m \big(\beta(H)/(m+n)\big)^{m+n}} & \text{for } \ 0 \le \tilde{t} \le \beta(H), \\ 0 & \text{for } \ \beta(H) < \tilde{t} \le T. \end{cases}$$

T [sec] is the duration of the cardiac cycle, $\beta(H)$ [sec] denotes the onset of relaxation, $H = 1/T$ [1/sec] denotes the heart rate, n and m characterize the contraction and relaxation phases, and P_p is the peak value of the activation. The $\tilde{t}$ is given by $\tilde{t} = t - nT$ [sec], where the nonnegative integer n is defined by $nT \le t < (n+1)T$. The ability to vary heart rate is included in the isovolumic pressure equation (3.45) by scaling time and peak values of the activation function f. The time for peak value of the contraction, t_p [sec], is scaled by introducing a sigmoidal function, that depends on the heart rate H, of the form

$$t_p = t_m + \frac{\theta^\nu}{H^\nu + \theta^\nu}(t_M - t_m),$$

where θ represents the median, ν represents the steepness, and t_m [sec] and t_M [sec] denote the minimum and maximum values, respectively. The peak ventricular pressure P_p [mmHg] is scaled similarly using a sigmoidal function of the form

$$P_p = P_m + \frac{H^\eta}{H^\eta + \phi^\eta}(P_M - P_m),$$

where ϕ represents the median, η represents the steepness of the sigmoidal curve, and p_m [mmHg] and p_M [mmHg] denote the minimum and maximum values, respectively.

Finally, the time for the onset of relaxation β is modeled by

$$\beta(H) = \frac{n+m}{n} t_p(H).$$

This equation is obtained by recognizing that, the time t_p for peak pressure is related to the parameter β in the isovolumic pressure model (3.45).

Gravitational effects

The effect of gravity, during postural change from sitting to standing, was modeled by adding a hydrostatic pressure to each of the compartments that represent the distance between the compartment and the heart. It is noted that only the compartments that represent the legs are affected by gravity. Consequently, the blood flow equations for F_{al} and F_{vl} are modified as follows:

$$F_{al} = \frac{P_{au} - (P_{al} + \rho g h)}{R_{al}},$$
$$F_{vl} = \frac{(P_{vl} + \rho g h) - P_{vu}}{R_{vl}},$$

where ρ [g/cm^3] is the density of blood, g [cm/sec^2] is the gravitational acceleration, and h [cm] is the height measured from the heart to the lower body compartment and is given by

$$h(t) = \frac{h_M}{1 + e^{-k(t - T_{up} - \delta)}}.$$

Here, T_{up} [sec] is the time at which the subject stands up, h_M [cm] is the maximum height needed for the mean arterial blood pressure in the finger to drop, as indicated by the experimental data, and δ [sec] is the latency for standing up.

Nonlinear passive resistances

From the theory of fluid mechanics, it is well known that the resistance depends on the radii of the vessels, and that the radii themselves depend nonlinearly on the corresponding transmural pressure. It has been shown (Olufsen et al., 2005) that it is important to include such dependencies in regions that represent vessels with large diameters and high blood pressure (in the large arteries), while they are less important in regions of low blood pressure (in the venous system) and in regions with small vessels (in the small arteries and arterioles), where autonomic responses are active and dominate the change in vessel diameters. To predict this dependency, the nonlinear resistances (R_{av}, R_{ac}, R_{au}, R_{al}, R_{af}) are modeled using a sigmoidally decreasing function of mean blood pressure of the form

$$R = (R_M - R_m) \frac{\alpha_2^k}{\bar{P}^k + \alpha_2^k} + R_m,$$

where R_M [mmHg sec/cm^3] and R_m [mmHg sec/cm^3] are the maximum and minimum values that the resistances can obtain, $\bar{P}$ [mmHg] is the mean blood pressure in the compartment that precedes the resistance, k represents the steepness of the sigmoid, and the

parameter α_2 is calculated to ensure that R returns to the known set-point value of the computed resistance. The mean pressure $\bar{P}$ is defined by

$$\bar{P} = \frac{1}{N}\int_0^t P(s)e^{-\nu(t-s)}\,ds,$$

where

$$N = \int_0^t e^{-\nu(t-s)}\,ds = \frac{1-e^{\nu t}}{\nu}$$

is a scaling parameter, so that we obtain the correct mean pressure when the pressure P is a constant.

Autonomic regulation

Two main control mechanisms play a role in blood flow regulation: autonomic regulation and cerebral autoregulation. Autonomic regulation is a part of the central control system. Autonomic reflexes are mediated via sympathetic and parasympathetic nervous responses. They are mainly activated by special receptors (baroreceptors), which are sensitive to pressure alterations. High-pressure receptors are located in the aortic arch and carotid sinuses, and low-pressure receptors are located in the atria and pulmonary circulation. These receptors buffer arterial blood pressure changes. They have cardiovascular and renal manifestations and they can adapt to a sustained alteration by resetting. During sit-to-stand approximately 500 [cm^3] (Joyner and Shephard, 1993) of blood is pooled in the legs as a result of gravitational force. As a consequence, the blood pressure in the trunk and upper extremities drops. To compensate for this drop in pressure, the frequency of afferent impulses in the aortic and carotid sinus nerves is reduced, which cause a reduction of activity in the medullary depressor area and stimulation of the pressor area. Fibers that descend from the cardiac and vasomotor centers of the medulla synapse with cells of the intermediolateral cell column of the spinal cord and travel via anterior spinal roots to the sympathetic chain. In addition, descending impulses from the cerebral cortex and hypothalamus may also, by way of these spinal pathways, induce sympathetic vascular responses. The increased sympathetic activity leads to an increased release of noradrenaline, which in turn helps to restore the blood pressure to normal by increasing heart rate, cardiac contractility, vasoconstrictor, and venoconstrictor tone. Furthermore, a decrease in parasympathetic activity leads to a decrease in the release of acetylcholine (Ach) in the heart and possibly in the brain. Decreased concentration of Ach in the heart leads to an increased heart rate. In the brain, a decreased Ach concentration may interact with cerebral autoregulation to obtain sufficient vasodilation to maintain constant cerebral perfusion.

The sympathetic nervous system normally responds more quickly to a decrease in blood pressure rather than an increase (i.e., it is more effective in combating hypotension than hypertension). The control forms a hysteresis effect, an increased sympathetic activity is typically initiated within seconds of the stimulus and it is able to increase the pressure within 5–10 seconds, whereas sudden inhibition of nervous stimulation requires 10–40 seconds to decrease the arterial blood pressure. In addition, a parasympathetic withdrawal (vagal stimulation) helps to restore the blood pressure. The parasympathetic response is faster than the sympathetic response; its effect will be implemented within 1–2 cardiac cycles. The parasympathetic response is greatest in the normal range of blood pressure

(from 80–150 [mmHg]) (Smith and Kampine, 1990). However, the baroreceptors are able to adapt to permanent or semipermanent alterations in arterial blood pressure. In (Olufsen et al., 2005; Olufsen et al., 2004), the autonomic regulation is modeled using a first-order differential set-point equation of the form

$$\frac{dx(t)}{dt} = \frac{-x(t) + x_{\text{ctr}}(\bar{P}_a)}{\tau},$$

where $x(t)$ is the controlled parameter, τ is a time constant that characterizes the time it takes for the controlled variable to obtain its full effect, x_{ctr} is the set-point function (a sigmoidal function) given by

$$x_{\text{ctr}} = (x_{\max} - x_{\min}) \frac{\hat{P}^k}{\hat{P}^k + \bar{P}^k} + x_{\min},$$

where $x_{\min}$ and $x_{\max}$ are the minimum and maximum values for the controlled parameter x, respectively, $\hat{P}$ is the pressure at which we want to achieve the value obtained during steady state (i.e., during sitting), and k denotes the steepness of the sigmoid. Controlled parameters include heart rate H [1/sec], cardiac contractility (S_{lv}, S_{la} [mmHg/cm^3]), peripheral systemic resistances (R_{aup}, R_{alp}, R_{afp} [mmHg sec/cm^3]), and systemic compliances (all c's [cm^3/mmHg] are shown in Figure 3.15).

Autoregulation

Cerebral autoregulation is essentially a local phenomenon mediated via changes in active tone in the small blood vessels. The aim of autoregulation is to keep the blood flow constant within some range of mean arterial blood pressure (from 80–160 [mmHg]). Organs with the smallest neurogenic tone (brain, heart, and kidney) show the highest autoregulatory ability. Although the ability to autoregulate is affected, to some extent, by neural and humoral influences such as vasoconstrictor tone and pH of blood, the autoregulatory response is largely intrinsic and occurs even when tissues are fully denervated and isolated. It is not clear exactly how this change is mediated. As discussed earlier, it is believed that several mechanisms, including responses to changes in myogenic tone, metabolic demand, and the concentration of CO_2 and O_2, are engaged. It is suggested that, a decreased perfusion pressure decreases the muscle tension in the vessel wall, stimulating it to dilate to increase the flow. Furthermore, it is believed that metabolically regulated flow can be described as a function of the O_2 concentration in the tissue; a decrease in flow will produce a decrease in local tissue O_2 concentration and an increase in tissue CO_2 concentration and other metabolites. The decrease of O_2 concentration or accumulation of vasoactive metabolites relax the arterioles and as a result the blood flow will rise. The physiological response to either of these mechanisms involves local regulation mediated via negative feedback mechanisms. For healthy young people, autoregulation is typically delayed by 5–10 seconds from when the change in flow was initiated.

Because of this complex interaction, it is not trivial to develop an accurate physiological model that describes cerebral autoregulation. One approach, which was considered in (Olufsen et al., 2005), was to treat the cerebrovascular resistance as an unknown function. To determine this function numerically, one can parameterize it using a combination

of known functions. The simplest one is to use piecewise linear functions with unknown coefficients as follows:

$$R_{\text{acp}}(t) = \sum_{i=1}^{n} \gamma_i \hat{H}_i(t),$$

where $\hat{H}_i$ are the standard "hat" functions given by

$$\hat{H}_i(t) = \begin{cases} \dfrac{t - t_{i-1}}{t_i - t_{i-1}}, & t_{i-1} \le t \le t_i, \\ \dfrac{t_{i+1} - t}{t_{i+1} - t_i}, & t_i \le t \le t_{i+1}, \\ 0, & \text{otherwise.} \end{cases}$$

Here, the time interval in the simulation studies [45, 90] (in seconds) is subdivided into n equally spaced subintervals with nodal points denoted by t_i. To capture sufficient dynamics in the cerebrovascular resistance $R_{\text{acp}}(t)$, we take n to be equal to 26. The unknown coefficients γ_i, which denote the approximation to the function $R_{\text{acp}}(t)$ at the nodal value $t = t_i$, will be estimated together with the other unknown parameters in the model. This approach was also used to estimate the resistance R_{au}, which may be affected by passive nonlinear resistances and autonomic regulation.

It is noted that a number of models have been developed to study autonomic regulation and cerebral autoregulation. One way to model the effect of cerebral autoregulation is to let the cerebrovascular resistance be a function of time as suggested in (Ursino and Lodi, 1998). However, this work does not include the effects of autonomic regulation. A second group of models has described parts of the control system without validation against experimental data (see, e.g., Melchior et al., 1992; Melchior et al., 1994; Rideout, 1991; Ottesen, 1997; Ottesen, 2000; Ursino, 1998; Warner, 1958). These models use closed-loop compartmental descriptions of the cardiovascular system combined with physiological descriptions of the cardiovascular control. While these models can provide qualitative analysis of the system, they cannot be used for quantitative comparisons with data. Furthermore, most of the models in the second group describe the effects of autonomic regulation without including the effects of cerebral autoregulation.

The cardiovascular model described above was validated against continuous physiological data obtained from a young and healthy subject during transition from sitting to standing. In particular, the data consist of arterial blood pressure measurements from the finger and arterial blood flow velocity measurements from the middle cerebral artery (Lipsitz et al., 2000). The subject was instrumented with a 3-lead echocardiogram (ECG) (Collins, TX, USA) to obtain heart rate and a photoplethysmographic cuff on the middle finger of the right hand, supported at the level of the right atrium to obtain noninvasive beat-by-beat blood pressure (Finapres, Ohmeda, CO, USA). The middle cerebral artery was insonated by placing a 2 MHz Doppler probe (Nicolet Companion, WI, USA) over the temporal window to obtain continuous measurements of blood flow velocity. The envelope of the velocity waveform was derived from the fast Fourier transform of the Doppler signal. All physiological signals were digitized at 500 Hz (Windaq, Dataq Instruments, OH, USA) and stored for off-line analysis. Blood pressure reduction of approximately 30 [mmHg]

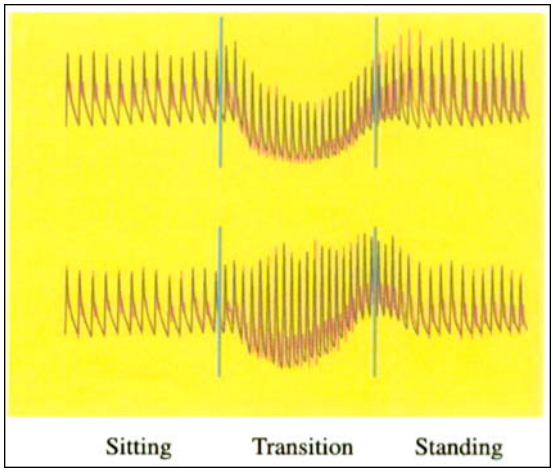

Figure 3.16: Comparison between model (black traces) and experimental data (red traces). Arterial finger blood pressure is depicted at the top and cerebral blood flow velocity is depicted at the bottom. The transition period (between green lines) specifies time frame for the sit-to-stand transition dynamics.

upon standing up was used as a challenge for cerebral autoregulation. The subject sat in a straight-backed chair with legs elevated at 90 degrees in front of them. Then the subject was asked to stand. Standing was defined as the moment when both feet touched the floor. Two trials were performed with 5-minute sitting followed by standing for 1 minute, and one trial of a 5-minute sitting followed by a 6-minute standing.

Using an OLS formulation of the problem to estimate the unknown parameters (compare Subsection 1.6.2), the model produces excellent agreement with the experimental data. The cost functional used in the OLS formulation and the obtained optimal parameters are discussed and reported in (Olufsen et al., 2005). Figure 3.16 illustrates that this model is able to predict the change in the overall profile during the transition from sitting to standing. The only minor difference is that the data include a small overshoot in the pressure in the transition region to standing. However, much work remains to be done. The models used in (Olufsen et al., 2005) and described above for the autonomic regulation and autoregulation are simple ones. For the model to be useful, especially in clinical settings, there is clearly a need for the development of more accurate and physiologically based models that can be used for quantitative comparisons with data.

This page intentionally left blank

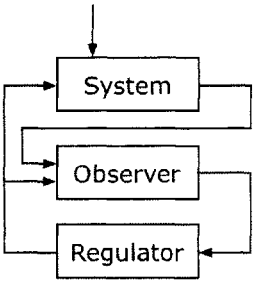

Chapter 4

Blood Volume and the Venous System

4.1 Introduction

The various needs of the circulation under different cardiovascular loads, which occur during exercise, orthostasis, and heat stress, require a well-orchestrated distribution of blood volume and blood flow to maintain proper cardiac filling. This must be accomplished without interfering too much with the pressure and flow relationship in the high- as well as low-pressure part of the circulation. These requirements are met by a system that can hold or release large amounts of blood volume with only small changes in systemic pressures. The system that accomplishes these requirements is essentially located in the highly distensible venous part of the circulation. A large part of this chapter deals with pressure, volume, and flow in distensible vessels and with the importance of volume for short-term cardiovascular control. The venous system not only holds a large volume, but also closes the loop for the circulation of the blood. In the closed-loop configuration, what the heart pumps into the arterial limb of the peripheral circulation, as cardiac output, eventually has to return to the heart through the venous limb as the so-called venous return. Problems in the understanding and interpretation of cardiovascular regulation, which result from this inherent circularity and which involve circular cause and effect relationships, are also addressed in this chapter.

The function of the venous reservoir not only depends on distensible vessel characteristics, but also depends on the filling volume, the blood, and on its major components, the red blood cells and the plasma. The regulation of both red blood cells and plasma volume remains the key for mid- to long-term cardiovascular control. A major part of this chapter deals with blood, plasma, and red blood cell volumes and their regulation, revisiting classic concepts and presenting more recent hypotheses, which may hold clues for long-term cardiovascular control. Finally, the issue of pressure and volume control is discussed in regards to the end-stage renal disease patient, where the disruption of long-term feedback control has serious consequences for volume and pressure homeostasis, and where a more or less stable state can only be obtained by renal replacement therapy such as hemodialysis. Hemodialysis, on the other hand, provides a unique environment to study the volume-pressure control system, also because of the direct access to the cardiovascular

system using an extracorporeal circulation for the treatment of blood. In this configuration, the volume-pressure system can be studied as it departs from the physiological state either spontaneously or using controlled perturbations. Last, but not least, the hemodialysis treatment itself can be considered a controlled perturbation, prescribed and performed by the medical staff, and hopefully optimized by adequate control algorithms.

This chapter begins with a more general consideration regarding the relationship of cardiovascular variables and parameters with body size. An understanding of scaling issues sheds light on functional and structural relationships, and also aids in understanding clinical parameters and data.

4.2 Scaling

In the development of physiological models, it is soon recognized that many variables and parameters must be adjusted to individual study subjects, especially when subjects differ in body size. Even when focusing on adult subjects, a factor of two for body weight is within the normal physiological range. The model structure, however, and this is important, can remain largely unchanged. When this thought is extended to comparisons among species with physiological resemblance, the factors relating individual parameters and variables may increase even further. What is the significance of such relationships? There are at least three areas where these relationships are of importance. First, mechanistic models can be made size independent when the size dependence of parameters and variables is known. For example, data and models established in experimental animals can be extrapolated for human application. Second, for comparison of normal ranges and to identify pathological conditions, many (but not all) clinically important variables and parameters have to be normalized to body mass or body surface area to eliminate the effect of variable body size. And third, the dependence of parameters and variables on body size across species can be studied to identify the common underlying building principles (or mechanistic models). This will provide improved insight into the relationship between structure and function. However, the dependence of variables and parameters on body size is not uniform. For example, while blood volume is related to body mass, and cardiac output is related to body surface area, arterial blood pressure apparently is independent of either. Why is this the case?

In this regard it may be helpful to investigate variables of interest in different species with comparable construction principles or physiology. This type of analysis has become known as scaling or allometric analysis. Scaling deals with the structural and functional consequences of the changes in size or scale among similar organisms (Schmidt-Nielsen, 1984). In the end, it is the aim to obtain measures for biological similarity (Stahl, 1963).

4.2.1 Isometric relationships

In geometry, similarity between bodies is described by isometric relationships. The linear relationship of isometric ratios is maintained when characteristics of the same dimension, such as the diameter or the circumference of a square, are examined. The transition to other dimensions changes this linearity. The surface of geometric bodies does not change in the same ratio as their linear dimension, nor does their volume. Thus, if a cube has a side twice as long as a smaller cube, its surface area will then be 2^2, or four times that of the smaller

cube, and its volume will be 2^3, or eight times as great. Thus, as $S \approx L^2$ and $V \approx L^3$, the ratio between the surface S and the volume V is $S \approx V^{2/3}$ for geometrical bodies. The same rule applies to any other geometrically similar or isometric three-dimensional bodies, whatever the shapes, and it also applies to irregularly shaped objects such as animals. If two dogs of different size are isometric, their surfaces and volumes will be in ratios related to their linear dimensions to their second and third powers, respectively. In a double logarithmic plot, the relationship between surface and volume is presented as a straight line with the slope $2/3$. If instead, the surface area per unit volume of the cube is plotted, the regression line shows that the relative surface area decreases with increasing size of the body. The slope of this relationship is $2/3 - 1 = -1/3$. This expresses another well-known fact, namely that smaller bodies have larger surface areas, relative to their volumes, than larger bodies.

4.2.2 Allometric relationships

Real organisms usually are not isometric, even when organized along similar patterns. Instead, certain proportions change in a distinct fashion. In biology, such nonisometric scaling is often referred to as allometric (from Greek $\alpha\lambda\lambda o\tilde{\iota}o\varsigma$, which means different). An amazing number of morphological and physiological variables y are scaled to body size x, according to allometric equations of the general form

$$y = ax^b, \tag{4.1}$$

where a is a constant and where the exponent b is of special interest. The exponent b can take on different values and can be either positive or negative, depending on the variable being considered. For $b \neq 0$, the physiological variable of interest is said to scale to body size, with the special case of $b = 1$ describing a linear relationship between the physiological variable and body size. For $b = 0$, the physiological variable y is independent of body size x. In the examination of physiological variables and their relationships to body size, the volume of physiological bodies is usually replaced by body mass M for practical reasons. This simplification is based on a uniform density of physiological bodies of $\rho \approx 1$. Often physiological entities are normalized for body mass to obtain a specific entity. Division of both sides of (4.1) by x gives the relationship for specific variables or parameters and the exponent in (4.1) is equal to $b - 1$. As mentioned above, specific entities can decline ($b - 1 < 0$), remain constant ($b - 1 = 0$; scale independent), or increase with increasing body mass ($b - 1 > 0$). Scaling is largely focused on variables that show some relationship to body mass, most notably metabolic rate. In terrestrial mammals, where body masses cover a range of 6 orders of magnitude—from the Etruscan shrew with a body mass of about 2 [grams] to the African elephant of up to $7 \cdot 10^6$ [grams]—metabolic rate was found to scale to body mass with an exponent of $b = 0.74$ (Kleiber, 1932). In this example, there is ongoing discussion on the exact value of the exponent, because of different biophysical interpretations, whether the exponent is closer to $2/3$ or $3/4$ (Dodds, Rothman, and Weitz, 2001; Schmidt-Nielsen, 1984; West, Brown, and Enquist, 1997). The interest in scaling recently resurfaced as the relationships, uncovered by this type of analysis, are expected to hold information on unifying concepts in the diversification of life up to the structure of ecosystems and societies (Enquist et al., 2003).

4.2.3 Cardiovascular entities

Blood volume increases linearly with body mass. The exponent b in (4.1), for the blood volume to body mass relationship, is not significantly different from unity ($b = 1.02$). When blood volume is normalized for body mass, specific blood volume (volume per mass, $\approx 70\,[\mathrm{cm}^3\,\mathrm{kg}^{-1}]$ body mass) is almost constant, and therefore is comparable among human subjects and most other mammals. Specific blood volume is scale independent. Therefore, to compare blood volumes between individuals, one also has to know their body mass. The same is true for the size of the mammalian heart, which scales with body mass with an exponent of $b = 0.98$. Another important cardiovascular variable is the heart rate, which in the resting mammal scales with an exponent of $b = -0.25$; i.e., the frequency decreases as body mass increases. This shows the importance of time as one of the components of space-time when scaling dynamic processes (Lambert and Teissier, 1927).

The exponent b in (4.1) for cardiac output (with the unit volume per time) in mammals of different body size is less than unity ($b = 0.81$). The value of b is closer to the exponent of $2/3$, describing the relationship between surface area and volume. In medical practice, cardiac output is therefore assumed to scale with body surface area. The difference in b between 0.81 and 0.67, however, could provide an explanation for problems indexing cardiac output relative to body surface (Turner and Reilly, 1995). The cardiac output normalized for body surface area, called cardiac index, is approximately $3\,[\mathrm{liter\,min}^{-1}\,\mathrm{m}^{-2}]$. Thus, to compare the cardiac output in subjects of different body size, one should know their body surface area. Body surface of an adult with average weight 70 [kg] is $S \approx 1.8\,[\mathrm{m}^2]$. The measurement of body surface area is more difficult than the measurement of body mass. Body surface area (S, in cm^2) is usually estimated from body mass (M, in kg) and body height (L, in cm) according to the formula proposed by Du Bois and Du Bois (1916),

$$S = aM^bL^c. \tag{4.2}$$

This formula is very popular, however, the values for the constants a, b, and c, originally obtained by Du Bois and Du Bois in a small group of adult subjects, should no longer be used. In a reanalysis of the original data using nonlinear least-squares regression, the coefficients were determined as $a = 94.9 \pm 26.7$, $b = 0.441 \pm 0.018$, and $c = 0.655 \pm 0.063$ (Tikuisis, Meunier, and Jubenville, 2001).

Unlike the heart that scales with body mass, the terminal branch of the vascular tree, where transport is governed by physical constants such as diffusion coefficients and solubilities, is scale independent ($b = 0$, (4.1)). To some extent, the transport of important chemical species can be facilitated, for example for O_2 by the presence of Hb or for CO_2 by the presence of carboanhydrase. But the properties of diffusion and solubility, determined by atomic and molecular sizes as well as the physicochemical properties of water such as density, viscosity, and heat capacity, are factors that biology can do nothing about; i.e., there is no way to control them. Thus, the dimensions of the terminal branch (and of its contents) are apparently given. Indeed, the diameter of red blood cells in the elephant ($9.2\,[\mu\mathrm{m}]$), man ($7.5\,[\mu\mathrm{m}]$), and mouse ($6.6\,[\mu\mathrm{m}]$) are not that different. Blood HB concentration, red cell size, hematocrit, plasma protein concentration, plasma viscosity, blood viscosity, colloid osmotic pressure, and — most important — blood pressure are scale independent, even though these properties are under biological control. There are some variations among species, but there is no general relationship to body size.

4.3 The Venous System

The venous system closes the loop for the circulation of the blood. Often it is just viewed as that, and more attention is given to the heart and the arterial side of the circulation, because these are providing the important vital signs such as the arterial pressure and pulse. In the closed-loop configuration, what the heart pumps into the arterial limb, as cardiac output, eventually has to return to the heart through the venous limb as so-called venous return. It is this inherent circularity which poses a considerable problem in the understanding of cardiovascular regulation. Because stroke volume and cardiac output increase with diastolic filling, it is often erroneously assumed that venous return (a flow) drives cardiac output. The problem with venous return (when interpreted as a flow), as a cause of cardiac output, is that such a system is inherently unstable due to positive feedback (Reddi and Carpenter, 2005). Venous return drives cardiac output, which will increase venous return because in the end, what flows out from the heart has to come back. The concept of venous return is fraught with misunderstandings (Figure 4.1).

It is one of the many achievements of Guyton and coworkers to have addressed this problem. They analyzed the mechanical coupling between the heart and the peripheral vasculature by cutting the loop and looking at each subsystem independently in a first step, and then, in a second step, by combing the subsystems, providing the steady state operation of the closed system (Guyton, 1955).

The function of the two subsystems is described by cardiac output curves for the heart, and by venous return curves for the vasculature (Figure 4.1). Cardiac output curves (as obtained by Guyton) describe the influence of preload, expressed as right atrial pressure P_{ra}, on cardiac output under conditions of fixed heart rate, afterload, and contractility. Cardiac output curves are obtained in the open-loop configuration; i.e., P_{ra} is independent of how the pressures in the vasculature are affected by the resultant cardiac output, because the loop is cut. Venous return curves describe the influence of blood flow, expressed as venous return, on P_{ra} under conditions of fixed vascular resistance and compliance, and under constant blood volume. Venous return curves are also obtained in the open-loop configuration; i.e., venous return is independent of how cardiac output is affected by changes in P_{ra}. A detailed discussion of the classic experiments that led to the venous return curves, together with a discussion of important dynamic effects, is presented by Brengelmann (2003). Notice the relationship between cause and effect. Flow (venous return) is the cause (input) and pressure P_{ra} is the effect (output) in the venous return curve, while flow (cardiac output) is the effect (output) and pressure P_{ra} is the cause (input) in the cardiac output curve. The cause-effect or input-output relationship of such systems is usually described by plotting the independent variable (input, cause) on the x-axis, and the dependent variable (output, effect) on the y-axis of an (x, y)-plot. Thus, for the cardiac output curve, P_{ra} is plotted on the x-axis and cardiac output is plotted on the y-axis. When the venous return curve is plotted with regard to cause and effect, or independent and dependent variables, P_{ra} must be plotted on the y-axis, while venous return is plotted on the x-axis. In fact this is the representation adopted by Levy's vascular function curves (Levy, 1979).

As described by Guyton, the intersection of the cardiac output and venous curves gives the steady state cardiac output and P_{ra} for the closed-loop systems (see Figure 4.1). However, when both dependent and independent variables are plotted on the proper y- and x-axes, the representations for cardiac output and vascular function curves cannot be

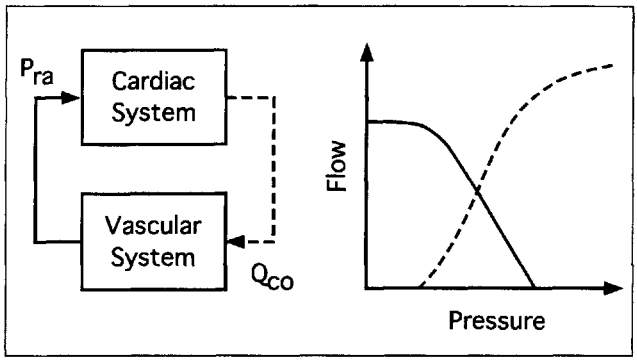

Figure 4.1: The cardiovascular system as interaction of two subsystems, the cardiac and vascular systems, acting on each other through cardiac output Q_{co} and right atrial pressure P_{ra} (left panel). The intersection of cardiac output (broken line) and venous return (full line) curves gives the steady state cardiac output.

combined, because the measures for pressure and flow to be combined are located on different axes. Therefore, the axes are exchanged for one of the relationships, which is then plotted in reverse "causality". Thus, whenever two systems interact in a negative feedback connection, like the interaction between the heart and the vasculature in this case, an (x, y)-plot that overlays their separate open-loop input-output properties, necessarily shows one of the systems plotted backwards.

In the interaction between the heart and the vasculature, this is done for the representation of the venous return curve, so that P_{ra} is plotted on the x-axis, and venous return is plotted on the y-axis (Figure 4.1), even though P_{ra} is the dependent variable. This is contrary to the customary representation of dependent and independent variables and it is the source of considerable confusion when reading the well-known combined cardiac output and venous return curves. Even if mathematically correct (and trivial), the change in representation of dependent and independent variables eventually leads to a mix-up of cause and effect (Brengelmann, 2003). But ultimately, it is the result of the circulation's intrinsic circularity which is liable to confound cause and effect. On the other hand, it also has been questioned whether the terms dependent and independent variable have a practical meaning in the closed-loop of the circulation (Rothe, 1993).

The reversed graphic evokes the misleading idea that in the vascular subdivision of the cardiovascular system, P_{ra} somehow determines venous return (Figure 4.1). It is true that a given level of P_{ra} (over the sloped segment) is uniquely associated with a corresponding level of flow, but it is not the cause, it is the effect. A frequent misinterpretation of the venous return curves is to mistake P_{ra} as a "back pressure," with the conclusion that increasing P_{ra} to the level of the mean systemic filling pressure $\approx$ 7 [mmHg] would stop venous return. Another misconception based on the picture of "back pressure," for example, is that reduced cardiac output, secondary to HF, is responsible for fluid accumulation in the interstitial space. In fact, it is the rise in venous and capillary pressures, resulting from decreased cardiac performance, that cause the various clinical symptoms such as prominent venous (jugular) pressure pulse, difficult breathing in the supine position, and

swollen feet. Also, trying to increase venous return by lowering P_{ra} will lead to serious complications.

As mentioned above, venous return curves are determined by vascular compliance, resistance, and blood volume. These are key characteristics of the venous system and are discussed in greater detail in the following sections.

4.4 Capacitance

In the arterial system, pressure is determined by flow and resistance. In the venous system, pressure is essentially determined by volume and vessel distensibility. The volume-pressure characteristics of the venous system provide a means to maintain and control pressure locally and globally, independently of flow, by passive and active mechanisms.

4.4.1 Passive mechanisms

The description of distensibility of the vascular system, in the various sections of the vascular tree, and of individual organs abounds with ambiguous, synonymous, and sometimes contradictory terms, depending on the aims and preferences of the authors. Since the emphasis here is on volume, the reservoir characteristics of blood vessels will be described in the volume-pressure diagram, where the volume V is the dependent variable plotted on the y-axis, and the distending pressure P is the independent variable plotted on the x-axis (Figure 4.2). The distending pressure, also known as transmural pressure P_t, refers to the pressure difference between the inside and the outside of the vessel. Volume changes caused by a change in transmural pressure can be considered as primarily passive. In this diagram, the volume-to-pressure relationship typically shows a nonzero, positive intercept at zero transmural pressure. As transmural pressure increases, volume also increases with a typical slope $\Delta V/\Delta P$ because of the distension and deformation of the vascular wall,

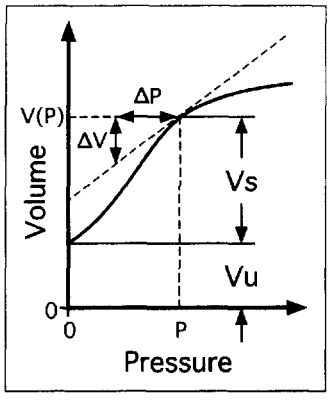

Figure 4.2: Volume-to-pressure relationship in a distensible vessel.

Compartment	V_u [ml]	c [ml mmHg^{-1}]
Right ventricle	50	1.2–20
Pulmonary arteries	90	4.3
Pulmonary veins	490	8.4
Left ventricle	50	0.4–10
Systemic arteries	715	2
Upper body systemic veins	650	8
Kidney veins	150	15
Splanchnic veins	1300	55
Lower limb veins	350	19
Abdominal veins	250	25
Inferior vena cava	75	2
Superior vena cava	10	19
Whole body	4180	217

Table 4.1: Volumes and compliances for a 71 to 75 [kg] normal male subject with an assumed total blood volume of $V_b = 5700$ [ml] (Heldt et al., 2002). Whole body compliance is calculated from $V_s = V_b - 4180$ [ml] and a mean circulatory filling pressure $P_{mcf} = 7$ [mmHg]. Notice that unstressed volume V_u and compliance c scale with body mass.

so that the vessel segment accommodates more volume. As pressure continues to rise, the steepness of the slope changes and the volume-to-pressure relationship flattens out before the vessel finally ruptures. The characteristics of this curve, a nonzero intercept and a nonlinear increase in volume as pressure increases, is typical for veins, individual organs, and arteries. The magnitudes for the intercepts and the slopes, however, vary in different sections of the cardiovascular system (Table 4.1). For different organs (arteries, veins, individual organs), one can make the simplifying assumption that the slope is constant within the operating range of individual physiological pressures. The volume-to-pressure relationship is characterized by important terms and parameters such as capacitance $V(P)$, stressed and unstressed volumes V_s, V_u, and compliance $c(P)$, as depicted in Figure 4.2.

Capacitance

Capacitance $V(P)$ relates to the overall volume of blood contained within a vessel, but it has only a precise meaning when the distending pressure P leading to this volume is known. The capacitance of a system is therefore described by the volume-to-pressure relationship, which results in its typical capacitance curve (see Figure 4.2 and equation (4.3)).

Compliance

The compliance at a given pressure ($c(P)$ [liter mmHg^{-1}]) is the slope of the capacitance curve,

$$c(P) = \frac{\Delta V}{\Delta P}.$$

As the capacitance curve is nonlinear, steep at low pressures and flatter at higher pressures, the compliance decreases as distending pressure increases.

Unstressed volume

Unstressed volume (V_u, in liters) is defined as the volume contained in the vessel at zero distending pressure, and refers to the intercept in the volume-to-pressure relationship discussed above (Figure 4.2). Unstressed volume is of special importance in the venous system. Usually, venous unstressed volume is not directly measured, but estimated by linear back-extrapolation of the volume-to-pressure relationship to zero pressure, as shown in Figure 4.2. This gives a reasonable estimate over the physiological pressure range (5–20 [mmHg]) for most tissues.

Stressed volume

Stressed volume is the additional volume in excess of V_u that causes a positive transmural distending pressure. It is computed as the mean filling pressure times compliance, assuming a linear relationship between the volume at zero pressure V_u and the volume at the distending pressure P.

To summarize, capacitance refers to the overall volume of blood contained within a vessel, whereas compliance, unstressed volume, and stressed volume are subsets of this total volume with specific meanings. Therefore, the volume of a vascular segment or organ cannot be completely described with a single number. Stressed and unstressed volumes are important conceptual volumes to understand the role of veins in circulatory control.

Over the physiological range of distending pressures, where the capacitance curve can be assumed as linear and compliance, therefore, can be assumed as constant, at least two parameters are needed to describe the volume of a vascular segment or organ according to the following relationship:

$$V(P) = c(P)P + V_u. \tag{4.3}$$

Capacitance at a given pressure is the sum of stressed and unstressed volumes. Passive changes refer to a change in vessel volume caused by a change in pressure.

Specific entities

With regard to issues of biological similarity and since blood volume scales with body mass, one can assume that capacitance and stressed and unstressed volumes also scale with body mass. Furthermore, since pressure is scale independent, compliance ($c = V/P$) can be assumed to scale like a volume, i.e., with body mass. Capacitance, volume, and compliance are, therefore, normalized to mass to provide specific capacitance [ml kg^{-1}], specific volume [ml kg^{-1}], and specific compliance [ml $mmHg^{-1}$ kg^{-1}], respectively, so that these characteristics can be compared between individuals. The same approach is also used to compare specific volumes and specific compliances of different vascular segments or organs. For consistency of units, it would be better to normalize for volume, however, since density of tissues is close to unity, and since weighing is easier and more accurate than measuring volume, these entities are usually normalized to organ mass.

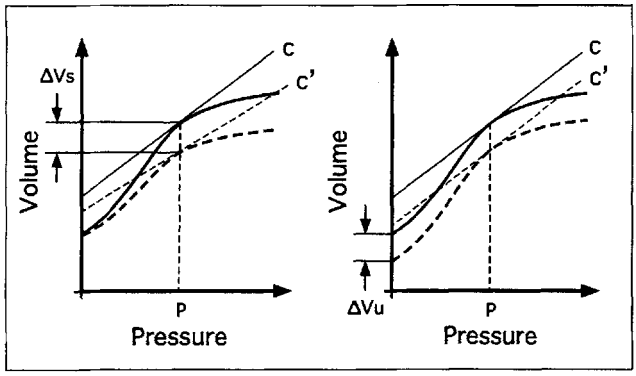

Figure 4.3: Active changes in vessel volume. An active change in volume is realized by a change ΔV_s in stressed volume caused by a change in compliance ($c \neq c'$) (left panel). An active change in volume is also realized by a change ΔV_u in unstressed volume at constant compliance ($c = c'$) (right panel).

4.4.2 Active mechanisms

Active change refers to a change in vessel volume without a change in pressure. Active volume changes are caused by active constriction or dilatation of the vessel wall, thereby changing the characteristics and the shape of the capacitance curve (Figure 4.3). As the idealized capacitance curve is characterized by the intercept V_u and the slope c, the capacitance curve can actively be changed by either changing V_u, c, or both in (4.3). First, assume that unstressed volume remains constant while stressed volume changes ($c \nrightarrow c'$) (Figure 4.3, left panel). This will cause an active volume change at constant pressure. Active changes are often misunderstood as being exclusively caused by changes in compliance. But a second mechanism is also possible. A change ΔV_u in unstressed volume causes a parallel shift in the capacitance curve without a change in compliance ($c = c'$) (Figure 4.3, right panel), resulting also in an active volume change, now at constant pressure as well as at constant compliance. Thus, volume can be mobilized at constant pressure by independent as well as by combined reductions in stressed and unstressed volumes.

With this feature, the venous vessels function as an almost ideal reservoir, where a change in volume will neither affect the pressure nor the compliance of the container. Note that the presence or absence of active vasoconstriction cannot be assessed from a change in compliance alone, and that the measurement of compliance or venous tone is not sufficient to assess venous capacitance.

4.4.3 Flow effects

The resistance to blood flow is much smaller in the venous system than in the arterial system, and the contribution of venous resistance to peripheral resistance is therefore small and often neglected. Venous resistance, however, still has an influence on venous capacitance and on regional distribution of blood volume, and for that reason venous resistance plays an important role in overall cardiovascular control. A detailed summary of the effects of

blood flow on venous capacitance has been given by Rowell (1986). The effects of venous blood flow and resistance on vascular capacitance and stressed and unstressed volumes are described in the following.

Assume the following idealized situation with a blood vessel of unit length beginning at $L = 0$ and ending at $L = 1$, radius $r = 1$, perfused at unit flow $Q = 1$ by a Newtonian fluid with unit viscosity $\eta = 1$. Pressure, given as a function of vessel length $P(L)$, is zero and constant at the vessel outflow ($P(1) = 0$). The relationships between pressure, radius, flow, resistance R, and compliance c can be modeled as follows:

$$\frac{dP}{dL} = R(L)Q,$$
$$\frac{dr}{dL} = \sqrt{\frac{R(L)cQ}{\pi}},$$

where

$$R(L) = \frac{8\eta}{r(L)^4\pi}$$

is the resistance of the vessel per unit length, as determined by the Hagen–Poiseuille law. If the vessel is noncompliant ($c = 0$), the radius is constant over the length of the vessel and the pressure drop is linear. In the special case where the outflow pressure is zero ($P(1) = 0$), the inflow pressure assumes a positive inflow pressure calculated as $P(0) \approx 2.55$ (Figure 4.4).

Now assume that the vessel is compliant ($c = 1$), and that the compliance is constant over the vessel length. The positive inflow pressure, required to drive the same flow, will distend the radius in upstream parts of the vessel. This distension falls as the pressure drops from the inflow ($L = 0$) to the outflow ($L = 1$) of the vessel. At the vessel outflow, the radius attains the undistended value because $P(1) = 0$.

As a small increase in vessel diameter greatly reduces flow resistance ($R = k/r^4$ for some constant k), the inflow pressure for a blood vessel, with a compliance $c = 1$, is now only $P(0) = 1.00$, compared to $P(0) = 2.55$ for the noncompliant vessel. It goes without saying that the capacitance of the vessel increases when the vessel becomes compliant. This discussion illustrates that, for a given flow, less pressure is needed to drive that flow in a compliant vessel due to the drop in resistance. This concomitant drop in pressure gradient as a result of the increase in compliance, however, is less intuitive.

In this example, the increase in compliance leads to an increase in capacitance. As compliance increases from $c = 0$ to $c = 1$, and while vessel inflow pressure $P(0)$ decreases from 2.55 to 1.00, total vessel capacitance increases from 3.14 to 5.48 (Figure 4.5, right panel).

Next, assume a decrease in flow with $c = 1$ under the condition that outflow pressure ($P(1) = 0$) remains unchanged, such as in a vessel opening to the ambient atmospheric pressure. If flow is reduced from $Q = 1$ to $Q = 0$, inflow pressure decreases from $P(0) = 1$ to $P(0) = 0$, and at the same time the capacitance of the vessel decreases from $V = 5.48$ to 3.14 because of this pressure drop (Figure 4.5, left panel). Notice that this change in volume is passive, does not change outflow pressure, and occurs without a change in compliance. This volume reduction in the compliant vessel, under these conditions of constant compliance and constant outflow pressure (not accounting for pressure distributed

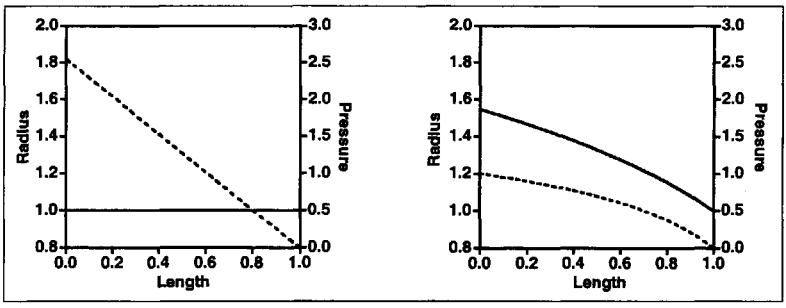

Figure 4.4: Resistance and compliance. Radius (full line) and pressure (broken line) in a noncompliant (left panel) and compliant tube (right panel) vs. tube length.

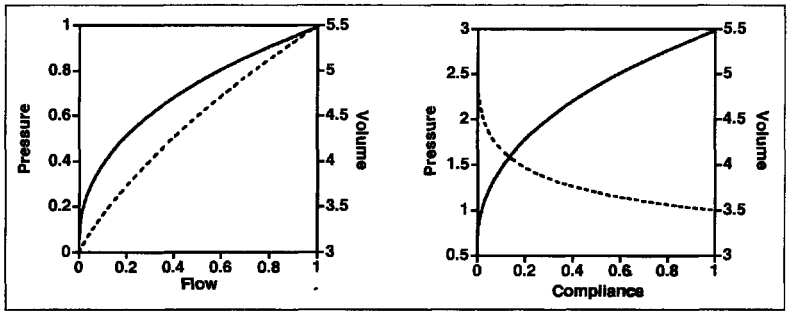

Figure 4.5: Flow effects on compliance. Inflow pressure (full line) and tube capacitance (broken line) as functions of flow (left panel) and tube compliance (right panel).

along the vessel), will thus appear to be a reduction in unstressed volume as defined above, where in fact it is stressed volume. Thus, in compartmental models where only a single pressure is given, the distinction between stressed and unstressed volumes can be obscured.

For cardiovascular control, it is important to recognize that venous capacitance passively reacts to the inflow of blood, which is determined by the arterial side of the vascular system. Regional venous capacitance is, therefore, importantly determined by arterial vasoconstriction or vasodilatation to different vascular beds. The magnitude of this effect, however, depends on venous compliance, which is especially high for the circulation of the skin (cutaneous) and that of the gastrointestinal (splanchnic) system. These circulations therefore play an important role in blood volume and blood pressure control.

When vessel volume is plotted against inflow pressure under variable flow conditions, the graph obtained very much resembles the volume-to-pressure relationship obtained under zero flow conditions, as depicted in Figure 4.6. In the absence of flow, the slope determined from the volume-to-pressure curve is defined as compliance (see above). In the presence of flow, however, the slope refers to an apparent compliance, since compliance was defined as $c = 1$ in the assumptions above and not changed for this thought experiment. This example points out the difficulties of compliance measurements and the

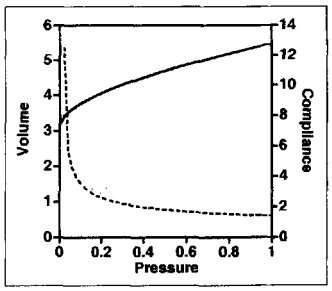

Figure 4.6: Apparent compliance. Volume-to-pressure diagram under variable flow conditions with capacitance (full line) and apparent compliance (broken line) curve. Data taken from simulations shown in Figure 4.5.

interpretation of V/P data. A change in flow causes passive changes in volume, which present as changes in compliance. When pressure is not measured at the outflow, but at some other level of the vessel, one can obtain volume-to-pressure curves as those shown in Figure 4.6. Therefore, in theory, the measurement of true compliance is only possible under static conditions.

4.4.4 Modeling and measurement

The relationships between flow, resistance, and capacitance document the necessity for distributed models to capture the effects of vascular pressure distribution on venous capacitance. As the circulation is often modeled by equivalent electric circuits, where flow corresponds to current, flow resistance corresponds to electrical resistance, and pressure corresponds to voltage, vascular capacitance is modeled by an electrical capacitor. However, when concerned about volume issues, the electrical capacitor is not a good model for vascular capacitance because of unstressed volume, which corresponds to a finite capacity at zero voltage.

The measurement of compliance requires a combined measurement of pressure and volume (or mass) at a sequence of different volumes and pressures. Volume is most easily changed by allowing blood flow to fill or drain the vasculature or the organ under consideration, however, the measurement of pressure and volume must occur under static conditions. Therefore, compliance is more easily measured in isolated organs. In humans, the measurement of venous compliance is limited to the measurement in the limbs, where blood flow can be occluded for short periods of time.

Whether static capacitance, compliance, and unstressed volume measurements can be substituted by dynamic measurements needs to be validated in each case. This was, for example, successfully shown for pig livers, where the infusion of noradrenaline reduced the capacitance (from 10.5 ± 0.6 to 6.9 ± 0.7 [ml kg^{-1}] at 7 [mmHg] pressure) and unstressed volume (from 3.1 ± 1.0 to -0.1 ± 1.2 [ml kg^{-1}]), but compliance remained essentially unchanged at 1.0 ± 0.1 [ml mmHg^{-1} kg^{-1}] whether measured with (dynamic) or without (static) blood flow (Kjekshus et al., 2000).

4.4.5 System of compliances

The vascular system consists of compliant vascular beds in serial and parallel arrangements (Table 4.1). Unlike total peripheral resistance, which depends upon whether vascular beds are connected in series or in parallel, total vascular capacitance is the sum of individual capacitances, independent of the arrangement of vascular beds. Changes in pressure, flow, peripheral resistance, and regional perfusion lead to characteristic changes in the distribution of blood volume as well as to changes in central venous and right arterial pressures. The arterial system, the microcirculation, the small venules, and large veins are connected in series. In the steady state, all segments are perfused by the same blood flow. The closed-loop configuration also implies a constant volume.

4.4.6 Mean circulatory filling pressure

Recall the situation when blood flow decreases in a compliant vascular bed (see Figure 4.5). In the open system, when outflow pressure is maintained at a constant level, capacitance decreases and unstressed volume is mobilized. In the closed cardiovascular system, however, without a change in volume, a stop in blood flow causes pressures to equilibrate throughout the vascular bed, albeit at a higher value than the initial outflow pressure. In the closed cardiovascular system, some blood will flow from the arterial side, where the pressure is high, to the venous side, where the pressure is low, until pressures equilibrate. The resulting pressure is called the mean circulatory filling pressure P_{mcf}. It is defined as the pressure that would be measured throughout the circulatory system at zero blood flow after all the blood has redistributed, according to the compliances of the vascular segments. For average man, mean circulatory filling pressure is about 7 [mmHg].

At zero flow, the blood volume is distributed depending on regional compliances, which are highest in the venous system. Most of the blood volume is, therefore, located in the venous part of the circulation. Since only stressed volume V_s can contribute to pressure, the mean filling pressure at zero flow of the model, shown in Figure 4.7, is given as

$$P_{\text{mcf}} = \frac{V_{\text{as}} + V_{\text{ps}} + V_{\text{vs}} + V_{\text{rs}}}{c_{\text{as}} + c_{\text{ps}} + c_{\text{vs}} + c_{\text{ra}}}. \tag{4.4}$$

As blood flow Q_{co} through the system begins, the pressures change because of flow resistance, as determined by the equivalent of Ohm's law,

$$P_{\text{as}} = Q_{\text{co}}(R_{\text{as}} + R_{\text{ps}} + R_{\text{vs}}) + P_{\text{ra}}, \tag{4.5}$$

$$P_{\text{ps}} = Q_{\text{co}}(R_{\text{ps}} + R_{\text{vs}}) + P_{\text{ra}}, \tag{4.6}$$

$$P_{\text{vs}} = Q_{\text{co}}R_{\text{vs}} + P_{\text{ra}}. \tag{4.7}$$

Since $V_s = cP$, insertion of (4.5), (4.6), and (4.7) into (4.4) and rearranging for P_{ra} give a relationship for the right atrial pressure as a function of cardiac output and the serial arrangement of compliances and resistances,

$$P_{\text{ra}} = -Q_{\text{co}} \frac{\left(c_{\text{vs}}R_{\text{vs}} + c_{\text{ps}}(R_{\text{ps}} + R_{\text{vs}}) + c_{\text{as}}(R_{\text{as}} + R_{\text{ps}} + R_{\text{vs}})\right)}{c_{\text{as}} + c_{\text{ps}} + c_{\text{vs}} + c_{\text{ra}}} + P_{\text{mcf}}. \tag{4.8}$$

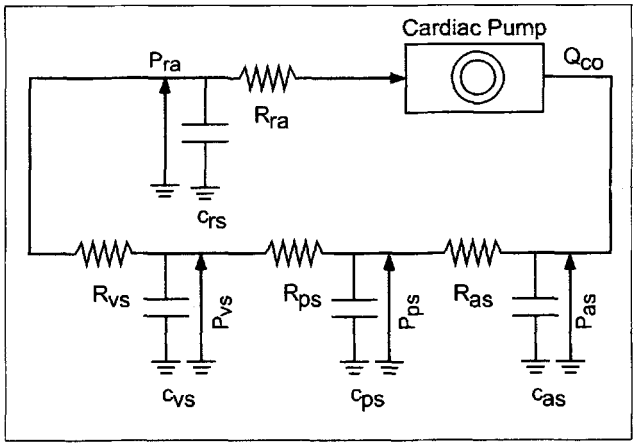

Figure 4.7: Serial arrangement of arterial, peripheral, venous, and right atrial resistances and compliances of the systemic circulation.

This is the venous return curve in the proper cause and effect relationship, describing right atrial pressure as a function of blood flow (also see Figure 4.9). When blood flow is plotted on the x-axis, and right atrial pressure is plotted on the y-axis of an (x, y)-plot, the intercept of (4.8) is determined by mean circulatory filling pressure, as described in (4.4), and the slope of (4.8) is determined by the combined effect of compliances and resistances. A change in compliance, therefore, does affect both the slope and the intercept of (4.8), whereas a change in stressed volume leads to an isolated change in P_{mcf} in (4.4), and to a parallel shift in the venous return curve (Figure 4.8). Notice that this parallel shift is caused by a change in stressed volume, which is not to be mistaken for a change in the whole blood volume. A change in unstressed volume will not have any effect on the venous return curve. A change in resistance leads to an isolated change in the slope of the venous return curve. The increase in arterial pressures causes an increase in arterial volume which, because of the constant volume requirement, is accompanied by a decrease in venous volume (Figure 4.9). The concomitant fall in venous pressure contributes to the decrease in venous volume. Thus, there is a volume shift from the venous side to the arterial side of the circulation. The volume shift is passive and, in the example presented here, this shift is of the order of 50 [ml]. The volume shift is thought to importantly contribute to the negative feedback control of cardiac output (Brengelmann, 2003; Reddi and Carpenter, 2005).

4.4.7 Parallel arrangement

The different regional circulations such as the myocardial, renal, muscular, cutaneous, and splanchnic circulations are arranged in parallel circuits. While this does not influence mean filling pressure at zero flow, changes in regional resistance, perfusion, and pressure have important effects on outflow pressure and volume.

When the vessel opens into a compliant ventricle, the condition of zero and constant outflow pressure is no longer maintained. However, mobilization of venous volume

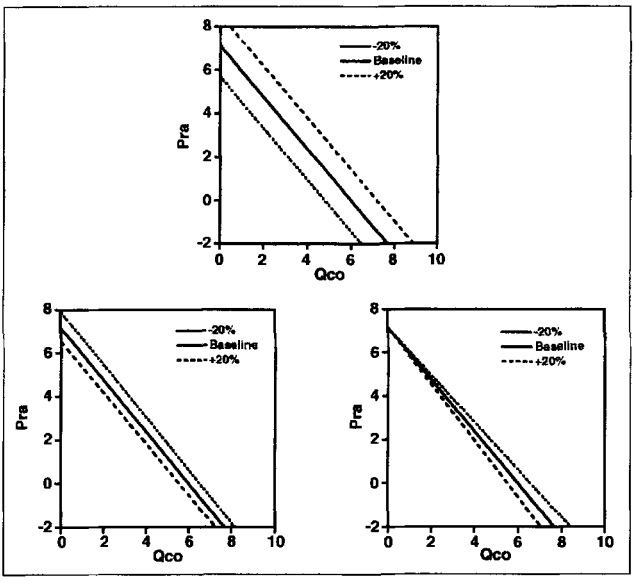

Figure 4.8: Venous return curves as derived from (4.8). Dependence of right atrial pressure P_{ra} (in mmHg) on flow through the vascular system Q_{co} (in liter min^{-1}) with a change in venous stressed volume V_{vs} (top panel), a change in venous systemic compliance c_{vs} (lower left panel), and a change in venous systemic resistance R_{vs} (lower right panel) (also see Figure 4.1).

by mechanisms discussed above leads to an increase in right atrial pressure P_{ra}, thereby supporting diastolic filling.

When blood flow resumes from the idealized no-flow condition, arterial pressure increases from 7 to 100 [mmHg], and hence, with a given arterial compliance, there is a measurable increase in arterial capacitance. On the other hand, central venous pressure decreases from 7 to 2 [mmHg], which therefore leads to a decrease in venous capacitance. Thus, there is a shift of blood volume from the venous to the arterial side of the circulation whenever blood flow increases at the same peripheral resistance.

4.5 Blood Volume

From the hemodynamic point of view, blood volume is largely inhomogeneous. Blood volume is reported to be distributed within the circulation approximately as 15% in the aorta, systemic arteries, and arterioles, 69% in the capillaries, venules and systemic veins, 9% in the pulmonary circulation, and 7% in the heart (Guyton, 1991b).

When viewed as a tissue, blood is macroscopically homogeneous. Microscopically, blood is inhomogeneous and consists of two phases, a continuous phase, termed plasma, and a discontinuous phase, the blood cells which are suspended in the plasma. Strictly speaking, the cell phase in itself is heterogeneous as it contains red blood cells, white blood cells, and platelets. But by far the most important cell fraction, especially with regard to volume, are the red blood cells (RBC). The blood volume V_b is then the sum of

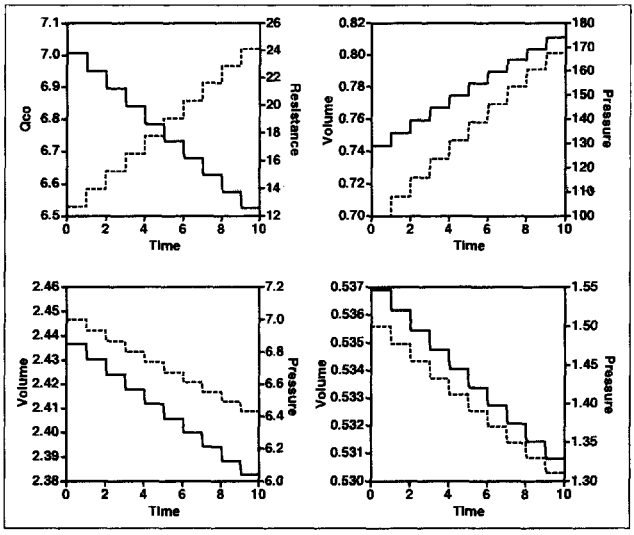

Figure 4.9: Serial arrangement of resistances and compliances. Passive effect of a stepwise 10% increase in peripheral systemic resistance R_{ps} (broken line), on vascular blood flow (full line, left upper panel) as well as on arterial (right upper panel), venous (lower left panel), and right atrial (right lower panel) volumes (full lines) and pressures (broken lines) for the model shown in Figure 4.7.

the plasma volume V_{pl} and the volume of all red blood cells V_{RBC}. The fractional blood volume occupied by RBC, i.e., the volume concentration of RBC, is termed hematocrit, C_{hct},

$$C_{hct} = \frac{V_{RBC}}{V_b} = \frac{V_{RBC}}{V_{pl} + V_{RBC}}. \tag{4.9}$$

The normal hematocrit in a blood sample taken from a peripheral vein is in the range of 45% of the total volume, although somewhat smaller in women than in men, and somewhat smaller in endurance trained subjects. Thus, there is an almost equal contribution of both cellular and noncellular components to total blood volume. With regard to blood flow and blood flow resistance, the rheologic effect of the RBC is much more important than the rheologic effect of the plasma. The situation is also complicated because the contribution of RBC to whole blood rheological properties depends on flow conditions such as shear rates and vessel dimensions (Cokelet, 1986). Thus, with regard to blood volume and blood flow, blood consists of two major components which are regulated by different means.

4.5.1 Characteristic times

One approach to separate the different aspects of blood volume regulation is based on differences in characteristic times for changes of specific components. For example, the turnover of the whole RBC population is in the range of 1% per day. Regulation of the RBC compartment through generation (erythropoiesis) or removal of RBC, therefore, can be considered as a long-term process. Similar considerations apply to albumin, the most

important plasma protein which has, among many other functions, a major influence on colloid osmotic pressure and on fluid exchange in the microcirculation.[10] However, the exchange of fluid volume between the blood and the extravascular compartment is about eight times the whole plasma volume per day. And finally, the formation of urine ranges from one fifth to three times the whole plasma volume per day. The regulation of the plasma compartment, therefore, involves much shorter time constants.

4.5.2 RBC

The kidney plays a major role in both long- and short-term regulation of blood volume, and hence in control of blood pressure. This has been studied extensively through the regulation of the plasma component. It is also well known that erythropoietin, the hormone stimulating RBC production and thereby regulating the RBC component of blood volume, is almost exclusively produced in the kidney. But the link between the regulation of the two components has remained unclear. Tissue hypoxia, whether caused by low blood volume, low Hb concentration, low blood flow, or low oxygenation, stimulates the release of erythropoietin from specialized fibroblasts (cells) located in the renal cortex. The action of this hormone increases the RBC count and the O_2 carrying capacity of blood within days, thereby correcting tissue hypoxia. Until recently, RBC regulation was focused on hypoxia overlooking effects on volume. It also appeared unexplainable why the sensor for long-term O_2 control was located in the kidney, given that other tissues such as heart and brain are more susceptible to hypoxia. Furthermore, kidney blood flow is exceptionally high (25% of cardiac output for less than 0.5% of body mass), whereas O_2 extraction and arteriovenous O_2 difference are exceptionally low (7% and 0.6 [mmol liter^{-1}]). It is now hypothesized that the volume of the RBC compartment (which is controlled by erythropoietin) has an important effect on renal perfusion. Since the perfusion is linked to glomerular[11] filtration, tubular[12] reabsorption, and tubular O_2 consumption, which all regulate plasma volume, the regulation of RBC volume is somehow linked to the regulation of plasma volume. The quantitative relationships for this control have not been established, but there is considerable clinical evidence for a close link between plasma and RBC volume regulation. The kidney apparently adjusts for an optimal partition between the two important blood components, and has therefore been termed as a "hematocrit meter" (Donnelly, 2001).

With regard to short-term regulation, total RBC count as well as total intravascular albumin mass may be considered as constant. Within the bounds of normal plasma osmolality (310 [mosmol kg^{-1}]), this assumption may be extended to RBC volume. A change in osmolality, however, affects RBC volume. An increase in plasma sodium concentration and osmolality, for example, induced by sweating, causes small but measurable shifts of fluid from the RBC to the plasma, thereby reducing total RBC volume. Alternately, a decrease in plasma osmolality, induced by drinking, causes osmotic swelling and increases RBC volume, even if RBC count remains constant. The magnitude of osmotic fluid shifts between RBC and plasma is limited, but osmotic shifts occur very rapidly and have to be considered

[10] Microcirculation is that part of the cardiovascular system between arteries and veins designed for exchange of fluid, solutes, and cells.

[11] Glomerulus is the structure in the kidney where the primary filtrate is obtained from filtration of plasma.

[12] Tubulus is the structure in the kidney processing the primary filtrate through controlled reabsorption and secretion of fluid and solutes, finally leading to the formation of urine.

when investigating short-term effects of volume regulation, for example, through the measurement of hematocrit.

4.5.3 Plasma

Short-term effects of blood volume regulation are confined to the plasma component, however, the whole blood volume is affected because plasma is one of the components of blood volume. Also, volume sensing occurs via the pressure exerted by the whole blood volume, so that the contribution of the RBC component must not be ignored. But the regulation of plasma volume is not limited to short-term effects, it covers a much wider range of physiological times, from the long-term range down to characteristic times of a few minutes.

4.5.4 Microvascular filtration

Short-term regulation essentially acts through the exchange of fluid volume with the extravascular compartment in the microcirculation. The distribution of water between the plasma (and the blood) and the extravascular compartment is governed by pressure gradients acting across the capillary wall, the permeability, and the area of the capillary wall, as described by the Starling hypothesis. Filtration Q_{fil} or reabsorption of fluid across the capillary wall is proportional to the effective filtration pressure P_{eff} gradient, which results from the difference in hydrostatic and oncotic (colloid-osmotic) pressure gradients, determined by four pressures: capillary hydrostatic P_{cap}, capillary oncotic Π_{cap}, tissue hydrostatic P_{tis}, and tissue oncotic Π_{tis},

$$Q_{\text{fil}} = K_{\text{fil}}\big((P_{\text{cap}} - P_{\text{tis}}) - (\Pi_{\text{cap}} - \Pi_{\text{tis}})\big). \tag{4.10}$$

The filtration coefficient K_{fil} refers to the product of the permeability times surface area of the microvascular wall and varies for different organs. Colloid osmotic pressures can be directly measured for plasma or calculated from protein concentration using the Landis–Pappenheimer equation (Landis and Pappenheimer, 1963).

The filtrate exchanged in the microcirculation, also known as ultrafiltrate, is cell free and protein poor. There is, however, a graded leak of protein, especially of albumin, into the extravascular space contributing to tissue oncotic pressure. The tightness of the microvascular barrier with regard to both albumin and water varies for different vascular beds. While the microcirculation in the splanchnic circulation is rather leaky for albumin, the renal glomerulus is highly permeable for water but almost impermeable for protein.

4.5.5 Volume regulation

Mid- to long-term plasma and blood volume regulation involves regulation against volume loss and volume gain. Since volume is not lost or gained as "pure volume," but in a combination of water and salt (NaCl), volume regulation is largely based on the regulation of these two components. Very detailed information on volume regulation is found in the textbook of Guyton (Guyton, 1991a).

Defense against volume loss

The defense against volume loss utilizes two strategies, reducing fluid and salt output on one hand, and stimulating fluid and salt intake through thirst and cravings for salt, so-called

salt appetite on the other hand. These strategies take two different pathways, using sensors located in the low- and high-pressure part of the cardiovascular system. A decrease in central venous pressure, secondary to volume loss, is sensed by central low-pressure sensors and communicated to the hypothalamus via vagal afferents to release antidiuretic hormone (ADH), (also known as arginine-vasopressin) from the posterior pituitary, and, concomitantly, to stimulate thirst and salt cravings. A decrease in arterial pressure is sensed by renal sensors to release renin from juxtaglomerular cells which, through intermediate steps, leads to the formation of angiotensin-II (Ang-II), and furthermore, to the release of aldosterone (see also Figure 3.3 and discussion on page 112 ff.). The whole sequence of steps is called the renin-angiotensin-aldosterone system (RAAS). Ang-II, among its many functions such as increasing peripheral resistance, reducing baroreflex sensitivity, and increasing sympathetic tone, also stimulates thirst. While ADH reduces renal water output and aldosterone reduces renal Na^+ output, a correction of the volume loss is only possible by replacing the combined volume and salt losses. Thirst stimulated by a loss in blood volume is also known as hypovolemic thirst. Since volume is usually lost with electrolytes, a replacement of volume loss by drinking water alone is inadequate. Therefore, full correction of volume homeostasis requires also the replacement of Na^+ loss, which is communicated through salt appetite. The final adjustment to balance salt and water uptake is done by osmoregulation, stimulating ADH release and osmotic thirst. Osmoregulation controls the input and output of water. Volume regulation controls the input and output of salt.

Defense against volume excess

The defense against volume excess is based on increased renal excretion of water and salt, also known as diuresis and natriuresis. This strategy may take three major pathways. An increase in volume stimulates the release of atrial natriuretic peptide (ANP) from the right atrium. ANP increases the filtration coefficient K_{fil} in (4.10) in the microcirculation. In the kidney, ANP increases glomerular filtration and reduces tubular reabsorption of sodium, thereby increasing the excretion of sodium (natriuresis) and volume (diuresis). Atrial stretch also inhibits the release of ADH, thereby increasing urinary flow through the so-called Gauer–Henry reflex. The third pathway, however, is assumed to be purely mechanical. Based on the observation that blood volume remains more or less constant despite a tremendous variation in the daily intake of water (from half a liter up to almost 10 liters without disruption of water homeostasis) and electrolytes (from 10 to 100 mmols), Guyton assumed that by far the most important basis for volume regulation is a purely mechanical mechanism, namely that increased arterial pressure greatly increases fluid volume output by the kidneys (Figure 4.10, top left panel). Increased salt output occurs along with diuresis. Guyton refers to these mechanical mechanisms as "pressure diuresis" and "pressure natriuresis" (Guyton, 1991a).

Pressure natriuresis revisited

While the mechanical concept of pressure diuresis and natriuresis has governed the thinking and understanding of volume regulation and pressure control for the past 35 years, and has tremendously contributed to the understanding of hypertension (Guyton and Coleman, 1969), there is a growing evidence that within the limits of normal physiological control, the role of pressure natriuresis needs to be revisited. For example, diurnal patterns

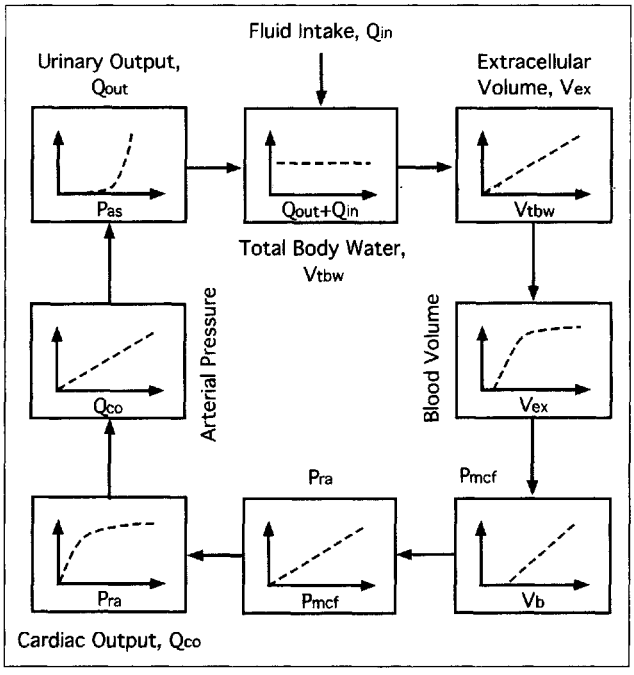

Figure 4.10: The body fluid and pressure balance system in a single control loop form, adapted from (Guyton and Coleman, 1969), with the concept of "pressure diuresis" shown in the left top panel.

reveal that changes in pressure are not accompanied by similar changes in urine volume and urine sodium, as one would expect from the pressure diuresis concept (Seeliger et al., 2005). Diurnal changes are rather related to sodium and water uptake. The lack of any positive correlation between spontaneous pressure changes, averaged over 20 [min], 1 [h], or 4 [h], and diuresis or natriuresis casts doubts onto a dominating role of pressure diuresis and natriuresis under physiological conditions. Even with sampling periods as short as 1 [min], there was no correlation between spontaneous pressure fluctuations and urine flow in conscious dogs.

Based on the pressure diuresis concept, one would also assume that a sustained reduction in renal perfusion pressure leads to a sustained reduction in diuresis and natriuresis. However, animal experiments done on freely moving dogs show that sodium balance is attained within two days in spite of sustained experimentally controlled reduction in renal perfusion pressures (Seeliger et al., 2005). This disruption between pressure and diuresis has been termed "pressure escape," in analogy to the well-known concept of "mineralcorticoid escape" (Seeliger et al., 2001). Such observations do not fit with an "infinite gain" blood pressure control system, which is meant to return pressure to normal, regardless of the size of the perturbation, by adjusting the excretion of water and salt (Guyton et al., 1972). In fact, many of the animal models of experimental hypertension that are regularly used to investigate the long-term control of blood pressure directly alter renal function either through removal of kidney mass, and/or clipping of the renal artery or through renal

acting hormones such as vasopressin, Ang-II, or aldosterone, document that an infinite gain is in fact absent.

Pressure diuresis and natriuresis is chiefly mediated by inhibition of tubular sodium reabsorption, because both total renal blood flow and glomerular filtration rate are efficiently autoregulated (see also Subsection 3.1.2). The sites for inhibition of tubular reabsorption are assumed to be located in proximal and distal parts of the nephron tubulus. These sites are located in the renal cortex (the outer part of the kidney, the "shell" of the kidney), but because the kidney is an encapsulated organ, an increase in pressure in other parts of the kidney such as the medulla (the core of the kidney), where regional blood flow is poorly autoregulated, will equilibrate throughout the kidney. Preventing the increase in renal interstitial hydrostatic pressure by renal decapsulation indeed blunts, but does not abolish, pressure natriuresis in rats (Garcia-Estan and Roman, 1989). The increase in renal interstitial hydrostatic pressure between 3 and 8 [mmHg] in response to arterial pressure changes from 50 to 90 [mmHg], therefore cannot fully account for the large decrease in tubular sodium reabsorption associated with pressure natriuresis. Another mechanical mechanism, discussed to explain pressure diuresis and natriuresis is based on washout of osmotic gradients by increased medullary blood flow (Selkurt, Womack, and Dailey, 1965). An increase in medullary blood flow, however, results only in slight changes in medullar osmotic gradients. It is also argued, in favor of the pressure diuresis concept, that chronic changes in blood volume caused by nervous or hormonal factors are usually moderate. While short-term changes often are dramatic, long-term changes are usually moderate. This may be true for the experimental situation, but this is not the case in pathological situations such as edema,[13] ascites,[14] and CHF. Pressure natriuresis appears to constitute a compensating mechanism that becomes active only under pathophysiological conditions.

Because of the difficulties relying on purely mechanical mechanisms for the regulation of blood volume, attention is now drawn to humoral and neuronal factors, especially to the RAAS and sympathetic nerve activity (SNA). For example, a 10% increase in renal perfusion pressure induced by saline loading did not contribute to the natriuretic response. Natriuresis was essentially achieved by RAAS suppression (Bie and Sandgaard, 2000). A 20% reduction in renal perfusion pressure caused a decrease of sodium excretion essentially by pressure-driven changes in the RAAS rather than by pressure natriuresis (Seeliger et al., 2005). It therefore appears that a change in renal perfusion pressure does not per se affect sodium excretion, but this effect is mediated by the RAAS. Pressure natriuresis is not an indispensable controller of extracellular volume. Its blockade does not result in ongoing sodium retention as long as the RAAS is operative. Thus, the existence of pressure diuresis and natriuresis is uncertain, at least in conscious dogs, and within the limits of autoregulation of glomerular filtration rate.

On the other hand, in the absence of a change in arterial pressure or glomerular filtration rate, renal sympathetic nerves are the main controllers of renin secretion. It is therefore hypothesized that renal SNA could play a major role in volume regulation (Guild, Barrett, and Malpas, 2005). If renal SNA is the critical signal, what are the main long-term controllers of that signal? One proposal is that hormonal signals, acting via circumventricular organs (where the blood-brain barrier is leaky), may provide an input to the central nervous

[13] Fluid accumulation in the extravascular space.

[14] Fluid accumulation in the peritoneal cavity.

system. There is substantial evidence that Ang-II contributes to the regulation of arterial pressure via actions on several brain sites that regulate the level of SNA. This is not without debate, as the increase in blood pressure caused by Ang-II will lead to baroreflex-mediated sympatho-inhibition. The role of sympathetic tone in volume regulation is very attractive, as increased sympathetic activity is assumed to stand at the beginning of many chronic diseases such as CHF and hypertension.

4.5.6 Volume measurement

Hemodynamic analysis of regional blood volume distribution covering the whole circulation would have a vast field of clinical applications. While current imaging techniques can provide regional blood distribution in different body segments, such measurements are limited to a few specialized investigations (Collins and Padhani, 2004). The measurement of regional blood flow and pressure, together with regional blood volume distribution, is not available at this time. However, because total and regional volumes are related, the measurement of total blood volume is still helpful for many clinical and experimental questions.

The classical measurement of blood volume is based on indicator dilution technique, where a known amount of tracer or indicator m_{ind} is introduced into the system and the concentration of the tracer C_{ind} is measured after complete mixing. The distribution volume of the indicator V_{ind} is then determined as

$$V_{\text{ind}} = \frac{m_{\text{ind}}}{C_{\text{ind}}}.$$

The ideal tracer is nontoxic, stable, easily to be measured, and completely as well as exclusively distributed in the volume or compartment of interest. Real tracers, however, are unstable and distribute incompletely or nonexclusively within the compartment of interest, and it is, therefore, not sufficient to rely on a single concentration measurement. Instead, it is necessary to take serial concentration measurements and to analyze the kinetics, for example, to identify a hypothetical concentration at the time of indicator injection ($C_{\text{ind}}(0)$).

Since blood consists of two major components, the measurement of blood volume requires two tracers, one for the RBC, and one for the plasma (Table 4.2). Classically, RBC volume has been measured using RBC tagged with radioactive isotopes such as ^{51}Cr, nonradiating isotopes such as ^{53}Cr, and dyes such as Sodium Fluorescein (Orth et al., 2001).

The RBC volume is more stable because RBC are confined to the vascular space and because generation and elimination rates are small compared to the duration of the dilution measurement. This is not the case for plasma volume because of significant fluid shifts

	Gender	V [ml m^{-2}]	V [ml kg^{-1}]
RBC	f	845 ± 56	24.0 ± 1.5
RBC	m	1108 ± 90	29.1 ± 2.7
Plasma	f	1395	
Plasma	m	1578	

Table 4.2: Human RBC volumes per [m^2] body surface area and per [kg] body weight (Orth et al., 2001).

between intravascular and extravascular compartments (as described above) and because albumin, the major plasma protein, escapes into the interstitial space. Plasma volume has been measured by injection of albumin tagged with radioactive isotopes such as ^{121}J and by dyes which bind to albumin such as Evans Blue. Both markers have become unpopular because of potential health hazards and accumulation which precludes repeated measurements. These shortcomings are overcome with Indocyanine Green (ICG), which also binds to albumin and which is completely cleared from the plasma by the healthy liver within 10 to 20 minutes. With new techniques that allow for a continuous measurement of ICG at high sampling rates transcutaneously, intravasally, or in the extracorporeal circulation without taking blood samples (Schneditz et al., 2005), the concentration at the time of injection ($C_{\text{ind}}(0)$) is easily back-extrapolated from the disappearance of measured ICG plasma concentrations.

4.5.7 RBC distribution

When both whole body RBC and plasma volume are measured simultaneously, the fraction of whole body RBC volume $V_{\text{RBC,wb}}$ to whole blood volume $V_{\text{b,wb}}$ gives the whole body hematocrit $C_{\text{hct,wb}}$ (also see (4.9)),

$$C_{\text{hct,wb}} = \frac{V_{\text{RBC,wb}}}{V_{\text{RBC,wb}} + V_{\text{pl,wb}}} = f_{\text{cell}} C_{\text{hct,lv}}.$$

This whole body hematocrit is in the range of 40% and it is significantly lower than the so-called large vessel hematocrit $C_{\text{hct,lv}}$, measured in a blood sample drawn from a peripheral vein or a large central vessel. The ratio of whole body to large vessel hematocrit, also known as f_{cell}, is in the range of 0.85 but may vary between 0.6 and 1.1 (Bauer and Brooks, 1981).

The discrepancy between RBC concentration, measured in all the blood or in a sample drawn from a large blood vessel such as a peripheral vein, originates from the microscopic heterogeneity of blood which leads to a graded separation of plasma and RBC flow in blood vessels when the vessel diameter ($d < 100\,[\mu\text{m}]$) approaches the dimension of the RBC ($d \approx 7.5\,[\mu\text{m}]$). Factors contributing to this effect were first described by Fåhræus and Lindqvist (1931). The most important factor is related to the blunted parabolic flow profile, with RBC rapidly flowing in the core of small vessels and plasma slowly flowing at the vessel wall, also known as plasma skimming. This two-phase flow leads to a significant reduction in small vessel hematocrit and viscosity, thereby also reducing flow resistance in small-diameter blood vessels. The hematocrit in small vessels may reach 20% compared to 45% measured in large vessels (Gaehtgens, 1980). A reduction in hematocrit is also found in microvascular networks (Pries, Ley, and Gaehtgens, 1986). Since blood volume contained in the microcirculation and small venules is a considerable fraction of total blood volume, whole body hematocrit is significantly smaller than large vessel hematocrit, where two-phase flow is not observed under normal conditions.

4.5.8 Hemoconcentration

Indicator dilution cannot be used for continuous measurement of absolute blood volume required for direct observation of dynamic processes. However, intrinsic properties of blood,

such as optical density, mass density (Kenner, 1982; Kenner, 1989), electrical conductivity (Olthof et al., 1994), and sound velocity (Schneditz et al., 1989), can be measured with high resolution for prolonged periods of time. When these intrinsic properties are related to the concentration of components confined to the vascular space, the continuous measurement can then be used to determine relative changes in plasma and blood volume. Often, it is sufficient to follow the relative changes in plasma or blood volume to obtain information on the exchange with the extravascular compartment and to determine the degree of hemoconcentration (degree of increase in cell phase proportion of blood) or hemodilution. In principle, this can be done when the concentration of some blood component confined to the vascular space is serially measured. The most prominent candidates for such serial measurements are Hb, total protein (the weighted sum of plasma protein and Hb), blood water (the weighted sum of plasma and RBC water), and RBC concentration (hematocrit).

The classic approach to determine relative hemoconcentration or hemodilution (also known as relative blood volume, $V_{b,rel}$) is based on serial hematocrit measurements, as this variable used to be easily measured by microcentrifugation (van Beaumont, 1972). From the volume balance ($V_b C_{hct} = V_{RBC}$), and under the assumption that both V_{RBC} and f_{cell} remain constant, the following classic relationship is obtained:

$$V_{b,rel}(t) = \frac{V_b(t)}{V_b(0)} = \frac{C_{hct}(0)}{C_{hct}(t)}.$$

The problems here reside with the assumptions used to derive this simple formula. For example, in hemodialysis where blood volume control, using relative blood volume measurements, has gained some importance, changes in electrolyte concentration and cell volume are common (Kouw et al., 1991). Also, changes in hemodynamic state apparently affect the intravascular distribution of RBC and f_{cell}, and a control based on measurements of hematocrit changes needs to be aware of these shortcomings.

The measurement of relative changes in plasma volume $V_{pl,rel}$ is not affected by these limitations. $V_{pl,rel}$ can be determined by measuring a plasma component confined to the intravascular plasma space ($V_{pl} C_{pl} = \text{const.}$), so that

$$V_{pl,rel}(t) = \frac{V_{pl}(t)}{V_{pl}(0)} = \frac{C_{pl}(0)}{C_{pl}(t)}.$$

The problem here is to find a suitable marker, which can be measured with the required accuracy. With a single hematocrit measurement, it is possible to estimate $V_{b,rel}$ from $V_{pl,rel}$ using

$$V_{b,rel}(t) = \frac{1 - V_{pl,rel}(t)}{C_{hct}(0)},$$

but this brings back the uncertainties mentioned above.

A more detailed analysis of problems of measuring relative blood volume changes is found elsewhere (van Beaumont, 1972; Dill and Costill, 1974; Graveney, 1981; Hinghofer-Szalkay, 1986). However, both hematocrit, Hb, and total protein concentration techniques fail to account for the variable f_{cell}. Blood volume changes calculated from these techniques rather relate to apparent distribution volumes. For example, if plasma is sequestered in the microcirculation because of changes in regional blood flow distribution, the local increase in venous and arterial hematocrit is interpreted as an apparent decrease in blood volume, even if true blood volume remains unchanged by the intravascular fluid shift.

4.6 Hemodialysis

One approach to analyze the characteristics of an intricately controlled system is to open the feedback loop and to analyze the system under impaired control capabilities. In fact, this is the usual experimental approach in medicine and especially in physiology, where the function of the intact system is often recognized only by studying the consequences of the defective system. In some cases, opening the feedback loop has catastrophic consequences such as the complete loss of insulin secretion in type-I diabetes mellitus which affects the sole control for glucose uptake to major tissue compartments. In other cases, opening the feedback loop has few consequences. For example, experimental denervation of arterial baroreceptors does not really affect long-term blood pressure control (Cowley and Guyton, 1972). The volume-pressure control system is, however, severely affected in chronic renal disease, where the capability to remove excessive fluid by the kidneys decreases gradually and finally ceases completely. The disruption of this loop has serious consequences for interstitial volume, blood volume, and blood pressure, and a more or less stable state can only be obtained by renal replacement therapy.

End stage renal disease is a unique environment to study the volume-pressure control system, because the control loop described above is disrupted by the defective kidneys. The system can be studied as it departs from the physiological state either spontaneously or by using controlled perturbations. Notice that the treatment itself can be considered a controlled perturbation, prescribed and performed by the medical staff.

The most effective and widely used treatment for end stage renal disease is hemodialysis. Other options are given by peritoneal dialysis and, of course, by transplantation which provides full replacement of kidney function. Hemodialysis refers to the treatment of blood in an extracorporeal system, which consists of blood lines, a blood pump, and a dialyzer, where the blood is separated from the dialysate by a thin and semipermeable membrane (Schneditz, 2005). The membrane allows for the exchange of low-molecular weight solutes and water from the blood to the dialysate, and vice versa, depending on the magnitude and direction of the driving forces. Since diffusion of solutes across a semipermeable membrane is known as dialysis, the process of clearing blood in an extracorporeal system has become known as hemodialysis.

It is the general perception that hemodialysis is first and foremost concerned with clearing the blood of toxins and metabolic waste products that accumulate in the body, but are no longer removed by the kidneys. The importance of hemodialysis for volume and pressure control is less recognized. Dietary intake of salt (NaCl) and the subsequent drinking of water to maintain a constant osmotic pressure, which is controlled by central osmoregulation, cause extracellular fluid to accumulate volume at a rate of 1 to 2 liters per day. In the absence of kidney function, this volume excess has to be removed from the body by ultrafiltration of blood in the extracorporeal circulation during hemodialysis. Current maintenance dialysis is usually done three times a week, with each session lasting 4 hours on average. This schedule is a compromise between delivering an adequate treatment dose within a minimum amount of time at a minimal frequency. Meanwhile, it has been recognized that increasing the frequency and reducing the duration of treatments may have major effects on treatment outcome. The duration and schedule of hemodialysis treatments are, in general, determined by the requirements to clear the blood from solutes (i.e., to provide a prescribed dose of dialysis), whereas the removal of excess fluid is done

within that time. The prescription and the delivery of an adequate dose of dialysis is a separate control problem, which has attracted major interest as it is related to long-term patient outcome. A discussion of this problem is beyond the scope of this chapter, but can be found in recent textbooks (Hörl et al., 2004; Nissenson and Fine, 2005). For acute morbidity, the removal of fluid, however, is more important.

Hemodialysis is especially well suited for studying the pressure-volume regulation system also because the presence of the extracorporeal circulation offers a special access to the cardiovascular system. The extracorporeal blood lines take the form of catheters to which transducers may be attached for the measurement of selected variables without direct patient contact. In addition, blood lines can be used for administration of markers, whereby some of these markers, such as hypertonic or isotonic saline solution, can be delivered by the extracorporeal machine under controlled and reproducible conditions. Maintenance hemodialysis is done on a regular basis for more than a million patients worldwide, and that number is increasing.

4.6.1 Ultrafiltration

The prescription of volume adjustment is done by measuring the patient weight before the treatment and by assuming a target weight, or the so-called dry weight, at which the patient is normohydrated. The difference between these weights is assumed to be due to fluid accumulation. It is this volume, the so-called ultrafiltration volume, which has to be removed from the body by ultrafiltration of blood. As simple as this sounds, there is a major problem with identifying the correct target weight which is essentially unknown. Errors in the estimation of target weight as small as ± 0.5 [kg] may be enough to cause complications during the treatment, on the one hand, or lead to gradual overhydration and long-term complications, such as hypertension and edema, on the other hand.

Up to now, apart from skilled clinical judgment, there is no generally accepted approach to estimate the correct ultrafiltration volume in the individual patient for the individual treatment. It is for this reason that mathematical modeling of the pressure-volume control system has attracted much interest in the past years.

4.6.2 Vascular refilling

During hemodialysis, ultrafiltration volume is first removed from the blood volume. The removal of fluid through the dialyzer membrane, which is almost impermeable to plasma protein, leads to an increase in hematocrit, an increase in plasma protein concentration, an increase in plasma colloid osmotic pressure, and a decrease in intravascular pressures. This will decrease the effective transcapillary pressure in the microcirculation ($P_{\text{eff}} = \Delta P - \Delta\Pi$, see (4.10)), and thereby stimulate the reabsorption of fluid from extravascular spaces, so-called vascular refilling.

Vascular refilling is of major importance for maintaining blood volume. Inadequate refilling, together with excessive ultrafiltration, will lead to an excessive drop in blood volume (hypovolemia), which is considered to be the most important single cause for hemodialysis induced complications such as cramps and hypotension (Daugirdas, 2001). Vascular refilling depends on treatment characteristics, such as the rate of extracorporeal ultrafiltration, and patient characteristics, such as body size, plasma volume, regional blood

flow distribution, plasma protein concentration, effective transcapillary pressure gradients, and fluid overload. Hence, vascular refilling is assumed to be an important marker for fluid overload, and there have been several attempts to quantify vascular refilling in order to optimize ultrafiltration and to identify the proper target weight.

Passive vascular refilling

Microvascular refilling Q_{fil} can be modeled as a fluid exchange between interstitial V_{is} and blood V_b compartments in the microcirculation using Starling's hypothesis (see (4.10)). There is also a continuous backflow of fluid from the interstitial space into the vascular space through lymphatic refilling Q_{ly}. With the inclusion of lymph flow and with a given ultrafiltration rate Q_{uf}, the following relationships are obtained:

$$\frac{dV_b}{dt} = Q_{\text{fil}} + Q_{\text{ly}} - Q_{\text{uf}}, \tag{4.11}$$

$$\frac{dV_{\text{is}}}{dt} = -Q_{\text{fil}} - Q_{\text{ly}}. \tag{4.12}$$

An analytic solution for this model has been obtained after linearization (Chamney et al., 1999). Only a few variables, required for the description of Q_{fil} in (4.10), are directly accessible. The difficulty especially resides with measurements in the interstitial space and the measurement of capillary pressure. Plasma colloid osmotic pressure, however, can be either measured or calculated from changes in plasma protein concentration using the Landis–Pappenheimer equations (Landis and Pappenheimer, 1963). An estimate for interstitial colloid osmotic pressure is obtained from interstitial protein concentration, which, in equilibrium, is close to one third of the plasma protein concentration C_{pl} (Ellmerer et al., 2000). Based on the observation that total plasma protein mass increases during ultrafiltration, it has been assumed that vascular refilling fluid contains a small but measurable amount of protein ($C_{\text{ref}} = 7\,[\text{g liter}^{-1}]$) (Schneditz et al., 1992).

Using the controlled perturbation of a short ultrafiltration pulse, the characteristics of vascular refilling were studied in a small group of stable maintenance hemodialysis patients (Schneditz et al., 1992). Relative blood volume changes and the degree of hemoconcentration, to estimate changes in plasma colloid osmotic pressure, were determined from changes in total protein concentration, measured by ultrasonic technique (Schneditz et al., 1990). The average whole body filtration coefficient K_{fil}, identified from fitting a two-compartment model to relative blood volume changes, was $5.6 \pm 1.6\,[\text{ml min}^{-1}\,\text{mmHg}^{-1}]$ per 50 [kg] lean body mass and in the same range as the filtration coefficient for skeletal muscle ($0.01\,[\text{ml min}^{-1}\,\text{mmHg}^{-1}]$ per 100 [g] muscle tissue).

The vascular and interstitial spaces in (4.11) and (4.12) may be considered as compliant elements c_{vs} and c_{is}, respectively (Chamney et al., 1999),

$$\frac{dV_{\text{vs}}}{dt} = c_{\text{vs}}\frac{dP_{\text{vs}}}{dt},$$

$$\frac{dV_{\text{is}}}{dt} = c_{\text{is}}\frac{dP_{\text{is}}}{dt}.$$

In this model all blood volume is located in the venous compartment and the pressure, therefore, refers to venous pressure. The interstitial volume-to-pressure curve is highly

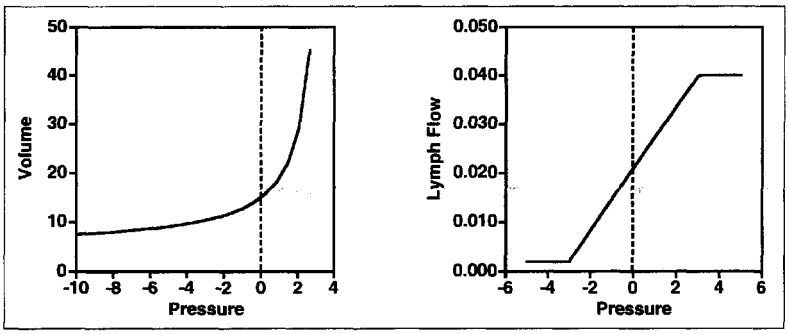

Figure 4.11: Interstitial volume (in liter, left panel) and lymph flow (in liter min^{-1}, right panel) as functions of interstitial pressure (in mmHg) for an average 70 [kg] subject.

non-linear in the range of interstitial pressures of interest, i.e., from 0 to -3 [mmHg]. Interstitial pressure importantly drives lymph flow Q_{ly} which may increase 20-fold with increasing pressure (Figure 4.11).

The relationship between interstitial pressure P_{is} (in mmHg) and volume V_{is} (in liter) is approximated by a hyperbola of the form $P_{is} = 3.5 - 35/(V_{is} - a)$. The constant a refers to the volume axis shift, which can be scaled to body mass M, so that $a = (10/70)M - 35/(3.5 + b)$, and where b is the normal interstitial pressure (-3 [mmHg]) for an interstitial volume of 10 [liter] in an average 70 [kg] subject (Chamney et al., 1999).

So far, the model falls short in describing larger perturbations when active control components to compensate for the drop in blood pressure come into play.

Active vascular refilling

A reduction in venous volume, reducing venous return, cardiac output, and arterial pressure, eventually leads to peripheral vasoconstriction because of barocontrol (Ursino and Innocenti, 1997a; Ursino and Innocenti, 1997b). This causes capillary pressure to decrease, thereby accelerating the refilling process (also see (4.10)).

Since vasoconstriction is a consequence of blood volume reduction, an arbitrary modulation gain function G_{cap} was introduced to describe the effect of a decrease in volume (Chamney et al., 1999). When all the blood volume is located in the venous compartment, the capillary hydrostatic pressure can be considered as the sum of venous pressure (P_{vs}, in this case) and the mean capillary pressure drop P_{dcap},

$$P_{cap} = P_{vs} + G_{cap} P_{dcap},$$
$$G_{cap} = k \frac{dV_{vs}}{dt} h(t - \tau).$$

The gain G_{cap} is assumed to be proportional to the rate of change in vascular volume, and the transport delay τ takes into account the lag before the active mechanism takes full effect (h denotes the Heaviside step function). This approach provides a much improved simulation of vascular refilling under changing conditions, where the passive model apparently fails (see Figure 4.12). On the other hand, the model does not attempt to elucidate the

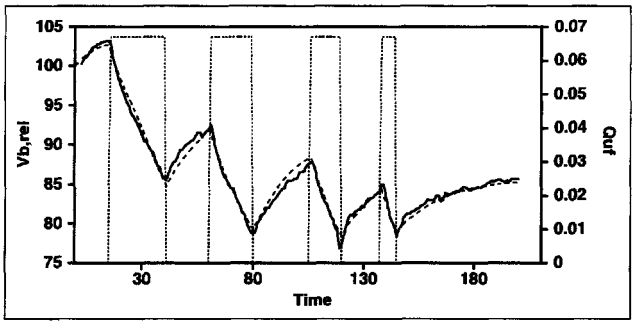

Figure 4.12: Response of V_b to ultrafiltration pulses. Measured (full lines) and modeled (broken lines) relative blood volume changes $V_{b,rel}$ (in %) in response to pulsed ultrafiltration Q_{uf} (in liter min^{-1}), using models with active control of vascular refilling Q_{fil}. An ultrafiltration volume of 4.2 [liter] was removed from a patient (97.5 [kg] pretreatment body weight) using four ultrafiltration pulses of identical pulse height and decreasing pulse duration.

details of the control mechanisms involved, but describes the aggregate gain for the overall physiological control loop. An analysis whether this aggregate gain is different in patients susceptible to ultrafiltration induced side effects, such as hypotension or cramps, has not been provided.

Blood pressure control

To address the question of individual susceptibility to intradialytic complications, it is necessary to take a closer look at the main compensatory reflexes to hypovolemia: the increase in peripheral resistance, heart rate, and heart contractility, as well as the decrease in unstressed venous volume (Ursino and Innocenti, 1997a; Ursino and Innocenti, 1997b). For this purpose the circulation is conveniently modeled using four compartments, three of which are located in the systemic circulation (also see Figure 4.7). The fourth compartment refers to right atrial volume and is part of the cardiac pump. Details of the model can be found in (Cavalcanti and Di Marco, 1999).

Pressure stabilization is achieved through the baroreflex loop, taking information from the high-pressure arterial and the low-pressure cardiopulmonary baroreceptors (Mark and Mancia, 1983). In the original model proposed by Cavalcanti and Di Marco (1999) and in subsequent adaptations of this model (Cavalcanti et al., 2004; Ciandrini et al., 2004), right atrial pressure P_{ra} is substituted for pressure sensed by low-pressure cardiopulmonary baroreceptors, because there is no pulmonary circulation. In this model the afferent tone T_{aff} is modeled by a linear superposition and reciprocal relationship of the two afferent limbs,

$$T_{aff} = (1 - G_{aff})\frac{P_{as} - P_{as}(0)}{P_{as}(0)} + (1 + G_{aff})\frac{P_{ra} - P_{ra}(0)}{P_{ra}(0)},$$

where $P_{as}(0)$ and $P_{ra}(0)$ refer to initial steady state pressures. The contribution of the afferent information is weighed by the afferent gain G_{aff} ($-1 \leq G_{aff} \leq 1$).

The four efferent limbs of the baroreflex loop to affect the system parameters X_i, such as heart rate, contractility, unstressed volume, and peripheral resistance, are modeled by the sigmoid functions,

$$X_i = X_i(0)\big(1 \pm G_{\text{eff},i} \tanh(2T_{\text{aff}})\big), \tag{4.13}$$

where $X_i(0)$ refers to initial steady state, and where plus or minus signs refer to a compensatory decrease or increase of the parameter of interest. The efferent gains $G_{\text{eff},i}$ can be assigned values between 0 (minimum gain) and 1 (maximum gain). Relative changes in blood volume are easily measured during hemodialysis by one of the continuous techniques discussed above. The same is true for heart rate, at least in the experimental situation. Therefore, as the focus is on blood pressure control, relative changes in blood volume and heart rate, continuously monitored over the duration of the whole treatment, can be used as model input. This eliminates a major source of uncertainty present in other experimental studies such as orthostasis or lower body negative pressure tests, which do not have a direct and continuous access to the circulation of the patient. Arterial pressure is the model output and can be fitted to measured mean arterial pressures by the tuning of model parameters, representing the efficiency in the regulation of venous capacity, peripheral resistance, and cardiac contractility.

This model has been used to identify the blood pressure control characteristics during hemodialysis and ultrafiltration, using different treatment modes in hypotension prone and hypotension resistant patients (Cavalcanti et al., 2004). While there was no significant difference in afferent gain G_{aff} between stable and unstable hemodialysis patients, the reduction in unstressed volume was less effective in hypotensive patients in spite of increased peripheral vasoconstriction (Cavalcanti and Di Marco, 1999). This result emphasizes the importance of vascular capacitance in the control of arterial blood pressure. It is also worth noting that the pressure responses of stable and unstable patients were not significantly different, because acute hypotension did not occur in these studies. The difference was most clearly documented in the gains of the control loops. In a different study, done in hypotension prone patients, the control of peripheral resistance and of cardiac contractility was especially impaired in the presence of acetate in the dialysate (Ciandrini et al., 2004).

4.6.3 Ultrafiltration control

There are, however, means to improve the process of fluid removal. It is generally accepted that the risk for hemodynamic instability increases during the second half and especially towards the end of the 4-hour hemodialysis and ultrafiltration treatment. One explanation for this observation is the excessive drop in blood volume observed at the end of treatments done with constant ultrafiltration rates. It was, therefore, suggested to stimulate vascular refilling at the beginning of the treatment with the potential to prevent the excessive drop in blood volume towards the end of ultrafiltration (Stiller et al., 1991). Also, during early treatment phases, vascular refilling is abundant because the tissue is overhydrated. Passive as well as active refilling models indicate that vascular refilling is importantly governed by the buildup of plasma colloid osmotic pressure, caused by ultrafiltration-induced hemoconcentration. With constant ultrafiltration rate, the buildup is slow and vascular refilling reaches its maximum only after a considerable period of time (Figure 4.13). High initial

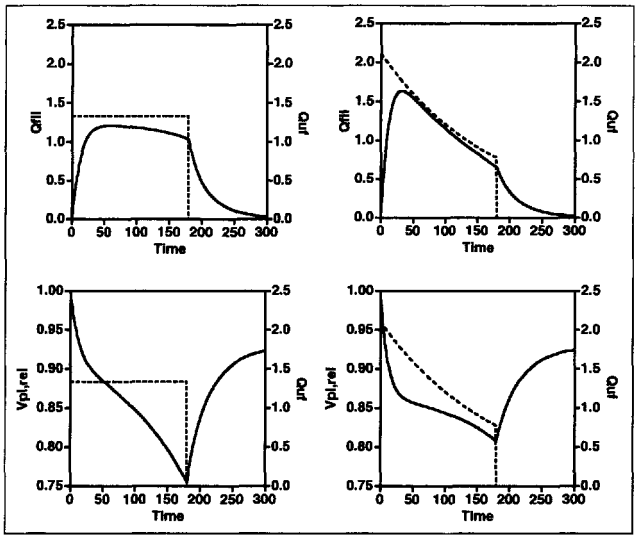

Figure 4.13: Ultrafiltration and vascular refilling. Effect of constant (left panels) or decreasing (right panels) ultrafiltration rate Q_{uf} (in liter min^{-1}, broken lines) on vascular refilling rate Q_{fil} (in liter h^{-1}, full lines, top panels), and relative changes in plasma volume $V_{pl,rel}$ (full lines, bottom panels) under identical treatment conditions and ultrafiltration volumes. Notice that plasma volume is better preserved by a decreasing Q_{uf} (bottom right panel).

ultrafiltration rates will lead to a faster increase in colloid osmotic pressure gradients and in vascular refilling rates at the beginning of the treatment (Schneditz, 1996). With the goal to remove the same ultrafiltration volume, ultrafiltration rates can then be lowered during late phases of the treatment. Thus, both enhanced refilling using increased ultrafiltration rates early in hemodialysis as well as reduction of ultrafiltration rates late in hemodialysis is expected to prevent an excessive decrease in blood volume, especially towards the end of the treatment. This approach is now available in many hemodialysis machines.

Different feedback control algorithms, covering the wide range from simple on-off techniques (Polaschegg, Knoflach, and Binswanger, 1996) to more complex fuzzy logic controllers, have been proposed (Giove and Nordio, 1994), but only two systems employing two different control approaches are used in dialysis machines today. More information on these and other control systems used in hemodialysis is found in (Lindsay and Schneditz, 2004).

Blood volume tracking

Blood volume tracking is designed to control the trajectory of relative blood volume changes, by adjusting the ultrafiltration rate and the dialysate composition of the hemodialysis process (Santoro et al., 1998). The control system requires the definition of a target for the three variables incorporated into this control, i.e., weight reduction, dialysate conductivity, and blood volume change. The rationale for inclusion of dialysate conductivity is based on the effects of sodium concentration on extracellular volume, vascular refilling,

and blood volume preservation (Fleming et al., 1987; Mann et al., 1996). Thus, in this system, vascular refilling early during dialysis is enhanced by both high ultrafiltration rate and high dialysate sodium concentration. Based on the target values for weight change and treatment duration, the system determines an exponential trajectory for intradialytic blood volume changes, which are to be followed with a certain tolerance. Ultrafiltration is limited to a maximum rate of 2 [liter/h]. Dialysate conductivity is controlled with the goal to provide the same sodium mass balance as a comparable treatment with constant dialysate conductivity. Ultrafiltration profiles obtained with this control system are anything but smooth. However, there is a trend for declining ultrafiltration rates as expected for exponential blood volume trajectories (Figure 4.13). Ultrafiltration rates are higher than average at the beginning of the treatment and gradually decrease towards the end of the treatment.

Critical hemoconcentration

The other system uses a critical hemoconcentration to define thresholds for ultrafiltration (Krämer, 1999). This system does not follow a blood volume trajectory and does not aim to reach a target blood volume reduction. Controlled fluid removal is achieved by a continuous adjustment of ultrafiltration rates following a set of rules. For example, in a treatment where the critical hemoconcentration is not approached, the algorithm provides a linear decrease in ultrafiltration rates, with ultrafiltration starting at double the constant ultrafiltration rate. If the linear decrease is not interrupted, and since the total ultrafiltration volume is not affected, the ultrafiltration rate at the end of the treatment is zero. However, when ultrafiltration induced hemoconcentration approaches a critical hemoconcentration, ultrafiltration rate is reduced in excess of the linear decrease. It is a characteristic of this approach that in case of system failure the algorithm can always fall back to an ultrafiltration rate, which will not be higher than the standard ultrafiltration rate of an uncontrolled treatment. This is a special aspect of control safety.

4.6.4 Blood pressure control

A system using both heart rate and relative blood volume as an input to identify the individual control characteristics, has the potential to be used in everyday practice. Both heart rate and relative blood volume changes can be measured in the extracorporeal circulation by noninvasive means (Moissl et al., 1999). The problem remains with the measurement of arterial blood pressure, which, in everyday practice, is available only in intervals of 30 minutes or more. The question therefore arises whether sporadic measurements of blood pressures are sufficient to identify patients at risk. On the other hand, the models could be used to make predictions and to request additional blood pressure measurements whenever the barocontrol system is reaching a critical state.

4.6.5 Time-variant system

Even though the models presented above adequately capture the dynamics of blood volume and of arterial blood pressure during hemodialysis, the question arises whether the system and its control parameters can be assumed to be constant for a perturbation lasting 4 hours

or even longer. The question is justified as adaptation and resetting are well known to occur in baroreflex control. How can this issue be addressed?

Complicated control problems, in which the parameters cannot be assumed to be time invariant, are often solved through adaptive techniques. This is a methodology by which the controller periodically performs certain tests in order to obtain parameter values, which may be considered constant over a limited period of time. Adaptive methods may be invoked by application of suitable test inputs such as intermittent ultrafiltration pulses (see Figure 4.12).

4.6.6 Ultrafiltration pulses

While ultrafiltration is usually prescribed at a constant rate for the whole dialysis session, the dynamics become more evident using a pronounced perturbation, where the amplitude of ultrafiltration rate is varied using different patterns such as a series of ultrafiltration pulses (see Figure 4.12). The resulting blood volume response may be monitored, from which certain properties of the physiological system may be deduced. This approach is particularly important, given the limitation of physiological knowledge regarding the operation of the patient's regulatory systems. A short ultrafiltration pulse also has the advantage that, other factors influencing intra- and extravascular fluid distribution, such as body position and fluid and/or food intake during the treatment, are better controlled for short periods of time. Pulses can be repeated, however, there are limitations with regard to the amplitude and the duration of such pulses. For example, the ultrafiltration pulse must not exceed a specified fraction of the extracorporeal plasma flow to avoid dialyzer problems and blood clotting. Also, the overall ultrafiltration must not exceed the prescribed ultrafiltration volume.

Such pulses were used to analyze the detection limit for volume overload of different available techniques (Krämer, Rode, and Wizemann, 2006). However, when compared to other means of measuring extracellular volume, such pulses did not do too well. Ultrafiltration pulses are part of the treatment in removing excess fluid water. In case of hemodynamic problems, the action of the ultrafiltration pulse cannot be reversed but must be stopped. To stabilize the blood pressure, an infusion has to be given. Also, there are limitations to pulse height and reversibility. Pulsed ultrafiltration has not been too successful, as patients undergoing such treatments experience exceptional fatigue. The reason for this is not well understood, but it is clear that valuable ultrafiltration time is lost with each phase between pulses, where ultrafiltration is reduced or even completely absent.

4.6.7 Blood volume sequestration

The extracorporeal circulation used in hemodialysis offers the possibility to provide a rapid and reversible sequestration of blood into the extracorporeal circulation without interfering with ultrafiltration requirements (Wimmer et al., 2004).

Operation of the artificial kidney requires the extracorporeal system to be filled with patient blood. This volume (usually less than 300 [ml]) is continuously replaced by extracorporeal blood flow, but the amount of blood volume sequestered in the extracorporeal circulation remains more or less stable during a treatment session. At the end of an extracorporeal treatment session, this volume is returned to the patient. However, for the purpose

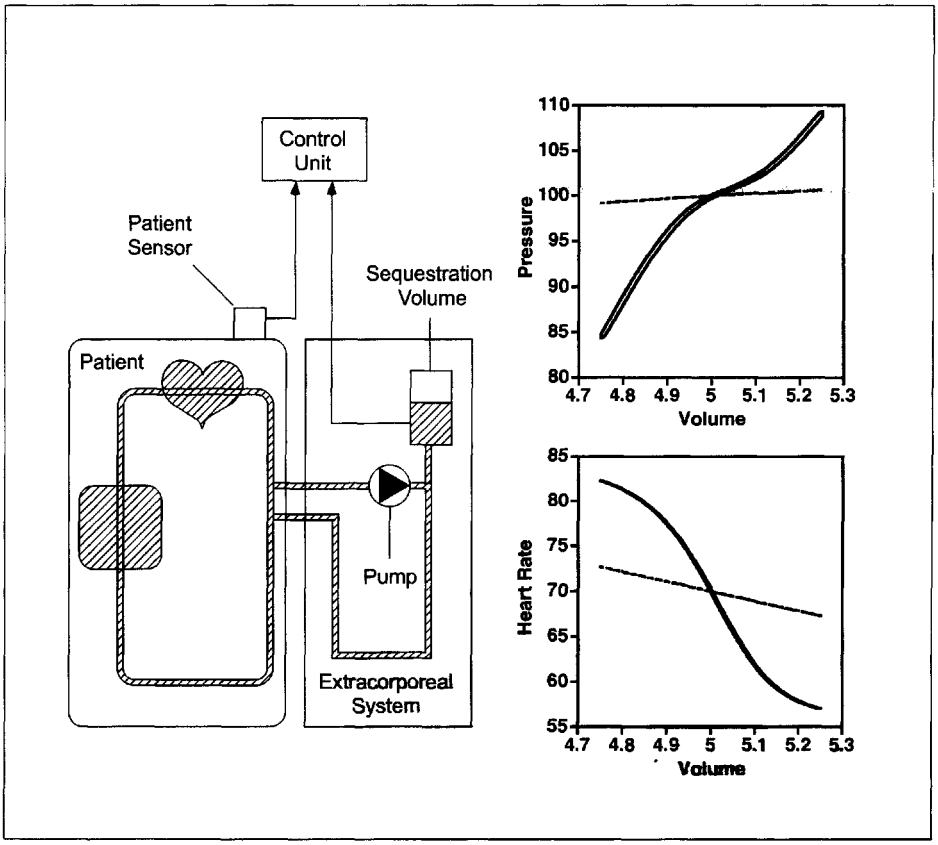

Figure 4.14: Extracorporeal sequestration of blood volume. Schematic view of sequestration of blood volume in the extracorporeal circulation connected to the patient circulation (left panel). Simulated changes in blood pressure (in mmHg, top right panel) and heart rate (in beats per minute, bottom right panel), with a reversible shift of 500 [ml] of blood volume assuming absent (full lines) and 50% (broken lines) compensation through reduction in unstressed volume (model adapted from (Ciandrini et al., 2004)).

of performing a controlled perturbation, the blood volume in the extracorporeal circulation can be further expanded by an additional and reversible volume shift. This can be done using a blood bag which is filled and emptied by extracorporeal blood flow under sterile conditions without much additional effort (Figure 4.14). To the patient circulation and to the cardiovascular control system, the shift of blood into the extracorporeal system therefore must appear as a "peripheral" sequestration, comparable to an increase in unstressed volume. An extracorporeal sequestration in the range of 500 [ml] compares to the peripheral sequestration of blood during upright standing. The reversible shift of volume between patient and extracorporeal circulations, therefore, corresponds to an orthostasis test without the patient changing body position. Such an extracorporeal sequestration test can then be used to measure short-term blood pressure control mechanisms during hemodialysis under well-controlled conditions.

Unlike other orthostasis tests such as tilt-table or lower body negative pressure experiments, the magnitude of the perturbation (the actual volume loss) is precisely known in this setting. Unlike fluid removed using ultrafiltration pulses, blood sequestered extracorporeally can rapidly be returned to the patient in case of hemodynamic instability. The perturbation does not by itself interfere with volume removal by ultrafiltration. The perturbation rate is determined by extracorporeal blood flow, which usually is in the range of 200 to 450 [ml min^{-1}], so that the test can be done within 1 to 3 [min]. This is much faster than the perturbation rate using ultrafiltration pulses, which reaches only 50 [ml min^{-1}]. Because of these characteristics, the test qualifies for repeated measurements to identify the pressure and volume control gains as they change throughout a 4-hour hemodialysis treatment. The cardiovascular response, measured by such a perturbation, can be analyzed to identify the individual blood volume sensitivity without making major modeling assumptions.

4.6.8 Blood volume sensitivity

Although many studies have investigated the relationship between blood volume and arterial blood pressure during hemodialysis, a precise and unique relationship could not be defined, because factors other than blood volume, such as peripheral resistance, cardiac output, and venous capacitance, also come into play. In some patients arterial pressure readily drops even with small reductions in blood volume, while in others blood pressure drops with a delay, and in a third group blood pressure increases as blood volume decreases. The differences between hypotension prone, delayed hypotensive, and hypotension resistant subjects have been explained by individual differences in the control gains to peripheral resistance and unstressed volume (see (4.13)) (Cavalcanti et al., 2002). In a blood volume sensitivity plot (Figure 4.14), patients can be distinguished by such different characteristics. Up to now, however, such data are available from the analysis of whole treatment sessions lasting several hours, and the question arises whether the response measured in these studies really refers to short-term control and whether the individual control systems remain unchanged during the whole treatment time. The system described above and shown in Figure 4.14 should be of some help to address this question, as a controlled perturbation can be performed at selected time intervals and within a short period of time. Also, with such a system, one should be able to make predictions on future blood pressure behavior. From the short-term control characteristics, measured for a known volume perturbation at one time point, one should be able to predict the hemodynamic state at later treatment time points, when a comparable blood volume drop is reached because of ultrafiltration and incomplete vascular refilling. A deviation of long-term prediction from short-term blood volume sensitivity data will have to be interpreted as long-term adaptation. Finally, a prediction of hemodynamic (in)stability could be used for automatic control of ultrafiltration rates and ultrafiltration volumes, without the immediate need to identify the physiological control system. On the other hand, identification of individual control strategies may also help to optimize long-term aspects of renal replacement therapy, for example, selecting the proper medication among the many pharmacological possibilities to specifically act on individual cardiovascular control mechanisms.

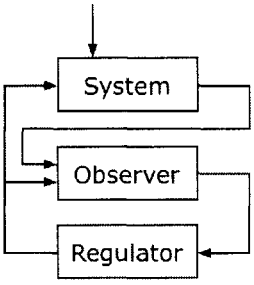

Chapter 5

Future Directions

5.1 Introduction

In recent years, the development of sophisticated experimental techniques and computational power has led to a large and ever increasing body of physiological knowledge related to the function and control of various aspects of the CVRS. How to integrate this diverse body of information, and how to apply this knowledge via clinically useful and personalized models in real time have become central questions to answer. In particular, issues of multiscale modeling, interfacing of hierarchical systems, and parameter identification for complex models are key topics to be addressed. In this chapter we will discuss some of the current questions and issues which exist in the field.

One point is clear: the topics presented in this book and other issues discussed in this chapter intersect in ways that require interdisciplinary cooperation, and such interdisciplinary interaction may lead to unexpected insights. Furthermore, even though particular clinical conditions are often approached as separate problems, multiple conditions regularly occur in the same patient and are linked in their function and pathophysiology. For example, the metabolic syndrome (syndrome-X) is characterized by the clustering of insulin resistance, obesity, and hypertension.

Another example where such interaction occurs is in the phenomenon of sleep apnea, which has been related to hypertension, and possibly to the progression of CHF. We have also seen that, blood pressure control depends on the interaction of numerous short-, mid-, and long-term systems, including regional volume distribution, regional and systemic changes in resistance and compliance, and the interaction of these quantities with respiratory gases, pH values, hypoxia, and renal influence.

In the introduction to a series of articles generated by a recent symposium "Neural, Hormonal, and Renal Interactions in Long-Term Blood Pressure Control", it was noted that, in the years since the introduction of the comprehensive computational model for blood pressure control by Guyton and colleagues (see, e.g., Guyton, Coleman, and Granger, 1972), "a new generalized integrative model has not been advanced." The authors went on to state that there was agreement among the symposium participants for the need to "launch

a collective international initiative to develop a fresh computational model for the long-term regulation of arterial pressure" (Evans et al., 2005).

Such a new generation model will include short-, mid-, and long-term elements and will also necessitate integrating respiratory function. We will mention here some of the directions in which research needs to go to develop such a model. However, the model will not be developed only by considering individual parts of the system, but also by stepping back and looking at how form and function interact in physiological systems. Vantage points for considering this integrative point of view are illustrated in the work of Weibel (2000).

Models of CVRS function and control will be of great benefit since, according to statistics of the American Heart Association, cardiovascular disease is directly responsible for 38% of all deaths in the United States each year and at least 70 million people in the United States have some form of cardiovascular disease.

5.2 Physiological Questions

In this section we discuss some areas in which physiological information needs to be developed, and important questions need to be posed. Genetic influences and issues of multiscale modeling will be discussed in Section 5.3.

Mid- and long-term control: The interaction of hormonal and neural control

The current paradigm is that long-term blood pressure control is essentially accomplished by pressure diuresis and natriuresis. This classical concept developed by Guyton and colleagues, which has contributed so much to the understanding of blood pressure control, has been recognized to be in need of major revision. While this approach captures the effects of large changes in arterial pressure, and is the basis for many experimental designs, there is growing awareness that moderate variations in blood pressure are not explained. This point must not be ignored, as small changes operating over extended periods of time apparently stand at the beginning of chronic and pathologic dysfunction.

Based on recent experiments in conscious and freely moving dogs, it was observed that diurnal patterns in arterial pressure were not accompanied by similar changes in urine volume and urine sodium (Seeliger et al., 2005). Diurnal variations in urine volume and urine sodium were rather related to sodium and water intake. Therefore, some other mechanism to control fluid and salt output, independent of direct blood pressure influence, must be operative (see, for example, Sandgaard et al., 2005).

It is well know that renal fine-tuning of water and sodium excretion is done by reabsorption of water and sodium from glomerular filtrate rather than by pressure mediated glomerular filtration. Even though reabsorption is influenced by pressure effects, it is mainly under hormonal control, including autonomic control pathways. This hormonal influence has led some researchers to postulate a long-term central control, including a central baroreceptor, rather than relying only on the long-term peripheral control by the kidney (Osborne, 2005).

Shifting the focus on long-term pressure and volume regulation from primarily mechanical factors (pressure and filtration) to neurohormonal factors has attracted much interest (Chapleau and Abboud, 2001). However, the possible neurohormonal mechanisms

and interactive pathways are vast, and an important step forward would be in identifying the most important players in that scenario.

Cardiac performance

A number of mechanisms and factors are involved in the process of filling the heart. Mechanoreceptors are found in the atria, ventricles, venoatrial junctions, and pulmonary and coronary arteries, while chemosensory nerves are found in the ventricles. These diverse receptors have different impacts, serve various roles, and interact in a complex manner. Furthermore, in trying to understand these interactions, it is not clear that animal models accurately reflect human physiology in this area. Heart rate, venous filling pressure, and sympathetic activity are primary factors influencing volume regulation. The balancing of these factors and the impact of afferent messages from various receptors, as well as baroreflex and other control influences, creates a complex web of interacting factors. As a consequence, it is not fully known how ventricular volume regulation is accomplished. A model of cardiac function needs to quantify how the heart balances its preload and afterload conditions, with its operating constraints imposed by the various cardiac sensory afferent signals that reflect ventricular stretch and other local cardiac conditions.

Vasoconstriction control

Vasoconstriction control involves a number of local and global influences, some of which have been detailed in Section 3.1. We wish to underscore the fact that there are a number of open questions in regard to the action and interaction of these factors. For example, how do global neural control and local influences (such as local active metabolites) interact to ensure appropriate vasoconstriction or vasodilation in tissues during dynamic exercise, while maintaining appropriate systemic blood pressure? Also, what role does muscle mechanical action play in controlling muscle blood flow and cardiac output? Does the control of local tissue blood flow influence metabolite accumulation, and consequently influence muscle chemoreflex action? It is also important to distinguish between skeletal and cardiac muscle with regards to vasodilation.

When considering only local tissue metabolic demand (which definitely influences local flow), the problem of specifying precisely which mechanisms are involved in generating this net flow effect, has not been adequately carried out. This is in part due to the redundancy in the system and overlapping influences whose dynamic interplay is hard to pin down. Such interactive problems are clear candidates for modeling studies.

Neural interaction and integration of RS *and* CVS *control centers*

While much work has been done in identifying the brain centers which correspond to various aspects of CVRS control, the neurophysiological basis for the interaction of the cardiovascular and respiratory controls (interaction and possible overlap of control regions) is still not well understood. Quantitative descriptions of integrated control, such as a description of how chemosensor stimulation is translated into (coordinated) respiratory and cardiovascular responses, are lacking. Another area where knowledge is lacking is in the interaction of the sleep-wake center with general CVRS control centers.

Feedback and feedforward control

The vast majority of models are based on feedback systems. Feedforward control certainly plays a role in the onset of exercise, and it may well be that feedforward components are operating in other settings of cardiovascular control as well. Such feedforward controls likely involve a form of learning and adaptation. Is this adaptive facility related to the capability to reset system set points in mid- and long-term control?

The set point or operating point defined by the system

Even though arterial pressure is maintained at a more or less constant level, the question of whether it is really pressure that is controlled is still a topic for debate. In other words, is the operating point of blood pressure an emergent quantity arising from satisfying other goals, or is it the primary controlled quantity? In the model proposed by Fink (2005), the circulation is controlled by the metabolic demands of organs and tissues, and these diverse demands are synthesized via a market model of supply, demand, and price. In this case blood pressure (which is inversely related to a defined price) is an emergent quantity determined by the interaction of market forces.

The question of determining a set point is linked to a wider debate about the roles of central versus peripheral control. Central control has, in the past, been the easier topic to approach with the periphery often modeled as a lumped system. Peripheral control requires a greater differentiation of levels and structures. The above market model represents a peripheral-control point of view.

On the other hand, taking a central-control point of view, some researchers, who try to resolve the problems of resetting, adaptation, and long-term pressure control, have postulated a central baroreceptor, analogous to the central chemoreceptor for respiratory control. There are some candidate areas in the brain where such a receptor could reside, but clear evidence for such a mechanism has not been established.

Questions involving the establishment of set points and operating points in the system have also been viewed in terms of the interplay between structure and function, which can help to account for the characteristics of performance (see, e.g., Weibel, 2000). A deeper description of cardiovascular control may also need to include self-organizing features, since a given malfunction of a single component does not necessarily completely disrupt the system. The self-organizing capability is reflected in the (apparent) redundancy of the sensory systems and feedback loops.

Noninvasive measurement

Continuous data measurement is necessary for model validation. By continuous data, we mean data that is sufficiently rich to capture detailed dynamics of a system. A key to future modeling will be the development of new methods for noninvasive measurement, which will allow for more accurate and convenient continuous measurement of currently accessible variables as well as measurement of new CVRS-related variables. The noninvasive feature will allow for easier acquisition of human data because of fewer ethical restrictions, wider accessibility to data, and ease of clinical application. While invasive measurements and delicate noninvasive experiments are continuously being performed to explore CVRS

function, such data is not easily obtainable especially in the clinical setting. We restrict our discussion to the problem of collecting data noninvasively in a clinical setting.

Noninvasive beat-to-beat measurement of heart rate is direct, and finger cuff measurement of P_{as} is nearly direct. Noninvasive measurements by monitoring other CVS quantities, such as cardiac output, stroke volume, parasympathetic and sympathetic activity, as well as total peripheral resistance, typically depend on algorithms to infer these quantities from direct measurements of the cardiac pulse, HRV, and other direct observations. These quantities are primarily useful (when carefully measured) for exhibiting dynamic behavior and relative changes, but are not in general accurate enough to provide direct absolute data. Continuous noninvasive direct measurement of ventilatory activity is available, while end-tidal and transcutaneous measurements of blood gases contain errors which can be partly adjusted by using blood test calibrations. Improved measurement techniques or estimation algorithms may be able to reduce the error in such derived measurements. Improvement in instrumentation and application in techniques, such as impedance and Doppler cardiography, will also be of value. Doppler tissue imaging and refined cardiac magnetic resonance imaging (MRI) techniques will also contribute to analyzing the structure and state of the CVRS and estimating fixed parameters. Even where continuous data measurement is not possible, extending the spectrum of quantities, accessible by noninvasive or minimally invasive steady-state measurement, will allow for more accurate estimate of steady state parameter values and for calibration of continuous data that are primarily useful for reflecting relative dynamic change.

New techniques, such as peripheral arterial tonometry (PAT), for measuring sympathetic drive are being developed. A key aspect of this development will be the validation of these new measurement techniques and the processing of noisy data. Implantable transducers (such as pressure transducers), telemetric signal transmission, and miniaturization may allow for long-term measurements of such diverse quantities as sympathetic nerve activity, glucose levels, and respiration. Such technology for long-term measurements will provide information for both research on long-term control and nonintrusive clinical applications, and, hence, such advances will be of use in validating complex models and also for deriving reduced models that can be applied clinically for predictions related to individual patients.

Exercise control and exercise versus nonexercise heart tissue remodeling

A number of important questions exist in regards to CVRS function during static and dynamic exercise. A succinct discussion of some of the main questions in regards to vascular response to exercise can be found in Rowell (2004). In addition, the current picture of the triggering process for the initial CVRS response in exercise onset (including the notion of a central command) is not complete.

Much remains to be learned in regards to understanding the mechanisms involved in the growth and remodeling of heart tissue in response to stress. Whereas exercise stress can be beneficial, other stresses imposed on the heart (such as due to increased vascular resistance) can be damaging. To what extent does this distinction depend on the triggering hormones or mechanisms associated with the growth or alteration of heart tissue, to what extent does it depend on the type of tissue which develops, and to what extent does it depend on tissue mechanical or chemical property effects that arise due to this stress? We know

that the remodeling of heart tissue, observed during the progression of chronic heart failure, plays a central role in this process. It has been recognized that the deteriorating heart function, characterizing the clinical course of this condition, is not simply the consequence of a failing or damaged heart pump, but the failing heart is the consequence of the interplay of a variety of factors, including mechanistic and control system response factors, genetic, cellular, and hormonal factors, as well as circulatory system functional status. Much work remains to unravel the dynamic interaction of these factors (Fedak et al., 2005). Clarifying the distinction between exercise-induced remodeling and destructive forms of remodeling may help unravel these complex interaction of factors involved in CHF. See also Section 5.4 for further discussion.

5.3 Mathematical and Modeling Issues

Multiscale systems

During recent years, our knowledge base has expanded significantly reflecting multiple levels of anatomy and physiology due to such data intensive efforts, as the Genome and Proteome projects, as well as due to the rapid development in instrumentation, data processing, and computational power. The term systems physiology, which is widely used but rarely well defined, has been used to encapsulate the effort to integrate levels of physiological knowledge. The approach is a bottom-up approach to knowledge integration that seeks to show how physiological levels from the gene to the whole body are functionally connected, and more important, to find ways to apply that knowledge to solve clinical problems. One aspect of this effort, which is of direct concern to the themes developed in this book, is that, because of this broad-based and extensive growth in our knowledge base, new techniques are needed for interfacing various levels of models.

An excellent example of the problem in blending together levels and types of models can be seen in the modeling methods exemplified by Quarteroni and Veneziani (2003). In that paper, a heterogeneous model is described that simulates local blood flow in a specific artery via Navier–Stokes equations. This arterial section is linked to the rest of the CVS, which is represented by a lumped zero-dimensional model, described by a system of ordinary differential equations (ODEs). The motivation is to be able to consider detailed localized behavior of fluid flow in cases such as a coronary bypass or stented artery, while utilizing certain interfaced state variables of a more generalized lumped-parameter CVS. This renders the problem computationally tractable.

Another example of the multiscale modeling approach can be seen in the work in the Lung Physiome project at Aukland University. Anatomical model meshes, derived from computed tomography (CT) data taken from lung structures, are developed and the problem considered is how to simulate air flow in these structures at various levels of detail depending on the physiological activity or problem of interest. Again, these models can include Navier–Stokes equations to model flow in larger vessels, and models of flow in the microcirculation using two-phase network flow models.

Multiscale system initiatives

A number of initiatives has been developed to coordinate modeling knowledge in physiology and to address some of the problems and issues associated with multiscale modeling

such as those problems just discussed. Of particular interest is the Physiome project, which is described in Bassingthwaighte (2000) as "a multicentric integrated program to design, develop, implement, test and document, archive, and disseminate quantitative information and integrative models of the functional behavior of molecules, organelles, cells, tissues, organs, and intact organisms from bacteria to man." A major goal of the Physiome project is to "provide the integrating scientific basis for the Genes to Health initiative, and make physiological genomics a reality applicable to whole organisms, from bacteria to man" (Bassingthwaighte, 2000). The Physiome project seeks to archive, cross-reference, and interadapt modeling submodules, which reflect a wide range of modeling levels. This archiving process will require addressing a number of bioinformatic organizational issues, such as making sure that submodules match up in units and level of detail, and also require that new techniques be developed for multiscale merging of submodules and submodels. Subprojects include such focus groups as the Cardiac and Pulmonary Structure and Function Group at the University of Aukland, the Integrative Cardiac Function Group at University of California at San Diego, the Cardiac Action Potential Modeling Group at Oxford Univiversity, and the Circulatory Flows and Exchanges and Cardiac Energy Metabolism Group at the University of Washington.

These efforts highlight the issues involved in multiscale modeling and represent a core beginning to organizing our knowledge base in such a way as to allow for maximal efficiency in the use of that knowledge.

The inverse problem and parameter identification of complex models

Many different mathematical models of CVRS dynamics have been published exhibiting a variety of complexity and purpose. Some models are based on lumped parameter representations of the vascular network, while others model one or more of the vascular beds, using fluid dynamics equations to represent flow through a distributed, compliant network. In addition, comprehensive models of the complex interaction of several control processes of the CVRS have been available for decades and have been progressively improving. However, when these mathematical models were validated against clinical data, most of them were carried out for a single subject, which is only sufficient for idealized study of mechanisms and responses. For a mathematical model to be useful for clinical considerations at the population level, the mathematical model is required to be integrated into a statistical framework (Davidian and Giltinan, 1995) characterizing variation within and across individuals in the population, and in the data. In particular, observable measurements on a given subject are potentially subject to measurement errors in addition to inherent intra-individual variation, that is not represented by the model. Moreover, intersubject fluctuation in dynamics is unavoidable, and understanding the extent and nature of this variation is essential if insights gained from mathematical models are to be translated to the clinical situations.

Techniques for model reduction for clinical application

The classical sensitivity analysis approach discussed in this book addressed the question of how particular model outputs depend on the input parameters. This is an important step in the modeling process for checking the sensitivity of the model response to uncertainty in values of the model parameters, as well as a powerful tool for checking the sensitivity of one

model parameter relative to other parameters. Generalized sensitivity analysis is beneficial in determining the direction of future data collection activities. Understanding which data the model is sensitive to should influence experimental design. However, one important issue that we did not address in this book is how to use sensitivity analysis to simplify or reduce model complexity. Complex models arise because it is necessary to incorporate interdependencies and interactions between subsystems in order to describe physiological systems with sufficient precision. Even if one focuses on a specific mechanism, it may be important to embed this mechanism into a larger system. The models obtained in this way usually have a large number of parameters and, in general, cannot be adapted for individual persons, which is required for clinical applications of the model. Therefore, in our opinion, it is important to develop methods of sensitivity analysis and parameter estimation, which will make it possible to single out those parameters in a complex model, which are of particular importance for a specific mechanism in the system, and to estimate these parameters with sufficient precision for individual persons. In addition, one needs methods for parameter estimation, which allows for validation of complex models for well-defined groups in a population.

5.4 Clinical Applications

In this section we discuss some clinical questions connected to CVRS control modeling.

Orthostatic stress

We have discussed several aspects of orthostatic stress and OID in Subsection 3.3.2. OID can lead to syncope and as the population ages, syncope-related falls and fractures will become even more prevalent. Models which can account for the interaction of the various control responses involved in countering the impact on the CVS of orthostatic stress, should be able to provide guidance on how best to treat OID, so as to avoid or minimize syncope and perhaps provide suggestions on how to design drug therapy that is individualized to the particular patient situation, especially as drugs can have complicating side effects for the CVS.

The role of sympathetic tone in CVS *disease*

Cardiovascular disease is the leading cause of death in developed countries and is about to replace infectious disease as the leading cause of death worldwide. Hypertension and CHF are chronic diseases whose understanding requires a long-term perspective. Short-term CVS control has received significantly more attention, and for that reason is better understood today, while less information is available for mid-term and long-term control. The initial events or perturbations that lead to cardiovascular disease are not well known, but there is a growing consensus that increased sympathetic activity may stand at the beginning of these chronic diseases.

In humans, sympathetic activity is measured by surrogates such as HRV or by noradrenaline (NA) spillover techniques. The latter requires invasive catheterization of the organ to be studied, and is therefore not possible in everyday clinical practice. Also, since NA spillover refers to the sum of NA release and uptake, the true sympathetic activity

may be masked. Other techniques using ganglionic blockade exert a global effect, including cardiac output and heart rate. While denervation has provided insight into feedback by opening the loops, such a procedure is impossible in humans, although such situations arise in patients, whose carotid bodies need to be removed, and in transplant recipients. Medicinal interruption and interference can also open a control loop, and these situations provide valuable, but restricted, information on control structure.

Given the emerging picture of the role of sympathetic activity in cardiovascular disease, and the importance of long-term pressure control, it seems imperative to perform long-term recordings of sympathetic activity, for example, by measuring SNA. In humans, noninvasive or minimally invasive measurement of SNA is restricted to the measurement of a limited set of accessible nerves (largely motor nerves) such as the peroneal nerve. Therefore, the question arises whether the sympathetic outflow measured in one nerve, targeted for a specific organ, really represents the sympathetic activity seen at other organs. There are a few studies on that subject. One study, using anesthetized rabbits, showed an increase in splanchnic SNA in response to hypoxia but a decrease in SNA to the heart and skin. An important future investigation will be to compare how SNA, recorded in accessible sites, compares with the activity of nerves to important target organs such as the kidney (Guild et al., 2005).

If SNA is the critical signal in long-term blood pressure control, what are the main long-term controllers of that signal? One proposal is that hormonal signals acting via circumventricular organs may provide an input to the central nervous system. There is substantial evidence that Angiotensin II contributes to the regulation of arterial pressure via actions on several brain sites that affect the level of SNA (Guild, Barrett, and Malpas 2005). These observations provide input to the discussion surrounding the idea of central control and the postulate of a central baroreceptor.

Hemodialysis and transfusion

The global number of dialysis patients is close to 1.3 million and growing by 6% annually. Up to 30% of all hemodialysis sessions are complicated by muscle cramps and/or hypotension, with such complications sometimes serious enough to terminate treatment. A model that explains the onset of such events may also lead to identifying parameters of significance for these events and to developing tests for identifying who has increased susceptibility (which may vary from day to day) as well as to anticipate or predict and ultimately to devise algorithmic adaptations to circumvent these events.

The problems of blood pressure control, during ultrafiltration of excess body water in hemodialysis, would be greatly reduced if either treatment frequency or treatment duration were increased. Such an approach, however, consumes scarce resources, and given the projections of the growing dialysis population, this simplest solution will likely not be feasible. Of course, longer and more frequent treatments are not favored by patients. Since a single treatment lasts 2 to 4 hours, blood pressure control involves already mid-term aspects. Such mechanisms have been discussed in Section 3.1, but the integration of controls into clinically useful quantitative mathematical models has not been achieved. Questions to be addressed must include aspects of regional metabolism and ischemia, for example, in the splanchnic circulation, and thermal balance, since peripheral vasoconstriction leads to heat accumulation. Both of these factors have the potential to cause detrimental vasodilatation

that can trigger or contribute to a hypotensive event. The influence of hormonal factors must also be included. The key issue is the reliable prediction of hemodynamic instability, so that countermeasures can be taken to prevent a hypotensive event and a premature termination of the treatment.

The above-described problem, associated with hemodialysis, centers on blood pressure control as a result of blood volume shifts. Similar issues arise in problems of stabilizing a patient during volume loss due to hemorrhage. A number of control responses come into play and a number of transfusion protocols are available. However, no quantitative model exists that allow for a full evaluation of these various treatment protocols.

Sudden infant death syndrome

Sudden infant death syndrome (SIDS) is still an unresolved mystery. A number of possible explanations have been put forward, which involves CVRS mechanisms, but none have been verified and some have been rejected as primary causes while still viewed as connected via risk factors or potentially connected in a chain of events. However, a number of these explanations (such as overheating and respiratory distress) are correlated in certain ways. This led to the key recommendation, which began to be extensively publicized in 1992, to have infants sleep in the supine position. This had an important impact on the number of SIDS cases after 1992, and, together with improved methods of diagnosis and descriptions of risk factors, has led to a significant drop in such SIDS cases after 1992. Yet no consensus exists on the mechanism(s) or sequence of events which triggers a SIDS case. Neonatal monitoring of CVRS parameters has not yet allowed for clear identification of infants at risk (Malloy, 2004). We know that a number of key developmental changes occur in the transition from fetus to neonate to infant (some discussed in Section 2.4). However, there is still insufficient knowledge about the details to be able to unambiguously identify the key vulnerabilities that may arise during this transitional time. Sleep architecture (Peirano, Algarin, and Uauy, 2003) and the chemical control system for respiration (Donnelly, 2000; Søvik and Lossius, 2004) are both developing during the neonatal period, and sleep deprivation is a risk factor for SIDS, but why? We have previously mentioned one recent study (Franco et al., 2004) that indicated that short-term sleep deprivation increased both the incidence of obstructive sleep apnea and raised the arousal (auditory) threshold in healthy infants. It is possible that either of these two factors, or a combination of both, could contribute to at least one chain of events that could lead to a SIDS case. It has also been suggested that problems with the peripheral control may be connected in some form to at least some SIDS cases (Donnelly, 2000).

CHF

There is no doubt that CHF is an increasing and more significant burden on health care systems as the proportion of elderly in the general population increases. It will be of great value to have models reflecting features of heart structure and function as well as the control mechanisms. Such models can provide insight into the self-reinforcing deterioration of the heart's pumping efficiency and can be used to study various drug treatments. They can also be used as an aid in decision making in regards to treatment alternatives based on vasodilators or beta-blockers in individual cases depending on CVS status.

Similar observations can be made about the increasing problem of hypertension, which is also a significant risk factor for CHF. As mentioned in the discussion on CHF in Section 3.3 and in the discussion above on the role of sympathetic tone in CVS disease, sympathetic activity and the Renin-Angiotensin system are important potential focal points for studying the etiology of these conditions. Apnea has also been associated with CHF, and while a number of possible mechanisms have been proposed, a detailed description of the mechanism involved in the development of CSR in CHF has not been accomplished, and if achieved, it would likely help to reveal what role that CSR and associated risk factors play in the progression of CHF.

This page intentionally left blank

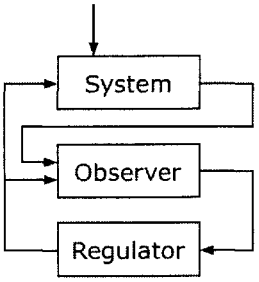

Appendix A

Supplemental Calculations

A.1 Equilibrium Computation for the CVS if P_{as} Is Given

If P_{as} at the equilibrium is given, then (1.38) and (1.43) imply

$$P_{vs} + A_{pesk} C_{a,O_2} F = P_{as} + A_{pesk} M_T.$$

This equation, together with (1.39), (1.40), and (1.5), gives the linear system

$$\begin{pmatrix} 1 & 0 & 0 & A_{pesk} C_{a,O_2} \\ 0 & 1 & -1 & -R_p \\ 0 & 0 & \mu_\ell(H) & -\nu_\ell(H) \\ c_{vs} & c_{ap} & c_{vp} & 0 \end{pmatrix} \begin{pmatrix} P_{vs} \\ P_{ap} \\ P_{vp} \\ F \end{pmatrix} = \begin{pmatrix} P_{as} + A_{pesk} M_T \\ 0 \\ 0 \\ V_{tot} - c_{as} P_{as} \end{pmatrix}$$

for P_{vs}, P_{ap}, P_{vp}, and F as functions of H, where we have set

$$\nu_\ell(H) = a_\ell(H) P_{as} + \lambda_\ell(H).$$

Defining

$$\tilde{D} = -c_{vs}\mu_\ell(H) A_{pesk} C_{a,O_2} + c_{ap}(\nu_\ell(H) + \mu_\ell(H) R_p) + c_{vp}\nu_\ell(H),$$

we obtain the solution

$$\begin{aligned} P_{vs}(H) &= \frac{1}{\tilde{D}}\Big(\big(c_{ap}(\nu_\ell(H) + \mu_\ell(H)R_p) + c_{vp}\nu_\ell(H)\big)(P_{as} + A_{pesk}M_T) \\ &\qquad - \mu_\ell(H)(V_{tot} - c_{as}P_{as})A_{pesk}C_{a,O_2}\Big), \\ P_{ap}(H) &= \frac{1}{\tilde{D}}\big(\nu_\ell(H) + \mu_\ell(H)R_p\big)\big(V_{tot} - c_{as}P_{as} - c_{vs}(P_{as} + A_{pesk}M_T)\big), \\ P_{vp}(H) &= \frac{1}{\tilde{D}}\nu_\ell(H)\big(V_{tot} - c_{as}P_{as} - c_{vs}(P_{as} + A_{pesk}M_T)\big), \\ F(H) &= \frac{1}{\tilde{D}}\mu_\ell(H)\big(V_{tot} - c_{as}P_{as} - c_{vs}(P_{as} + A_{pesk}M_T)\big). \end{aligned} \tag{A.1}$$

Finally, (1.41) implies

$$a_r(H)F(H)P_{ap}(H) - \mu_r(H)P_{vs}(H) + \lambda_r(H)F(H) = 0, \tag{A.2}$$

which is a nonlinear equation for H. Once we have computed H from (A.2), we get P_{vs}, P_{ap}, P_{vp}, and F from (A.1), R_s from (1.43), and S_ℓ, S_r from (1.37).

A.2 The Jacobian of $\mathcal{F}(x, p, W, 0)$ with Respect to x

We recall first that

$$x = \left(P_{as}, P_{vs}, P_{ap}, S_\ell, \sigma_\ell, S_r, \sigma_r, R_s, H\right)^T,$$

and that the coordinates of $\mathcal{F}(x, p, W, 0)$ are given by (1.34) with $u(t) \equiv 0$. We set

$$a_{ij} = \frac{\partial \mathcal{F}_i}{\partial x_j}(x, p, W, 0), \quad i, j = 1, \ldots, 9,$$

and get

$$a_{11} = \frac{1}{c_{as}}\left(\frac{\partial Q_\ell}{\partial P_{as}} - \frac{1}{R_s}\right), \qquad a_{12} = \frac{1}{c_{as}}\left(\frac{\partial Q_\ell}{\partial P_{vs}} + \frac{1}{R_s}\right),$$

$$a_{13} = \frac{1}{c_{as}}\frac{\partial Q_\ell}{\partial P_{ap}}, \qquad a_{14} = \frac{1}{c_{as}}\frac{\partial Q_\ell}{\partial S_\ell},$$

$$a_{15} = a_{16} = a_{17} = 0, \qquad a_{18} = \frac{P_{as} - P_{vs}}{c_{as}R_s^2}, \quad a_{19} = \frac{1}{c_{as}}\frac{\partial Q_\ell}{\partial H},$$

$$a_{21} = \frac{1}{c_{vs}R_s}, \qquad a_{22} = -\frac{1}{c_{vs}}\left(\frac{1}{R_s} + \frac{\partial Q_r}{\partial P_{vs}}\right),$$

$$a_{23} = -\frac{1}{c_{vs}}\frac{\partial Q_r}{\partial P_{ap}}, \qquad a_{24} = a_{25} = 0,$$

$$a_{26} = -\frac{1}{c_{vs}}\frac{\partial Q_r}{\partial S_r}, \qquad a_{27} = 0,$$

$$a_{28} = -\frac{P_{as} - P_{vs}}{c_{vs}R_s^2}, \qquad a_{29} = -\frac{1}{c_{vs}}\frac{\partial Q_r}{\partial H},$$

$$a_{31} = -\frac{c_{as}}{c_{ap}c_{vp}R_p}, \qquad a_{32} = \frac{1}{c_{ap}}\left(\frac{\partial Q_r}{\partial P_{vs}} - \frac{c_{vs}}{c_{vp}R_p}\right),$$

$$a_{33} = \frac{1}{c_{ap}}\frac{\partial Q_r}{\partial P_{ap}} - \frac{1}{c_{ap}R_p}\left(1 + \frac{c_{ap}}{c_{vp}}\right), \qquad a_{34} = a_{35} = 0,$$

$$a_{36} = \frac{1}{c_{ap}}\frac{\partial Q_r}{\partial S_r}, \quad a_{37} = a_{38} = 0, \qquad a_{39} = \frac{1}{c_{ap}}\frac{\partial Q_r}{\partial H},$$

$$a_{41} = a_{42} = a_{43} = a_{44} = 0, \quad a_{45} = 1, \quad a_{46} = a_{47} = a_{48} = a_{49} = 0,$$

$$a_{51} = a_{52} = a_{53} = 0, \quad a_{54} = -\alpha_\ell, \quad a_{55} = -\gamma_\ell,$$
$$a_{56} = a_{57} = a_{58} = 0, \quad a_{59} = \beta_\ell,$$

$$a_{61} = a_{62} = a_{63} = a_{64} = a_{65} = a_{66} = 0, \quad a_{67} = 1, \quad a_{68} = a_{69} = 0,$$

$$a_{71} = a_{72} = a_{73} = a_{74} = a_{75} = 0, \quad a_{76} = -\alpha_r, \quad a_{77} = -\gamma_r, \quad a_{78} = 0,$$
$$a_{79} = \beta_r,$$

$$a_{81} = \frac{1}{K}\Big(\frac{A_{\text{pcsk}} C_{a,O_2}}{R_s} - 1\Big), \qquad a_{82} = \frac{1}{K}\Big(1 - \frac{A_{\text{pcsk}} C_{a,O_2}}{R_s}\Big),$$

$$a_{83} = a_{84} = a_{85} = a_{86} = a_{87} = 0, \qquad a_{88} = -\frac{A_{\text{pcsk}} C_{a,O_2}(P_{as} - P_{vs})}{K R_s^2},$$

$$a_{89} = 0,$$

$$a_{91} = a_{92} = a_{93} = a_{94} = a_{95} = a_{96} = a_{97} = a_{98} = a_{99} = 0.$$

Next, we have to compute the derivatives of Q_ℓ and Q_r (see (1.35) for the definition of Q_ℓ and Q_r),

$$\frac{\partial Q_\ell}{\partial P_{as}} = \frac{c_\ell a_\ell(H) H S_\ell}{c_{vp}} \cdot \frac{a_\ell(H)\big(c_{vs} P_{vs} + c_{ap} P_{ap} - V_{tot}\big) - c_{as} k_\ell(H) S_\ell}{\big(a_\ell(H) P_{as} + k_\ell(H) S_\ell\big)^2},$$

$$\frac{\partial Q_\ell}{\partial P_{vs}} = -\frac{c_\ell c_{vs}}{c_{vp}} \cdot \frac{a_\ell(H) H S_\ell}{a_\ell(H) P_{as} + k_\ell(H) S_\ell},$$

$$\frac{\partial Q_\ell}{\partial P_{ap}} = -\frac{c_\ell c_{ap}}{c_{vp}} \cdot \frac{a_\ell(H) H S_\ell}{a_\ell(H) P_{as} + k_\ell(H) S_\ell},$$

$$\frac{\partial Q_\ell}{\partial S_\ell} = \frac{c_\ell a_\ell(H)^2 H\big(V_{tot} - c_{as} P_{as} - c_{vs} P_{vs} - c_{ap} P_{ap}\big) P_{as}}{c_{vp}\big(a_\ell(H) P_{as} + k_\ell(H) S_\ell\big)^2},$$

$$\frac{\partial Q_\ell}{\partial H} = \frac{c_\ell S_\ell\big(V_{tot} - c_{as} P_{as} - c_{vs} P_{vs} - c_{ap} P_{ap}\big)}{c_{vp}\big(a_\ell(H) P_{as} + k_\ell(H) S_\ell\big)^2}$$
$$\times \Big(a_\ell(H)^2 (P_{as} - S_\ell) + S_\ell\Big(1 - k_\ell(H)\Big(1 - \frac{H}{c_\ell R_\ell} t_d'(H)\Big)\Big)\Big),$$

$$\frac{\partial Q_r}{\partial P_{vs}} = H \frac{c_r a_r(H) S_r}{a_r(H) P_{ap} + k_r(H) S_r},$$

$$\frac{\partial Q_r}{\partial P_{ap}} = -H\frac{c_r a_r(H)^2 P_{vs} S_r}{\big(a_r(H)P_{ap} + k_r(H)S_r\big)^2},$$

$$\frac{\partial Q_r}{\partial S_r} = H\frac{c_r a_r(H)^2 P_{vs} P_{ap}}{\big(a_r(H)P_{ap} + k_r(H)S_r\big)^2},$$

$$\frac{\partial Q_r}{\partial H} = \frac{c_r P_{vs} S_r}{\big(a_r(H)P_{ap} + k_r(H)S_r\big)^2} \times \Big(a_r(H)^2(P_{ap} - S_r) + S_r\Big(1 - k_r(H)\Big(1 - \frac{H}{c_r R_r}t_d'(H)\Big)\Big)\Big),$$

where we have used

$$k_\ell'(H) = -\frac{1}{c_\ell R_\ell}k_\ell(H)t_d'(H), \quad k_r'(H) = -\frac{1}{c_r R_r}k_r(H)t_d'(H),$$
$$t_d'(H) = \frac{1}{H^2}\Big(\frac{\kappa}{2}H^{1/2} - 1\Big).$$

A.3 Sensitivity with Respect to a Variable

Let the variable y be a function of the variable x,

$$y = y(x), \quad x \in D,$$

where D is some open interval and y is differentiable on D. Let $x_0 \in D$ be given and assume that $x_0 \neq 0$, $y_0 = y(x_0) \neq 0$. Corresponding to Δx with $x_0 + \Delta x \in D$, we define $\Delta y = y(x_0 + \Delta x) - y(x_0)$. In view of our assumption on x_0 and y_0, it makes sense to consider the relative errors $\Delta x/x_0$ and $\Delta y/y_0$. The *sensitivity* $\sigma_{y,x}(x_0)$ of y with respect to x at x_0 is defined by

$$\sigma_{y,x}(x_0) = \lim_{\Delta x \to 0}\frac{\Delta y/y_0}{\Delta x/x_0}.$$

A simple computation gives

$$\sigma_{y,x}(x_0) = \frac{x_0}{y_0}y'(x_0). \tag{A.3}$$

From the definition of $\sigma_{y,x}$, it is easily seen that the sensitivity is invariant against changes of units for x or y. In case of $y(x) = cx^r$, $x \in \mathbb{R}$, with some constants $c, r \in \mathbb{R}$, we immediately get from (A.3)

$$\sigma_{y,x}(x_0) = r \quad \text{for all } x_0 \neq 0.$$

If a third variable z is given by $z = z(x) = y(x)x$, $x \in D$, then an easy calculation using (A.3) shows

$$\sigma_{z,x}(x_0) = 1 + \sigma_{y,x}(x_0).$$

A.4 Generalized Sensitivity Functions

In Thomaseth and Cobelli (1999), the authors proposed a type of sensitivity function, which provides information on the relevance of measurements of output variables of a system for the identification of certain parameters. In other words, generalized sensitivity functions describe the sensitivity of parameter estimates with respect to measurements. Following the presentation in Thomaseth and Cobelli (1999), we consider a single output system where the output of the model is given by

$$y(t) = f(t, \theta), \quad 0 \le t \le T,$$

where $\theta = \mathrm{col}(\theta_1, \ldots, \theta_p)$ is the vector of the model parameters and f is a sufficiently smooth function. At times

$$0 \le t_1 < \cdots < t_M \le T,$$

we have measurements ξ_k corresponding to the model outputs $y(t_k)$, $k = 1, \ldots, M$. We assume that the measurements have the form

$$\xi_k = z(t_k) + e_k, \quad k = 1, \ldots, M,$$

where $z(t)$, $0 \le t \le T$, is the "true" output of the system and e_k is the measurement noise for the measurement ξ_k. We impose the following conditions on the e_k's:

(i) e_k has zero mean, $k = 1, \ldots, M$.

(ii) The e_k's are identically distributed.

(iii) The variance σ_k^2 of e_k is not dependent on θ.

We introduce the vectors

$$\begin{aligned} \xi &= \mathrm{col}(\xi_1, \ldots, \xi_M), \\ F(\theta) &= \mathrm{col}(f(t_1, \theta), \ldots, f(t_M, \theta), \\ e &= \mathrm{col}(e_1, \ldots, e_k), \end{aligned}$$

in $\mathbb{R}^M$. It will be convenient (but, in general, not realistic) to assume that there exists a unique θ_0 such that

$$z(t_k) = f(t_k, \theta_0), \quad k = 1, \ldots, M.$$

Note that we do not assume that $z(t) = f(t, \theta_0)$ for all $t \in [0, T]$. Under this assumption we have

$$\xi = F(\theta_0) + e.$$

In order to measure the deviation between the model output and the measurements we introduce the functional

$$J(x, \theta) = \big(x - F(\theta)\big)^{\mathsf{T}} D\big(x - F(\theta)\big), \quad x \in \mathbb{R}^M, \ \theta \in \mathbb{R}^p, \tag{A.4}$$

where

$$D = \mathrm{diag}\Big(\frac{1}{\sigma_1^2}, \ldots, \frac{1}{\sigma_M^2}\Big).$$

We assume that

(iv) for any θ in a neighborhood of θ_0, the functional $\tau \to J(F(\theta) + e, \tau)$ has a unique minimum.

This assumption amounts to unique local identifiability. Then, for any θ in a neighborhood of θ_0, the estimate $\hat{\theta} = \hat{\theta}(\theta)$ is obtained as

$$\hat{\theta}(\theta) = \operatorname*{argmin}_{\tau} J(\xi, \tau), \quad \xi = F(\theta) + e.$$

Note that, for any θ in a neighborhood of θ_0, $\hat{\theta}(\theta)$ is a random variable. In view of assumption (iv) the estimate $\hat{\theta}(\theta)$ satisfies[15]

$$h(\theta) = \nabla_\tau J(F(\theta) + e, \tau)\big|_{\tau=\hat{\theta}(\theta)} = 0, \tag{A.5}$$

$$H(\theta) = \nabla_{\tau\tau} J(F(\theta) + e, \tau)\big|_{\tau=\hat{\theta}(\theta)} \text{ is positive definite.} \tag{A.6}$$

Using $\xi = F(\theta) + e$ and (A.4) we get

$$h(\theta) = -2F_\theta(\hat{\theta}(\theta))^\mathsf{T} D\big(F(\theta) + e - F(\hat{\theta}(\theta))\big),$$
$$H(\theta) = 2F_\theta(\hat{\theta}(\theta))^\mathsf{T} DF_\theta(\hat{\theta}(\theta)) - 2F_{\theta\theta}(\hat{\theta}(\theta))^\mathsf{T} D\big(F(\theta) + e - F(\hat{\theta}(\theta))\big).$$

We are interested in the Jacobian $\partial\hat{\theta}/\partial\theta$. For θ in a neighborhood of θ_0 we have (see (A.5)) $h(\theta) \equiv 0$, which implies $h'(\theta) \equiv 0$ or—after some computations—

$$H(\theta)\frac{\partial\hat{\theta}}{\partial\theta} = F_\theta(\hat{\theta}(\theta))^\mathsf{T} DF_\theta(\theta). \tag{A.7}$$

From (A.6) we see that $H(\theta)$ is invertible. We impose the following assumption concerning the estimates $\hat{\theta}(\theta)$:

(v) The estimates $\hat{\theta}(\theta)$ are unbiased, i.e., we have $\mathrm{E}\big(x\hat{\theta}(\theta)\big) = \theta$, for θ in a neighborhood of θ_0.

Taking expected values in (A.7) we get (observe $\mathrm{E}(e) = 0$)

$$\mathrm{E}\Big(\frac{\partial\hat{\theta}(\theta)}{\partial\theta}\Big) \approx \Big(F_\theta(\theta)^\mathsf{T} DF_\theta(\theta)\Big)^{-1} F_\theta(\theta)^\mathsf{T} DF_\theta(\theta) \equiv I. \tag{A.8}$$

The explicit form of the matrix $F_\theta(\theta)^\mathsf{T} DF_\theta(\theta)$ is

$$F_\theta(\theta)^\mathsf{T} DF_\theta(\theta) = \sum_{k=1}^{M} \frac{1}{\sigma_k^2}\Big(\frac{\partial f(t_k, \theta)}{\partial\theta_i} \cdot \frac{\partial f(t_k, \theta)}{\partial\theta_j}\Big)_{i,j=1,\dots,p}$$
$$= \sum_{k=1}^{M} \frac{1}{\sigma_k^2}\big(\nabla_\theta f(t_k, \theta)\big)^\mathsf{T} \nabla_\theta f(t_k, \theta).$$

[15] $\nabla_\theta J(\xi, \hat{\theta}) = (\partial J(\xi, \hat{\theta})/\partial\theta_1, \dots, \partial J(\xi, \hat{\theta})/\partial\theta_p) \in \mathbb{R}^{1\times p}$.

Note that we consider $\nabla_\theta f$ to be a row vector. Equation (A.8) now can be written as

$$\mathrm{E}\Big(\frac{\partial\hat{\theta}(\theta)}{\partial\theta}\Big) \approx \sum_{k=1}^{M} \frac{1}{\sigma_k^2}\Bigg(\Big(\sum_{j=1}^{M}\frac{1}{\sigma_j^2}\big(\nabla_\theta f(t_j,\theta)\big)^{\mathrm{T}}\nabla_\theta f(t_j,\theta)\Big)^{-1} \times \big(\nabla_\theta f(t_k,\theta)\big)^{\mathrm{T}}\Bigg)\nabla_\theta f(t_k,\theta) \equiv I. \tag{A.9}$$

This equation shows that the expected estimate of the ith component $\hat{\theta}_i$ of $\hat{\theta}$ depends, in the first approximation only, on the variation of θ_i (which reflects assumption (v)).

In equation (A.9) all available measurements $\xi_1, \ldots, \xi_M$ are used. It is of interest to consider the case, where the deviations from all measurements still enter the cost functional (A.4), but for some reason we only have access to the measurements $\xi_1, \ldots, \xi_{k_0}$, $1 \le k_0 \le M$, i.e., we can compute the sensitivities with respect to the parameters θ for the measurements $\xi_1, \ldots, \xi_{k_0}$ only. We set

$$\xi^{(k_0)} = \big(\xi_1, \ldots, \xi_{k_0}\big)^{\mathrm{T}}$$

and consider first the estimate $\hat{\theta}$ as a function of the measurements $\xi^{(k_0)}$ (compare also Remark 1 below). Equation (A.5) takes the form $\nabla_\tau J(\xi,\tau)\big|_{\tau=\hat{\theta}} \equiv 0$. Differentiating this equation with respect to $\xi^{(k_0)}$, we obtain

$$\nabla_{\tau\tau}J(\xi,\tau)\big|_{\tau=\hat{\theta}}\frac{\partial\hat{\theta}}{\partial\xi^{(k_0)}} + \nabla_{\xi^{(k_0)},\theta}J(\xi,\tau)\big|_{\tau=\hat{\theta}} \equiv 0,$$

which implies (using the chain rule)

$$\nabla_{\tau\tau}J(\xi,\tau)\big|_{\tau=\hat{\theta}}\frac{\partial\hat{\theta}}{\partial\theta} + \nabla_{\xi^{(k_0)},\theta}J(\xi,\tau)\big|_{\tau=\hat{\theta}}\frac{\partial\xi^{(k_0)}}{\partial\theta} \equiv 0. \tag{A.10}$$

Simple computations show

$$\begin{aligned}\nabla_{\tau\tau}J(\xi,\tau) &= 2F_\tau(\tau)^{\mathrm{T}}DF_\tau(\tau) - 2F_{\tau\tau}(\tau)^{\mathrm{T}}D\big(\xi - F(\tau)\big),\\ \nabla_{\xi^{(k_0)},\tau}J(\xi,\tau) &= -2F_\tau(\tau)^{\mathrm{T}}DI_{k_0},\end{aligned}$$

where I_{k_0} is the $M \times k_0$-matrix with elements $\alpha_{i,i} = 1$, $i = 1, \ldots, k_0$, and $\alpha_{i,j} = 0$ for $i \neq j$. Taking expected values in (A.10) and proceeding as above in the case where we had access to all measurements, we obtain

$$\mathrm{E}\Big(\frac{\partial\hat{\theta}}{\partial\theta}\Big) \approx -\big(\nabla_{\theta\theta}J(F(\theta),\theta)\big)^{-1}\nabla_{\xi^{(k_0)}\theta}J(F(\theta),\theta)\frac{\partial\xi^{(k_0)}}{\partial\theta}. \tag{A.11}$$

Using the explicit expressions for $\nabla_{\tau\tau} J(\xi, \tau)$ and $\nabla_{\xi^{(k_0)}\tau} J(\xi, \tau)$ as given above, we can write (A.11) as

$$\begin{aligned} \mathrm{E}\Big(\frac{\partial\hat{\theta}}{\partial\theta}\Big) &\approx \sum_{k=1}^{k_0} \frac{1}{\sigma_k^2} \Bigg(\Big(\sum_{j=1}^{M} \frac{1}{\sigma_j^2} \big(\nabla_\theta f(t_j,\theta)\big)^{\mathrm{T}} \nabla_\theta f(t_j,\theta) \Big)^{-1} \\ &\qquad \times \big(\nabla_\theta f(t_k,\theta)\big)^{\mathrm{T}} \Bigg) \nabla_\theta f(t_k,\theta) \\ &= \Bigg(\sum_{j=1}^{M} \frac{1}{\sigma_j^2} \big(\nabla_\theta f(t_j,\theta)\big)^{\mathrm{T}} \nabla_\theta f(t_j,\theta) \Bigg)^{-1} \\ &\qquad \times \sum_{k=1}^{k_0} \frac{1}{\sigma_k^2} \big(\nabla_\theta f(t_k,\theta)\big)^{\mathrm{T}} \nabla_\theta f(t_k,\theta). \end{aligned} \tag{A.12}$$

If the components of the parameter vector θ are completely independent, then the matrices $\mathrm{E}(\partial\hat{\theta}/\partial\theta)$, as given in (A.12) for $k_0 = 1, \ldots, M$, are diagonal matrices. In general, however, this is not the case. But it still motivates us to consider the elements in the main diagonal and to define the *generalized sensitivity function* $g_i(t_{k_0})$ with respect to the parameter θ_i at the time instant t_{k_0} to be the ith element in the main diagonal of the matrix given in (A.12); i.e., for θ in a neighborhood of θ_0 we have

$$\begin{aligned} g_i(t_{k_0}) = \sum_{k=1}^{k_0} \frac{1}{\sigma_k^2} \Bigg(\Bigg(\sum_{j=1}^{M} \frac{1}{\sigma_j^2} \big(\nabla_\theta f(t_j,\theta)\big)^{\mathrm{T}} \nabla_\theta f(t_j,\theta) \Bigg)^{-1} \\ \times \big(\nabla_\theta f(t_k,\theta)\big)^{\mathrm{T}} \Bigg)_i \big(\nabla_\theta f(t_k,\theta)\big)_i. \end{aligned} \tag{A.13}$$

Equation (A.12) implies that $g_i(t_M) = 1$, $i = 1, \ldots, p$. Therefore, it is meaningful to define $g_i(t) = 0$ for $t < t_1$ and $g_i(t) = 1$ for $t \geq t_M$.

We also introduce the *incremental generalized sensitivity function* $g_{\mathrm{inc},i}(\cdot)$ by

$$g_{\mathrm{inc},i}(t_{k_0}) = g_i(t_{k_0}) - g_i(t_{k_0-1}), \quad k_0 = 1, \ldots, M.$$

Using the representation of $g_i(\cdot)$ from above, we get

$$\begin{aligned} g_{\mathrm{inc},i}(t_{k_0}) = \frac{1}{\sigma_{k_0}^2} \Bigg(\Bigg(\sum_{j=1}^{M} \frac{1}{\sigma_j^2} \big(\nabla_\theta f(t_j,\theta)\big)^{\mathrm{T}} \nabla_\theta f(t_j,\theta) \Bigg)^{-1} \\ \times \big(\nabla_\theta f(t_{k_0},\theta)\big)^{\mathrm{T}} \Bigg)_i \big(\nabla_\theta f(t_{k_0},\theta)\big)_i, \\ k_0 = 1, \ldots, M,\ i = 1, \ldots, p. \end{aligned} \tag{A.14}$$

Assuming that the measurement noise is normally distributed, we can compute the Fisher information matrix as (see, for instance, Seber and Wild, 1989)

$$\mathcal{J}(\theta) = \sum_{j=1}^{M} \frac{1}{\sigma_j^2} \big(\nabla_\theta f(t_j, \theta)\big)^{\mathrm{T}} \nabla_\theta f(t_j, \theta) \eta_j, \tag{A.15}$$

where η_j is the weight for the measurement ξ_j at time t_j. We choose $\eta_j = 1$, $j = 1, \ldots, M$. The information on the parameters provided by the measurement ξ_j is quantified by the derivative of an information index with respect to η_j. A frequently used information index is $\ln \det \mathcal{J}(\theta)$. Let $a_j^{(i)} = \big(a_j^{(i,1)}, \ldots, a_j^{(i,p)}\big)$ denote the ith row of the matrix $\big(\nabla_\theta f(t_j, \theta)\big)^{\mathrm{T}} \nabla_\theta f(t_j, \theta)/\sigma_j^2$, $i = 1, \ldots, p$. Then the derivative of $\det \mathcal{J}(\theta)$ is given by

$$\frac{\partial}{\partial \eta_k} \det \mathcal{J}(\theta) = \sum_{i=1}^{p} \det \mathcal{J}_i(\theta),$$

where

$$\mathcal{J}_i(\theta) = \operatorname{col}\left(\sum_{\ell=1}^{M} a_\ell^{(1)} \eta_\ell, \ldots, \sum_{\ell=1}^{M} a_\ell^{(i-1)} \eta_\ell, a_k^{(i)}, \sum_{\ell=1}^{M} a_\ell^{(i+1)} \eta_\ell, \ldots, \sum_{\ell=1}^{M} a_\ell^{(p)} \eta_\ell \right).$$

We denote by $\hat{A}$ the adjoint matrix for $\mathcal{J}(\theta)$, i.e., $\hat{A} = \big(\det \mathcal{J}(\theta)\big)\, \mathcal{J}(\theta)^{-1}$. Expansion of the determinants with respect to the ith rows yields

$$\frac{\partial}{\partial \eta_k} \det \mathcal{J}(\theta) = \sum_{i=1}^{p} \sum_{j=1}^{p} a_k^{(i,j)} \hat{A}_{i,j}.$$

Observing $a_k^{(i,j)} = \sigma_k^{-2} \big(\partial f(t_k, \theta)/\partial \theta_i\big) \big(\partial f(t_k, \theta)/\partial \theta_j\big)$, we get

$$\begin{aligned} \frac{\partial}{\partial \eta_k} \det \mathcal{J}(\theta) &= \frac{1}{\sigma_k^2} \sum_{i=1}^{p} \sum_{j=1}^{p} \frac{\partial f(t_k, \theta)}{\partial \theta_i} \cdot \frac{\partial f(t_k, \theta)}{\partial \theta_j} \hat{A}_{i,j} \\ &= \frac{\det \mathcal{J}(\theta)}{\sigma_k^2} \nabla_\theta f(t_k, \theta) \mathcal{J}(\theta)^{-1} \big(\nabla_\theta f(t_k, \theta)\big)^{\mathrm{T}}. \end{aligned}$$

This implies

$$\begin{aligned} \frac{\partial}{\partial \eta_k} \ln \det \mathcal{J}(\theta) &= \frac{1}{\det \mathcal{J}(\theta)} \frac{\partial}{\partial \eta_k} \det \mathcal{J}(\theta) \\ &= \frac{1}{\sigma_k^2} \nabla_\theta f(t_k, \theta) \mathcal{J}(\theta)^{-1} \big(\nabla_\theta f(t_k, \theta)\big)^{\mathrm{T}}. \end{aligned} \tag{A.16}$$

Comparing (A.14) and (A.16), we see that

$$\frac{\partial}{\partial \eta_k} \ln \det \mathcal{J}(\theta) = \sum_{i=1}^{p} g_{\mathrm{inc},i}(t_k). \tag{A.17}$$

Remarks. 1. We can write (A.7) also as

$$\left(H(\theta) \frac{\partial \hat{\theta}}{\partial \xi} - F_\theta(\hat{\theta}(\theta))^T D \right) \frac{\partial \xi}{\partial \theta} \equiv 0.$$

This implies

$$E\left(\frac{\partial \hat{\theta}}{\partial \xi} \right) \approx \left(F_\theta(\theta)^T D F_\theta(\theta) \right)^{-1} F_\theta(\theta)^T D$$

and

$$E\left(\frac{\partial \hat{\theta}(\theta)}{\partial \theta} \right) \approx E\left(\frac{\partial \hat{\theta}(\theta)}{\partial \xi} \right) \cdot \frac{\partial \xi(\theta)}{\partial \theta},$$

which is (A.8). This shows that we have computed the sensitivity of the parameter estimate $\hat{\theta}$, with respect to changes in the "true" parameters θ, as the composition of the sensitivity of the parameter estimate $\hat{\theta}$ with respect to the output ξ of the system and the sensitivity of ξ with respect to θ.

2. The Fisher information matrix is positive semidefinite. Thus, (A.17) shows that

$$\sum_{i=1}^{p} g_{\text{inc},i}(t_k) \geq 0, \quad k = 1, \ldots, M, \tag{A.18}$$

which implies that $\left(\sum_{i=1}^{p} g_i(t_k) \right)_{k=1,\ldots,M}$ is an increasing sequence.

3. Equation (A.17) also indicates that the incremental generalized sensitivities at a time t_k reflect the distribution onto the individual parameters of the information provided by the measurement ξ_k.

4. We assume that the parameter identification procedure considered is not only unbiased, but also efficient; i.e., the covariance of the estimates $\operatorname{Cov} \hat{\theta}$ equals the Cramer–Rao (lower) bound (see Goodwin and Payne, 1977),

$$\operatorname{Cov} \hat{\theta} = \mathcal{J}(\hat{\theta})^{-1}. \tag{A.19}$$

5. The generalized sensitivity functions g_i are, in general, not monotonically increasing for $k = 1, \ldots, M$ (compare Remark 2). However, a comparison between (A.19), (A.13), and (A.15) indicates that in case of independent parameters, the individual generalized sensitivity functions are monotonically increasing. In this case the measurements in that time interval, where the generalized sensitivity function of a parameter has most of its increase from zero to one, are the measurements which carry most of the information on that parameter. Examples show that this interval can be considerably shorter than the time interval for all measurements. In cases where the parameters are rather strongly correlated, we see considerable oscillations in the generalized sensitivity functions.

Many of the facts given above are demonstrated in Section 1.7 for the basic model of the cardiovascular system.

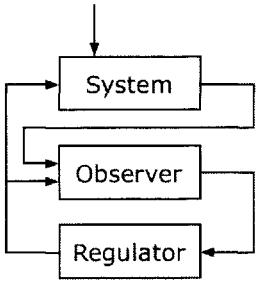

Appendix B

A Nonlinear Feedback Law

In this appendix we describe another possibility for constructing a feedback law for the cardiovascular model described in Chapter 1. This approach is based on results in the nonlinear systems theory concerned with systems which are linear in the controls (see Isidori, 1995).

B.1 The Relative Degree of a System

Given the mappings $f, g : \mathbb{R}^n \to \mathbb{R}^n$ and $h : \mathbb{R}^n \to \mathbb{R}$, we consider single-input single-output control systems of the form

$$\begin{aligned} \dot{x} &= f(x) + g(x)u(t), \\ y &= h(x). \end{aligned} \tag{B.1}$$

In order to define the relative degree of system (B.1), we have to consider the derivative of h along f,

$$\big(L_f h\big)(x) := \sum_{i=1}^{n} \frac{\partial h}{\partial x_i}(x) f_i(x) =: \frac{\partial h}{\partial x}(x) f(x), \quad x \in \mathbb{R}^n.$$

Note that $L_f h$ is a mapping $\mathbb{R}^n \to \mathbb{R}$. Analogously, we define the derivative of h along g. The derivatives L_f^k, $k = 1, 2, \ldots$, are defined recursively by

$$\big(L_f^k h\big)(x) = \frac{\partial L_f^{k-1} h}{\partial x}(x) f(x), \quad x \in \mathbb{R}^n.$$

Assume that the functions f, g, and h are sufficiently smooth. The relative degree of system (B.1), at some point $x_0 \in \mathbb{R}^n$, is r if and only if the following two conditions are satisfied:

(i) $\left(L_g L_f^k h\right)(x) = 0$ for all x in a neighborhood of x_0 and all $k = 0, \ldots, r-2$.

(ii) $\left(L_g L_f^{r-1} h\right)(x_0) \neq 0$.

Note that the relative degree of system (B.1) at a point x_0 may not exist. In case $r = 1$, conditions (i) and (ii) reduce to

$$(L_g h)(x_0) \neq 0.$$

In order to show the meaning of the relative degree, we assume that $x_0 = x(t_0)$, where $x(t)$ is a solution of (B.1) corresponding to a control $u(t)$ existing in a neighborhood of t_0. The control $u(t)$ does not show up explicitly at the output, $y(t) = h(x(t))$. Differentiating $y(t)$, we obtain

$$\begin{aligned}\dot{y}(t) &= \frac{\partial h}{\partial x}(x(t))\dot{x}(t) = \frac{\partial h}{\partial x}(x(t))\big(f(x(t)) + g(x(t))u(t)\big)\\ &= (L_f h)(x(t)) + (L_g h)(x(t))u(t).\end{aligned}$$

If the relative degree of the system at x_0 is $r = 1$, then

$$\dot{y}(t_0) = (L_f h)(x_0) + (L_g h)(x_0)u(t_0), \quad \text{where } (L_g h)(x_0) \neq 0;$$

i.e., the control $u(t_0)$ shows up explicitly in the first derivative of the output at t_0. If $r \geq 2$, then

$$\dot{y}(t) = (L_f h)(x(t)) \quad \text{for } t \text{ in a neighborhood of } t_0,$$

and we get

$$\ddot{y}(t) = (L_f^2 h)(x(t)) + (L_g L_f h)(x(t))u(t).$$

If $r = 2$, then $(L_g L_f h)(x_0) \neq 0$, and we see that $u(t_0)$ shows up explicitly in $\ddot{y}(t_0)$. Continuing in this way we arrive at the following result.

If the relative degree of (B.1) *is* $r \geq 1$, *then*

$$y^{(k)}(t) = \big(L_f^k h\big)(x(t))$$

for all $k = 0, \ldots, r-1$ *and all* t *in a neighborhood of* t_0, *and*

$$y^{(r)}(t) = \big(L_f^r h\big)(x(t)) + \big(L_g L_f^{r-1} h\big)(x(t))u(t).$$

In particular, for $t = t_0$, *we have* $(L_g L_f^{r-1} h)(x_0) \neq 0$; *i.e.,* $u(t_0)$ *shows up explicitly in* $y^{(r)}(t_0)$.

B.2 A Nonlinear Coordinate Transform

Let the relative degree of (B.1) at x_0 be $r \geq 1$. Then the functions h, $L_f h, \ldots, L_f^{r-1} h$ can be used as the first r functions of a local coordinate transformation in a neighborhood of x_0. This follows from the following result (see Isidori, 1995, Lemma 4.1.1 and Proposition 4.1.3).

The row vectors

$$\frac{\partial h}{\partial x}(x_0), \ \frac{\partial L_f h}{\partial x}(x_0), \ldots, \ \frac{\partial L_f^{r-1} h}{\partial x}(x_0)$$

are linearly independent.

Suppose that system (B.1) *has relative degree* $r \geq 1$ *at* x_0. *Then the following are true.*

(a) $r \leq n$.

(b) *We set*

$$\phi_i(x) = L_f^{i-1}h(x), \quad i = 1, \ldots, r.$$

If $r = n$, *then the Jacobian of the mapping*

$$\Phi(x) := \big(\phi_1(x), \ldots, \phi_n(x)\big)^{\mathsf{T}} \tag{B.2}$$

is nonsingular in a neighborhood of x_0. In case $r < n$, it is always possible to find $n - r$ functions $\phi_{r+1}(x), \ldots, \phi_n(x)$ such that the Jacobian of the mapping (B.2) is nonsingular at x_0. Moreover, we can choose $\phi_{r+1}(x), \ldots, \phi_n(x)$ such that $L_g\phi_i(x) = 0$ for $i = r + 1, \ldots, n$ and all x in a neighborhood of x_0.

This result shows that

$$z = \Phi(x) \tag{B.3}$$

defines a coordinate transformation in a neighborhood of x_0.

Next, we compute the control system, which we get from (B.1), by applying the coordinate transformation (B.3). Simple computations show

$$\begin{aligned}
\dot{z}_1(t) &= \frac{\partial \phi_1}{\partial x}(x(t))\dot{x}(t) = \frac{\partial h}{\partial x}(x(t))\big(f(x(t)) + g(x(t))u(t)\big) \\
&= L_f h(x(t)) = \phi_2(x(t)) = z_2(t), \\
&\vdots \\
\dot{z}_{r-1}(t) &= \frac{\partial \phi_{r-1}}{\partial x}(x(t))\dot{x}(t) = \frac{\partial L_f^{r-2}h}{\partial x}(x(t))\dot{x}(t) \\
&= \big(L_f^{r-1}h\big)(x(t)) = \phi_r(x(t)) = z_r(t), \\
\dot{z}_r(t) &= \big(L_f^r h\big)(x(t)) + \big(L_g L_f^{r-1}h\big)(x(t))u(t).
\end{aligned}$$

We set

$$\begin{aligned}
a(z) &= \big(L_g L_f^{r-1}h\big)\big(\Phi^{-1}(z)\big), \\
b(z) &= \big(L_f^r h\big)\big(\Phi^{-1}(z)\big).
\end{aligned}$$

Then the last equation can be rewritten as

$$\dot{z}_r(t) = b(z(t)) + a(z(t))u(t).$$

Note that $a(z_0) \neq 0$ for $z_0 = \Phi(x_0)$, by definition. Thus, the coefficient $a(z)$ is also nonzero for all z in a neighborhood of z_0.

Moreover, if $\phi_{r+1}(x), \ldots, \phi_n(x)$ have been chosen such that $L_g\phi_i(x) = 0$ for $i = r + 1, \ldots, n$, then

$$\begin{aligned}
\dot{z}_i(t) &= \frac{\partial \phi_i}{\partial x}(x(t))\big(f(x(t)) + g(x(t))u(t)\big) \\
&= \big(L_f\phi_i\big)(x(t)) + \big(L_g\phi_i\big)(x(t))u(t) = \big(L_f\phi_i\big)(x(t)), \quad i = r + 1, \ldots, n.
\end{aligned}$$

Setting $q_i(z) := \big(L_f\phi_i\big)\big(\Phi^{-1}(z)\big)$, $i = r+1,\dots,n$, we obtain

$$\dot{z}_i(t) = q_i(z(t)), \quad i = r+1,\dots,n.$$

Moreover, we define a new control $v(t)$ by

$$v(t) = b(z(t)) + a(z(t))u(t), \quad \text{respectively} \quad u(t) = \frac{1}{a(z(t))}\big(v(t) - b(z(t))\big).$$

Thus, the coordinate transform (B.3) transforms (B.1) to the following normal form:

$$\frac{d}{dt}\begin{pmatrix} z_1 \\ \vdots \\ \vdots \\ \vdots \\ z_r \end{pmatrix} = \begin{pmatrix} 0 & 1 & 0 & \cdots & 0 \\ \vdots & \ddots & \ddots & \ddots & \vdots \\ \vdots & & \ddots & \ddots & 0 \\ \vdots & & & \ddots & 1 \\ 0 & \cdots & \cdots & \cdots & 0 \end{pmatrix}\begin{pmatrix} z_1 \\ \vdots \\ \vdots \\ \vdots \\ z_r \end{pmatrix} + \begin{pmatrix} 0 \\ \vdots \\ \vdots \\ 0 \\ v(t) \end{pmatrix}, \tag{B.4}$$

$$\begin{aligned} \dot{z}_{r+1} &= q_{r+1}(z), \\ &\vdots \\ \dot{z}_n &= q_n(z), \end{aligned} \tag{B.5}$$

$$y(t) = z_1(t). \tag{B.6}$$

The input-output behavior of the transformed system is completely determined by the linear part (B.4). The nonlinear part (B.5) has no influence on the linear part and the output.

In general, it is not easy to construct $n-r$ functions $\phi_{r+1}(x),\dots,\phi_n(x)$ such that $(L_g\phi_i)(x) = 0$, $i = r+1,\dots,n$, for all x in a neighborhood of x_0, because this amounts to solving a system of $n-r$ partial differential equations. Therefore, one usually chooses the functions $\phi_{r+1}(x),\dots,\phi_n(x)$ with the only property that the Jacobian of $\Phi(x)$ is non-singular at x_0, which is sufficient so that (B.3) defines a coordinate transformation. Instead of (B.5), we get

$$\begin{aligned} \dot{z}_{r+1} &= q_{r+1}(z) + \frac{p_{r+1}(z)}{a(z)}\big(v(t) - b(z)\big), \\ &\vdots \\ \dot{z}_n &= q_n(z) + \frac{p_n(z)}{a(z)}\big(v(t) - b(z)\big), \end{aligned}$$

where

$$\begin{aligned} q_i(z) &:= \big(L_f\phi_i\big)\big(\Phi^{-1}(z)\big), \\ p_i(z) &:= \big(L_g\phi_i\big)\big(\Phi^{-1}(z)\big), \quad i = r+1,\dots,n. \end{aligned}$$

B.3 Construction of the Feedback Law

In this section we construct a feedback law for the nonlinear system (B.3) following the approach given in Isidori (1995, Section 4.2). To start with, we first consider the transformed system (B.4)–(B.6) and choose a linear feedback

$$v = k_0 z_1 + \cdots + k_{r-1} z_r, \quad k_i \in \mathbb{R}.$$

The linear subsystem (B.4), with this control, has the form

$$\frac{d}{dt}\begin{pmatrix} z_1 \\ \vdots \\ \vdots \\ \vdots \\ z_r \end{pmatrix} = \begin{pmatrix} 0 & 1 & 0 & \cdots & 0 \\ \vdots & \ddots & \ddots & \ddots & \vdots \\ \vdots & & \ddots & \ddots & 0 \\ 0 & \cdots & \cdots & 0 & 1 \\ k_0 & k_1 & \cdots & \cdots & k_{r-1} \end{pmatrix} \begin{pmatrix} z_1 \\ \vdots \\ \vdots \\ \vdots \\ z_r \end{pmatrix}.$$

The characteristic polynomial of the system matrix is given by

$$p(\lambda) = (-1)^r \left(\lambda^r - k_{r-1}\lambda^{r-1} - \cdots - k_1\lambda - k_0\right).$$

This tells us that we have to choose the coefficients k_i, $i = 0, \ldots, r-1$, such that the polynomial $p(\lambda)$ has all roots in the left half plane, in order to get a stabilizing feedback control.

Substituting the expressions for $z_1, \ldots, z_r$ and for $a(z)$, $b(z)$, we get the following nonlinear feedback law for system (B.1) in a neighborhood of x_0:

$$u(x) = \frac{-(L_f^r h)(x) + \sum_{i=0}^{r-1} k_i (L_f^i h)(x)}{(L_g L_f^{r-1} h)(x)}. \tag{B.7}$$

Note that we do not need to determine the functions $\phi_{r+1}, \ldots, \phi_n$ in order to compute the nonlinear feedback law (B.7).

B.4 The Nonlinear Feedback Law for the Cardiovascular Model

In this section we show how the construction in the previous sections can be used to construct a nonlinear feedback law for the cardiovascular model presented in Chapter 1.

Since we want to design a control which steers system (1.33) to the equilibrium x^{exer}, we introduce, as in Section 1.4, the coordinate transformation

$$\xi = x - x^{\text{exer}}.$$

This transforms system (1.33) into

$$\begin{aligned} \dot{\xi} &= \mathcal{F}(\xi + x^{\text{exer}}, p^{\text{exer}}, W^{\text{exer}}, u(t)) \\ &= \mathcal{F}(\xi + x^{\text{exer}}, p^{\text{exer}}, W^{\text{exer}}, 0) + (0, \ldots, 0, 1)^{\mathrm{T}} u(t) \end{aligned} \tag{B.8}$$

with the output

$$y(t) = (q_{\text{as}}, 0, \ldots, 0)^{\mathrm{T}}\xi. \tag{B.9}$$

Thus, we have

$$\begin{aligned} f(\xi) &= \mathcal{F}(\xi + x^{\text{exer}}, p^{\text{exer}}, W^{\text{exer}}, 0), \\ g(\xi) &\equiv (0, \ldots, 0, 1)^{\mathrm{T}}, \\ h(\xi) &= (q_{\text{as}}, 0, \ldots, 0)\xi. \end{aligned} \tag{B.10}$$

Simple computations—using also (1.34) and the formulas given in Section A.2 of Appendix A—give the following results:

$$\frac{\partial h}{\partial \xi} \equiv (q_{\text{as}}, 0, \ldots, 0),$$

$$\big(L_f h\big)(\xi) = \frac{\partial h}{\partial \xi}(\xi) f(\xi) = q_{\text{as}} \mathcal{F}_1(\xi + x^{\text{exer}}, p^{\text{exer}}, W^{\text{exer}}, 0), \tag{B.11}$$

$$\big(L_g h\big)(\xi) = \frac{\partial h}{\partial \xi}(\xi) g(\xi) \equiv 0,$$

$$\begin{aligned} \big(L_g L_f h\big)(\xi) &= q_{\text{as}} \frac{\partial \mathcal{F}_1}{\partial H}(x, p^{\text{exer}}, W^{\text{exer}}, 0)\Big|_{x=\xi+x^{\text{exer}}} \\ &= q_{\text{as}} \frac{\partial Q_\ell}{\partial H}(x, p^{\text{exer}})\Big|_{x=\xi+x^{\text{exer}}} \\ &= \frac{q_{\text{as}} c_\ell x_4 \big(V_{\text{tot}} - c_{\text{as}} x_1 - c_{\text{vs}} x_2 - c_{\text{ap}} x_3\big)}{c_{\text{as}} c_{\text{vp}} \big(a_\ell(x_9) x_1 + k_\ell(x_9) x_4\big)^2} \\ &\quad \times \Bigg(a_\ell(x_9)^2 (x_1 - x_4) \\ &\qquad + x_4 \Big(1 - k_\ell(x_9)\Big(1 - \frac{\xi_9}{c_\ell R_\ell} t_d'(\xi_9)\Big)\Big)\Bigg)\Bigg|_{x=\xi+x^{\text{exer}}}. \end{aligned} \tag{B.12}$$

We see that

$$\big(L_g L_f h\big)(0) > 0,$$

provided $P_{\text{as}}^{\text{exer}} > S_\ell^{\text{exer}}$ (compare (1.19)), $P_{\text{vp}}^{\text{exer}} > 0$, and

$$1 - k_\ell(H^{\text{exer}})\Big(1 - \frac{H^{\text{exer}}}{c_\ell R_\ell} t_d'(H^{\text{exer}})\Big) > 0. \tag{B.13}$$

Numerical computations with physiologically meaningful values for the parameters show that condition (B.13) is satisfied for the values of H^{exer} considered in our bicycle ergometer tests. This implies that we have

$$r = 2$$

for system (B.8), (B.9).

The feedback law (B.7) takes the form

$$u(\xi) = \frac{k_0 h(\xi) + k_1 (L_f h)(\xi) - (L_f^2 h)(\xi)}{(L_g L_f h)(\xi)},$$

where $k_0 < 0$ and $k_1 < 0$. For the original system (1.33), we get

$$u(x) = \frac{k_0 h(x - x^{\text{exer}}) + k_1 (L_f h)(x - x^{\text{exer}}) - (L_f^2 h)(x - x^{\text{exer}})}{(L_g L_f h)(x - x^{\text{exer}})}.$$

From (B.10), (B.11), and (B.12), we get

$$\begin{aligned}
h(x - x^{\text{exer}}) &= q_{\text{as}}(P_{\text{as}} - P_{\text{as}}^{\text{exer}}),\\
(L_f h)(x - x^{\text{exer}}) &= \frac{q_{\text{as}}}{c_{\text{as}}}\Big(Q_\ell(x) - \frac{1}{R_{\text{s}}}(P_{\text{as}} - P_{\text{vs}})\Big),\\
(L_g L_f h)(x - x^{\text{exer}}) &= \frac{q_{\text{as}} c_\ell S_\ell \big(V_{\text{tot}} - c_{\text{as}} P_{\text{as}} - c_{\text{vs}} P_{\text{vs}} - c_{\text{ap}} P_{\text{ap}}\big)}{c_{\text{as}} c_{\text{vp}} \big(a_\ell(H) P_{\text{as}} + k_\ell(H) S_\ell\big)^2}\\
&\quad \times \Big(a_\ell(H)^2 (P_{\text{as}} - S_\ell)\\
&\qquad + S_\ell\Big(1 - k_\ell(H)\Big(1 - \frac{H}{c_\ell R_\ell} t_d'(H)\Big)\Big)\Big).
\end{aligned}$$

In addition, we also need

$$\big(L_f^2 h\big)(x - x^{\text{exer}}) = q_{\text{as}} \sum_{i=1}^{9} \frac{\partial \mathcal{F}_1}{\partial x_i}(x) \mathcal{F}_i(x).$$

Using the formulas given in Section A.2 of Appendix A, we get

$$\begin{aligned}
\frac{\partial \mathcal{F}_1}{\partial P_{\text{as}}}(x)\mathcal{F}_1(x) &= \frac{1}{c_{\text{as}}^2}\Big(\frac{\partial Q_\ell}{\partial P_{\text{as}}}(x) - \frac{1}{R_{\text{s}}}\Big)\Big(Q_\ell(x) - \frac{1}{R_{\text{s}}}(P_{\text{as}} - P_{\text{vs}})\Big),\\
\frac{\partial \mathcal{F}_1}{\partial P_{\text{vs}}}(x)\mathcal{F}_2(x) &= \frac{1}{c_{\text{as}} c_{\text{vs}}}\Big(\frac{\partial Q_\ell}{\partial P_{\text{vs}}}(x) + \frac{1}{R_{\text{s}}}\Big)\Big(\frac{1}{R_{\text{s}}}(P_{\text{as}} - P_{\text{vs}} - Q_{\text{r}}(x)\Big),\\
\frac{\partial \mathcal{F}_1}{\partial P_{\text{ap}}}(x)\mathcal{F}_3(x) &= \frac{1}{c_{\text{as}} c_{\text{ap}}} \frac{\partial Q_\ell}{\partial P_{\text{ap}}}(x)\Big(Q_{\text{r}}(x)\\
&\quad - \frac{1}{R_{\text{p}}^{\text{exer}}}\Big(P_{\text{ap}} - \frac{1}{c_{\text{vp}}}\big(V_{\text{tot}} - c_{\text{as}} P_{\text{as}} - c_{\text{vs}} P_{\text{vs}} - c_{\text{ap}} P_{\text{ap}}\big)\Big)\Big),\\
\frac{\partial \mathcal{F}_1}{\partial S_\ell}(x)\mathcal{F}_4(x) &= \frac{1}{c_{\text{as}}} \frac{\partial Q_\ell}{\partial S_\ell}(x)\sigma_\ell,\\
\frac{\partial \mathcal{F}_1}{\partial \sigma_\ell}(x)\mathcal{F}_5(x) &\equiv 0,\\
\frac{\partial \mathcal{F}_1}{\partial S_{\text{r}}}(x)\mathcal{F}_6(x) &\equiv 0,
\end{aligned}$$

$$\frac{\partial \mathcal{F}_1}{\partial \sigma_T}(x)\mathcal{F}_7(x) \equiv 0,$$
$$\frac{\partial \mathcal{F}_1}{\partial R_s}(x)\mathcal{F}_8(x) = \frac{P_{as} - P_{vs}}{c_{as} K R_s^2}\left(A_{pcsk}^{exer}\left(\frac{P_{as} - P_{vs}}{R_s} C_{a,O_2} - M_{tis}^{exer}\right) - P_{as} + P_{vs}\right),$$
$$\frac{\partial \mathcal{F}_1}{\partial H}(x)\mathcal{F}_9(x) \equiv 0.$$

It remains to determine the negative constants k_0 and k_1. One possibility is to define a quadratic cost functional

$$\tilde{J}(v(\cdot)) = \int_0^\infty \left(\rho^2 z_1(t)^2 + v(t)^2\right) dt,$$

where ρ^2 is a weighting factor. Associated with this cost functional, we consider the linear control system

$$\dot{z}_1 = z_2, \quad \dot{z}_2 = v(t), \quad y(t) = z_1(t).$$

The solution of this linear quadratic control problem is a feedback law of the form

$$v(t) = k_0 z_1(t) + k_1 z_2(t).$$

We have $z_1 = q_{as}(P_{as} - P_{as}^{exer})$. However, z_2 is already a very complicated function of the original state variables, and, consequently, so is $v(t)$. Therefore, it is very difficult to give a meaningful interpretation of the weighting factor ρ^2. Compare this with the situation of the linear quadratic problem described in Section 1.4. There, the weighting factor q_{as}^2 describes how much weight is put on the deviations $P_{as}(t) - P_{as}^{exer}$ in comparison to the rate of change of the heart frequency (note that $u(t) = \dot{H}(t)$). Because of this difficulty, we preferred the other possibility to determine k_0 and k_1. We include these two constants in the set of parameters which have to be identified. Of course, one has to observe the constraints $k_0 < 0$ and $k_1 < 0$. See Section 1.7 for numerical results.

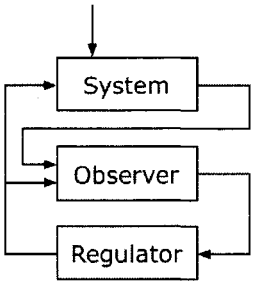

Appendix C

Retarded Functional Differential Equations: Basic Theory

In this appendix we discuss delay differential equations, a type of equations becoming increasingly important as a modeling tool in various areas, and in particular cardiovascular-respiratory modeling, as can be seen in Subsection 2.2.5 and Section 2.3. Here we present some of the basic notions, consider fundamental results, and indicate some of the most important directions for the development of the theory for delay equations. There exist several excellent textbooks on hereditary systems (Bellman and Cooke, 1963; Driver, 1977; Stépán, 1989; Hale and Lunel, 1993; Diekman et al., 1995).

C.1 Basic Notions

By a *retarded functional differential equation* (also called hereditary system, system with memory, or delay system) we mean a dynamical system where the rate of change $\dot{x}(t)$ of the "state" $x(\cdot)$ at time t depends not only on the present value $x(t)$, but also on past values of $x(\cdot)$. A simple example of a retarded functional differential equation is given by

$$\dot{x}(t) = f(t, x(t), x(t-h)), \tag{C.1}$$

where $x(t) \in \mathbb{R}^n$ and $h > 0$. Equations of type (C.1) for obvious reasons are called differential-difference equations. In order to solve (C.1) starting at $t = t_0$, we must not only specify $x(t_0)$ but also $x(t)$ for t in some interval $[t_0 - h, t_0 - h + \epsilon)$, $\epsilon > 0$. In fact, if we want to solve (C.1) on $[t_0, t_0 + h]$, we have to provide $x(t)$ for $t \in [t_0 - h, t_0]$, i.e., $x(t_0 + \theta) = \phi(\theta)$, $\theta \in [-h, 0]$. If this information is given, then, for $t \in [t_0, t_0 + h]$, (C.1) is equivalent to the Cauchy problem

$$\begin{aligned} \dot{x}(t) &= f(t, x(t), \phi(t-h)), \ t_0 \le t \le t_0 + h, \\ x(t_0) &= \phi(0). \end{aligned} \tag{C.2}$$

Assume that f is continuous and satisfies a Lipschitz condition with respect to the second argument, and that ϕ is continuous. Then the Cauchy problem (C.2) has a unique solution on some interval $[t_0, t_0 + \epsilon)$, $0 < \epsilon \le h$. If this solution exists on $[t_0, t_0 + h]$, we obtain, on $[t_0 + h, t_0 + 2h]$, a problem analogous to (C.2). This problem again has a local solution.

Continuing in this way, we can compute the solution of (C.1) on its maximal interval of existence. This method of solving equations of type (C.1) is known as the *method of steps*. As an example, consider the scalar problem

$$\begin{aligned} \dot{x}(t) &= x(t-1), \quad t \geq 0, \\ x(t) &= 1, \quad -1 \leq t \leq 0, \end{aligned} \tag{C.3}$$

i.e., we have $\phi \equiv 1$. For $0 \leq t \leq 1$, we have to solve the problem

$$\dot{x}(t) = 1, \quad 0 \leq t \leq 1, \quad x(0) = 1,$$

which yields $x(t) = t + 1, 0 \leq t \leq 1$. For $1 \leq t \leq 2$, we get

$$\dot{x}(t) = (t-1) + 1 = t, \quad 1 \leq t \leq 2, \quad x(1) = 2,$$

i.e., $x(t) = 3/2 + t^2/2 = 1 + t + (t-1)^2/2, 1 \leq t \leq 2$. By a simple induction, we see that the solution of (C.3) is given by

$$x(t) = \sum_{k=0}^{N} \frac{(t-k+1)^k}{k!}, \quad N-1 \leq t \leq N, \ N = 1, 2, \ldots .$$

Assume that the function f is continuous and that the solution of (C.1), with initial condition $x(t_0 + s) = \phi(s)$, $-h \leq s \leq 0$, exists on $t_0 \leq t < t_{\max}$. Then, it is easy to see that $\dot{x}$ is continuous on $t_0 < t < t_{\max}$. However, $\dot{x}(t_0)$ in general does not exist. As can be seen from example (C.3), we may have $\dot{x}(t_0 + 0) = f(t_0, x(t_0), \phi(-h)) \neq \dot{\phi}(0-0)$, even if ϕ is differentiable on $[-h, 0]$.

Differential-difference equations are special in the sense that the right-hand side of such an equation depends on the past history of $x(\cdot)$ only through values at discrete times. In general, the right-hand side of a functional-differential equation may depend on all values of $x(\cdot)$ on the interval $[t-h, t]$. A simple example of such an equation is

$$\dot{x}(t) = f(t, x(t), x(t-h)) + \int_{-h}^{0} g(t, s, x(t+s))\, ds.$$

Equations of this type are called functional-differential equations with distributed delays. It is clear that for equations with distributed delays, the method of steps does not work.

The special cases of functional-differential equations we have considered up to now already show that, in order to continue a solution of such an equation beyond t, we have to know $x(\cdot)$ on the interval $[t-h, t]$. This indicates how we have to define the state, at time t, of a functional-differential equation. Since the state of a dynamical system has to contain all information needed in order to predict the future behavior of the system, it is clear that the state of a functional-differential equation at time t is the function (see also Figure C.1)

$$s \to x(t+s), \quad -h \leq s \leq 0,$$

which we denote by x_t, i.e., $x_t(s) = x(t+s)$, $-h \leq s \leq 0$. For differential-difference equations, it was appropriate to choose the initial function ϕ, i.e., the initial state $x_{t_0} = \phi$,

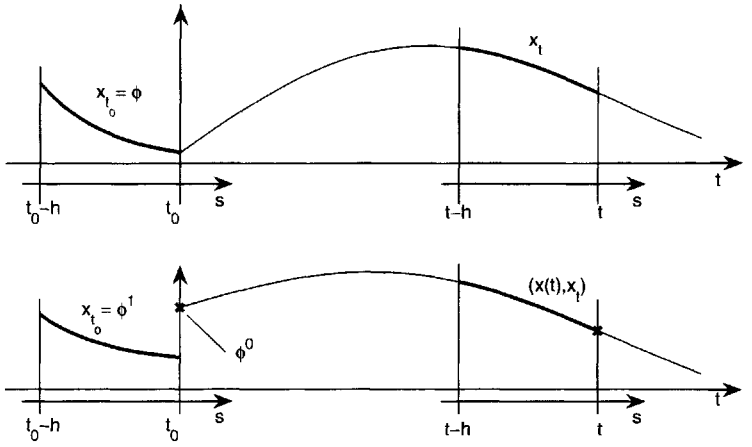

Figure C.1: State of a delay system in $C(-h, 0; \mathbb{R}^n)$ (upper panel) and in $\mathbb{R}^n \times L^2(-h, 0; \mathbb{R}^n)$ (lower panel).

as a continuous function on $[-h, 0]$. This motivates us to consider the states of a system to be elements in the function space $C([-h, 0]; \mathbb{R}^n)$. This also shows that delay equations are inherently infinite-dimensional systems. Therefore, a general Cauchy problem for a hereditary functional-differential equation has the form

$$\begin{aligned} \dot{x}(t) &= f(t, x_t), \\ x_{t_0} &= \phi \in C([-h, 0]; \mathbb{R}^n), \end{aligned} \tag{C.4}$$

where f is a function $G \to \mathbb{R}^n$ with G being an open subset of $\mathbb{R} \times C([-h, 0]; \mathbb{R}^n)$, and where $(t_0, \phi) \in G$. As we have seen above, the problem of establishing existence and uniqueness for solutions of differential-difference equations can be reduced, by the method of steps, to the corresponding problem for ordinary differential equations. This is not possible for delay equations with distributed delay. However, by an easy generalization of the proof for ordinary differential equations, we get the following basic existence and uniqueness result for functional-differential equations of type (C.4) (see, for instance, Hale and Lunel, 1993).

> *Let f be continuous on G and Lipschitz-continuous with respect to the second argument.*[16] *Then for any $(t_0, \phi) \in G$, there exists a unique solution of* (C.4) *on some interval $[t_0 - h, t_0 + \epsilon)$, $\epsilon > 0$. Moreover, solutions of* (C.4) *depend continuously on initial values.*

We denote the unique solution of (C.4), existing according to this result, by $x(t; t_0, \phi)$. In order to stress the importance of introducing the past history x_t as the state of a functional-differential equation at time t and not $x(t)$, we mention that uniqueness of solutions means that, for two solutions with different initial states $\phi \neq \psi$ at t_0, we also have $x_t(t_0, \phi) \neq x_t(t_0, \psi)$ for all $t \geq t_0$, for which both solutions exist. On the other hand, uniqueness of solutions is perfectly compatible with $x(t_1; t_0, \phi) = x(t_1, t_0, \psi)$ for some $t_1 \geq 0$.

[16] This means that for any bounded subset B of G, there exists a constant $L_B > 0$ such that, for all $(t, \phi), (t, \psi) \in B$, we have $\|f(t, \phi) - f(t, \psi)\|_{\mathbb{R}^n} \leq L_B \|\phi - \psi\|_C$.

Functional-differential equations may also have the form

$$\dot{x}(t) = f(t, x(t), x(t - \tau(t))),$$

where $\tau(\cdot)$ is a continuous function satisfying $0 \leq \tau(t) \leq h$. More generally, we may have $\tau = \tau(t, x_t)$, where τ is a continuous function $\mathbb{R} \times C([-h, 0]; \mathbb{R}^n) \supset \tilde{G} \to [-h, 0]$. In this case, the delay τ depends on t and also on the state of the system at time t. Such equations are called functional-differential equations with state-dependent delay. The theory for such equations presently is not fully developed. The respiratory control model, that we presented in Section 2.2, shows that hereditary systems with state-dependent delays are becoming important as models, in particular in the biosciences. For results on well-posedness of such equations, see (Driver, 1963), (Ito and Kappel, 1995), or (Ito and Kappel, 2002, Section 11.2). One should have in mind that delay equations with state- or time-dependent delays, in general, do not satisfy the assumption concerning Lipschitz-continuity of the right-hand side for the existence and uniqueness result given above. In order to get existence and uniqueness of solutions for those equations, one has to restrict the admissible initial states.

Finally, we want to mention that the rate of change of $x(\cdot)$ at time t may also depend on its own past values. Such systems are called neutral functional-differential equations. A simple example of a neutral functional-differential equation is the neutral differential-difference equation,

$$\dot{x}(t) = f(t, x(t), x(t - h), \dot{x}(t - h)).$$

We will not consider further equations of this type, but we refer the reader to Hale and Lunel (1993).

C.2 Linear Equations and the Linear-Quadratic Regulator Problem

In this section we turn our attention to linear retarded equations of the form

$$\dot{x}(t) = A_0 x(t) + \sum_{k=1}^{N} A_k x(t - h_k) + \int_{-h}^{0} A(s) x(t + s)\, ds, \tag{C.5}$$

where $x(\cdot) \in \mathbb{R}^n$, A_k, $k = 0, 1, \ldots, N$, are $n \times n$ matrices, $A(\cdot)$ is an integrable $n \times n$ matrix on $[-h, 0]$, and $0 = h_0 < h_1 \leq h_2 \leq \cdots \leq h_N \leq h$ are the discrete delays. It is easy to see that the right-hand side of (C.5) defines a bounded linear functional $L : C([-h, 0]; \mathbb{R}^n) \to \mathbb{R}^n$,

$$L(\phi) = \sum_{k=0}^{N} A_k \phi(-h_k) + \int_{-h}^{0} A(s)\phi(s)\, ds, \quad \phi \in C([-h, 0]; \mathbb{R}^n).$$

It is well known that any bounded linear functional $C([-h, 0]; \mathbb{R}^n) \to \mathbb{R}^n$ can be written as a Riemann–Stieltjes integral (see, for instance, Hewitt and Stromberg, 1969). Since we are not dealing with more general equations than (C.5) and do not make explicit use of the representation by Riemann–Stieltjes integrals, we refer the reader to the literature for further discussions of general linear autonomous functional-differential equations (see, for

instance, Hale and Lunel, 1993). The existence and uniqueness result quoted in Section C.1 applies immediately to (C.5). Moreover, it is not difficult to prove that all solutions exist for $t \to \infty$. Since (C.5) is autonomous, we always can take $t_0 = 0$, and we shall write $x(t;\phi)$ instead of $x(t;0,\phi)$. It is easy to see that a solution $x(t;\phi)$ of (C.5) is k-times continuously differentiable on $((k-1)h, \infty)$ with $\lim_{t \downarrow (k-1)h} x^{(k)}(t)$ existing, i.e., (C.5) has a smoothing property concerning solutions. An analogous result is true for equations of type (C.4), provided f has derivatives of arbitrary order. In contrast to the situation for hereditary functional-differential equations, smoothing of solutions does not occur for equations of neutral type.

Let $x(t) = x(t;\phi)$ be a solution of (C.5) with $x_0 = \phi$. Then we can define the mappings $T(t) : C([-h,0];\mathbb{R}^n) \to C([-h,0];\mathbb{R}^n)$, $t \geq 0$, by

$$T(t)\phi = x_t(\phi), \quad \phi \in C([-h,0];\mathbb{R}^n).$$

This family of mappings corresponds to the exponential matrices e^{At}, $t \geq 0$, in case of the ordinary differential equation $\dot{x}(t) = Ax(t)$ and has the following three analogous properties.

(i) $T(t)$ is a bounded linear operator for $t \geq 0$ and $T(0) = I$.

(ii) For any $\phi \in C([-h,0];\mathbb{R}^n)$, the mapping $t \to T(t)\phi$ is continuous from $[0,\infty)$ to $C([-h,0];\mathbb{R}^n)$.

(iii) $T(t+s) = T(t)T(s)$ for $t, s \geq 0$.

A family of operators with properties (i)–(iii) is called a *strongly continuous* (property (ii)) *semigroup* (property (iii)) *of bounded linear operators* (property (i)). Since in case of e^{At} any function $x(t) = e^{At}x_0$, $t \geq 0$, is a solution of $\dot{x}(t) = Ax(t)$, one would expect that a similar result holds for the "functions" $T(t)\phi$, $t \geq 0$, in the space $C([-h,0];\mathbb{R}^n)$. It is easy to see that $t \to T(t)\phi$ is continuously differentiable as a function $[0,\infty) \to C([-h,0];\mathbb{R}^n)$ if and only if the solution $x(t) = x(t;\phi)$ of (C.5) is continuously differentiable on $[-h,\infty)$. The latter property holds if and only if $\phi \in C^1([-h,0];\mathbb{R}^n)$ and $\dot{\phi}(0) = \lim_{\theta \uparrow 0} \dot{\phi}(\theta) = L(\phi)$. If we define an operator $\mathcal{A}$ on $C([-h,0];\mathbb{R}^n)$ by

$$\begin{aligned} \operatorname{dom}\mathcal{A} &= \{\phi \in C^1([-h,0];\mathbb{R}^n) \mid \dot{\phi}(0) = L(\phi)\}, \\ \mathcal{A}\phi &= \dot{\phi}, \quad \phi \in \operatorname{dom}\mathcal{A}, \end{aligned}$$

then it can be shown that for $\phi \in \operatorname{dom}\mathcal{A}$, the function $v(t) = T(t)\phi$, $t \geq 0$, is a solution of the abstract Cauchy problem

$$\dot{v}(t) = \mathcal{A}v(t), \; t \geq 0, \quad v(0) = \phi.$$

Thus, delay differential equations can be viewed as abstract differential equations in the state space $C([-h,0];\mathbb{R}^n)$. The operator $\mathcal{A}$ is called the *infinitesimal generator* of the solution semigroup $T(\cdot)$. Many results on delay differential equations are established in this abstract setting. We refer the interested reader to Hale and Lunel (1993).

For modeling the baroreceptor and other control loops in Chapters 1 and 3, we formulate a linear quadratic regulator problem and use results from the control theory in order to

obtain the feedback controls. In Chapter 3 the underlying system is a delay system. In the special case of constant delays, we can use the same approach to obtain a linear quadratic control problem, where the state equation is a linear delay system with discrete delays,

$$\dot{x}(t) = L(x_t) + Bu(t),\ t \geq 0, \quad x_0 = \phi,\ \phi \in C([-h, 0], \mathbb{R}^n), \tag{C.6}$$

where $B \in \mathbb{R}^{n\times p}$ and $u \in L^2(0, \infty; \mathbb{R}^p)$. We have to find $\hat{u} \in L^2(0, \infty; \mathbb{R}^p)$ such that

$$J(\hat{u}, \phi) = \min_{u\in L^2(0,\infty;\mathbb{R}^p)} J(u, \phi),$$

where

$$J(u, \phi) = \int_0^\infty \left(x(t; \phi)^\mathrm{T} Q x(t; \phi) + u(t)^\mathrm{T} R u(t)\right) dt.$$

The matrix $Q \in \mathbb{R}^{n\times n}$, respectively $R \in \mathbb{R}^{p\times p}$, is positive semidefinite, respectively, positive definite. The appropriate setting for such control problems is not in the state space $C([-h, 0]; \mathbb{R}^n)$, but in the Hilbert space $M^2 = \mathbb{R}^n \times L^2(-h, 0; \mathbb{R}^n)$. For equations of type (C.5), it is easy to see that for any $\phi^0 \in \mathbb{R}^n$ and $\phi^1 \in L^2(-h, 0; \mathbb{R}^n)$, there exists a unique solution $x(t) = x(t; \phi^0, \phi^1)$ on $[-h, \infty)$. Similarly, as in the case of the state space $C([-h, 0]; \mathbb{R}^n)$, we have a smoothing property for solutions: $x(\cdot; \phi^0, \phi^1) \in W^{k,2}_{\mathrm{loc}}([(k-1)h, \infty); \mathbb{R}^n)$, $k = 0, 1, 2, \ldots$, where $W^{k,2}_{\mathrm{loc}}([(k-1)h, \infty); \mathbb{R}^n)$ is the Sobolev space of functions y which, on every compact subinterval I of $[(k-1)h, \infty)$ are k-times differentiable in the distributional sense with $y^{(k)} \in L^2(I; \mathbb{R}^n)$.[17]

For a solution $x(t) = x(t; \phi^0, \phi^1)$, we define, as state of the system at time t, the pair $(x(t), x_t) \in M^2$. By

$$\tilde{T}(t)(\phi^0, \phi^1) = (x(t; \phi^0, \phi^1), x_t(\phi^0, \phi^1)), \quad (\phi^0, \phi^1) \in M^2,\ t \geq 0,$$

we define again a semigroup of bounded linear operators $(\tilde{T}(t))_{t\geq 0}$ now on the state space M^2. It is not very difficult to see that a "function" $t \to \tilde{T}(t)(\phi^0, \phi^1)$ is differentiable on $[0, \infty)$ if and only if $x(t; \phi^0, \phi^1)$ is differentiable in the L^2-sense on $[-h, \infty)$, i.e., if and only if $\phi^1 \in W^{1,2}([-h, 0]; \mathbb{R}^n)$ and $\phi^1(0) = \phi^0$. If we define the operator $\tilde{A}$ on M^2 (analogously as we defined A on $C([-h, 0]; \mathbb{R}^n)$) by

$$\begin{aligned}
\operatorname{dom} \tilde{A} &= \{(\phi^0, \phi^1) \in M^2 \mid \phi^1 \in W^{1,2}([-h, 0]; \mathbb{R}^n) \text{ and } \phi^0 = \phi^1(0)\},\\
\tilde{A}(\phi^0, \phi^1) &= (L(\phi), \dot{\phi}^1), \quad (\phi^0, \phi^1) \in \operatorname{dom} \tilde{A},
\end{aligned}$$

then we can write (C.6) as an abstract differential equation in M^2,

$$\dot{z}(t) = \tilde{A}z(t) + (Bu(t), 0),\ t \geq 0, \quad z(0) = (\phi^0, \phi^1) \in M^2.$$

Then the linear quadratic regulator problem for the delay system (C.6) can be considered as a special case of linear quadratic regulator problems in Hilbert spaces, for which a complete theory exists (see, for instance, Curtain and Pritchard, 1978; Gibson, 1983). The use of the

[17] Since the argument varies in an interval, this is equivalent to saying that y is $(k-1)$-times continuously differentiable on $[(k-1)h, \infty)$, and $y^{(k-1)}$ is absolutely continuous on any compact subinterval I with $y^{(k)}$, which exists almost everywhere, being in $L^2(I; \mathbb{R}^n)$.

state space M^2 goes back to Krasovskij (1964, 1966). Many authors have used this state space for control problems (see, e.g., Delfour and Mitter, 1972; Delfour and Mitter, 1975). A first proof of existence and uniqueness for solutions was given in Borisovič and Turbabin (1969); see also (Bernier and Manitius, 1978).

In order to solve linear quadratic regulator problems for delay systems, a number of approximation schemes have been developed. Usually the delay system is approximated by a sequence of finite-dimensional systems (which are described by ordinary differential equations). One solves the linear-quadratic regulator problem for the finite-dimensional systems and gets an approximating sequence of feedback laws for infinite-dimensional delay system. Of the numerous papers concerned with this approach, we mention Banks and Burns (1978), Banks and Kappel (1979), Kappel and Propst (1984), Ito and Teglas (1986), Kappel and Salamon (1987), Lasiecka and Manitius (1988), Ito and Tran (1989), Kappel and Salamon (1990), Tran (1991), Ito and Kappel (1991), and Manitius and Tran (1994). A rather complete survey on approximation of linear-quadratic control problems for delay systems is given in Kappel (1991).

C.3 Eigenvalues and Local Stability

In this section we give a brief review of eigenvalues and stability of linear autonomous retarded functional differential equations. At the end of the section we refer the reader to results concerned with computation of eigenvalues.

The definition of stability of equilibria of equations of type (C.4) is analogous to that for ordinary differential equations. Assume that in (C.4) we have $G = \mathbb{R} \times C([-h, 0]; \mathbb{R}^n)$ and $f(t, 0) \equiv 0$, so that $x \equiv 0$ is an equilibrium solution. The solution $x \equiv 0$ of (C.4) is said to be *stable* if and only if for any $t_0 \in \mathbb{R}$ and any $\epsilon > 0$, there exists a $\delta = \delta(\epsilon, t_0) > 0$ such that for any initial function ϕ with $\|\phi\|_C < \delta$, we have $\|x_t(t_0, \phi)\|_C < \epsilon$ for $t \geq t_0$. The solution $x \equiv 0$ is said to be *asymptotically stable* if it is stable, and for any $t_0 \in \mathbb{R}$, there exists an $\eta = \eta(t_0) > 0$ such that $\|\phi\| < \eta$ implies $\lim_{t\to\infty} \|x_t(t_0, \phi)\|_C = 0$.

In the following, we consider only linear autonomous functional-differential equations of type (C.5) and assume that $A(s) \equiv 0$, so that (C.5) takes the form

$$\dot{x}(t) = \sum_{k=0}^{N} A_k x(t - h_k), \tag{C.7}$$

where $0 = h_0 < h_1 < \cdots < h_N =: h$. Such equations may be the result of linearizing an autonomous functional-differential equation around an equilibrium solution. As for linear autonomous ordinary differential equations, we expect that also for equations of type (C.7), stability of the zero solution can be characterized by the location of the eigenvalues. In order to obtain the eigenvalues of (C.7), we look for solutions of the form $x(t) = ce^{\lambda t}$, $t \in \mathbb{R}$, where $c \neq 0$. Inserting this into (C.7), we obtain $(\lambda I - \sum_{k=0}^{N} A_k e^{-h_k\lambda})c = 0$. This equation has a nontrivial solution c if an only if

$$\det \Delta(\lambda) = 0, \quad \text{where}$$

$$\Delta(\lambda) := \lambda I - \sum_{k=0}^{N} A_k e^{-h_k\lambda}.$$

The function $\det \Delta(\lambda)$ is the *characteristic function* corresponding to (C.7) and the zeros of this function are called the *eigenvalues* of (C.7). For an eigenvalue λ, the functions $ce^{\lambda\theta}$, $\theta \in [-h, 0]$, with $\Delta(\lambda)c = 0$, are called the *eigenfunctions* of (C.7). It turns out that the set of all eigenvalues of (C.7) is the spectrum $\sigma(\mathcal{A})$ of the infinitesimal generator for the solution semigroup of (C.7) (see, for instance, Hale and Lunel, 1993). Since the characteristic function is an entire function (i.e., analytic on $\mathbb{C}$), the results on the distribution of eigenvalues in the complex plane follow from well-known results concerning the distribution of zeros of entire functions (see Bellman and Cooke, 1963; Hale and Lunel, 1993).

(i) *All eigenvalues are isolated and of finite multiplicity.*

(ii) *There exists a constant $\rho > 0$ independent of the delays such that all eigenvalues are contained in the exponential sector (see Figure C.2)*

$$\{\lambda \in \mathbb{C} \mid \operatorname{Re}\lambda \geq 0 \text{ and } |\lambda| \leq \rho\} \cup \{\lambda \in \mathbb{C} \mid \operatorname{Re}\lambda < 0 \text{ and } |\lambda| \leq \rho e^{-hn\operatorname{Re}\lambda}\}.$$

(iii) *All eigenvalues lie asymptotically (i.e., for $|\lambda| \to \infty$ or, equivalently, for $\operatorname{Re}\lambda \to \infty$) on a finite number of curves,*

$$|\lambda^{\mu_r} e^{\lambda}| = \kappa_r, \quad r = 1, \ldots, M,$$

where μ_r and κ_r are positive constants, which can be calculated from $\Delta(\lambda)$.

In fact, one can give asymptotic (for $|\lambda| \to \infty$) formulas for the eigenvalues (see Bellman and Cooke, 1963, Chapter 12). Note that the constants μ_r above are positive, because (C.7) is of retarded type. Properties (i) and (ii) are simple consequences of the fact that the characteristic function is entire. Property (iii) needs deeper results on exponential polynomials (see Bellman and Cooke, 1963). From (i) and (ii), it follows immediately that

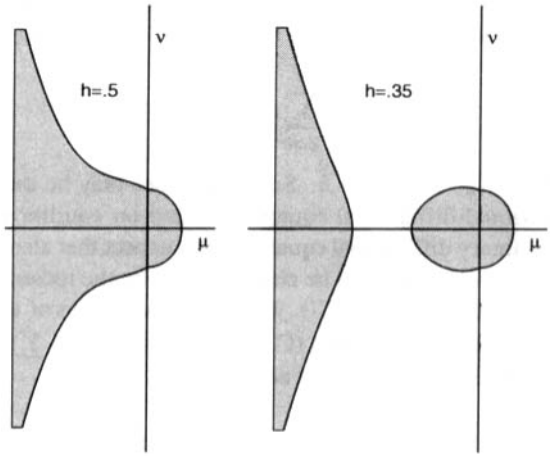

Figure C.2: Exponential sectors (shaded areas) for the spectrum of a linear delay equation with $\rho = n = 1$ and $h = 0.5$ (left), respectively $h = 0.35$ (right).

in any vertical strip $\alpha \leq \operatorname{Re}\lambda \leq \beta$, with $-\infty < \alpha \leq \beta \leq \infty$, there are at most finitely many eigenvalues. Moreover, if all eigenvalues have negative real part, then there exists a $\delta > 0$ such that $\operatorname{Re}\lambda \leq -\delta$ for all $\lambda \in \sigma(\mathcal{A})$.

As in the case of linear autonomous ordinary differential equations, the stability properties of the zero solution are also, in case of (C.7), determined by the location of its eigenvalues (Kappel and Wimmer, 1976).

(i) *The zero solution of* (C.7) *is asymptotically stable if and only if* $\operatorname{Re}\lambda < 0$ *for all* $\lambda \in \sigma(\mathcal{A})$. *If this is the case, then, for all* $\epsilon > 0$, *there exists a* $K(\epsilon) > 0$ *such that*

$$\|x(t;\phi)\|_{\mathbb{R}^n} \leq K(\epsilon)\|\phi\|_C e^{(\sigma_0+\epsilon)t}, \quad t \geq 0,\ \phi \in C([-h,0];\mathbb{R}^n),$$

where $\sigma_0 = \max\{\operatorname{Re}\lambda \mid \lambda \in \sigma(\mathcal{A})\}$.

(ii) *The zero solution of* (C.7) *is stable if and only if* $\operatorname{Re}\lambda \leq 0$ *for all* $\lambda \in \sigma(\mathcal{A})$ *and the following property holds for those* $\lambda \in \sigma(\mathcal{A})$ *with* $\operatorname{Re}\lambda = 0$: *let* $\operatorname{Re}\lambda_0 = 0$ *and let* m *be the multiplicity of* λ_0 *as a zero of* $\det \Delta(\lambda)$. *Then either*

$$m < n \text{ and } \operatorname{rank}\Delta(\lambda_0) = n - m \text{ or}$$
$$m = n,\ \Delta(\lambda_0) = 0 \text{ and } \operatorname{rank}\Delta'(\lambda_0) = n.$$

In case of a scalar nth-order linear autonomous delay equation,

$$x^{(n)}(t) + \sum_{p=0}^{n-1}\sum_{k=0}^{N} a_{p,k}x^{(p)}(t-h_k) = 0, \tag{C.8}$$

which can be written as a system of type (C.7), we have, instead of (ii), the following result.

(ii′) *The zero solution of* (C.8) *is stable if and only if* $\operatorname{Re}\lambda \leq 0$ *for all* $\lambda \in \sigma(\mathcal{A})$, *and the* λ_0*'s in* $\sigma(\mathcal{A})$ *with* $\operatorname{Re}\lambda_0 = 0$ *are simple zeros of* $\det \Delta(\lambda)$.

Computation of the eigenvalues for (C.7) is not a trivial task. In Manitius et al. (1987), an algorithm was developed for finding the eigenvalues of (C.7) with commensurate delays (i.e., there exists an $h > 0$ such that $h_k = n_k h$, $k = 1,\ldots,N$, with integers m_k) using the characteristic function $\det \Delta(\lambda)$. Essentially, the method consists of two subalgorithms. The eigenvalues, which are contained in some bounded region around the origin, are approximated by using an adaptation of a combinatorial algorithm (Kuhn, 1974) for approximation of zeros of ordinary polynomials. For eigenvalues with large modulus, which (as we have seen) are distributed asymptotically along some curves, are computed directly from the asymptotic formulas mentioned above.

An interesting part of the algorithm, presented in Manitius et al. (1987), is an algorithm to compute the characteristic equation. The characteristic equation has the form

$$\lambda^n + \theta_1\lambda^{n-1} + \cdots + \theta_{n-1}\lambda + \theta_n = 0,$$

where

$$\theta_i = \theta_i(\eta_1,\ldots,\eta_N), \quad i = 1,\ldots,n,$$

with $\eta_k = e^{-h_k\lambda}$, $k = 1, \ldots, N$. The θ_i thus can be considered as polynomial in N indeterminates. We set

$$\hat{A}(\eta_1, \ldots, \eta_N) = \sum_{k=0}^{N} A_k \eta_k.$$

The polynomials θ_i, $i = 1, \ldots, N$, can be determined using the following recursive formulas (Buslowicz, 1980):

$$\begin{aligned} F_1 &= I, \\ \theta_i &= -\frac{1}{i} \operatorname{tr}(\hat{A} F_i), \quad i = 1, 2, \ldots, n, \\ F_{i+1} &= \hat{A} F_i + \theta_i I, \quad i = 1, 2, \ldots, n-1. \end{aligned} \tag{C.9}$$

For commensurate delay, the matrix $\hat{A}$ is a polynomial matrix in one indeterminate only, $\hat{A} = \hat{A}(\eta)$ with $\eta = e^{-h\lambda}$. Consequently, also the polynomials θ_i are polynomials in η. In this case, it is easy to obtain from (C.9) recursive formulas for the coefficients of the θ_i.

Through extensive numerical tests, the method was found to work well and reliable even on relative high-order systems of retarded equations with commensurate delays (the largest system that has been tested was of dimension $n = 10$).

Bibliography

Adams, Jr., K. F. (2001). New epidemiologic perspectives concerning mild-to-moderate heart failure, *Am. J. Med.* **110**: S6–S13.

Altman, P. L. and Dittmer, D. S. (eds.) (1971). *Biological Handbooks, Respiration and Circulation*, Md Federation of American Societies for Experimental Biology, Bethesda, MD.

Aratow, M., Fortney, S. M., Watenpaugh, D. E., Crenshaw, A. G., and Hargens, A. R. (1993). Transcapillary fluid responses to lower body negative pressure, *J. Appl. Physiol.* **74**: 2763–2770.

Ayappa, I. and Rapoport, D. M. (2003). The upper airway in sleep: Physiology of the pharynx, *Sleep Med. Rev.* **7**: 9–33.

Ballantyne, D. and Scheid, P. (2001). Central chemosensitivity of respiration: A brief overview, *Respir. Physiol.* **129**: 5–12.

Banks, H. T. and Burns, J. A. (1978). Hereditary control problems: Numerical methods based on averaging approximations, *SIAM J. Control Optim.* **16**: 169–208.

Banks, H. T. and Kappel, F. (1979). Spline approximations for functional differential equations, *J. Differential Equations* **34**: 496–522.

Barbieri, R., Triedman, J. K., and Saul, J. P. (2002). Heart rate control and mechanical cardiopulmonary coupling to assess central volume: A systems analysis, *Am. J. Physiol. Regul. Integr. Comp. Physiol.* **283**: R1210–R1220.

Bassingthwaighte, J. B. (2000). Strategies for the physiome project, *Ann. Biomed. Eng.* **28**: 1043–1058.

Batzel, J. J., Kappel, F., and Timischl-Teschl, S. (2005). A cardiovascular-respiratory control system model including state delay with application to congestive heart failure in humans, *J. Math. Biol.* **50**: 293–335.

Batzel, J. J. and Tran, H. T. (2000a). Modeling instability in the control system for human respiration: Applications to infant non-REM sleep, *Appl. Math. Comput.* **110**: 1–51.

Batzel, J. J. and Tran, H. T. (2000b). Stability of the human respiratory control system. I. Analysis of a two-dimensional delay state-space model, *J. Math. Biol.* **41**: 45–79.

Batzel, J. J. and Tran, H. T. (2000c). Stability of the human respiratory control system. II. Analysis of a three-dimensional delay state-space model, *J. Math. Biol.* **41**: 80–102.

Bauer, J. and Brooks, C. (1981). Body fluid composition in chronic renal failure, *Clin. Nephrol.* **16**: 114–118.

Bazett, H. C. (1920). An analysis of the time-relations of electrocardiograms, *Heart* **7**: 353–370.

Becker, H. F., Piper, A. J., Flynn, W. E., McNamara, S. G., Grunstein, R. R., Peter, J. H., and Sullivan, C. E. (1999). Breathing during sleep in patients with nocturnal desaturation, *Am. J. Respir. Crit. Care Med.* **159**: 112–118.

Bellman, R. and Cooke, K. L. (1963). *Differential-Difference Equations*, Academic Press, New York.

Bennett, L. S., Langford, B. A., Stradling, J. R., and Davies, R. J. (1998). Sleep fragmentation indices as predictors of daytime sleepiness and nCPAP response in obstructive sleep apnea, *Am. J. Respir. Crit. Care Med.* **158**: 778–786.

Bernier, C. and Manitius, A. (1978). On semigroups in $\boldsymbol{R}^n \times L^p$ corresponding to differential equations with delays, *Canad. J. Math.* **30**: 897–914.

Bevier, W. C., Bunnell, D. E., and Horvath, S. M. (1987). Cardiovascular function during sleep of active older adults and the effects of exercise, *Exp. Gerontol.* **22**: 329–337.

Bie, P. and Sandgaard, N. C. F. (2000). Determinants of the natriuresis after acute, slow sodium loading in conscious dogs, *Am. J. Physiol. Regul. Integr. Comp. Physiol.* **278**: R1–R10.

Blackmer, J. (1997). Orthostatic hypotension in spinal cord injured patients, *J. Spinal Cord Med.* **20**: 212–217.

Boese, F. (1998). Stability with respect to the delay: On a paper of K. L. Cooke and P. van den Driessche, *J. Math. Anal. Appl.* **228**: 293–321.

Borisovič, J. and Turbabin, A. S. (1969). On the Cauchy problem for linear nonhomogeneous differential equations with retarded arguments, *Soviet Math. Dokl.* **10**: 401–405.

Brack, T. (2003). Cheyne-Stokes respiration in patients with congestive heart failure, *Swiss Med. Wkly.* **133**: 605–610.

Bradley, T. D. and Floras, J. S. (2003). Sleep apnea and heart failure. Part I: Obstructive sleep apnea, *Circulation* **107**: 1671–1678.

Brengelmann, G. L. (2003). A critical analysis of the view that right atrial pressure determines venous return, *J. Appl. Physiol.* **94**: 849–859.

Brian, Jr., J. E. (1998). Carbon dioxide and the cerebral circulation, *Anesthesiology* **88**: 1365–1386.

Brown, C. M., Hecht, M. J., Neundorfer, B., and Hilz, M. J. (2003). Effects of lower body negative pressure on cardiac and vascular responses to carotid baroreflex stimulation, *Physiol. Res.* **52**: 637–645.

Buckwalter, J. B., Taylor, J. C., Hamann, J. J., and Clifford, P. S. (2004). Role of nitric oxide in exercise sympatholysis, *J. Appl. Physiol.* **97**: 417–423.

Burton, A. C. (1969). *Physiologie und Biophysik des Kreislaufs*, F. K. Schatlauer Verlag, Stuttgart.

Buslowicz, M. (1980). Inversion of polynomial matrices, *Internat. J. Control* **33**: 977 –984.

Buxton, R. B. and Frank, L. R. (1997). A model for the coupling between cerebral blood flow and oxygen metabolism during neural stimulation, *J. Cereb. Blood Flow Metab.* **17**: 64–72.

Carley, D. W. and Shannon, D. C. (1988). A minimal mathematical model of human periodic breathing, *J. Appl. Physiol.* **65**: 1400–1409.

Cavalcanti, S., Cavani, S., and Santoro, A. (2002). Role of short-term regulatory mechanisms on pressure response to hemodialysis-induced hypovolemia, *Kidney Int.* **61**: 228–238.

Cavalcanti, S., Ciandrini, A., Severi, S., Badiali, F., Bini, S., Gattiani, A., Cagnoli, L., and Santoro, A. (2004). Model-based study of the effects of the hemodialysis technique on the compensatory response to hypovolemia, *Kidney Int.* **65**: 1499–1510.

Cavalcanti, S. and Di Marco, L. Y. (1999). Numerical simulation of the hemodynamic response to hemodialysis-induced hypovolemia, *Artif. Organs* **23**: 1063–1073.

Chamney, P. W., Johner, C., Aldridge, C., Krämer, M., Valasco, N., Tattersall, J. E., Aukaidey, T., Gordon, R., and Greenwood, R. N. (1999). Fluid balance modelling in patients with kidney failure, *J. Med. Eng. Technol.* **23**: 45–52.

Chapleau, M. W. and Abboud, F. M. (eds.) (2001). *Neuro-cardiovascular Regulation: From Molecules to Man*, The New York Academy of Sciences, New York.

Cherniack, N. S. (1999). Apnea and periodic breathing during sleep, *N. Engl. J. Med.* **341**: 985–987.

Christie, J., Sheldahl, L. M., Tristani, F. E., Sagar, K. B., Ptacin, M. J., and Wann, S. (1987). Determination of stroke volume and cardiac output during exercise: Comparison of two-dimensional and Doppler echocardiography, Fick oximetry, and thermodilution, *Circulation* **76**: 539–547.

Ciandrini, A., Cavalcanti, S., Severi, S., Garred, L. J., and Avanzolini, G. (2004). Effects of dialysis technique on acute hypotension: A model-based study, *Cardiovasc. Eng.* **4**: 163–171.

Cleave, J. P., Levine, M. R., Fleming, P. J., and Long, A. M. (1986). Hopf bifurcations and the stability of the respiratory control system, *J. Theor. Biol.* **119**: 299–318.

Cohen, G., Malcolm, G., and Henderson-Smart, D. (1997). Ventilatory response of the newborn infant to mild hypoxia, *Pediatr. Pulmonol.* **24**: 163–172.

Cokelet, G. R. (1986). Rheology and tube flow of blood, *in* R. Skalak and S. Chien (eds.), *Handbook of Bioengineering*, McGraw–Hill, New York, pp. 14.1–14.17.

Collins, D. A. and Padhani, A. R. (2004). Dynamic magnetic resonance imaging of tumor perfusion, *IEEE Eng. Med. Biol. Mag.* **23**: 65–83.

Convertino, V. A., Ludwig, D. A., and Cooke, W. H. (2004). Stroke volume and sympathetic responses to lower-body negative pressure reveal new insight into circulatory shock in humans, *Auton. Neurosci.* **111**: 127–134.

Cooke, K. L. and Turi, J. (1994). Stability, instability in delay equations modeling human respiration, *J. Math. Biol.* **32**: 535–543.

Cooke, K. L. and van den Driessche, P. (1986). On zeroes of some transcendental equations, *Funkcial. Ekvac.* **29**: 77–90.

Cooke, W. H., Ryan, K. L., and Convertino, V. A. (2004). Lower body negative pressure as a model to study progression to acute hemorrhagic shock in humans, *J. Appl. Physiol.* **96**: 1249–1261.

Cowley, Jr. A. W. and Guyton, A. C. (1972). Quantification of intermediate steps in the renin-angiotensin-vasoconstrictor feedback loop in the dog, *Circ. Res.* **30**: 557–566.

Cunningham, D. J. C., Robbins, P. A., and Wolff, C. B. (1986). Integration of respiratory responses to changes in alveolar pressures of CO_2, O_2 and in arterial pH, *in* A. P. Fishman, N. S. Cherniack, and J. G. Widdicombe (eds.), *Handbook of Physiology, Section 3: The Respiratory System*, Vol. II, Control of Breathing, Part 2, American Physiol. Soc., Bethesda, MD, pp. 475–528.

Curtain, R. F. and Pritchard, A. J. (1978). *Infinite Dimensional Linear Systems Theory*, Springer-Verlag, Berlin.

Dampney, R. A., Coleman, M. J., Fontes, M. A., Hirooka, Y., Horiuchi, J., Li, Y. W., Polson, J. W., Potts, P. D., and Tagawa, T. (2002). Central mechanisms underlying short- and long-term regulation of the cardiovascular system, *Clin. Exp. Pharmacol. Physiol.* **29**: 261–268.

Danielsen, M. and Ottesen, J. T. (2001). Describing the pumping heart as a pressure source, *J. Theor. Biol.* **212**: 71–81.

Dankelman, J., Stassen, H. G., and Spaan, J. A. (1999). Interaction between Gregg's phenomenon and coronary flow control: A model study, *Med. Biol. Eng. Comput.* **37**: 742–749.

Daugirdas, J. T. (2001). Pathophysiology of dialysis hypotension: An update, *Am. J. Kidney Dis.* **38**: S11–S17.

Davidian, M. and Giltinan, D. M. (1995). *Nonlinear Models for Repeated Measurement Data*, CRC Press/Chapman and Hall, London.

Davis, T. L., Kwong, K. K., Weisskoff, R. M., and Rosen, B. R. (1998). Calibrated functional MRI: Mapping the dynamics of oxidative metabolism, *Proc. Natl. Acad. Sci. USA* **95**: 1834–1839.

De Burg Daly, M. (1986). Interactions between respiration and circulation, *in* A. P. Fishman, N. S. Cherniack, J. G. Widdicombe, and S. R. Geiger (eds.), *Handbook of Physiology, Section 3: The Respiratory System*, Vol. II, Control of Breathing, Part 2, Am. Phys. Soc., Bethesda, MD, pp. 529–594.

deBoer, R. W., Karemaker, J. M., and Strackee, J. (1987). Hemodynamic fluctuations and baroreflex sensitivity in humans: A beat-to-beat model, *Am. J. Physiol.* **253**: H680–H689.

Delfour, M. C. and Mitter, S. K. (1972). Controllability, observability and optimal feedback control of affine hereditary differential systems, *SIAM J. Control Optim.* **10**: 298–328.

Delfour, M. C. and Mitter, S. K. (1975). Hereditary differential systems with constant delays. II. A class of affine systems and the adjoint problem, *J. Differential Equations* **18**: 18–28.

Delivoria-Papadopoulos, M. and DiGiacomo, J. E. (1992). Oxygen transport and delivery, *in* R. Polin and W. W. Fox (eds.), *Fetal and Neonatal Physiology*, W. B. Saunders, Philadelphia, pp. 801–813.

Despopoulos, A. and Silbernagl, S. (1991). *Colour Atlas of Physiology*, 4th ed., Georg Thieme, Stuttgart.

DiCarlo, S. E. and Bishop, V. S. (2001). Central baroreflex resetting as a means of increasing and decreasing sympathetic outflow and arterial pressure, *Ann. N. Yo. Acad. Sci.* **940**: 324–337.

Diekman, O., van Gils, S. A., Lunel, S. M. V., and Walther, H.-O. (1995). *Delay Equations: Functional-, Complex-, and Nonlinear Analysis*, Springer-Verlag, New York.

Dieudonné, J. A. (1960). *Foundations of Modern Analysis*, Academic Press, New York.

Dill, D. and Costill, D. (1974). Calculation of percentage changes in volumes of blood, plasma, and red cells in dehydration, *J. Appl. Physiol.* **37**: 247–248.

Dobkin, B. (1989). Orthostatic hypotension as a risk factor for symptomatic occlusive cerebrovascular disease, *Neurology* **305**: 30–34.

Dodds, P. S., Rothman, D. H., and Weitz, J. S. (2001). Re-examination of the "3/4-law" of metabolism, *J. Theor. Biol.* **209**: 9–27.

Donnelly, D. F. (2000). Developmental aspects of oxygen sensing by the carotid body, *J. Appl. Physiol.* **88**: 2296–2301.

Donnelly, S. (2001). Why is erythropoietin made in the kidney? The kidney functions as a critmeter, *Am. J. Kidney Dis.* **38**: 415–425.

Dowden, S. and Allen, G. (1997). Relationships between anxiety senstivity, hyperventilation, and emotional reactivity to displays of facial emotions, *J. Anxiety Disord.* **11**: 63–75.

Driver, R. D. (1963). Existence theory for a delay-differential equation, *Contr. Diff. Eqs.* **1**: 317–336.

Driver, R. D. (1977). *Ordinary and Delay Differential Equations*, Springer-Verlag, New York.

Du Bois, D. and Du Bois, E. (1916). A formula to estimate the approximate surface area if height and weight be known, *Arch. Int. Med.* **17**: 863–871.

Duffin, J. (1972). A mathematical model of the chemoreflex control of ventilation, *Respir. Physiol.* **15**: 277–301.

Duffin, J. (2004). Functional organization of respiratory neurones: A brief review of current questions and speculations, *Exp. Physiol.* **89**: 517–529.

Duffin, J. (2005). Role of acid-base balance in the chemoreflex control of breathing, *J. Appl. Physiol.*, **99**: 2255–2265.

Eigenbrodt, M. (2000). Orthostatic hypotension as a risk factor for stroke, *Stroke* **31**: 2307–2313.

Ellmerer, M., Schaupp, L., Brunner, G. A., Sendlhofer, G., Wutte, A., Wach, P., and Pieber, T. R. (2000). Measurement of interstitial albumin in human skeletal muscle and adipose tissue by open-flow microperfusion, *Am. J. Physiol. Endocrinol. Metab.* **278**: E352–E356.

Ely, E. W. and Bernard, G. R. (1999). Editorial: Transfusions in critically ill patients, *New England J. Med.* **340**: 467–468.

Enquist, B. J., Economo, E. P., Huxman, T. E., Allen, A. P., Ignace, D. D., and Gillooly, J. F. (2003). Scaling metabolism from organisms to ecosystems, *Nature* **423**: 639–642.

Evans, R. G., Malpas, S. C., Osborne, J. W., and Fink, G. D. (2005). Neural, hormonal and renal interactions in long-term blood pressure control, *Clin. Exp. Pharmacol. Physiol.* **32**: 372–373.

Evans, R. W. (1995). Neurologic aspects of hyperventilation syndrome, *Semin. Neurol.* **15**: 115–125.

Fåhræus, R. and Lindqvist, T. (1931). The viscosity of blood in narrow capillary tubes, *Am. J. Physiol.* **96**: 562–568.

Fedak, P. W., Verma, S., Weisel, R. D., and Li, R. K. (2005). Cardiac remodeling and failure: From molecules to man (Part I), *Cardiovasc. Pathol.* **14**: 1–11.

Fehske, W. (1988). *Praxis der konventionellen und farbkodierten Doppler-Echokardiographie*, Hans-Huber-Verlag, Bern, Stuttgart, Toronto.

Feldman, J. L., Mitchell, G. S., and Nattie, E. E. (2003). Breathing: Rhythmicity, plasticity, chemosensitivity, *Annu. Rev. Neurosci.* **26**: 239–266.

Fincham, W. F. and Tehrani, F. T. (1983a). A mathematical model of the human respiratory system, *J. Biomed. Eng.* **5**: 125–133.

Fincham, W. F. and Tehrani, F. T. (1983b). On the regulation of cardiac output and cerebral blood flow, *J. Biomed. Eng.* **5**: 73–75.

Fink, G. D. (2005). Hypothesis: The systemic circulation as a regulated free-market economy. A new approach for understanding the long-term control of blood pressure, *Clin. Exp. Pharmacol. Physiol.* **32**: 377–383.

Fink, M., Batzel, J. J., and Kappel, F. (2004). An optimal control approach to modeling the cardiovascular-respiratory system: An application to orthostatic stress, *Cardiovasc. Eng.* **4**: 27–38.

Fishman, A. P., Cherniack, N. S., and Widdicombe, J. G. (eds.) (1986). *Handbook of Physiology, Section 3: The Respiratory System*, Vol. II, Control of Breathing, Part 2, American Physiol. Soc., Bethesda, MD.

Fleming, S., Wilkinson, J., Greenwood, R. N., Aldridge, C., and Baker, L. (1987). Effect of dialysate composition on intercompartmental fluid shift, *Kidney Int.* **32**: 267–273.

Fogel, R. B., White, D. P., Pierce, R. J., Malhotra, A., Edwards, J. K., Dunai, J., Kleverlaan, D., and Trinder, J. (2003). Control of upper airway muscle activity in younger versus older men during sleep onset, *J. Physiol.* **553**: 533–544.

Fowler, A. C. and Kalamangalam, G. P. (2002). Periodic breathing at high altitude, *IMA J. Math. Appl. Med. Biol.* **19**: 293–313.

Francis, D. P., Willson, K., Davies, L. C., Coats, A. J., and Piepoli, M. (2000). Quantitative general theory for periodic breathing in chronic heart failure and its clinical implications, *Circulation* **102**: 2214–2221.

Franco, P., Seret, N., Van Hees, J. N., Scaillet, S., Vermeulen, F., Groswasser, J., and Kahn, A. (2004). Decreased arousals among healthy infants after short-term sleep deprivation, *Pediatrics* **114**: e192–e197.

Furlan, R., Jacob, G., Palazzolo, L., Rimoldi, A., Diedrich, A., Harris, P. A., Porta, A., Malliani, A., Mosqueda-Garcia, R., and Robertson, D. (2001). Sequential modulation of cardiac autonomic control induced by cardiopulmonary and arterial baroreflex mechanisms, *Circulation* **104**: 2932–2937.

Gaehtgens, P. (1980). Flow of blood through narrow capillaries: Rheological mechanisms determining capillary hematocrit and apparent viscosity, *Biorheology* **17**: 183–189.

Gallagher, K. M., Fadel, P. J., Stromstad, M., Ide, K., Smith, S. A., Querry, R. G., Raven, P. B., and Secher, N. H. (2001). Effects of exercise pressor reflex activation on carotid baroreflex function during exercise in humans, *J. Physiol.* **533**: 871–880.

Garcia-Estan, J. and Roman, R. J. (1989). Role of renal interstitial hydrostatic pressure in the pressure diuresis response, *Am. J. Physiol. Renal. Physiol.* **256**: F63–F70.

Ghazanshahi, S. D. and Khoo, M. C. K. (1993). Optimal ventilatory patterns in periodic breathing, *Ann. Biomed. Eng.* **21**: 517–530.

Giardino, N. D., Glenny, R. W., Borson, S., and Chan, L. (2003). Respiratory sinus arrhythmia is associated with efficiency of pulmonary gas exchange in healthy humans, *Am. J. Physiol. Heart Circ. Physiol.* **284**: H1585–H1591.

Gibson, J. S. (1983). Linear-quadratic optimal control of hereditary differential systems: Infinite dimensional Riccati equations and numerical approximations, *SIAM J. Control Optim.* **21**: 95–139.

Giove, S. and Nordio, M. (1994). Proposal of an adaptive fuzzy control module for hemodialysis, *in* B. Patterson (ed.), *Modeling and Control in Biological Systems*, University of Texas Medical Branch and Shriners Burns Institute, Galveston, TX, pp. 212–213.

Glass, L. (2001). Synchronization and rhythmic processes in physiology, *Nature* **410**: 277–284.

Glass, L. and Mackey, M. C. (1979). Pathological conditions resulting from instabilities in physiological control systems, *Ann. N. Y. Acad. Sci.* **316**: 214–235.

Goodwin, G. C. and Payne, R. L. (1977). *Dynamical System Identification: Experimental Design and Data Analysis*, Mathematics in Science and Engineering, Vol. 136, Academic Press, New York.

Graveney, M. J. (1981). Gravimetric density analysis of blood: A means of investigating compartmental blood volume changes, *Technical report*, Royal Air Force Institute of Aviation Medicine, Farnborough, UK.

Gray, J. S. (1946). The multiple factory theory of the control of respiratory ventilation, *Science* **103**: 739–744.

Greenough, A. (2000). Breathing patterns, oxygen and carbon dioxide levels during infancy, *Acta Paediatr.* **89**: 1275–1277.

Grodins, F. S. (1959). Integrative cardiovascular physiology: A mathematical synthesis of cardiac and blood vessel hemodynamics, *Quart. Rev. Biol.* **34**: 93–116.

Grodins, F. S. (1963). *Control Theory and Biological Systems*, Columbia University Press, New York.

Grodins, F. S., Buell, J., and Bart, A. J. (1967). Mathematical analysis and digital simulation of the respiratory control system, *J. Appl. Physiol.* **22**: 260–276.

Grodins, F. S., Gray, J. S., Schroeder, K. R., Norins, A. L., and Jones, R. W. (1954). Respiratory responses to CO_2 inhalation: A theoretical study of a nonlinear biological regulator, *J. Appl. Physiol.* **7**: 283–308.

Guild, S. J., Barrett, C. J., and Malpas, S. C. (2005). Long-term recording of sympathetic nerve activity: The new frontier in understanding the development of hypertension, *Clin. Exp. Pharmacol. Physiol.* **32**: 433–439.

Guyton, A. C. (1955). Determination of cardiac output by equating venous return curves with cardiac response curves, *Physiol. Rev.* **35**: 123–129.

Guyton, A. C. (1991a). Renal regulation of blood volume and extracellular fluid volume: Excretion and regulation of urea, potassium and other substances, *in* A. C. Guyton (ed.), *Textbook of Medical Physiology*, 8th ed., W. B. Saunders, Philadelphia, pp. 320–329.

Guyton, A. C., Coleman, T. G., Cowley, A. V., J., Scheel, K. W., Manning, R. D., J., and Norman, R. A., J. (1972). Arterial pressure regulation. Overriding dominance of the kidneys in long-term regulation and in hypertension, *Am. J. Med.* **52**: 584–594.

Guyton, A. C., Coleman, T. G., and Granger, H. J. (1972). Circulation: Overall regulation, *Ann. Rev. Physiol.* **34**: 13–46.

Guyton, A. C. (ed.) (1991b). *Textbook of Medical Physiology*, 8th ed., W. B. Saunders, Philadelphia.

Guyton, A. and Coleman, T. (1969). Quantitative analysis of the pathophysiology of hypertension, *Circ. Res.* **24**: I1–I14.

Haldane, J. S. and Priestley, J. G. (1905). The regulation of the lung-ventilation, *J. Physiol. London* **32**: 225–266.

Hale, J. and Lunel, S. M. V. (1993). *Introduction to Functional Differential Equations*, Springer-Verlag, New York.

Hamilton, G. S., Solin, P., and Naughton, M. T. (2004). Obstructive sleep apnoea and cardiovascular disease, *Intern. Med. J.* **34**: 420–426.

Hand, I. L., Noble, L., Wilks, M., Towler, E., Kim, M., and Yoon, J. J. (2004). Hering-Breuer reflex and sleep state in the preterm infant, *Pediatr. Pulmonol.* **37**: 61–64.

Harris, M. D., Terrio, J., Miser, W. F., and Yetter 3rd, J. F. (1998). High-altitude medicine, *Am. Fam. Physician* **57**: 1907–1914.

Helbling, D., Boutellier, U., and Spengler, C. M. (1997). Modulation of the ventilatory increase at the onset of exercise in humans, *Respir. Physiol.* **109**: 219–229.

Heldt, T., Shim, E. B., Kamm, R. D., and Mark, R. G. (2002). Computational modeling of cardiovascular response to orthostatic stress, *J. Appl. Physiol.* **92**: 1239–1254.

Hewitt, E. and Stromberg, K. (1969). *Real and Abstract Analysis*, Springer-Verlag, Berlin.

Hinghofer-Szalkay, H. (1986). Method of high-precision microsample blood and plasma mass densitometry, *J. Appl. Physiol.* **60**: 1082–1088.

Hoffmann, M., Bybee, K., Accurso, V., and Somers, V. K. (2004). Sleep apnea and hypertension, *Minerva Med.* **95**: 281–290.

Horemuzova, E., Katz-Salamon, M., and Milerad, J. (2000). Breathing patterns, oxygen and carbon dioxide levels in sleeping healthy infants during the first nine months after birth, *Acta Paediatr.* **89**: 1284–1289.

Horgan, J. D. and Lange, R. L. (1963). Digital computer simulation of the human respiratory system, *IEEE International Conference Record,* pp. 149–157.

Hörl, W. H., Koch, K. M., Lindsay, R. M., Ronco, C., and Winchester, J. F. (eds.) (2004). *Replacement of Renal Function by Dialysis*, 5th ed., Kluwer Academic Publishers, Dordrecht, Boston, London.

Hughson, R. L., O'Leary, D. D., Shoemaker, J. K., Lin, D. C., Topor, Z. L., Edwards, M. R., and Tulppo, M. P. (2004). Searching for the vascular component of the arterial baroreflex, *Cardiovasc. Eng.* **4**: 155–162.

Ichinose, M. and Nishiyasu, T. (2005). Muscle metaboreflex modulates the arterial baroreflex dynamic effects on peripheral vascular conductance in humans, *Am. J. Physiol. Heart Circ. Physiol.* **288**: H1532–H1538.

Ichinose, M., Saito, M., Kitano, A., Hayashi, K., Kondo, N., and Nishiyasu, T. (2004). Modulation of arterial baroreflex dynamic response during mild orthostatic stress in humans, *J. Physiol.* **557**: 321–330.

Isidori, A. (1995). *Nonlinear Control Systems*, 3rd ed., Springer-Verlag, New York.

Ito, K. and Kappel, F. (1991). A uniform differentiable approximation scheme for delay systems using splines, *Appl. Math. Optim.* **23**: 217–262.

Ito, K. and Kappel, F. (1995). Approximation of semilinear equations, *Nonlinear Anal.:* **24**: 51–80.

Ito, K. and Kappel, F. (2002). *Evolution Equations and Approximations*, World Scientific, Singapore.

Ito, K. and Teglas, R. (1986). Legendre-tau approximations for functional differential equations, *SIAM J. Control Optim.* **24**: 737–759.

Ito, K. and Tran, H. T. (1989). Linear quadratic optimal control problem for linear systems with unbounded input and output operators: Numerical approximations, *in* F. Kappel, K. Kunisch, and W. Schappacher (eds.), *Internat. Ser. Numer. Math.*, Vol. 91, Birkhäuser, Basel, pp. 171–196.

Javaheri, S. (1999). A mechanism of central sleep apnea in patients with heart failure, *New England J. Med.* **341**: 949–954.

Jessup, M. and Brozena, S. (2003). Heart failure, *New England J. Med.* **348**: 2007–2018.

Jiang, C., Rojas, A., Wang, R., and Wang, X. (2005). CO_2 central chemosensitivity: Why are there so many sensing molecules?, *Respir. Physiol. Neurobiol.* **145**: 115–126.

Jordan, J., Shannon, J. R., Diedrich, A., Black, B., Costa, F., Robertson, D., and Biaggioni, I. (2000). Interaction of carbon dioxide and sympathetic nervous system activity in the regulation of cerebral perfusion in humans, *Hypertension* **36**: 383–388.

Joyner, M. J. and Proctor, D. N. (1999). Muscle blood flow during exercise: The limits of reductionism, *Med. Sci. Sports Exerc.* **31**: 1036–1040.

Joyner, M. and Shephard, J. (1993). Autonomic regulation of circulation, *in* P. Low (ed.), *Clinical Autonomic Disorders: Evaluation and Management*, Little, Brown, Boston, pp. 61–72.

Kahn, A., Groswasser, J., Franco, P., Scaillet, S., Sawaguchi, T., Kelmanson, I., and Bernard, D. (2002). Sudden infant deaths: Arousal as a survival mechanism, *Sleep Med.* **3**: S11–S14.

Kappel, F. (1991). Approximation of LQR-problems for delay systems: A survey, *in* K. L. Bowers and J. Lund (eds.), *Progress in Systems and Control Theory*, Birkhäuser, Boston, pp. 187–224.

Kappel, F. and Peer, R. O. (1993). A mathematical model for fundamental regulation processes in the cardiovascular system, *J. Math. Biol.* **31**: 611–631.

Kappel, F. and Propst, G. (1984). Approximation of feedback control for delay systems using Legendre polynomials, *Conf. Sem. Mat. Univ. Bari* **201**: 1–36.

Kappel, F. and Salamon, D. (1987). Spline approximation for retarded systems and the Riccati equation, *SIAM J. Control Optim.* **25**: 1082–1117.

Kappel, F. and Salamon, D. (1990). An approximation theorem for the algebraic Riccati equation, *SIAM J. Control Optim.* **28**: 1136–1147.

Kappel, F. and Wimmer, H. K. (1976). An elementary divisor theory for linear autonomous functional differential equations, *J. Differential Equation* **21**: 134–147.

Kara, T., Narkiewicz, K., and Somers, V. K. (2003). Chemoreflexes–physiology and clinical implications, *Acta Physiol. Scand.* **177**: 377–384.

Keidl, W. (ed.) (1985). *Kurzgefasstes Lehrbuch der Physiologie*, 6th ed., Georg Thieme Verlag, Stuttgart.

Kenner, T. (1982). Physiological measurement in circulation research. A review on the biological application of a new method, *Med. Prog. Technol.* **9**: 67–74.

Kenner, T. (1989). The measurement of blood density and its meaning, *Basic Res. Cardiol.* **84**: 111–124.

Kenner, T., Baertschi, A. J., Allison, J. L., and Ono, K. (1974). Amplitude dependence of the carotid sinus reflex, *Pflügers Arch.* **346**: 49–59.

Khoo, M. C. K. (1989). A model of respiratory variability during non-REM sleep, *in* G. D. Swanson, F. S. Grodins, and R. L. Hughson (eds.), *Respiratory Control: A Modeling Perspective*, Plenum Press, New York, pp. 327–336.

Khoo, M. C. K. (2000). *Physiological Control Systems: Analysis, Simulation, and Estimation*, IEEE Press, New York.

Khoo, M. C. K., Anholm, J. D., Ko, S. W., Downey 3rd, R., Powles, A. C., Sutton, J. R., and Houston, C. S. (1996). Dynamics of periodic breathing and arousal during sleep at extreme altitude, *Respir. Physiol.* **103**: 33–43.

Khoo, M. C. K., Gottschalk, A., and Pack, A. I. (1991). Sleep-induced periodic breathing and apnea: A theoretical study, *J. Appl. Physiol.* **70**: 2014–2024.

Khoo, M. C. K. and Kronauer, R. E. (1983). Estimation of cardiopulmonary parameters for quasi-optimal inputs, *1983 Proc. 2nd Am. Control Conf.*, pp. 46–51.

Khoo, M. C. K., Kronauer, R. E., Strohl, K. P., and Slutsky, A. S. (1982). Factors inducing periodic breathing in humans: A general model, *J. Appl. Physiol.* **53**: 644–659.

Khoo, M. C. K. and Yamashiro, S. M. (1989). Models of control of breathing, *in* H. K. Chang and M. Paiva (eds.), *Respiratory Physiology: An analytical approach*, Marcel Dekker, New York, pp. 799–829.

Kjekshus, H., Risoe, C., Scholz, T., and Smiseth, O. A. (2000). Methods for assessing hepatic distending pressure and changes in hepatic capacitance in pigs, *Am. J. Physiol. Heart Circ. Physiol.* **279**: H1796–H1803.

Klabunde, R. E. (2005). *Cardiovascular Physiology Cencepts*, Lippincott Williams & Wilkins, Baltimore, MD.

Kleiber, M. (1932). Body size and metabolism, *Hilgardia* **6**: 315–353.

Knobloch, H. W. and Kwakernaak, H. (1985). *Lineare Kontrolltheorie*, Springer-Verlag, Berlin.

Koch, G. (1968). Alveolar ventilation, diffusing capacity and the A-a PO2 difference in the newborn infant, *Respir. Physiol.* **4**: 168–192.

Koulouris, N. G., Latsi, P., Dimitroulis, J., Jordanoglou, B., Gaga, M., and Jordanoglou, J. (2001). Noninvasive measurement of mean alveolar carbon dioxide tension and Bohr's dead space during tidal breathing, *Eur. Respir. J.* **17**: 1167–1174.

Kouw, P., Olthof, C., Gruteke, P., de Vries, P., Meijer, J., Oe., P., and Donker, A. (1991). Influence of high and low sodium dialysis on blood volume preservation, *Nephrol. Dial. Transplant.* **6**: 876–880.

Krämer, M. (1999). New strategies for reducing intradialytic symptoms, *Sem. Dial.* **12**: 389–395.

Krämer, M., Rode, C., and Wizemann, V. (2006). Detection limit of methods to assess fluid status in dialysis patients, *Kidney Int.* **69**: 1609–1620.

Krasovskij, N. N. (1964). The approximation of a problem of analytic design of controls in a system with time lag, *Appl. Math. Mech.* **28**: 876–885.

Krasovskij, N. N. (1966). Approximation of an optimal control problem for a system with delay, *Soviet Phys. Dokl.* **11**: 219–221.

Krieger, J., Maglasiu, N., Sforza, E., and Kurtz, D. (1990). Breathing during sleep in normal middle-aged subjects, *Sleep* **13**: 143–154.

Kuhn, H. (1974). A new proof of the fundamental theorem of algebra, *Math. Prog. Stud.* **1**: 148–158.

Kwakernaak, H. and Sivan, R. (1972). *Linear Optimal Control Systems*, Wiley Interscience, New York.

Kwan, I., Bunn, F., and Roberts, I. (2003). Timing and volume of fluid administration for patients with bleeding, *Cochrane Database Syst. Rev.* **3**: 1–14.

Lahiri, S. and Forster II, R. E. (2003). CO_2/H^+ sensing: Peripheral and central chemoreception, *Int. J. Biochem. Cell Biol.* **35**: 1413–1435.

Lambert, R. and Teissier, G. (1927). Théorie de la similitude biologique, *Ann. Physiol.* **3**: 212–246.

Lambertsen, C. J. (1980). Chemical control of respiration at rest, *in* V. B. Montcastle (ed.), *Medical Physiology*, 14th ed., Vol. 2, Ch. 71, C. V. Mosby Company, St. Louis, MO, pp. 1447–1487.

Landis, E. and Pappenheimer, J. (1963). Exchange of substances through the capillary walls, *in* W. Hamilton and P. Dow (eds.), *Handbook of Physiology, Circulation*, Section II, Vol. 2, Chapter 29, American Physiological Society, Washington, DC, pp. 961–1024.

Lanfranchi, P. A. and Somers, V. K. (2003). Sleep-disordered breathing in heart failure: Characteristics and implications, *Respir. Physiol. Neurobiol.* **136**: 153–165.

Lasiecka, I. and Manitius, A. (1988). Differentiability and convergence rates of approximating semigroups for retarded functional differential equations, *SIAM J. Numer. Anal.* **25**: 883–907.

Leuenberger, U. A., Hardy, J. C., Herr, M. D., Gray, K. S., and Sinoway, L. I. (2001). Hypoxia augments apnea-induced peripheral vasoconstriction in humans, *J. Appl. Physiol.* **90**: 1516–1522.

Levick, J. R. (2003). *An Introduction to Cadiovascular Physiology*, 4th ed., Oxford University Press, New York.

Levine, M., Cleave, J. P., and Dodds, C. (1995). Can periodic breathing have advantages for oxygenation? *J. Theor. Biol.* **172**: 355–368.

Levine, M., Hathorn, M. K., and Cleave, J. P. (2000). Optimization of inspiratory work in periodic breathing in infants, *Pediatr. Res.* **47**: 256–265.

Levy, M. N. (1979). The cardiac and vascular factors that determine systemic blood flow, *Circ. Res.* **44**: 739–747.

Lindsay, R. M. and Schneditz, D. (2004). Online monitoring and biofeedback, *in* W. H. Hörl, K. M. Koch, R. M. Lindsay, C. Ronco, and J. F. Winchester (eds.), *Replacement of Renal Function by Dialysis*, 5th ed., Kluwer Academic Publishers, Dordrecht, Boston, London, pp. 555–584.

Lipsitz, L., Mukai, S., Hammer, J., Gagnon, M., and Babikian, V. (2000). Dynamic regulation of middle cerebral artery blood flow velocity in aging and hypertension, *Stroke* **32**: 1897–1903.

Lloyd, B. B. and Cunningham, D. J. C. (1963). A quantitative approach to the regulation of human respiration, *in* D. J. C. Cunningham and B. B. Lloyd (eds.), *The Regulation of Human Respiration*, Blackwell Scientific Publications, Oxford, UK, pp. 331–349.

Loeppky, J. A., Caprihan, A., Altobelli, S. A., Icenogle, M. V., Scotto, P. and Melo, M. F. V. (2006). Validation of a two-compartment model of ventilation/perfusion distribution, *Respir. Physiol. Neurobiol.*, **151**: 74–92.

Loewi, O. (1921). Über humorale Übertragbarkeit der Herznervenwirkung, *Pflügers Archiv* **189**: 239–242.

Loewi, O. and Navatril, E. (1926). Über humorale Übertragbarkeit der Herznervenwirkung. X. Mitteilung: Über das Schicksal des Vagusstoffs, *Pflügers Archiv* **214**: 678–688.

Longobardo, G. S., Cherniack, N. S., and Fishman, A. P. (1966). Cheyne-Stokes breathing produced by a model of the human respiratory system, *J. Appl. Physiol.* **21**: 1839–1846.

Longobardo, G. S., Cherniack, N. S., and Gothe, B. (1989). Factors affecting respiratory system stability, *Ann. Biomed. Eng.* **17**: 377–396.

Longobardo, G. S., Gothe, B., Goldman, M. D., and Cherniack, N. S. (1982). Sleep apnea considered as a control system instability, *Respir. Physiol.* **50**: 311–333.

Lorenzi-Filho, G., Rankin, F., Bies, I., and Douglas Bradley, T. (1999). Effects of inhaled carbon dioxide and oxygen on Cheyne-Stokes respiration in patients with heart failure, *Am. J. Respir. Crit. Care Med.* **159**: 1490–1498.

Lundvall, J., Bjerkhoel, P., Edfeldt, H., Ivarsson, C., and Lanne, T. (1993). Dynamics of transcapillary fluid transfer and plasma volume during lower body negative pressure, *Acta Physiol. Scand.* **147**: 163–172.

Magder, S. and De Varennes, B. (1998). Clinical death and the measurement of stressed vascular volume, *Crit. Care Med.* **26**: 1061–1064.

Magistretti, P. J., Pellerin, L., and Martin, J. (1995). Brain energy metabolism: An integrated cellular perspective, *in* F. E. Bloom and D. J. Kupfer (eds.), *Psychopharmacology: The Fourth Generation of Progress*, Raven Press, New York, pp. 921–932.

Magosso, E. and Ursino, M. (2004). Modelling study of the acute cardiovascular response to hypocapnic hypoxia in healthy and anaemic subjects, *Med. Biol. Eng. Comput.* **42**: 158–166.

Malloy, M. H. (2004). SIDS—a syndrome in search of a cause, *N. Engl. J. Med.* **351**: 957–959.

Mancia, G. (1993). Autonomic modulation of the cardiovascular system during sleep, *N. Engl. J. Med.* **328**: 347–349.

Manitius, A., Tran, H., Payre, G., and Roy, R. (1987). Computation of eigenvalues associated with functional differential equations, *SIAM J. Sci. Statistic. Comput.* **8**: 222–247.

Manitius, A. and Tran, H. T. (1994). Numerical approximations for hereditary systems with input and output delays: Convergence results and convergence rates, *SIAM J. Control Optim.* **32**: 1332–1363.

Mann, H., Stefanidis, I., Reinhardt, B., and Stiller, S. (1996). Prevention of haemodynamic risk by continuous blood volume measurement and control, *Nephrol. Dial. Transplant.* **11**: S48–S51.

Mark, A. L. and Mancia, G. (1983). Cardiopulmonary baroreflexes in humans, *in* J. T. Shepherd, F. M. Abboud, and S. R. Geiger (eds.), *Handbook of Physiology. The Cardiovascular System. Peripheral Circulation and Organ Blood Flow,* Section 2, Vol. III, part 2, Chapter 21, Am. Physiol. Soc., Bethesda, MD, pp. 795–813.

Mateika, J. H., Mateika, S., Slutsky, A. S., and Hoffstein, V. (1992). The effect of snoring on mean arterial blood pressure during non-REM sleep, *Am. Rev. Respir. Dis.* **145**: 141–146.

Melchior, F. M., Srinivasan, R. S., and Clere, J. M. (1992). Modeling of the human response to LBNP, *Physiologist* **35**: 204–205.

Melchior, F. M., Srinivasan, R. S., Thullier, P. H., and Clère, J. M. (1994). Simulation of cardiovascular response to lower body negative pressure from 0 mmHg to 40 mmHg, *J. Appl. Physiol.* **77**: 630–640.

Milhorn, Jr., H. T., Benton, R., Rose, R., and Guyton, A. C. (1965). A mathematical model of the human respiratory control system, *Biophys.* **5**: 27–46.

Mintun, M. A., Lundstrom, B. N., Snyder, A. Z., Vlassenko, A. G., Shulman, G. L., and Raichle, M. E. (2001). Blood flow and oxygen delivery to human brain during functional activity: Theoretical modeling and experimental data, *Proc. Natl. Acad. Sci. USA* **98**: 6859–6864.

Mohan, R. and Duffin, J. (1997). The effect of hypoxia on the ventilatory response to carbon dioxide in man, *Respir. Physiol.* **108**: 101–115.

Moissl, U., Wabel, P., Leonhardt, S., Isermann, R., and Krämer, M. (1999). Continuous observation and analysis of heart rate during hemodialysis treatment, *Med. Biol. Eng. Comput.* **37**: S558–S559.

Moller, K., Paulson, O. B., Hornbein, T. F., Colier, W. N., Paulson, A. S., Roach, R. C., Holm, S., and Knudsen, G. M. (2002). Unchanged cerebral blood flow and oxidative metabolism after acclimatization to high altitude, *J. Cereb. Blood Flow Metab.* **22**: 118–126.

Moore, F. A., McKinley, B. A., and Moore, E. E. (2004). The next generation in shock resuscitation, *Lancet* **363**: 1988–1996.

Mulkey, D. K., Stornetta, R. L., Weston, M. C., Simmons, J. R., Parker, A., Bayliss, D. A., and Guyenet, P. G. (2004). Respiratory control by ventral surface chemoreceptor neurons in rats, *Nat. Neurosci.* **7**: 1360–1369.

Muza, S. R., Rock, P. B., Fulco, C. S., Zamudio, S., Braun, B., Cymerman, A., Butterfield, G. E., and Moore, L. G. (2001). Women at altitude: Ventilatory acclimatization at 4,300 m, *J. Appl. Physiol.* **91**: 1791–1799.

Nattie, E. (1999). CO_2, brainstem chemoreceptors and breathing, *Prog. Neurobiol.* **59**: 299–331.

Neder, J., Corso, S. D., Malaguti, C., Reis, S., Fuccio, M. B. D., Schmidt, H., Fuld, J. P., and Nery, L. E. (2003). The pattern and timing of breathing during incremental exercise: A normative study, *Eur. Respir. J.* **21**: 530–538.

Nelson, N. M. (1976). Respiration and circulation after birth, *in* C. A. Smith and N. M. Nelson (eds.), *Physiology of the Newborn Infant*, 4th ed., Thomas, Springfield, Ill., pp. 200–250.

Nissenson, A. R. and Fine, R. N. (eds.) (2005). *Clinical Dialysis*, 4th ed., McGraw–Hill, New York.

Nofzinger, E. A., Buysse, D. J., Miewald, J. M., Meltzer, C. C., Price, J. C., Sembrat, R. C., Ombao, H., Reynolds, C. F., Monk, T. H., Hall, M., Kupfer, D. J., and Moore, R. Y. (2002). Human regional cerebral glucose metabolism during non-rapid eye movement sleep in relation to waking, *Brain* **125**: 1105–1115.

Novak, P., Novak, V., Spies, J., Gordon, V., Lagerlund, T., and Petty, G. (1997). Evaluation of cerebral autoregulation in orthostatic hypotension and POTS, *Clin. Auton. Res.* **7**: 238.

Novak, V., Chowdhary, A., Farrar, B., Nagaraja, H., Braun, J., Kanard, R., and Novak, P. (2003). Altered cerebral vasoregulation in hypertension and stroke, *Neurol.* **60**: 1657–1663.

Novak, V., Novak, P., Spies, J. M., and Low, P. A. (1998). Autoregulation of cerebral blood flow in orthostatic hypotension, *Stroke* **29**: 104–111.

Nugent, S. T. and Finley, J. P. (1987). Periodic breathing in infants: A model study, *IEEE Trans. Biomed. Eng.* **34**: 482–485.

Numa, A. H. and Newth, C. J. (1996). Anatomic dead space in infants and children, *J. Appl. Physiol.* **80**: 1485–1489.

Ochs, M., Nyengaard, J. R., Jung, A., Knudsen, L., Voigt, M., Wahlers, T., Richter, J., and Gundersen, H. J. (2004). The number of alveoli in the human lung, *Am. J. Respir. Crit. Care Med.* **169**: 120–124.

O'Dell, K. M., Kalus, J. S., Kucukarslan, S., and Czerska, B. (2005). Nesiritide for secondary pulmonary hypertension in patients with end-stage heart failure, *Am. J. Health Syst. Pharm.* **62**: 606–609.

Olthof, C., Kouw, P., Donker, A., de Lange, J., and de Vries, P. (1994). Non-invasive conductivity technique to detect changes in haematocrit: In vitro validation, *Med. Biol. Eng. Comput.* **32**: 495–500.

Olufsen, M. S., Ottesen, J. T., and Tran, H. T. (2004). Modeling cerebral blood flow control during posture change from sitting to standing, *J. Cardiov. Eng.* **4**: 47–58.

Olufsen, M. S., Ottesen, J. T., Tran, H. T., Ellwein, L. M., Lipsitz, L. A., and Novak, V. (2005). Blood pressure and blood flow variation during postural change from sitting to standing: Model development and validation, *J. Appl. Physiol.* **99**: 1523–1537.

Orth, V. H., Rehm, M., Haller, M., Thiel, M., and Finsterer, U. (2001). Die Messung des Blutvolumens—aktueller Stand, *Anaesthesist* **50**: 562–568.

Osborne, J. W. (2005). Hypothesis: Set-points and long-term control of arterial pressure. A theoretical argument for a long-term arterial pressure control system in the brain rather than the kidney, *Clin. Exp. Pharmacol. Physiol.* **32**: 384–393.

Ottesen, J. T. (1997). Modelling the baroreflex-feedback mechanism with time-delay, *J. Math. Biol.* **36**: 41–63.

Ottesen, J. T. (2000). Modelling the dynamical baroreflex-feedback control, *Math. Comput. Modelling* **31**: 167–173.

Ottesen, J. T. and Danielsen, M. (2003). Modeling ventricular contraction with heart rate changes, *J. Theor. Biol.* **222**: 337–346.

Ottesen, J. T., Olufsen, M. S., and Larsen, J. K. (2004). *Applied Mathematical Models in Human Physiology*, Monographs on Mathematical Modeling and Computation 9, SIAM, Philadelphia.

Panerai, R. B. (1998). Assessment of cerebral pressure autoregulation in humans—a review of measurement methods, *Physiol. Meas.* **19**: 305–338.

Pang, C. C. (2001). Autonomic control of the venous system in health and disease: Effects of drugs, *Pharmacol. Ther.* **90**: 179–230.

Pawelczyk, J. A. and Raven, P. B. (1989). Reductions in central venous pressure improve carotid baroreflex responses in conscious men, *Am. J. Physiol.* **257**: H1389–H1395.

Pearce, W. J. (1995). Mechanisms of hypoxic cerebral vasodilatation, *Pharmacol. Ther.* **65**: 75–91.

Peirano, P., Algarin, C., and Uauy, R. (2003). Sleep-wake states and their regulatory mechanisms throughout early human development, *J. Pediatr.* **143**: S70–S79.

Peskin, C. S. (1981). Lectures on mathematical aspects of physiology, *in* F. C. Hoppensteadt (ed.), *Mathematical Aspects of Physiology*, Vol. 19 of *Lectures on Applied Mathematics*, American Mathematical Society, Providence, RI, pp. 1–107.

Phillipson, E. A. and Bowes, G. (1986). Control of breathing during sleep, *in* A. P. Fishman, N. S. Cherniack, J. G. Widdicombe, and S. R. Geiger (eds.), *Handbook of Physiology, Section 3: The Respiratory System*, Vol. II, Control of Breathing, Part 2, Amer. Phys. Soc., Bethesda, MD, pp. 649–689.

Pinna, G. D., Maestri, R., Mortara, A., La Rovere, M. T., Fanfulla, F. and Sleight, P. (2000). Periodic breathing in heart failure patients: Testing the hypothesis of instability of the chemoreflex loop, *J. Appl. Physiol.* **89**: 2147–2157.

Podszus, T. (1997). Kreislauf und Schlaf, *in* H. Schulz (ed.), *Kompendium Schlafmedizin für Ausbildung, Klinik und Praxis*, Deutsche Gesellschaft für Schlafforschung und Schlafmedizin, Ecomed-Verl.-Ges., Landsberg/Lech., VII–1.1, pp. 1–3.

Polaschegg, H. D., Knoflach, A., and Binswanger, U. (1996). Ultrafiltrationskontrolle mittels Hämatokritmessung bei der Hämodialyse, *Biomed. Technik* **41**: 374–375.

Polin, R. A., Fox, W. W., and Abman, S. (eds.) (2004). *Fetal and Neonatal Physiology*, Vol. 1 and 2, 3rd ed., W. B. Saunders, Philadelphia.

Prabhakar, N. R. and Peng, Y. J. (2004). Peripheral chemoreceptors in health and disease, *J. Appl. Physiol.* **96**: 359–366.

Pries, A. R., Ley, K., and Gaehtgens, P. (1986). Generalization of the Fahraeus principle for microvessel networks, *Am. J. Physiol.* **251**: H1324–H1332.

Quarteroni, A. and Veneziani, A. (2003). Analysis of a geometrical multiscale model based on the coupling of ODEs and PDEs for blood flow simulations, *Multiscale Model. Simul.* **1**: 173 –195.

Reddi, B. A. J. and Carpenter, R. H. S. (2005). Venous excess: A new approach to cardiovascular control and its teaching, *J. Appl. Physiol.* **98**: 356–364.

Revow, M., England, S. J., O'Beirne, H., and Bryan, A. C. (1989). A model of the maturation of respiratory control in the newborn infant, *IEEE Trans. Biomed. Eng.* **36**: 414–423.

Richardson, D. W., Wasserman, A. J., and Patterson, Jr., J. L. (1961). General and regional circulatory responses to change in blood pH and carbon dioxide tension, *J. Clin. Invest.* **40**: 31–43.

Rideout, V. C. (1991). *Mathematical and Computer Modeling of Physiological Systems*, Biophysics and Bioengineering Series, Prentice–Hall, Englewood Cliffs, NJ.

Risk, M. R., Lirofonis, V., Armentano, R. L., and Freeman, R. (2003). A biphasic model of limb venous compliance: A comparison with linear and exponential models, *J. Appl. Physiol.* **95**: 1207–1215.

Robert, C., Guilpin, C., and Limoge, A. (1998). Review of neural network applications in sleep research, *J. Neurosci. Methods* **79**: 187–193.

Rothe, C. (1993). Mean circulatory filling pressure: Its meaning and measurement, *J. Appl. Physiol.* **74**: 499–509.

Roux, F., D'Ambrosio, C., and Mohsenin, V. (2000). Sleep-related breathing disorders and cardiovascular disease, *Am. J. Med.* **108**: 396–402.

Rowell, L. B. (1986). *Human Circulation Regulation During Physical Stress*, Oxford University Press, New York.

Rowell, L. B. (2004). Ideas about control of skeletal and cardiac muscle blood flow (1876-2003): Cycles of revision and new vision, *J. Appl. Physiol.* **97**: 384–392.

Rowland, T. W. (2005). Circulatory responses to exercise: Are we misreading Fick ?, *Chest* **127**: 1023–1030.

Russell, D. R. (1979). *Mathematics of Finite-dimensional Control Systems: Theory and Design*, Marcel Dekker, New York.

Salvaggio, A., Insalaco, G., Marrone, O., Romano, S., Braghiroli, A., Lanfranchi, P., Patruno, V., Donner, C. F., and Bonsignore, G. (1998). Effects of high-altitude periodic breathing on sleep and arterial oxyhaemoglobin saturation, *Eur. Respir. J.* **12**: 408–413.

Samaja, M. (1997). Blood gas transport at high altitude, *Respiration* **64**: 422–428.

Sandgaard, N. C., Andersen, J. L., Holstein-Rathlou, N. H., and Bie, P. (2005). Saline-induced natriuresis and renal blood flow in conscious dogs: Effects of sodium infusion rate and concentration, *Acta Physiol. Scand.* **185**: 237–250.

Santoro, A., Mancini, E., Paolini, F., Cavicchioli, G., Bosetto, A., and Zucchelli, P. (1998). Blood volume regulation during hemodialysis, *Am. J. Kidney Dis.* **32**: 739–748.

Saunders, K. B., Bali, H. N., and Carson, E. R. (1980). A breathing model of the respiratory system: The controlled system, *J. Theor. Biol.* **84**: 135–161.

Scarpelli, E. M. (ed.) (1990). *Pulmonary Physiology: Fetus, Newborn, Child, Adolescent*, 2nd ed., Lee and Febiger, Philadelphia.

Schäfer, C., Rosenblum, M. G., Abel, H. H., and Kurths, J. (1999). Synchronization in the human cardiorespiratory system, *Phys. Rev. E. Stat. Phys. Plasmas Fluids Relat. Interdiscip. Topics* **60**: 857–870.

Schmidt-Nielsen, K. (1984). *Scaling: Why is Animal Size so Important?* Cambridge University Press, Cambridge, UK.

Schneditz, D. (1996). Pathophysiology of refilling, *in* G. D'Amico and G. Colasanti (eds.), *Issues in Nephrosciences*, Vol. 6, Wichtig Editore, Milano, pp. 173–180.

Schneditz, D. (2005). Technological aspects of hemodialysis and peritoneal dialysis, *in* A. R. Nissenson and R. Fine (eds.), *Clinical Dialysis*, 4th ed., McGraw–Hill, New York, pp. 47–83.

Schneditz, D., Kenner, T., Heimel, H., and Stabinger, H. (1989). A sound speed sensor for the measurement of total protein concentration in disposable, blood perfused tubes, *J. Acoust. Soc. Am.* **86**: 2073–2080.

Schneditz, D., Mekaroonkamol, P., Haditsch, B., and Stauber, R. (2005). Measurement of indocyanine green dye concentration in the extracorporeal circulation, *ASAIO J.* **51**: 376–378.

Schneditz, D., Pogglitsch, H., Horina, J., and Binswanger, U. (1990). A blood protein monitor for the continuous measurement of blood volume changes during hemodialysis, *Kidney Int.* **38**: 342–346.

Schneditz, D., Roob, J. M., Oswald, M., Pogglitsch, H., Moser, M., and Kenner, T. (1992). Nature and rate of vascular refilling during hemodialysis and ultrafiltration, *Kidney Int.* **42**: 1425–1433.

Schneider, H., Schaub, C. D., Andreoni, K. A., Schwartz, A. R., Smith, P. L., Robotham, J. L., and O'Donnell, C. P. (1997). Systemic and pulmonary hemodynamic responses to normal and obstructed breathing during sleep, *J. Appl. Physiol.* **83**: 1671–1680.

Schubert, R. and Mulvany, M. J. (1999). The myogenic response: Established facts and attractive hypotheses, *Clin. Sci. (Lond.)* **96**: 313–326.

Seber, G. A. F. and Wild, C. J. (1989). *Nonlinear Regression*, J. Wiley, New York.

Secher, N. H., Jacobsen, J., Friedman, D. B., and Matzen, S. (1992). Bradycardia during reversible hypovolaemic shock: Associated neural reflex mechanisms and clinical implications, *Clin. Exp. Pharmacol. Physiol.* **19**: 733–743.

Seeliger, E., Persson, P. B., Boemke, W., Mollenhauer, G., Nafz, B., and Reinhardt, H. W. (2001). Low-dose nitric oxide inhibition produces a negative sodium balance in conscious dogs, *J. Am. Soc. Nephrol.* **12**: 1128–1136.

Seeliger, E., Wronski, T., Ladwig, M., Rebeschke, T., Persson, P. B., and Reinhardt, H. W. (2005). The 'Body Fluid Pressure Control System' relies on the Renin-Angiotensin-Aldosterone system: Balance studies in freely moving dogs, *Clin. Exp. Pharmacol. Physiol.* **32**: 394–399.

Selkurt, E. E., Womack, I., and Dailey, W. N. (1965). Mechanism of natriuresis and diuresis during elevated renal arterial pressure, *Am. J. Physiol.* **209**: 95–99.

Severinghaus, J. W. (1979). Simple, accurate equations for human blood O_2 dissociation computations, *J. Appl. Physiol.* **46**: 599–602.

Shepard, Jr., J. W. (1985). Gas exchange and hemodynamics during sleep, *Med. Clin. North. Am.* **69**: 1243–1264.

Smith, J. C., Butera, R. J., Koshiya, N., Del Negro, C., Wilson, C. G., and Johnson, S. M. (2000). Respiratory rhythm generation in neonatal and adult mammals: The hybrid pacemaker-network model, *Respir. Physiol.* **122**: 131 – 147.

Smith, J. and Kampine, J. (1990). *Circulatory Physiology*, Williams and Wilkins, Baltimore.

Solin, P., Roebuck, T., Johns, D. P., Walters, E. H., and Naughton, M. T. (2000). Peripheral and central ventilatory responses in central sleep apnea with and without congestive heart failure, *Am. J. Respir. Crit. Care Med.* **162**: 2194–2200.

Somers, V. K., Dyken, M. E., Mark, A. L., and Abboud, F. M. (1993). Sympathetic-nerve activity during sleep in normal subjects, *New England J. Med.* **328**: 303–307.

Søvik, S. and Lossius, K. (2004). Development of ventilatory response to transient hypercapnia and hypercapnic hypoxia in term infants, *Pediatr. Res.* **55**: 302–309.

Spanoudaki, S. and Myrianthefs, P. (2004). Alveolar-arterial oxygen difference increase during exercise, *Pneumon.* **17**: 265–271.

Stahl, W. R. (1963). The analysis of biological similarity, *in* J. H. Lawrence, J. W. Gofman, and T. L. Hayes (eds.), *Advances in Biological and Medical Physics*, Vol. 9, Academic Press, New York, pp. 355–464.

Starc, V. (2004). Effect of myogenic and metabolic mechanisms on the autoregulation of blood flow through muscle tissue: A mathematical model study, *Cardiovasc. Eng.*, **4**: 81–88.

Stefanovska, A. (2002). Cardio-respiratory interactions, *Nonlinear Phenomena in Complex Systems* **5**: 462–469.

Stépán, G. (1989). *Retarded Dynamical Systems: Stability and Characteristic Functions*, Longman Group UK Limited, Essex, UK.

Stiller, S., Wirtz, D., Waterbär, F., Gladziwa, U., Dakshinamurty, K. V., and Mann, H. (1991). Less symptomatic hypotension using blood volume controlled ultrafiltration, *ASAIO Transactions* **37**: M139–M141.

Swanson, G. D., Grodins, F. S., and Hughson, R. L. (eds.) (1990). *Respiratory Control: A Modeling Perspective*, Plenum Press, New York.

Taylor, J. A., Myers, C. W., Halliwill, J. R., Seidel, H., and Eckberg, D. L. (2001). Sympathetic restraint of respiratory sinus arrhythmia: Implications for vagal-cardiac tone assessment in humans, *Am. J. Physiol. Heart Circ. Physiol.* **280**: H2804–H2814.

Tehrani, F. T. (1993). Mathematical analysis and computer simulation of the respiratory system in the new born infant, *IEEE Trans. Biomed. Eng.* **40**: 475–481.

Thomaseth, K. and Cobelli, C. (1999). Generalized sensitivity functions in physiological system identification, *Ann. Biomedical Eng.* **27**: 607–616.

Thrasher, T. N. (2004). Baroreceptors and the long-term control of blood pressure, *Exp. Physiol.* **89**: 331–335.

Tikuisis, P., Meunier, P., and Jubenville, C. E. (2001). Human body surface area: Measurement and prediction using three dimensional body scans, *Eur. J. Appl. Physiol.* **85**: 264–271.

Timischl, S. (1998). *A Global Model of the Cardiovascular and Respiratory System*, PhD thesis, University of Graz, Graz, Austria.

Tran, H. T. (1991). Numerical studies of the linear quadratic control problem for retarded systems with delay in control, *in* K. Bowers and J. Lund (eds.), *Progress in Systems and Control Theory*, Birkhäuser, Boston, pp. 307–324.

Tremblay, L. N., Rizoli, S. B., and Brenneman, F. D. (2001). Advances in fluid resuscitation of hemorrhagic shock, *Can. J. Surg.* **44**: 172–179.

Tsuruta, H., Sato, T., Shirataka, M., and Ikeda, N. (1994). Mathematical model of cardiovascular mechanics for diagnostic analysis and treatment of heart failure, Part 1: Model description and theoretical analysis, *Med. Biol. Eng. Comput.* **32**: 3–11.

Turner, S. and Reilly, S. (1995). Fallacy of indexing renal and systemic hemodynamic measurements for body surface area, *Am. J. Physiol.* **268**: R978–R988.

Ursino, M. (1998). Interaction between carotid baroregulation and the pulsating heart: A mathematical model, *Am. J. Physiol.* **275**: H1733–H1747.

Ursino, M., Fiorenzi, A., and Belardinelli, E. (1996). The role of pressure pulsatility in the carotid baroreflex control: A computer simulation study, *Comput. Biol. Med.* **26**: 297–314.

Ursino, M. and Innocenti, M. (1997a). Mathematical investigation of some physiological factors involved in hemodialysis hypotension, *Artif. Organs* **21**: 891–902.

Ursino, M. and Innocenti, M. (1997b). Modeling arterial hypotension during hemodialysis, *Artif. Organs* **21**: 873–890.

Ursino, M. and Lodi, C. A. (1998). Interaction among autoregulation, CO_2 reactivity, and intracranial pressure: A mathematical model, *Am. J. Physiol.* **274**: H1715–H1728.

Ursino, M. and Magosso, E. (2003). Short-term autonomic control of cardiovascular function: A mini-review with the help of mathematical models, *J. Integr. Neurosci.* **2**: 219–247.

Ursino, M., Magosso, E., and Avanzolini, G. (2001a). An integrated model of the human ventilatory control system: The response to hypercapnia, *Clin. Physiol.* **21**: 447–464.

Ursino, M., Magosso, E., and Avanzolini, G. (2001b). An integrated model of the human ventilatory control system: The response to hypoxia, *Clin. Physiol.* **21**: 465–477.

van Beaumont, W. (1972). Evaluation of hemoconcentration from hematocrit measurements, *J. Appl. Physiol.* **32**: 712–713.

Van Mil, A. H., Spilt, A., Van Buchem, M. A., Bollen, E. L., Teppema, L., Westendorp, R. G., and Blauw, G. J. (2002). Nitric oxide mediates hypoxia-induced cerebral vasodilation in humans, *J. Appl. Physiol.* **92**: 962–966.

Warner, H. R. (1958). The frequency dependent nature of blood pressure regulation by carotid sinus studied with an electric analog, *Circ. Res.* **6**: 35–40.

Wasserman, K., Whipp, B. J., and Casaburi, R. (1986). Respiratory control during exercise, *in* A. P. Fishman, N. S. Cherniack, J. G. Widdicombe, and S. R. Geiger (eds.), *Handbook of Physiology, Section 3: The Respiratory System*, Vol. II, Control of Breathing, Part 2, Amer. Phys. Soc., Bethesda, MD, pp. 595–619.

Weibel, E. R. (2000). *Symmorphosis: On Form and Function in Shaping Life*, Harvard University Press, Cambridge, Mass.

Weibel, E. R. and Hoppeler, H. (2004). Modeling design and functional integration in the oxygen and fuel pathways to working muscle, *Cardivasc. Eng.* **4**: 5–19.

Weil, J. (1986). Ventilatory control at high altitude, *in* A. P. Fishman, N. S. Cherniack, J. G. Widdicombe, and S. R. Geiger (eds.), *Handbook of Physiology, Section 3: The Respiratory System*, Vol. II, Control of Breathing, Part 2, Amer. Phys. Soc., Bethesda, MD, pp. 703–727.

West, G. B., Brown, J. H., and Enquist, B. J. (1997). A general model for the origin of allometric scaling laws in biology, *Science* **276**: 122–126.

West, J. B. (2000). Human limits for hypoxia. The physiological challenge of climbing Mt. Everest, *Ann. N. Y. Acad. Sci.* **899**: 15–27.

Westerhof, N., Stergiopulos, N., and Noble, M. I. M. (2005). *Snapshots of Hemodynamics*, Basic Science for the Cardiologist, Vol. 18, Kluwer Academic Publishers, Dordrecht.

White, D. P., Gleeson, K., Pickett, C. K., Rannels, A. M., Cymerman, A., and Weil, J. V. (1987). Altitude acclimatization: Influence on periodic breathing and chemoresponsiveness during sleep, *J. Appl. Physiol.* **63**: 401–412.

Wickramasinghe, H. and Anholm, J. D. (1999). Sleep and breathing at high altitude, *Sleep Breath.* **3**: 89–101.

Wimmer, J., Haditsch, B., Holzer, H., and Schneditz, D. (2004). Measurement of volume sensitivity during hemodialysis (HD) by a reversible blood volume shift, *J. Am. Soc. Nephrol.* **15**: 593A. Abstract.

Yang, F. and Khoo, M. C. K. (1994). Ventilatory response to randomly modulated hypercapnia and hypoxia in humans, *J. Appl. Physiol.* **76**: 2216–2223.

Yasuma, F. and Hayano, J. (2004). Respiratory sinus arrhythmia: Why does the heartbeat synchronize with respiratory rhythm, *Chest* **125**: 683–690.

Index